

Advances on Vortex Fluidics for Processing Soft Matter Nanomaterials

By

Nikita Joseph

*Thesis
Submitted to Flinders University
for the degree of*

Doctor of Philosophy

College of Science & Engineering

22/09/2021

TABLE OF CONTENTS

Declaration	v
Acknowledgements	vi
Abstract	vii
Published and Submitted Articles.....	i
Presentation Contributions	ii
List of Figures	iii
List of Tables.....	xv
Abbreviation List of Chemicals and Symbols.....	xvi
Chapter 1. Introduction and Research Aims.....	1
1.1 Review on the Fundamentals of the Soft-Matter Sciences.....	1
1.1.1 What is Soft Matter?.....	1
1.1.2 Key Components of Soft Matter.....	2
1.1.3 A Soft Matter Perspective in Liposomal and Drug Delivery Technology.	3
1.1.4 A Soft Matter Perspective in Food Science Technology.....	8
1.2 Applications of Microfluidic Technology in Liposomal and Drug Delivery Processing.....	12
1.2.1 Flow-focusing and Co-flow droplet-based microfluidics for controlled size of liposomal and drug delivery systems.....	14
1.2.2 T-junction droplet-based microfluidics for controlled size of liposomal and drug delivery systems	17
1.3 Application of Microfluidic Technology in Food Processing.....	20
Author Contributions.....	20
Abstract	20
1.3.1. Introduction	21
1.3.2 Microfluidic devices.....	23
1.3.3. Applications of microfluidic devices in food processing	29
1.3.4 Microfluidic device for food safety control.....	33
1.3.5 Microfluidic devices for other food processing.....	36
1.3.6 Future research and development directions	37
1.3.7 Conclusions	43
Appendix: The print of published review article first page	44
1.4 The Vortex Fluidic Device (VFD).....	45

1.4.1 Applications of Vortex Fluidics in Materials Transformations.....	47
1.4.2 Applications of Vortex Fluidics in Chemicals Transformations.....	49
1.4.3 Applications of Vortex Fluidics in Biomaterials Processing.....	51
1.5 Research Program.....	54
1.5.1 Aims of the Program	55
1.5.2 Thesis Outline.....	55
References	58

Chapter 2: Continuous Flow Thin Film Microfluidic Mediated Nano Encapsulation of Fish-Oil.....70

Author Contributions.....	70
Abstract	70
2.1 Introduction	71
2.2 Materials.....	74
2.3 Methods.....	74
2.4 Results and Discussions	76
2.5 Conclusion.....	82
Acknowledgements	83
References	83
Appendix: The print of published article first page.....	85

Chapter 3: Vortex Fluidic Mediated Food Processing86

Author Contributions.....	86
Abstract	86
3.1 Introduction	87
3.2 Materials.....	90
3.3 Methods.....	90
3.4 Results and Discussions	93
3.5 Conclusion.....	98
Acknowledgements	98
References	98
Appendix: The print of published article first page.....	101

**Chapter 4: Vortex Fluidic Mediated Encapsulation of Functional FishOil Featuring
inSitu Probed Small Angle Neutron Scattering 102**

Author Contributions.....	102
Abstract	103
4.1 Introduction	104
4.2 Materials.....	105
4.3 Methods.....	105
4.4 Results and Discussion.....	112
4.4 Conclusion.....	127
Acknowledgements	128
References	128
Appendix: The print of published article’s first page.....	131

**Chapter 5: Vortex Fluidics Mediated Non-Covalent Physical Entanglement of
Tannic Acid and Gelatin for Entrapment of Nutrients 132**

Author Contributions.....	132
Abstract	132
5.1 Introduction	133
5.2 Materials.....	135
5.3 Methods.....	136
5.4 Results and Discussion.....	139
5.5 Conclusion.....	150
Acknowledgements	150
References	150
Appendix: The print of published article’s first page.....	152

Chapter 6: Vortex Fluidic Regulated Equilibria Involving Liposomes Down to Solvated Phospholipids 153

Author Contributions..... 153
Abstract 154
6.1 Introduction 155
6.2 Materials..... 157
6.3 Methods..... 158
6.4 Results and Discussions 161
6.5 Conclusion..... 175
Acknowledgements 175
References 176

Chapter 7: Conclusions and Future Work..... 178

7.1 Conclusions 178
7.2 Future Work 180
Acknowledgements 183
References 183

Declaration

I certify that this thesis does not incorporate without acknowledgment any material previously submitted for a degree or diploma in any university; and that to the best of my knowledge and belief it does not contain any material previously published or written by another person except where due reference is made in the text.

Signed..... *Nikita Joseph*

Date..... 02/03/2021

Acknowledgements

I would like to sincerely acknowledge Prof. Colin Raston for his excellent guidance, motivation and all of the mentoring towards this learning curve of life. These four years guidance and learning is going to be a stepping stone for the upcoming future. Thank you, Colin, for all the life stories and advice not only limited to research but also for becoming a better person in life. I would like to acknowledge Assoc. Prof. Shan He for all the help with the research and publications. Thank you, Shan, for keeping this journey full of enthusiasm with new ideas and lots of fun together. I would also like to acknowledge Prof. Harshita Kumari and Marzieh Mirzammani for their assistance and help with neutron scattering experiments. I thank all the Raston Lab members for keeping a high-spirited environment and helping each other at every point of time.

I am grateful towards my family for giving me this opportunity in life and will always be appreciated. Lastly, a very special thanks to my partner Dhaval Desai for making me believe in myself and keeping faith in me at every step. Today this journey is possible all because of his boundless love, patience and commitment.

Abstract

The Vortex Fluidic Device (VFD) is a versatile microfluidic platform with a range of applications under its umbrella. In this thesis, the research is focused on developing applications for the soft-matter discipline in manipulating soft-materials at nano-domains. The VFD imparts controlled mechanical energy and shear stress in the thin-film liquid in the device. Soft-materials can be easily manipulated under this controlled mechano-energy. Crucial parameters such as controlled size, shape and scalability are some challenges which determines the fate of any new technology coming in the market. In this thesis VFD gives a new direction to these challenges via a cost-effective and a sustainable pathway for food, pharmaceuticals and cosmetic industries.

A process for fabricating soft-nanoparticles such as Water/Oil/Water (W/O/W) emulsions is demonstrated in a scalable environment. The mechano-energy of the liquid in the VFD controls the size of these particles at the nanometer dimensions. Parameters such as flow-rate, rotational-speed are altered for a favorable application in the food-industry. A number of different food models have been tested in determining the potential of VFD in the food technology sector. From improving the time-efficiency in raw milk pasteurization to improving enzymatic hydrolysis of the milk powder has been established for providing a sustainable environment for the benefit of the community in day to day life. In addition, improved O/W formulation with higher nutritional values has been established in the VFD. This process provides a new route in the health industry where fish-oil is often under-rated due to its taste, odor, chemical structure and viscosity.

With increasing customer demand for plant-based material and super foods with better nutritional values in terms of protein or vitamins there is always a research niche awaiting. Herein, we utilize the potential of VFD in fabricating stronger gelatin gels when cross-linked with polyphenols non-covalently. These crosslinked gels are further utilized to entrap nutrients without using any toxic chemicals or reagents which unequivocally meets the criteria of green chemistry metrics. These mentioned applications embrace major challenges in the food technology sector and have given a new direction for the VFD technology.

Moreover, with this VFD thin-film microfluidic flow reactor one of the widely utilized soft material in health, food and pharmaceutical industry “liposomes” are fabricated. Liposomes of *ca* 100 nm are fabricated from a phospholipid suspension when processed at its optimized conditions in the VFD. This study also includes the *in-situ* small angle neutron scattering which reveals *ca* 100 nm are the stable bottom-up self-assembly process thermodynamically, and this is in accord with cellular processing of exosomes and endosomes which are of similar dimensions.

Overall, the results in this thesis further contribute to the remarkable versatility of the VFD. It is a new cutting-edge technology in the field of microfluidics with a plethora of applications and provides insights on the rudimentary disciplines of science. It is a benign process intensification platform which is high in green chemistry metrics and the applications exhibited in this thesis opens are just the start to the future applications.

Published and Submitted Articles

1. He, Shan, Joseph, Nikita, Luo, Xuan, & Raston, Colin. (2019). Continuous flow thin film microfluidic mediated nano-encapsulation of fish oil. **Food Science & Technology**, *103*, 88-93.
2. He, Shan, Joseph, Nikita, Luo, Xuan, & Raston, Colin L. (2019). Vortex fluidic mediated food processing. **PloS One**, *14*(5), E0216816.
3. He, Shan, Joseph, Nikita, Mirzamani, Marzieh, Pye, Scott J, Al-anataki, Ahmed Hussein Mohammed, Whitten, Andrew E, Chen, Yaonan, Kumari, Harshita, and Raston, Colin L. Vortex fluidic mediated encapsulation of functional fish oil featuring in situ probed small angle neutron scattering. **NPJ Science of Food**, *4*(1), 12.
4. Cao, X, Joseph, N, Jellicoe, M, Alantak, A, Luo, X, & Su, D. et al. (2020). Vortex fluidics mediated non-covalent crosslinking of tannic acid and gelatin for entrapment of nutrients. **Food & Function**. doi: 10.1039/d0fo02230f.
5. He, S, Joseph, N, Feng, S, Jellicoe, M, & Raston, C. (2020). Application of microfluidic technology in food processing. **Food & Function**, *11*(7), 5726-5737. doi: 10.1039/d0fo01278e.
6. Joseph, N, Mirzammani, Marzieh., Al-anataki, Ahmed Hussein Mohammed, Whitten, Andrew E, Raston, Jellicoe, M., Harvey., David., P, Crawley., Emily., Raston, Colin L. Vortex fluidic regulated equilibria involving liposomes down to solvated phospholipids. (close to submission)
7. Tavakoli, Javad, Joseph, Nikita, Raston, Colin L, & Tang, Youhong. (2020). A hyper-branched polymer tunes the size and enhances the fluorescent properties of aggregation-induced emission nanoparticles. **Nanoscale Advances**, *2*(2), 633-641.
8. Tavakoli, J., Joseph, N., Chuah, C., Raston, C., & Tang, Y. (2020). Vortex fluidic enabling and significantly boosting light intensity of graphene oxide with aggregation induced emission luminogen. **Materials Chemistry Frontiers**, *4*(7), 2126-2130. doi: 10.1039/d0qm00270d.

Presentation Contributions

1. Nano-centre Annual Conference-Flinders 2017/2018/2019/, Australia, Poster Presentation.
2. Royal Centenary Congress (RACI) 100 years July 2017, Australia, Poster Presentation.
3. International Conference on Nanoscience and Nanotechnology (ICONN-2018) Jan-2018, Australia, Poster Presentation.
4. International Conference on Nanoscience and Nanotechnology (ICONN-2020) Feb - 2020, Australia, Poster Presentation.
5. International Conference on Nanoscience and Nanotechnology (ICONN-2020) Feb - 2020, Australia, Oral Presentation.

List of Figures

Figure 1.1: classification of soft matter materials. (Left) The soft matter triangle which was originally proposed by Gomper, Dhont and Richter ³ indicates the multi dimensions of molecules and materials. The gradients depict the amphiphilicity and elongation/flexibility of the materials. (Right) A colloidal length scale mapping different soft-matter particle ².

Figure 1.2: Soft matter perspective on nanoparticles induced stability to liposomes. (Top) A schematic approach towards supported lipid bilayer formation on nanoparticles where the radius of the nanoparticle is greater than the liposomes. (Bottom) A schematic approach on nanoparticle internalization where the particle size is smaller than the liposome ⁸.

Figure 1.3: Schematic structure of different types of liposomes for multiple functions. Liposomes can be used for carrying different active agents by manipulating their aqueous core region or outer bilayers based on the functions such as Conventional, PEGylated, Ligand targeted or Theranostic liposomes ¹².

Figure 1.4: Different protein based nano-carriers for drug-delivery technology. Nanofibers, Nanoparticles, films, sponges, microneedles processed from naturally occurring proteins such as Silk, Resilin, Keratin and Collagen ¹⁵.

Figure 1.5: Microscopic structure of ice-cream, yoghurt and cheese. The images were obtained from Confocal Scanning Laser Microscopy (CLSM) images with fluorescent dyes fats (green) and protein is (red) ²².

Figure 1.6: Schematic representation of protein-polysaccharide stabilization of oil droplets in oil-water emulsions. These types of interactions can lead to several gel networks where the extended protein can be in random coil or partially folded state ²⁷.

Figure 1.7: Device geometries for droplet-based microfluidics. Different types of drug delivery systems 1, 11, 111 are prepared through co-flow, flow focusing and T-junction geometries ⁴⁰.

Figure 1.8: Flow focusing droplet based microfluidic geometry. (left) Formation of liposomes from a double emulsion template ⁴². (Right) formation of PLGA micro particles with a model drug through flow focused microfluidic setup ⁴³.

Figure 1.9: Applications of T-shaped geometry in droplet based microfluidic systems. (1) T-junction combining co-flow and Y-junction for fabricating Janus particles ⁴⁰. (2) formation of droplet interface bilayers (DIBs) via T-junction and co-axial flow geometry (a) T-junction schematics (b) side view of the microfluidic platform, (c) and (d) aqueous droplets in oil phase with continuous alginate flow. (e) a continuous alginate flow encapsulates the constructs in alginate shell ⁴⁷. (3) schematic representation of T-junction microfluidic platform for fabricating ca-alginate microcapsules ⁴⁸.

Figure 1.10: Length scale for microfluidics. Range of the length scale of material involved in microfluidics, microfluidic devices, and microfluidic applications. (Images are reprinted from “Applications of Microfluidic devices in food engineering”, Food Biophys., 2008, 3, 1–15 with permission from Springer)

Figure 1.11: Capillary microfluidic devices. (a) A co-flow microcapillary device, and (b) A flow-focusing microcapillary devices. (Images are reprinted from “Controlled production of emulsions and particles by milli- and microfluidic techniques”, Engl, et al., Curr. Opin. Colloid Interface Sci., 2008, 13, 206–216 with permission from ELSEVIER)

Figure 1.12: Planar geometry devices. (a) A co-flow T-junction, (b) A co-flow Y-junction, and (c) A cross-junction. (Images are reprinted from “Microfluidic emulsification in food processing”, Abid, et al., J. Food Eng., 2015, 147, 1–7 with permission from ELSEVIER).

Figure 1.13: Schematic of a terrace geometry microfluidic device. (Images are reprinted from “Spontaneous droplet formation techniques for monodisperse emulsions preparation– Perspectives for food applications”, Abid, et al., J. Food Eng., 2011, 107, 334–346 with permission from ELSEVIER)

Figure 1.14: Schematic of a microfluidic device with two successive T-junctions. 1) (Images are reprinted from “Controlled production of monodisperse double emulsions by two-step droplet breakup in microfluidic devices”, Shingo, et al., Langmuir, 2004, 20, 9905–9908 with permission from the American Chemical Society). 2) Schematic of a microfluidic device with the combined capillaries of a circular cross section (images are reprinted from “Controlled production of emulsions and particles by milli- and microfluidic techniques”, Engl, et al., Curr. Opin. Colloid Interface Sci., 2008, 13, 206–216 with permission from ELSEVIER).

Figure 1.15 A microfluidic device with linear sequences of multiple cross-junction micro-channels. (Images are reprinted from “Microfluidic emulsification in food processing”, Abid, et al., J. Food Eng., 2015, 147, 1–7 with permission from ELSEVIER).

Figure 1.16: Vortex Fluidic Device (VFD). (a). Photograph of the VFD, highlighting its salient features. (b) Schematic of the VFD showing the fluid flow.

Figure 1.17: Schematic representation of the VFD. (a, b) Average film thickness vs rotating speed. (c), Behavior of thin film at different rotational speeds ¹²⁸.

Figure 1.18: Applications of vortex fluidics in materials transformation. (1) Schematic representation for VFD mediated SWCNT coiled rings (a) SWCNTs entangled pre-processing VFD, (b) Schematic of the VFD setup, (c) Post processing coiled SWCNTs and (d) Defining parameters for the coiled rings.¹³⁶ (2) VFD manipulated graphite into highly conducting scrolls, (a) Schematic representation of the VFD processing from graphite flakes into graphene scrolls (b) AFM phase images and SEM images for the graphene scrolls (c) Raman spectra of the graphene and as receive graphite flakes (d) TEM and HRTEM characterization for the graphene scrolls¹³⁷. (3) An inverted VFD for fabricating exfoliating and scrolling Hexagonal Boron Nitride (h-BN). (a) Schematic representation of the VFD (b) A zoomed in illustration for the delivery of liquid inside the VFD tube. (c) Schematics for exfoliation of h-BN and scrolling of h-BN. (d) Photograph of the VFD in inverted position -45° relative to the horizontal position¹³⁸. (4) VFD mediated exfoliation and fragmentation of two dimensional Mxene (Ti_2CT_x)¹³⁹. (a) Schematic representation of the VFD (b)& (c) Indicates two different setups of VFD in continuous and confined mode with an images of the post VFD product in IPA and water.

Figure 1.19: Application of vortex fluidics in chemical transformations. 1- a) Schematic mechanism for ethenolysis type – Olefin Methathesis (OM) reaction. 1-b) Schematic illustration for VFD mediated processing of methyl oleate (MO)¹⁴⁰. 2) Schematic illustration for processing chemoselectivity of biobased molecule cyrene via utilizing cellulose immobilized palladium nanoparticles onto the VFD tube for a continuous scalable process¹⁴¹. 3 – top) Schematic illustration for utilizing VFD for Azide-Alkyne cycloaddition reactions, 3-bottom) Optimized conditions and total conversion for the VFD processed cycloaddition product with water as a suitable solvent for the reaction¹⁴².

Figure 1.2: Applications of vortex fluidics in biomaterials processing. 1-a) Schematic representation of aggregation induced emission alginate hydrogel with fluorescence properties excited at 350 nm in presence of UV light. 1-b) Schematic representation of AIE hyper-branched self-assembly and change its structure by utilizing VFD¹⁴⁶.

2-a), Data analysis for elongation at the break for PVA alone and PVA with AIE 2-b), Crosslinking with borax and self-healing properties for PVA alone and PVA with AIE. 2-c) PVA crosslinked with borax images ¹⁴⁶. 3-a) Schematic representation of the VFD and rotational effects on the BSA incorporated Nano-Flowers (BNFs) 3-b) BNFs processing at 2, 10 and 30 min. 3-c) Encapsulation Efficiency of BSA on BNFs at different rotational speed 3-d) Encapsulated Efficiency of BSA at given concentrations 3-e) Encapsulated Efficiency at optimized conditions 5000 rpm for 30min and 2-day incubation ¹⁴⁵.

Figure 2.1: Photograph of the vortex fluidic device (VFD) highlighting its salient features. The reagents are delivered via syringe pump into the bottom of the glass tube, gets processed at optimized conditions and collected in the vial.

Figure 2.2: Photographs of different samples of fish oil. (a) As received fish oil. (b) Fish oil formulation processed using the homogenization method (speed: 13,500 rpm; time: 10 min; temperature: 25 °C; sonication: 20 min; homogenizer: T25 digital ULTRA-TURRAX). (c) Fish oil formulation processed using a vortex fluidic device (VFD) (dispersed phase: 2 g/100 mL, lipid/oil: 1/1 (w/ w), speed: 8000 rpm, flow-rate: 0.1 mL/min, tilt angle: 45°, temperature: 25 °C; sonication post VFD processing for 20 min).

Figure 2.3. SEM images of fish oil encapsulation in phospholipids. (a) Generated using the homogenization method (speed: 13,500 rpm; time: 10 min; temperature: 25 °C, sonication: 20 min). (b) Generated using VFD processing. Samples in (a) and (b) were coated with 2 nm Pt; dispersed phase: 2 g/ 100 mL, lipid/oil: 1/1 (w/w), speed: 8000 rpm, flowrate: 0.1 mL/min, tilt angle: 45°, temperature: 25 °C; sonication: 20 min.

Figure 2.4: Dynamic light scattering (DLS) data. (Temperature 25 °C; HeNe laser: 633 nm; detector angle: 173°) for encapsulated particles produced using VFD processing, for the optimized processing parameters in Fig. 2.3 caption

Figure 2.5: Transmission electron microscopy images. Encapsulated particles produced using VFD processing under different magnification, for the optimized processing parameters in Fig. 2. (Sample volume: 20 μ L; staining: 2 g/100 mL uranyl acetate solution).

Figure 2.6: Atomic Force Microscopy image. (Sample volume: 20 μ L, dispersed phase: 2 g/100 mL, lipid/oil: 1/1 (w/w), speed: 8000 rpm, flow-rate: 0.1 mL/ min, tilt angle: 45°, temperature: 25 °C; sonication post VFD processing for 20 min).

Figure 3.1: Photograph of the vortex fluidic device (VFD) highlighting its salient features. The reagents are delivered via syringe pump into the bottom of the glass tube, gets processed at optimized conditions and collected in the vial.

Figure 3.2. Enzymatic hydrolysis of protein. (Left) Appearance of dissolved milk powder with (a) no treatment; milk powder: water = 1:5 (w/v). (b) VFD-enzymatic hydrolyzation; milk powder: water = 1:5 (w/v); temperature at 55°C; processing time of 20 mins; VFD speed at 8000 rpm; VFD tilt angle of 45°. (c) Conventional enzymatic hydrolyzation; milk powder: water = 1:5 (w/v); temperature at 55°C; processing time of 20 min. (Right) MALDI mass spectra analysis of dissolved milk powder before and after different treatments (a) No treatment; milk powder: water = 1:5 (w/v). (b) VFD-enzymatic hydrolyzation; milk powder: water = 1:5 (w/v); temperature at 55°C; processing time of 20 mins; VFD speed at 8000 rpm; VFD tilt angle at 45°. (c) Conventional enzymatic hydrolyzation; milk powder: water = 1:5 (w/v); temperature at 55°C; processing time of 20 min.

Figure 3.3: Curcumin encapsulation of O/W emulsions. 1-a) O/W emulsion homogenized 1-b) O/W emulsion of VFD. 2) Particle size data for homogenized and VFD samples. 3) Fluorescence spectrum of homogenized and VFD samples. 4) UV-spectrum of homogenized and VFD samples.

Figure 3.4: Pasteurization of raw milk. The effect of VFD-pasteurization with different processing times (5–30 min) and temperatures (40–60°C) on raw milk (VFD Mode: confined mode; VFD rotation speed: 9000 rpm; VFD tilt angle: 45°).

Figure 4.1: Fish oil encapsulation with tween 20. (A) Homogenization processed mixture (speed: 13,500 rpm; time: 10 min; temperature: 25°C) immediately after processing (H) and VFD processed mixture (rotational speed: 9000 rpm; flow rate: 0.3 mL/min; tilt angle: 45°; temperature: 25°C) immediately after processing (V). (B) The mixtures in (A) after 24 hours. (C) and (D) Epi-fluorescence microscopic images (20 X long-working-distance; exposure time 100 ms; frame rate 10 fps) for the homogenization and VFD processed mixtures in (A) respectively. (E) Emulsion stability of homogenization and VFD processed mixtures in (A). (F) Dynamic light scattering (temperature: 25°C; He-Ne wavelength: 633 nm detector angle: 173°) results of homogenization and VFD mixtures prepared in (A)

Figure 4.2: Small-angle neutron scattering. (A) SANS data overlay of real-time VFD data of 10wt% Tween 20 alone, (B) SANS data overlay of post-VFD data of 10wt% Tween 20 alone, (C) SANS data overlay of real-time VFD data of 10wt% Tween 20 with 10wt% of fish oil, (D) SANS data overlay of post-VFD data of 10wt% Tween 20 with 10wt% of fish oil, (E) top-down view schematic representation for in situ VFD SANS where the neutron beam is normal to the x-z plane of the VFD tube and the tube is tilted 45° from vertical, (F) picture of the VFD installed on the sample staging area of the Bilby beam line while out of the path of the neutron beam. The curves shown in the data overlays in (A)-(D) were offset by powers of 3 to improve clarity.

Figure 4.3: Representative fits to the data from the models described above. a) Gauss Sphere with screened Coulomb interaction model fitted to the 10 wt% of Tween 20-alone sample at 0 rpm (static), b summed Power Law + Gauss Sphere model fitted to the 10 wt% of Tween 20 with 10 wt% of fish oil

sample while being sheared at 4000 rpm. The fits to the other data sets shown in the SI are similar in fit quality.

Figure 4.4: Application of encapsulated fish oil using vortex fluidic device. a) Sensory evaluation of apple juices with and without fish oil and encapsulated fish oil. b) Fatty acid profile of fresh fish oil and encapsulated fish oil by VFD processing (speed: 9000 rpm; flow rate: 0.3 mL/min; tilt angle: 45°; temperature: 25 °c) before and after 14 days storage.

Figure 4.5: Encapsulation capacity for curcumin and quercetin. a) Dynamic light scattering (DLS) measurements for encapsulated emulsions. b, c) Fluorescence spectra for curcumin and quercetin encapsulated emulsions, respectively. d, e) Confocal micrographic images (wavelength: 420 and 370 nm) of encapsulated fish oil containing curcumin and quercetin, respectively, homogenously suspended in water

Figure 5.1: Vortex Fluidic Device (VFD). (a). Photograph of the VFD, highlighting its salient features. (b). Schematic of the VFD showing the fluid flow (images are reprinted from our previous publication “Application of microfluidic technology in food processing”, He, et al., Food and Function, 2020, advance article, with permission from the Royal Society of Chemistry).

Figure 5.2: Physical characteristics of cross-linked tannic acid-gelatin materials produced using the vortex fluidic device (VFD). (Total concentration: 0.18 g mL⁻¹, gelatin/tannic acid: 2 : 0.375(w/w); speed: 7000 rpm; flow rate: 0.3 mL min⁻¹; tilt angle: 45 °C; temperature: 25° C) and homogenization (speed: 13 500 rpm; time: 10 min; temperature: 25 °C; homogenizer: T25 digital ULTRA-TURRAX). (a) Viscosity data: measured immediately after processing. Images in (a): taken 12 h after the material was prepared. (b) Dynamic light scattering (DLS) data.

Figure 5.3: Scanning electron microscopy (SEM) images of cross-linked tannic acid-gelatin materials. (a) Material produced using homogenization processing (speed: 13 500 rpm; time: 10 min; temperature: 25 °C; homogenizer: T25 digital ULTRA-TURRAX) immediately drop casted onto a silicon wafer and air dried overnight, followed by platinum sputter coating. (b) Material produced using VFD processing (total concentration: 0.18 g mL⁻¹, gelatin/tannic acid: 2 : 0.375 (w/w); speed: 7000 rpm; flow rate: 0.3 mL min⁻¹; tilt angle: 45 °C; temperature: 25 °C) immediately drop casted onto a silicon wafer and air dried overnight, followed by platinum sputter coating. (c). Material produced using homogenization processing (speed: 13 500 rpm; time: 10 min; temperature: 25 °C; homogenizer: T25 digital ULTRA-TURRAX) after freeze-drying and platinum sputter coating. (d) Material produced using VFD processing (total concentration: 0.18 g mL⁻¹, gelatin/tannic acid: 2 : 0.375 (w/w); speed: 7000 rpm; flow rate: 0.3 mL min⁻¹; tilt angle: 45 °C; temperature: 25 °C) after freeze-drying and platinum sputter coating.

Figure 5.4: Fourier transform infrared (FTIR) spectra of physically entangled tannic acid-gelatin materials produced using the vortex fluidic device (VFD). (Total concentration: 0.18 g mL⁻¹, gelatin/tannic acid: 2 : 0.375 (w/w); speed: 7000 rpm; flow rate: 0.3 mL min⁻¹; tilt angle: 45°; temperature: 25° C) and homogenization (speed: 13 500 rpm; time: 10 min; temperature: 25 °C; homogenizer: T25 digital ULTRA-TURRAX).

Figure 5.5: Nutrients Entrapment capacity. Appearances of ground nutrient supplements of minerals and vitamins entrapped by different cross-linked tannic acid-gelatin materials after freeze-drying the sample prepared using VFD processing (gelatin/tannic acid/ground nutrient supplement: 2 : 0.375 : 1.25 (w/w/w); speed: 7000 rpm; flow rate: 0.3 mL min⁻¹; tilt angle: 45 °C; temperature: 25° C) and using a homogenizer (gelatin/tannic acid/ground nutrient supplement: 2 : 0.375 : 1.25 (w/w/w); speed: 13 500 rpm; time: 10 min; temperature: 25 °C; homogenizer: T25 digital ULTRA-TURRAX).

Figure 5.6: Percentage of entrapped mineral in cross-linked tannic acid-gelatin prepared using homogenization processing. (speed: 13 500 rpm; time: 10 min; temperature: 25 °C; homogenizer: T25 digital ULTRA-TURRAX) and a VFD (total concentration: 0.18 g mL⁻¹, gelatin/tannic acid: 2: 0.375. (w/w); speed: 7000 rpm; flow rate: 0.3 mL min⁻¹; tilt angle: 45°; temperature: 25 °C).

Figure 5.7: Percentage of each entrapped vitamin in cross-linked tannic acid-gelatin prepared using homogenization processing (speed: 13 500 rpm; time: 10 min; temperature: 25 °C; homogenizer: T25 digital ULTRA-TURRAX) and a VFD (total concentration: 0.18 g mL⁻¹, gelatin/tannic acid: 2 : 0.375(w/w); speed: 7000 rpm; flow rate: 0.3 mL min⁻¹; tilt angle: 45°; temperature: 25 °C).

Figure 6.1: Schematic representation of The Vortex Fluidic Device. The phospholipid suspension is passed to the bottom of the tube through one jet feed at a concentration of 1mg/mL, 9000 rpm, 0.1 mL/min, 45° tilt angle in continuous flow in a hydrophobic tube. The collected product yields unilamellar liposomes of ~ 100 nm in size.

Figure 6.2: VFD processed liposomes. (A) Nanoparticle tracking analysis size distribution data with maximum concentration of particles at 90 nm. (B) pre-VFD and post VFD solutions for 1mg/mL phospholipid (POPC) solution in MQ-water processed at 9000 rpm, 0.1 mL/min, 45° tilt angle in continuous flow in a hydrophobic tube. (C) Scanning Electron Microscopy (SEM) image for VFD processed liposomes at 9000 rpm, 0.1 mL/min, 45° tilt angle in continuous flow in a hydrophobic tube, the sample was sputter coated with 2 nm Pt deposition before imaging. Scale bar is 500 nm. (d) Atomic Force Microscopy (AFM) image for VFD processed liposomes at 9000 rpm, 0.1 mL/min, 45° tilt angle in continuous flow in a hydrophobic tube, the sample was imaged with fast scan assist peak force microscope in a tapping mode on a silicon surface. Scale bar is 200 nm (e) Transmission Electron Microscopy (TEM) image for VFD processed liposomes at 9000 rpm, 0.1 mL/min, 45° tilt angle in continuous flow in a hydrophobic tube. Samples were stained with 2% uranyl acetate and air dried on copper grid before imaging. The voltage applied was 80 – 100 kv. Scale bar is 200 nm.

Figure 6.3: Influence of different size VFD tube. (A) Schematic representation for VFD hydrophobic coated tube having OD 10mm and 15 mm VFD tube. (B) Pre-VFD and post VFD solutions processed at 9000 rpm in confined mode, 1mg/mL concentration at an angle 45° in 10 mm and 15mm tubes. (c) Scanning Electron Microscopy (SEM) image for VFD processed liposomes, the sample was sputter coated with 2 nm Pt deposition before imaging. Scale bar is 500 nm. (d) Atomic Force Microscopy (AFM) images and height distribution profile for VFD processed liposomes. The samples were scanned with SPM multimode 2 in tapping mode on silicon surface. The scale bars are 500 nm. (E) The lamellarity was observed through AFM height thickness, the maximum thickness for the 10mm sample is widely distributed and a heterogeneous population is observed. (F) The 15mm tube sample is observed to be more homogeneous and a height profile of 11 – 17 nm is shown indicating more unilamellar - bilamellar liposomes.

Figure 6.4: SANS data overlays of POPC liposomes in D₂O at each shear level generated at the specified rotational speeds. (a) Overhead-view schematic of the VFD tube, the sample film, and the neutron beam passing through and being scattered by the tube and sample film before meeting the 2D-detector; (b) BILBY sample staging area depicting the VFD setup; (c) Real-time VFD-SANS data as a function of increasing rotational speeds (d) Static SANS measurements after each real-time VFD study, (e) Schematic mechanism on the observed lipid self-assembly at each rotational speed as determined via in-situ SANS and post-shear static SANS. Each data set in (a) and (b) were offset by powers of 6 for improved visibility.

Figure 6.5: Fluorophore labelling and exchange of labelled liposomes. (a) Schematics for VFD NBD-PE liposomes and VFD Rh-PE liposomes and mixed fluorophore labelled liposomes processed through VFD at given conditions of 5000 rpm, 0.1% of fluorophore dye, confined mode, 1 mL of solution at 45° in 20 mm VFD tube. (b) Atomic Force Microscopy (AFM) images and height distribution profile for VFD processed fluorophore labelled liposomes and mixed fluorophore VFD liposomes. (c) DLS size distribution for VFD NBD-PE liposomes and VFD Rh-PE labelled liposomes and mixed fluorophore

VFD liposomes. (d) Fluorescence spectrum for the VFD NBD-PE liposomes, (e) VFD Rh-PE fluorophore labelled liposomes and (f) VFD mixed liposomes.

Figure 7.1: Application of VFD in drug delivery technology. 1) TEM images of the protein carrier ferritin. 2) photograph of the VFD with the heating unit assembled. 3) protein recovery rate for the VFD at different speeds and water bath system. Loading efficiency of the drug in the protein at different speeds and the water bath system.

List of Tables

Table 1.1 Different structure of Microfluidic Devices.

Table 1.2. Microfluidic devices result in improvements compared to conventional processing methods, especially associated with processing of emulsification and downstream processing of food safety control.

Table 4.1. Sphere radius and polydispersity during and after VFD treatment at each speed for 10 wt% of Tween 20 by itself and 10 wt% of Tween 20 with 10 wt% of fish-oil at ratio 1:1.

Table 6.1. SANS fitting results for the real-time VFD-SANS data at increasing VFD speeds.

Table 6.2. SANS fitting results to the post-shear data sets.

Abbreviation List of Chemicals and Symbols

AFM	Atomic Force Microscopy
BET	Brunauer, Emmett, and Teller Analysis
D ₂ O	Deuterium Dioxide
DLS	Dynamic Light Scattering
DNA	Deoxyribonucleic Acid
DTPA	Diethylenetriamine pentaacetic acid
EDAX	Energy-Dispersive 360 X-ray Spectroscopy
K _B	Boltzman constant
MALDI	Matrix-Assisted Laser Desorption/Ionization
NBD-PE	1-oleoyl-2-hydroxy-sn-glycero-3-phosphoethanolamine-N- [tetra (ethylene-glycol)]-N'-(7-nitro-2-1,3benzoxadiazol-4-yl) (ammonium salt)
PEG	Poly-Ethylene Glycol
POPC	1-palmitoyl-2-oleoyl-sn-glycerol-3-phosphocholine
Rh-PE	1,2-dipalmitoyl-sn-glycero-3-phosphoethanolamine-N-(lissamine rhodamine B sulfonyl) (ammonium salt)
SANS	Small-Angle Neutron Scattering
SEM	Scanning Electron Microscopy
SLB	Supported Lipid Bilayer
TEM	Transmission Electron Microscopy
VFD	Vortex Fluidic Device

Chapter 1. Introduction and Research Aims

This chapter serves as the cornerstone for the research program that is undertaken for this thesis. Different areas of science and its applications are introduced and a detailed literature review is conducted. This chapter is divided into four major subclasses which incorporate current trends of processing offered in the soft matter areas to different microfluidic technologies which are utilized for food processing applications. A detailed background and review on the novel applications delivered from the newly developed microfluidic platform of the Vortex Fluidic Device (VFD) is provided. The ability to manipulate different areas of processing in different areas of science in terms of their size and morphology is presented. A detailed research program and overall aims of this thesis are presented at the end of the chapter.

1.1 Review on the Fundamentals of the Soft-Matter Sciences.

The section provides an overview on the nature and properties of the soft matter. After this introduction, the focus turns to the different areas of research that are encompassed under the definition of soft-matter umbrella. Furthermore, different characterization and experimental techniques are discussed which are widely utilized in the area of soft matter. The development and highlights in the soft matter areas will be presented.

1.1.1 What is Soft Matter?

Soft matter science is a study of area of materials which are physically “soft”. These materials possessing properties of soft matter can range from different types of materials from polymer solutions to liquid like colloidal solutions. A more precise definition is provided from the Nobel Laureate Pierre-Gilles de Gennes, who was awarded “Nobel Prize in Physics in 1991”, characterized soft-matter particles that give a “large response to small perturbations under an external stimulus such as mechanical forces, electric or magnetic

fields”¹. Such materials which undergo deformations under external stimulus can be identified as “soft matter” materials¹. There are various other concepts and definitions for soft matter, one of the key underlying concepts is related to the thermal energy of the materials. The materials possess weak intermolecular interactions and possess low thermal energies than the energy possessed by a crystalline solid. At room temperature, the materials have thermal energy $K_B T$, where K_B is the Boltzmann constant ($1.38 \times 10^{-23} \text{ m}^2 \text{ kg/s}^2 \text{ K}$) and T is the temperature of the material measured in Kelvin which has the energy at approximately 26 MeV (or 4.2×10^{-21} Joules). Thus, most of the soft materials can be altered at low temperatures. Another characteristic of the soft materials includes short-range atomic arrangement compared to a crystalline solid where there are regular short and long-range arrangements are observed¹.

1.1.2 Key Components of Soft Matter

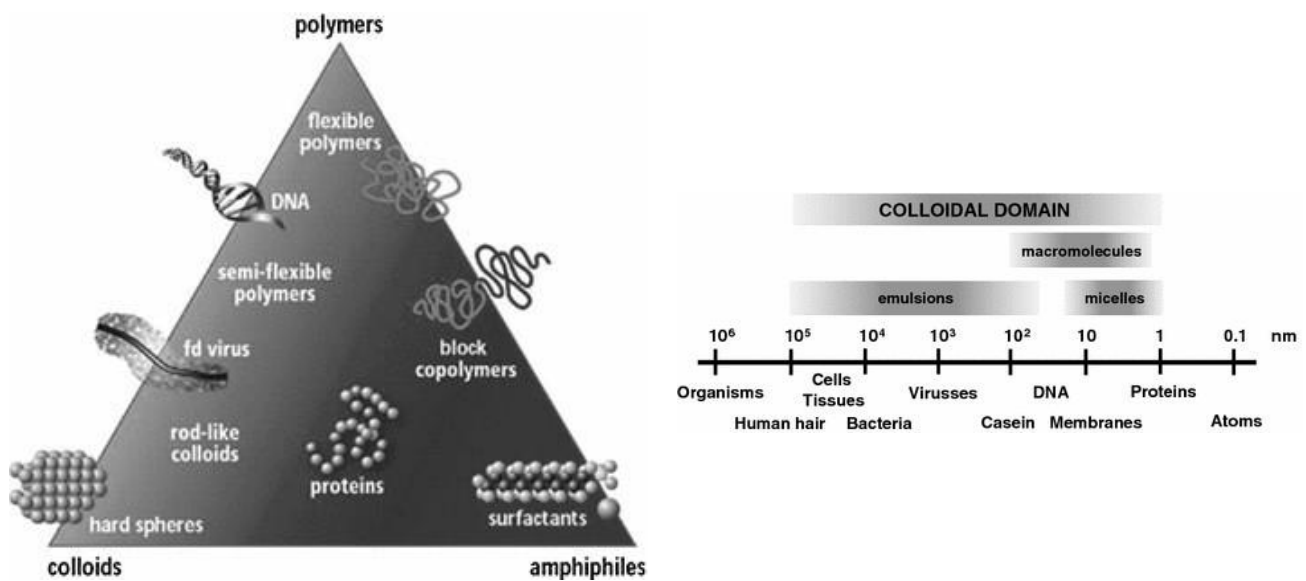


Figure 1.1: classification of soft matter materials. (left) The soft matter triangle which was originally proposed by Gomper, Dhont and Richter³ indicates the multi dimensions of molecules and materials. The gradients depict the amphiphilicity and elongation/flexibility of the materials. (right) A colloidal length scale mapping different soft-matter particles².

Soft matter or soft particles are divided into a plethora of building block components. These particles typically range from 1 – 1000 nm often referred to as nanoparticles. The different classification includes polymers, surfactants such as phospholipids, proteins, colloids which includes silica spheres and virus capsids. Various biological self-assembly is also a building block of soft matter. An example built from scaffolds of soft matter is of a globular enzyme which keeps its tertiary structure intact in its native state, but which quickly unfolds and denatures in the presence of urea². DNA nanotechnology is another example, as material built from the scaffolds of soft materials. In the 1980's, Seeman and co-workers introduced this biological self-assembly, where the weak intermolecular interactions were manipulated and a desired self-assembly of rigid nanostructures such as cubes and octahedrals were obtained^{4,5}.

Another such example of soft matter sciences is to control the wetting properties, colloidal instability and viscoelastic properties. These properties have led to excellent formulations in the personal care industry where foams, detergents and colloidal formulations have maintained their soft matter perspective ⁶. Various other areas are discussed in detailed in the following sections. These areas were explored and the research is an integral part of this thesis.

1.1.3 A Soft Matter Perspective in Liposomal and Drug Delivery Technology.

Liposomes are soft phospholipid bilayer membranes which are enclosed in a spherical structure with an aqueous core in the center. Due to their malleable and highly versatile properties these liposomes are often used to deliver drugs and nutrients across cell membranes. Phospholipid membranes have a flexible and dynamic nature which allows a lot of study into their deformation and viscoelastic behavior. Fasciolo et.al reported ⁷ the membrane elasticity behavior by squeezing a micropipette across a liposome whose diameter is larger than that of pipette. These fluid-like properties determine the membrane behavior and elasticity and determines the fate of liposomes in the body when utilized as a drug delivery vehicle ⁷.

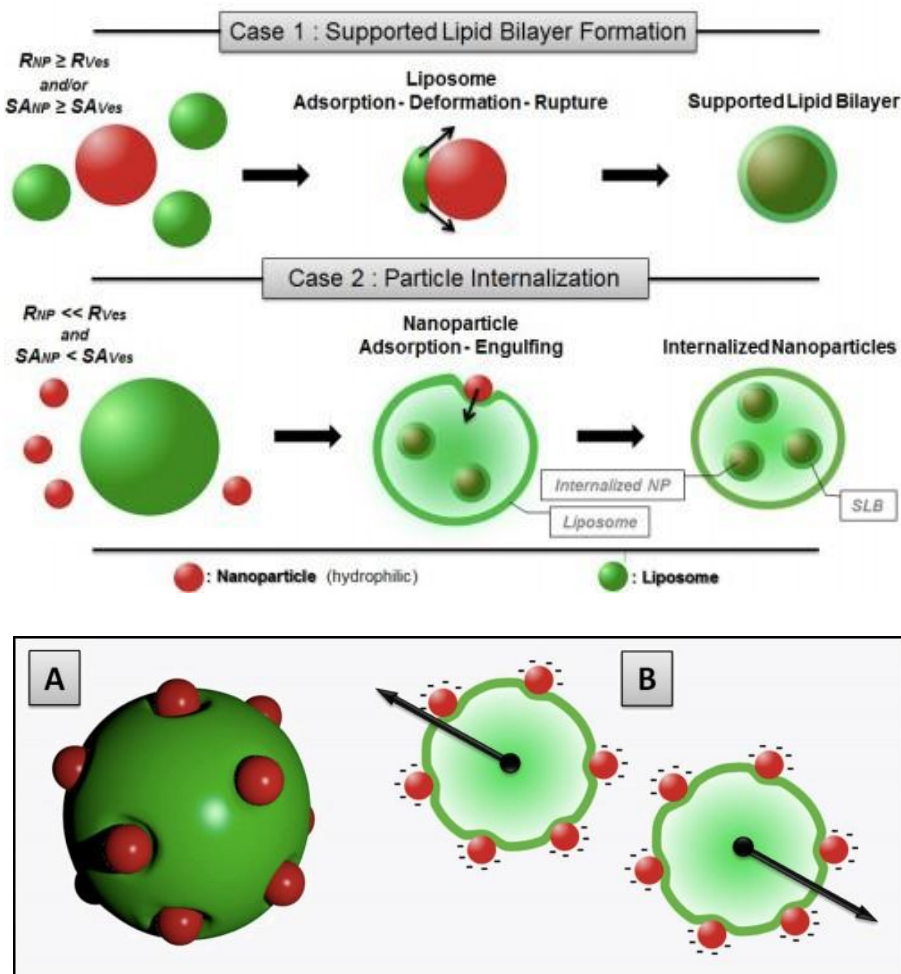


Figure 1.2: Soft matter perspective on nanoparticles induced stability to liposomes. (Top) A schematic approach towards supported lipid bilayer formation on nanoparticles where the radius of the nanoparticle is greater than the liposomes. (Bottom) A schematic approach on nanoparticle internalization where the particle size is smaller than the liposome ⁸.

Michel et.al ⁸ reported interactions of colloidal particles on the liposome formation and membrane stability. The study investigated into Supported Lipid Bilayer (SLB) & particle internalization. In the vicinity of silica Np's where the radius is less than the radius of vesicles, the vesicles form a SLB on the surface of silica Np's and there after it invaginates and engulfs the nanoparticles. This process is similar to cellular uptake in living organisms ⁸. Similarly, in another case, not all the nanoparticles are engulfed inside the liposomes, the kinetic energy of the engulfing process is slowed down when the radius of the nanoparticle reaches a critical value.

Hydrophilic nanoparticles adhere to the surface of the vesicles due to attraction between the nanoparticle and the membrane surface. Thus, there is partial wrapping of the nanoparticles and they are decorated on the surface⁸. Due to this phenomenon, there is electrostatic repulsion between the liposomes and an overall colloidal stability is achieved.

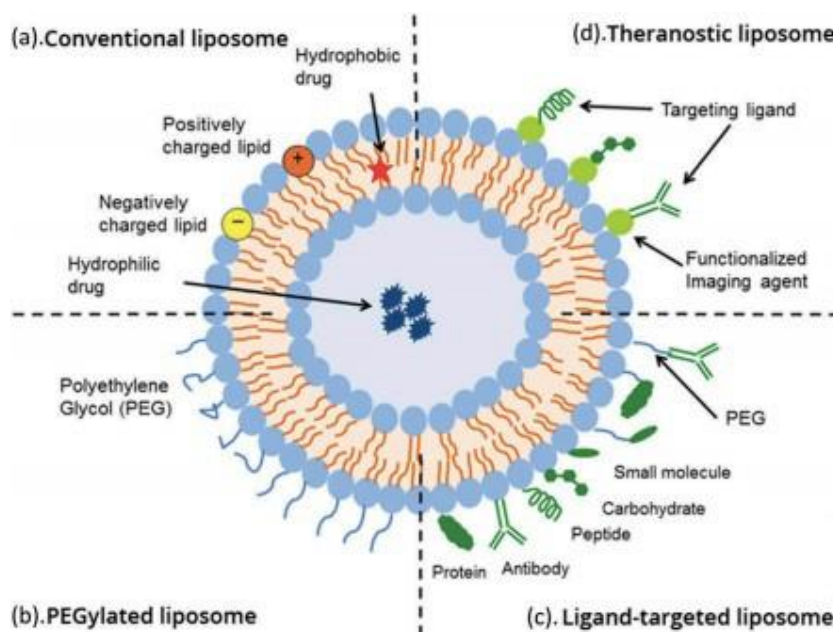


Figure 1.3: Schematic structure of different types of liposomes for multiple functions. Liposomes can be used for carrying different active agents by manipulating their aqueous core region or outer bilayers based on the functions such as Conventional, PEGylated, Ligand targeted or Theranostic liposomes¹².

The unique structure of liposomes allows the encapsulation of different active agents such as hydrophilic substances in the hydrophilic core and hydrophobic substances in the hydrophobic lamellar region. These liposomes also have an excellent renal clearance property and doesn't accumulate in a specific region⁹. Estelrich et.al¹² reported multiple advantages of liposomes as a Magnetic Resonance Imaging (MRI) contrast agents. Due to the toxic properties and high concentration requirements for the element Gadolinium (Gd) in therapeutic applications, these Gd are encapsulated in liposomes and used as Gd-based paramagnetic carriers or by introducing Fe- based superparamagnetic carriers¹⁰ for radionuclide imaging applications. Due to the latent toxicity of the free Gd-chelate, the encapsulated Gd-chelate are often required in higher concentration and high volume in order to receive good signal as a contrast agent

during MRI imaging. Different polymers are introduced to provide stability to the suspension, with polyethylene glycol (PEG) is often introduced as a linker in the amphiphilic chains of the liposomes also known as Stealth Liposomes ¹¹. Diethylene-triamine-pentaacetic acid (DTPA) labelled with ⁶⁴Cu, ¹¹¹In, ⁹⁹mTc are an excellent examples of radionuclide imaging agents with a better blood circulation time and 90 % labelling efficiency ¹².

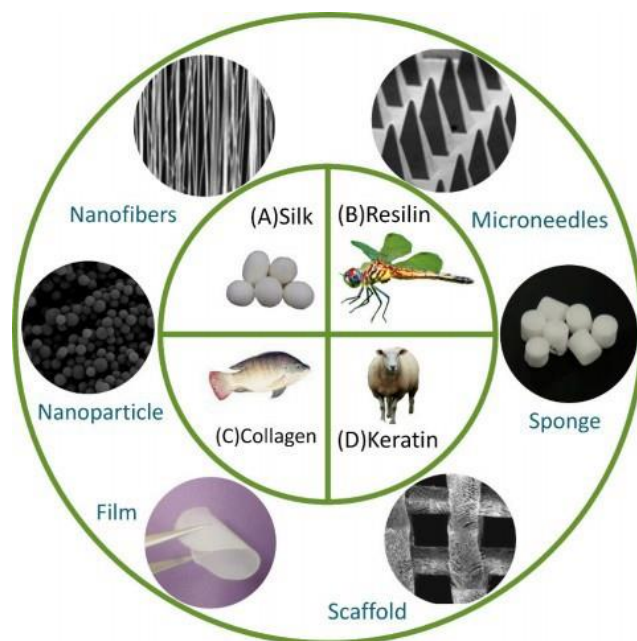


Figure 1.4: Different protein based nano-carriers for drug-delivery technology. Nanofibers, Nanoparticles, films, sponges, microneedles processed from naturally occurring proteins such as Silk, Resilin, Keratin and Collagen ¹⁵.

Another rapidly progressing area in soft matter science is protein-based drug delivery technology. Liposomes have been an area of interest for a number of years as a potential candidate for drug carriers, most recently advancing into different colloidal materials ¹³, nanoparticles ¹⁴ and protein and peptides self-assembly based carriers ¹⁵. Protein based nano-carriers are biocompatible, biodegradable and interactions can be site specific to the target site. Various natural proteins under research include silk, collagen and keratin which process nano-fibers, nanoparticles, gels and sponges for an active drug delivery response.

Collagen is widely used in skin and nasal delivery formulations due its excellent bio-compatible properties. Sun-hee cho et al. ¹⁶ reported collagen-based photothermal modulated drug delivery hydrogels. Their hydrogels reported to be theranostic platform for various molecular imaging probes ¹⁶. Different molecular weights of the proteins have effects on the drug-release rate. Pritchard et.al. ¹⁷ reported that silk fibroin fibers drug release can be controlled through their degumming times, better the degumming time better is the release profile ¹⁷. Various other proteins are also served as an excellent candidate one such example is of Ferritin protein which is gaining interest in recent years as a potential drug delivery candidate. Ferritin which is responsible for the iron storage in human body is composed of 24-subunits. These units are modified and formed spherical nano-cages which are actively used as drug delivery candidate ¹⁸. Zhen et.al. ¹⁹ reported modifying ferritin nano-cages genetically and loaded them with doxorubicin anti-cancer drug for targeting overexpressing tumor protein integrin. This method increased the blood circulation time and loading efficiency increased up to 73 wt% with decreased cardiotoxicity than the free doxorubicin itself.

Thus, a variety of factors are involved while designing a suitable soft-matter based delivery approach. From colloidal soft particles to Protein-based self-assembly, all of them are a major cornerstone in today's research platforms. There are various other soft-matter approaches for drug-delivery such as microemulsions, organogels, dendrimers and solid-lipid nanoparticles which are not discussed in detail and are not relevant to the research in this thesis.

1.1.4 A Soft Matter Perspective in Food Science Technology.

Soft matter has gained prominence in the area of food technology in recent years. From controlling the structure of the food to improving the edible properties of the food, scientists have researched it from the soft matter perspective. Our day to day intake consists of variety of soft matter-based foods. One such example is of ice-cream where milk protein casein is embedded in sugar solution with fat crystals and air bubbles entrapped. Various research is carried out based on the food-structure and now we have different types of ice-cream with multiple flavors and consistencies²⁰. Yoghurt is another example where food research is carried out from soft matter perspective and nowadays different plant-based yoghurts are developed with same nutritional values as in a normal animal dairy product. All the manufactured food is available in colloidal states such as emulsions, foams, gels and dispersions. A very fundamental principle is applied here at the mesoscale to alter the properties of food texture and complexity. The interactions occurring at the mesoscale are more dominated by the entropy than the chemical moieties itself. The mesoscopic properties depend on the size, flexibility and amphiphilicity of the interparticle attraction/repulsions, hydrocolloids network and controlled array of amphiphiles in emulsions. These all properties decides the macroscopic mouth-feel of the food²¹.



Figure 1.5: Microscopic structure of ice-cream, yoghurt and cheese. The images were obtained from Confocal Scanning Laser Microscopy (CLSM) images with fluorescent dyes fats (green) and protein is (red)²².

Encapsulation of the food active agents plays a vital role from a soft matter perspective. Entrapping the active agents in a soft shell or embedded in a matrix gives the food better long life and controlled release of the agents. The encapsulates are determined by their particle sizes depending on their application. They can range from nanometers to micrometers. There are a number of advantages by encapsulating the active agents such as off-smell masking, improving the shelf-life of the products and a better handling of the products if they are in liquid form. Improving these mentioned characteristics improves the flavors and colors of the final food product for better sense of taste and smell ²³. Encapsulation also protects from the damages due to high heat, moisture and pH. Turasan et.al. ²⁴ reported an essential oil encapsulation for better storage and stability. Rosemary oil was reported to be encapsulated in the presence of maltodextrin (MD) and whey protein concentrate which were freeze-dried to microcapsules and stability was monitored for days. Another group Sultana et.al. ²⁵ reported encapsulations of probiotic bacteria in alginate starch-based gel beads and their survival in the gastrointestinal tract was reported to be improved

²⁵. Different hydrocolloids such as carrageenan, carboxymethylcellulose, alginate, pectin etc. are often found as stabilizers in our food products. These hydrocolloids act as a thickening agent in food formulations. Various acidic or flavored dairy products, yoghurts or infant formulations include stabilizers for better shelf-life and improved food texture. When two or more hydrocolloids are mixed it is known as mixing of biopolymer solutions. These interactions give rise to various intermolecular interactions and sometimes are not entropically favored. These constraints cause separation of the solution and are incompatible to each other ²⁶. Such biopolymers are often interacted with the food matrix and the food texture is altered. Protein and polysaccharide interactions form a strong amphiphile conjugate which is adsorbed at the emulsions interfaces and provide colloidal stability. These type of interactions give rise to various aggregates and produce a gelling behavior

²⁷.

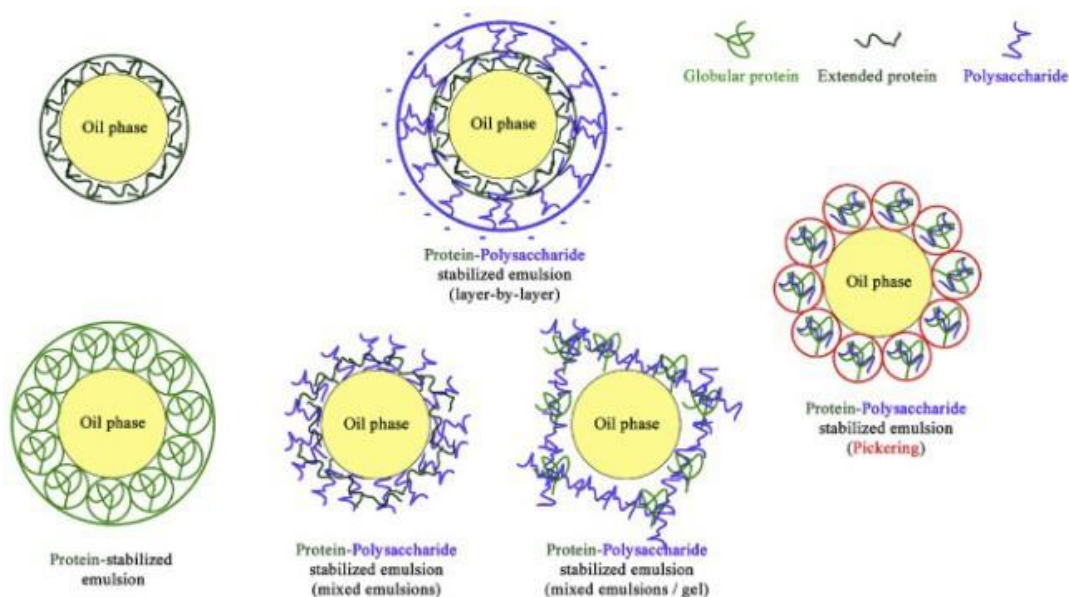


Figure 1.6: Schematic representation of protein-polysaccharide stabilization of oil droplets in oil-water emulsions. These types of interactions can lead to several gel networks where the extended protein can be in random coil or partially folded state ²⁷.

Baeza et.al.²⁸ reported K-carrageenan protein interaction in presence of lactoglobulin protein and denatured soy protein isolates which caused increase in the gelation temperatures and storage moduli than the single k-gel itself. These additions of proteins increased the gel hardness, cohesiveness, gumminess and springiness. These altered properties can be applied in designing new food formulations ²⁸. Another group peanparkdee et.al.²⁹ reported encapsulation of mulberry extract flavonoids in a complex coacervates which are typically small liquid droplets of two immiscible phases formed due to protein and polysaccharide interactions. Based on the interactions they produced high quality microcapsules ²⁹.

Thus, we can see the food technology is based on amalgamation of soft matter concepts. Altering the structure, taste and other properties depends on a number of these concepts. In recent years the focus is shifting from macroscopic properties such as viscosity, turbidity, interfacial tension to various length scales in bulk interfaces, structure, dynamics and kinetics.

These studies link the physico-chemical properties and also allow replacement of animal proteins by plant proteins². The next section of thesis discusses the underlying processes involved for production of these materials. Also, a detailed discussion on how new technologies such as microfluidics are becoming a paradigm in soft matter area for a benign future.

1.2 Applications of Microfluidic Technology in Liposomal and Drug Delivery Processing.

Phospholipids are the building block components of liposomes and are ubiquitous in Nature. In water, these amphiphilic molecules tend to organize into a vesicular structure due to maximizing hydrophobic interactions and to entropically minimizing free energy. Fabricating liposomes with a target size between 50 nm to 200 nm is important for drug delivery applications through enhanced cellular uptake, but processing these liposomes for medical and industrial applications is challenging³⁰. The primary goal for approving liposomal formulations was to alter the therapeutic index, reducing the toxicity of the parent drug, improving the bio-distribution, rendering the formulation non-toxic and weakly immunogenic, optimizing the residence clearance times of drugs from the body, and also providing enhanced permeability rates of the drug (EPR). The very first liposomal pharmaceutical product approved by the Food and Drug administration (FDA) was Doxil, introduced in 1995, which is a chemotherapy drug known as doxorubicin encapsulated into PEGylated liposomes for Kaposi's Sarcoma, ovarian and breast cancer treatments³³. Depending on the type of phospholipids, the liposomes can be cationic, anionic or neutral at physiological pH, with surface charge playing an important role on the stability of the liposome, both in formulation and in serum. Incorporation of other lipophilic compounds such as cholesterol reduces the fluidity within the liposomal bilayers and also induces premature drug leakage from the liposomes. Thus, introducing polymer conjugated on the surface of liposomes provides enhanced stability through improved steric repulsion and also prevents aggregation and subsequent endocytosis by the phagocytes. Apart from drug-delivery application, liposomes are widely exploited in the field of nutraceuticals and cosmetics where the term "natural", "organic" or "no added preservatives" are the driving force for the consumer market. The active ingredient is encapsulated within the liposome and a controlled release system is obtained through them at the target site^{34,35,36}. The primary aim behind targeting liposomes is associated with better therapeutic outcome of anti-cancer drugs, and drugs in general, in animal tumor

models compared to non-targeted liposomes, preventing premature drug leakage at the healthy tissue sites, and thus providing a controlled release system at the targeted site. Fabricating such liposomes for uptake of drug molecules, for example, involves multi-step procedures including dispersing the hydrophobic/hydrophilic drug dissolved into a suitable solvent to then prepare multi-lamellar vesicles (MLV) using the lipid thin film hydration technique and formation of Large Unilamellar Vesicles (LUVs) through rapid freeze and thawing, followed by repetitive extrusion through polycarbonate filters ³¹. Various improvements have been made in the field of microfluidics to reduce this multistep processing. Microfluidic methods such as electro formation & hydration, extrusion, pulse jetting, double emulsion templating, ice droplet hydration, transient membrane injection, droplet emulsion transfer and hydrodynamic focusing ^{30,31,32} have been used to fabricate liposomes with control over size and polydispersity compared to traditional batch-processes ³². Droplet based microfluidics is an important sub category of microfluidic devices which is widely utilized in fabrication, encapsulation, sorting and cell analysis ^{37,38,39}.

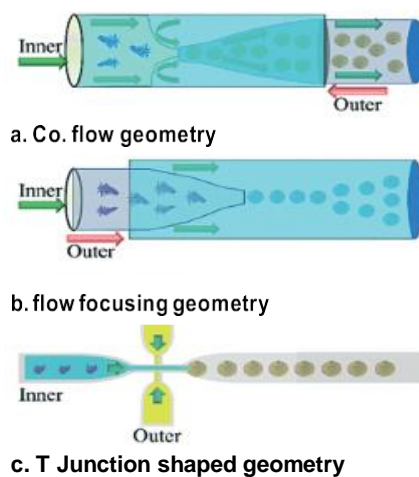


Figure 1.7: Device geometries for droplet-based microfluidics. Different types of drug delivery systems 1, 11, 111 are prepared through co-flow, flow focusing and T-junction geometries ⁴⁰.

In droplet-based microfluidics two immiscible phases are manipulated and generated into different droplet sizes through jetting or dripping regime. The droplet phase is called dispersed phase and medium

phase is known as continuous phase. Based on the droplet microfluidics there are three different geometries available such as co-flow, flow focusing and T-junction. These geometries depend on the shape of the junction which helps to define two immiscible flows and controls the final fabrication of the drug delivery systems⁴⁰. Different droplet-based microfluidics geometries are discussed in the next section which are widely used to overcome the above-mentioned challenges.

1.2.1 Flow-focusing and Co-flow droplet-based microfluidics for controlled size of liposomal and drug delivery systems.

In this type of flow focused geometry, the dispersed and continuous phase flows through two sides of the channel and meets before the orifice of the inner capillary and starts the formation of droplets at the orifice (Fig 1.7 b). Both dripping and jetting regime can be applied in this type of microfluidic geometry⁴⁰. The co-flow geometry setup is defined where the dispersed phase is in the inner capillary and it flows through the orifice of a defined dimension into continuous flow from the outer capillary both in same direction (Fig 1.7 a). This type of flow is typically produced due to Rayleigh-plateau instability and thus jetting regime is often involved⁴⁰. Single emulsions, such as Oil/Water (O/W) or Water/Oil (W/O) and double emulsions such as Oil/Water/Oil (O/W/O) or Water/Oil/Water (W/O/W) can be fabricated. Biocompatible polymers such as poly (lactic-co-glycolic acid) PLGA and hydroxypropyl methylcellulose acetate succinate (HPMCAS) can be fabricated with uniform size and distribution while carrying the drug at the same time⁴¹. Shum et.al.⁴² reported a flow focusing setup for the fabrication of liposomes from a double emulsion template. Here the phospholipid was dissolved in a volatile solvent and the model drug is an aqueous solution which forms the inner phase of the system. Once the droplets are formed at the orifice of the capillary the volatile solvent is evaporated and the phospholipids concentrate and forms bilayers⁴². Typically, in O/W emulsions the polymers which are used as a wall material can be evaporated from the solvent or can diffuse out from the droplets. The concentration of the polymers is a crucial step while deciding the setup due to the size of the droplets. The size of the final particles can be controlled by the droplet size and how much the final droplet shrinks. Polymers such as PLGA are

challenging when it comes to emulsification and drug loading. With microfluidic set ups, this can be achieved through rapid mixing and better dissolution of the polymer matrix ⁴⁰.

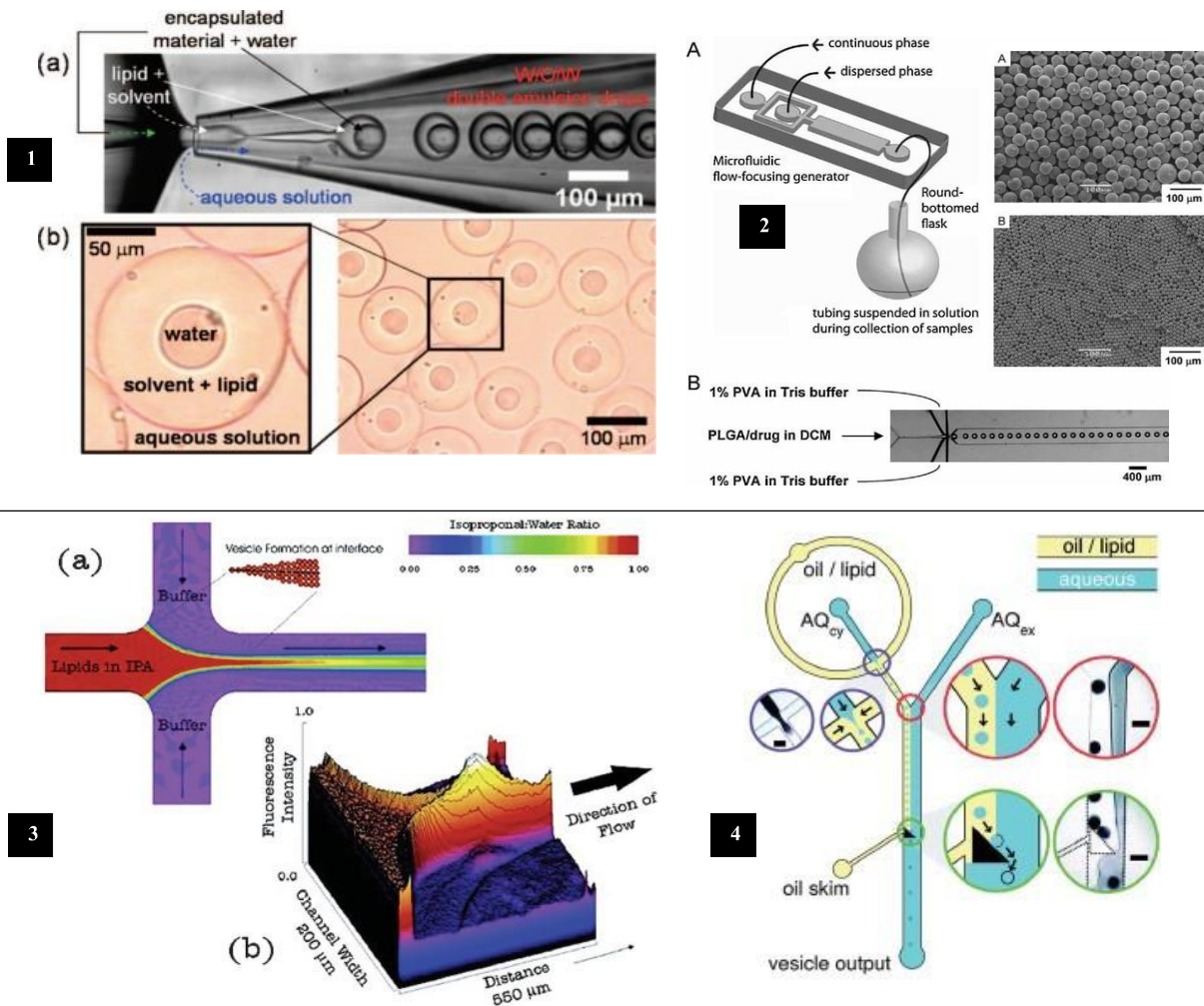


Figure 1.8: Flow focusing droplet based microfluidic geometry. (left) Formation of liposomes from a double emulsion template⁴². (Right) formation of PLGA micro particles with a model drug through flow focused microfluidic setup⁴³.

Another group Xu et.al.⁴³ reported similar microfluidic flow focusing setup for formation of PLGA micro particles. This group reports fabricating uniform size distribution of PLGA micro particles ranging from 10 μm to 50 μm. A model amphiphilic drug (Bupivacaine) was incorporated and the kinetic studies revealed that drug release is slower than most conventional methods. Thus, the homogenous fabrication of micro particles delivered drug release with lower initial burst is achieved through this flow focusing setup.

Jahn et.al. ⁴⁴ proposed another method based on the flow focused setup. Here the lipid solution is suspended in an Isopropyl Alcohol (IPA) solution which is passed throughout the center flow while it is being intersected by aqueous buffer solutions on the sides. As the alcohol solution gets diluted and passes the critical concentration the lipids spontaneously self-assemble into liposomes. The size distribution for liposomes is from 50-150 nm which is dependent on the flow-rates. Large or micron size vesicles are not formed through this method ⁴⁴. Matosevic et.al. ⁴⁵ proposed another method which includes emulsion transfer method integrated on a microfluidic device. In his work water in oil droplets were formed by focusing a stream of water in oil which was stabilized by lipid at a microfluidic junction and then forced across an oil-water interface by a ramp-shaped barrier (Fig 1.8-4). While moving from organic to aqueous phase the droplets picked up a second monolayer of lipids at the oil-water interface forms a bilayer and then into liposomes. This method often caused disruption of droplets and the efficiency drops to 83% ⁴⁵. Giant unilamellar vesicles are formed through this proposed method. Often single emulsions are prepared easily with a flow focusing setup, However, in certain double emulsions or drug delivery systems processing the flow focused and co-flow it is combined T-junction setups for a better loading of multiple active drugs in the carriers that are fabricated simultaneously. A number of such setups along with a combination approach using T-junctions are discussed in the next section.

1.2.2 T-junction droplet-based microfluidics for controlled size of liposomal and drug delivery systems.

T-junction microfluidic systems consist of micro-channels where the dispersed phase is separated by an immiscible continuous liquid phase. Factors such as interfacial tension, viscosity and shearing pressure drop affects this type of microfluidic systems ⁴⁶. In this type of microfluidic devices, the continuous phase flows through the main straight channel while the dispersed phase flows through side channels and enters the main channel by forming a cross flow. This affords a monodisperse droplets for homogenous fabrication ⁴⁰. Janus particles are unique type of particles which can be fabricated through this setup. Janus particles consists of two or more distinct materials on their surfaces for example one part is hydrophobic and another is hydrophilic part. Such type of particles can be formed through this geometry when combined with flow focusing geometry, nanoparticles can be aggregated on one side of geometry and Janus particles are formed after the droplet takes place from flow focused from the other side (Fig 1.9-1) ⁴⁰.

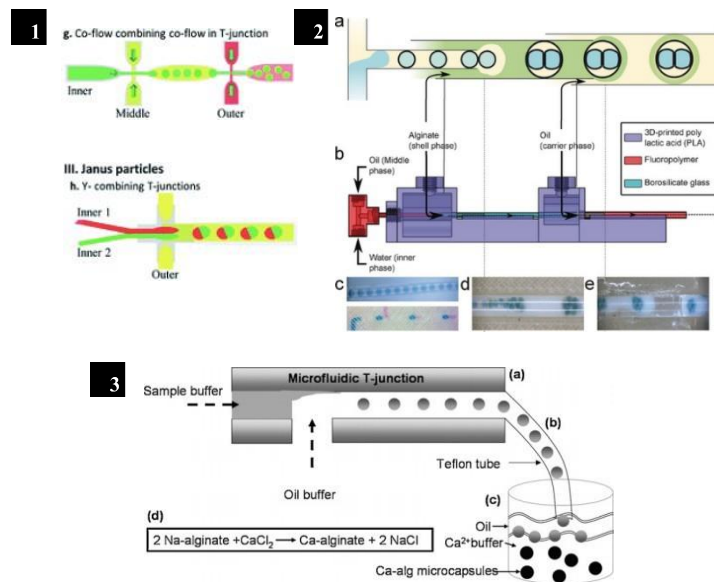


Figure 1.9: Applications of T-shaped geometry in droplet based microfluidic systems. (1) T-junction combining co-flow and Y-junction for fabricating Janus particles ⁴⁰. (2) formation of droplet interface bilayers (DIBs) via T-junction and co-axial flow geometry (a) T-junction schematics (b) side view of the microfluidic platform, (c) and (d) aqueous droplets in oil phase with continuous alginate flow. (e) a

*continuous alginate flow encapsulates the constructs in alginate shell*⁴⁷. (3) *schematic representation of T-junction microfluidic platform for fabricating ca-alginate microcapsules*⁴⁸.

Baxani et.al.⁴⁷ demonstrated a method for fabricating droplet interface bilayers (DIBs) through their combined geometry of T-junction and co-axial flow (Fig 1.9-2). Due to stability issues for DIBs the group reports a fabrication of multiphase hierarchy with the help of microfluidic platform and construct a hydrogel shell outside for the stability and support of the DIBs. The DIBs are stable in air, water and oil. Such novel smart materials are fabricated with the aid of combining different geometry microfluidic devices⁴⁷. Another group yeh et.al.⁴⁸ reports fabrication of calcium and alginate microcapsules by utilizing T-junction microfluidic platform. Ca-Ag microspheres are widely utilized *in-vivo* for targeted drug delivery and immobilization of enzymes and proteins. They are often restricted for applications due to their size influences the clearance rate. Herein, the group reports fabricating monodispersed ca-ag microspheres with controlled size. A simple W/O emulsion was produced from the biopolymer sodium alginate in oil-phase which was then collected into a bath of calcium ions to form microspheres. These microspheres were further utilized to encapsulate silver and gold nanoparticles⁴⁸.

Microfluidics deliver a plethora of applications, but still some questions are always unexplored. Despite this control over size and polydispersity, processing these carriers for medical, industrial and bulk processing while addressing scalability still remains a challenge. There is also no broad comparison of microfluidic devices with conventional methods. When it comes to liposomes there is lipid concentration administered is somewhere between 0.1 mM to 2.0 mM while the already suspended formulations administered clinically is from 5mM – 25mM. Thus, through microfluidics typically a low concentration liposome is fabricated⁴⁹. Also, very few studies have been carried out to demonstrate the encapsulation efficiency and release profile fabricated from such devices⁴⁹.

In the next few sections we discuss the microfluidics application utilized in food processing technology also with a new paradigm in microfluidic platforms known as The Vortex Fluidic Device (VFD). There are number of applications in materials, chemicals, biomaterials and food processing which are discussed in detail in coming sections.

1.3 Application of Microfluidic Technology in Food Processing.

(This section of the review is published)

Nikita Joseph^{2, ^}, Shan He^{1,2^*}, Shilun Feng^{3^}, Matt Jellicoe², Colin L. Raston^{2, *}

1 Department of Food Science, School of Chemistry and Chemical Engineering, Guangzhou University, Guangzhou, Guangdong, 510006, China.

2 Flinders Institute for Nanoscale Science and Technology, College of Science and Engineering, Flinders University, Bedford Park, South Australia, 5042, Australia

3 School of Electrical and Electronic Engineering, Nanyang Technological University, 639798, Singapore.

[^] These Authors Contributed Equally to This Work

Author Contributions

NJ, SH contributed towards the writing of VFD and introduction part and SF wrote the microfluidics section in the original Manuscript. MJ made the schematics for the VFD. C.L.R Supervised the Project.

Abstract

Microfluidic technology is interdisciplinary with a diversity of applications including in food processing. the rapidly growing global population demands more advanced technologies in food processing to produce more functional and safer food, and for such processing microfluidic devices are a popular choice. This review critically critiques the state-of-the-art designs of microfluidic devices and their applications in food processing, and identifies the key research trends and future research directions for maximizing the value of microfluidic technology. capillary, planar, and terrace droplet generation systems are currently used in the design of microfluidic devices, each with their strengths and weaknesses as applied in food processing, for emulsification, food safety measurements, and bioactive compound

extraction. conventional channel-based microfluidic devices are prone to clogging, and have high labor costs and low productivity, and their “directional pressure” restricts scaling-up capabilities. These disadvantages can be overcome by using “inside-out centrifugal force” and the new generation continuous flow thin-film microfluidic vortex fluidic device (VFD) which facilitates translating laboratory processing into commercial products. also highlighted is controlling protein-polysaccharide interactions and the applications of the produced ingredients in food formulations as targets for future development in the field.

1.3.1. Introduction

Microfluidics is defined as a system that processes and manipulates small amounts of fluid, up to 10^{-6} to 10^{-9} L (Fig 1) ⁵⁰. Microfluidic technology is interdisciplinary covering physics, chemistry, engineering, biotechnology, and other fields. The dimensions of the devices ranging from micrometers to a few millimeters ⁵¹. The strengths of microfluidic devices come from two of their properties, namely the reduced particle size generated and the laminar flow characteristics of fluids. These devices offer several advantages, including low fabrication costs, rapid processing, and the reuse of molds ⁵². As such they help to ameliorate important scientific problems that are difficult to resolve by applying conventional technologies. Moreover, compared with conventional fluidic systems, microfluidic devices are cheap to fabricate, using less chemical reagent as well as offering improved analytical performance, chemical reactivity, and biocompatibility. These advantages greatly contribute to the development of sustainable technologies with reduced financial burden ⁵³. Applications of microfluidic devices emerged at the beginning of the 1990s, and encompass blood rheology ⁵⁴ and chemical analyses ⁵⁵. Subsequently, applications have expanded into capillary electrophoresis ⁵⁶, flow cytometry ⁵⁷, multiple component reactions ⁵⁸, bio-sensors ⁵⁹, genetic analyses ⁶⁰, and drug screening ⁶¹. The overall market value for microfluidics related products has an expected annual growth rate of 15.5% and reached USD 13.5 billion in 2019, and it is predicted to be over USD 44 billion in 2025 ⁶².

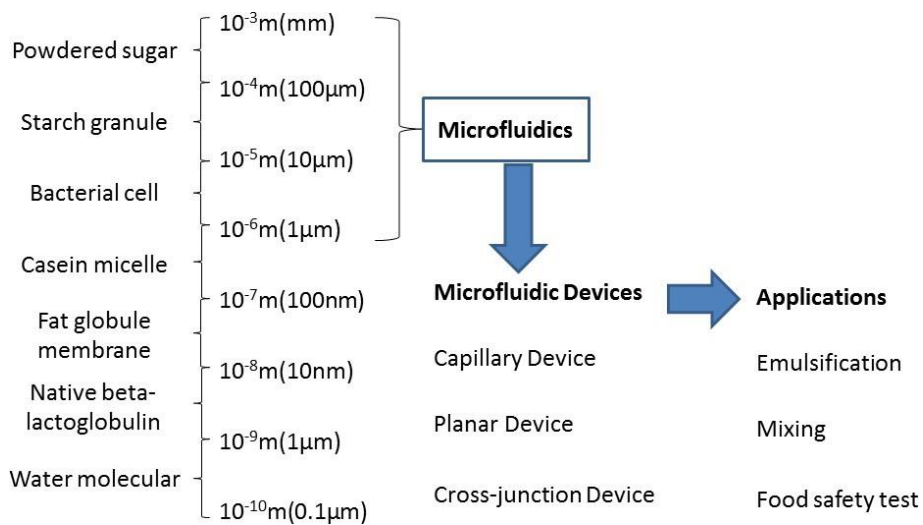


Figure 1.10: Length scale for microfluidics. Range of the length scale of material involved in microfluidics, microfluidic devices, and microfluidic applications. (Images are reprinted from “Applications of Microfluidic devices in food engineering”, *Food Biophys.*, 2008, 3, 1–15 with permission from Springer)

With the rapidly growing global population, there is an increasing demand for the development of more advanced technologies in food processing to provide safer and more functional food. Among these new food processing technologies, microfluidic technology has received considerable attention in recent times and is rapidly growing, as evidenced by the number of relevant publications and patents in the field. Food emulsification using microfluidic techniques is reproducible with highly controllable operational conditions⁶³. Relative to conventional emulsification techniques, such as homogenization and high-pressure homogenization⁶⁴, microfluidic techniques have faster reactions, are smaller in size and have greater control of the defined interface between two phases due to lower power dissipation, and have strictly laminar flow⁶⁵. Applications of microfluidic technology in food processing have been extended to other fields. For example, in food safety measurements, the current industry practice of using 1.0 mg/L free chlorine requires more than 1.0 s total contact to achieve a reduction in an E.coli population, whereas by using a microfluidic device, 10.0 $\mu\text{g/L}$ free chlorine solution is effective for a reduction in as little as

0.25 s⁶⁶. In bio-compound detection, a newly developed microfluidic flow injection analyzer allows determining the total polyphenols in white wine with the relative errors reduced by more than 13% in comparison with the conventional flow-injection analysis method⁶⁷. Microfluidic chips are also efficient tools in the extraction of bioactive compounds from plant-based products using a solvent, for example, the extraction of strychnine⁶⁸. T-junction style microfluidic devices are effective in the production of microporous calcium alginate gels by incorporating monodisperse air bubbles 177 μ m in diameter. This increases the volume to energy content ratio of the product with improved homogeneity of the material⁶⁹. However, while broad applications of microfluidic technology in food processing have been developed, a comprehensive treatise of the field in a review is wanting. Several existing reviews on food safety control and emulsification using microfluidics^{70, 71} provide the overarching achievements of previous studies in the field.

However, since these reviews there have been significant advances in microfluidic systems in food processing, based on thin film microfluidics rather than conventional micro-channel-based systems. Accordingly, we have reviewed the existing research and applications of microfluidic systems that are relevant to food processing. This includes discussion on the limitations and future perspectives at a time of an emerging need for food research and product development, and the development of the vortex fluidic device.

1.3.2 Microfluidic devices

Researchers have investigated microfluidic devices according to different methods of droplet generation (Table 1) which fall under three major categories, namely capillaries, planar, and terrace systems. Microfluidic devices with various functions have been comprehensively explored. The droplet generation mode is the foundation for the design of these devices, and is vital for the subsequent functionality of the material. Consequently, microfluidic devices have been categorized herein according to different modes of droplet generation

Table 1.1 Different structure of Microfluidic Devices.

Type		Application	Ref.
Capillary microfluidic device	Co-flow	Synthesis of emulsion (oil-in-water) Synthesis of emulsion (for sensitive cells encapsulation)	Luoran, <i>et al.</i> , 2014 Seyed, <i>et al.</i> , 2015
	Flow-focus	Synthesis of emulsion (generating emulsions independent of the surface wettability)	Goran, <i>et al.</i> , 2017
Planar geometries	T-junction	Food safety control (biosensor for pathogen detection in food)	Yiming, <i>et al.</i> , 2019
		Synthesis of emulsion (monodisperse emulsion for scaling-up)	Goran, <i>et al.</i> , 2017
	Y-junction	Synthesis of emulsion (for cell encapsulation)	Seyed, <i>et al.</i> , 2015
		Component monitoring (small changes of free calcium in solution in real time)	Xuan, <i>et al.</i> , 2017
Cross-junction	Formation of microporous materials (microporous calcium alginate gel)	Kazuhiko, <i>et al.</i> , 2018	
	Food safety control (modern analytical technology for hazardous compounds in food)	Nora, <i>et al.</i> , 2017	
Terrace geometries	Cross-junction	Bioactive compound extraction (polyphenols)	Yiming, <i>et al.</i> , 2019
		Synthesis of emulsion (for the high-throughput production of colloidal monodisperse droplets)	Goran, <i>et al.</i> , 2016
	T-junction	Synthesis of emulsion (numerical study on microfluidic emulsification at the cross-junction, using 5 cSt silicone oil as the continuous phase and 52% glycerol/48% water mixture containing surfactants as the dispersed phase)	Goran, <i>et al.</i> , 2016
		Bioactive compound extraction (Astaxanthin)	Shinji, <i>et al.</i> , 2001
Y-junction	Food safety control (detection of benzoic acid in food)	Jiaming, <i>et al.</i> , 2018	
	Food safety control (real-time cell allergic response)	Katarina, <i>et al.</i> , 2015	

I. Capillary microfluidic device

Capillary microfluidic devices use positive pressure generated by droplets deposited at different inlets and outlets to control the speed and direction of flow, with smaller droplets generating higher positive pressures and self-flowing via a conduit into larger droplets⁷¹. In capillary microfluidic devices, droplets are formed by dripping, squeezing, or jetting regimes. Dripping and squeezing regimes occur at the tip of the junction or tube orifice. The squeezing regime happens when the interfacial tension is larger than the shear force, with the droplet growing until it blocks the cross-section of the channel; the thin film between the droplet and the walls of the channel will be filled with the continuous phase. When the pressure upstream of the droplet increases, the detachment of the droplet neck occurs⁷².

In the dripping regime, since there is still room for the continuous phase flow, the droplet will detach⁷³. The jetting regime leads to the formation of a long stream of inner fluid where the point of droplet detachment can be variable, resulting in a broader size distribution. In this regime, based on the principle of Rayleigh-Plateau instability, perturbations in the jet increase the Laplace pressure when the droplet is generated. When this pressure is high, the jet becomes so thin that it breaks the stream into droplets⁷⁴. In the dripping jetting regimes, they are assemblies of coaxial capillary microfluidic devices (Fig 1.11), with two coaxially located with different diameters. These devices are widely used for the generation of vesicles, droplets, and microparticles⁷⁵.

For single emulsions in coaxial micro-capillaries, co-flow and flow-focusing arrangements are widely used. As for the co-flow arrangement (Fig 1.11-A), two fluids move in the same direction, and the continuous phase flows between the capillaries while the dispersed phase flows in the inner smaller diameter capillary. As for the flow-focusing arrangement, at the two ends of the external capillary, two kinds of fluids will be introduced in opposite directions (Fig 1.11-B). Both phases will flow into the narrow inner capillary with an open end inside the external capillary, and the dispersed phase from one side will be constricted by the continuous phase. This breaks as droplets in the jetting or dripping regime move into the small inner capillary, depending on the operational conditions⁷⁶.

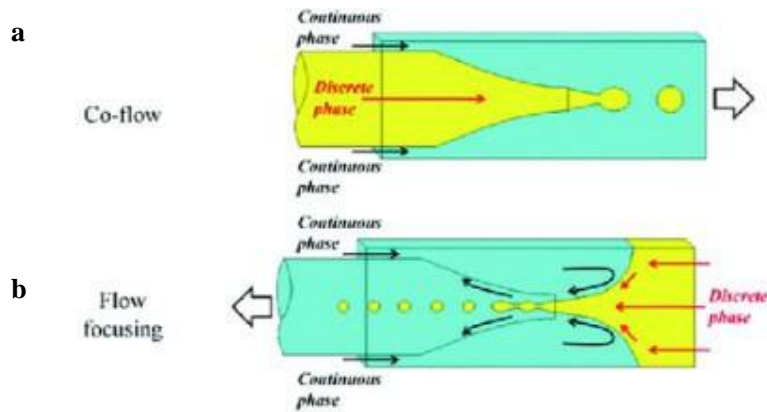


Figure 1.11: Capillary microfluidic devices. (a) A co-flow microcapillary device, and (b) a flow-focusing microcapillary devices (images are reprinted from “Controlled production of emulsions and particles by milli- and microfluidic techniques”, Engl, et al., *Curr. Opin. Colloid Interface Sci.*, 2008, 13, 206–216 with permission from ELSEVIER)

One advantage of the coaxial micro-capillaries is that the effects of the interfacial forces between the two phases can be increased with the droplets surrounded by the outer phase. However, alignment and fabrication of the tubes are two main obstacles for scale-up processing of microfluidic device using a coaxial micro-capillary⁷⁷.

II. Planar microfluidic devices

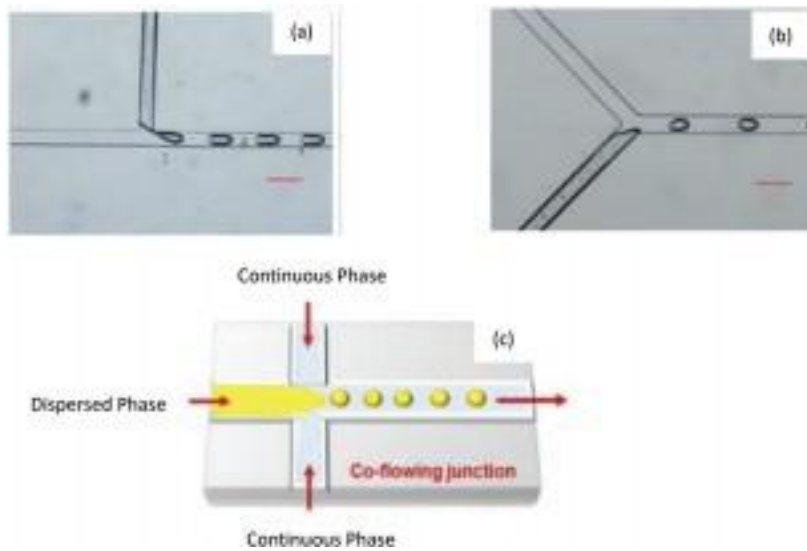


Figure 1.12: Planar geometry devices: (a) A co-flow T-junction, (b) a co-flow Y-junction, and (c) a cross-junction (images are reprinted from “Microfluidic emulsification in food processing”, Abid, et al., *J. Food Eng.*, 2015, 147, 1–7 with permission from ELSEVIER)

Planar microfluidic devices feature channels with rectangular cross-sections constructed using different materials using different techniques. Depending on the type of junction between the channels, they can be classified as T-, Y-, and cross-junctions. These are the most common types of planar devices used for droplet generation (Fig 1.12) In T-junction devices (Fig 1.12-A), fluids are pumped in two perpendicular micro-channels for generating monodisperse droplets. Capillary number (Ca) is a parameter representing the relative effect of viscous drag forces versus surface tension forces acting across an interface between two immiscible liquids. In the squeezing regime, Ca is low in value, where droplet detachment is less favorable. For this system, droplet generation occurs in two steps, initially droplet growth followed by droplet detachment⁷⁴. For a Y-junction device (Fig 1.12B), the angle between the channels is usually $> 90^\circ$, which influences droplet generation due to the shear effect imposed by the continuous phase on the dispersed phase. Unlike in a T-junction device, the droplet detachment mechanism in a Y-junction device involves a single step⁷⁸.

This simpler process results in a higher dependence on shear and interfacial forces, as well as on the operating conditions for generating the droplets. Nevertheless, processing using this geometry depends directly on the balance between the shear forces and the interfacial tension, with no droplets formed at low Ca ⁷⁹. A cross-junction microfluidic device presents four crossed perpendicular or oblique channels, where the flow of the lateral channels usually constricts the fluid flow in the main channel, as a hydrodynamic flow focusing process ⁸⁰. This geometry is the most commonly used for self- assembled structure formation, such as liposomes, due to the control over the molecular diffusion between two fluids ⁸¹. Besides, this geometry is used for droplet formation. Compared with T- or Y- junctions, cross-junction geometries have higher shear since it is imposed by a continuous phase arising from flow both sides of the dispersed phase stream. Consequentially, this configuration can lead to the formation of smaller droplets. Planar geometries are attractive in being easily designed and fabricated, with the ability to create more elaborate configurations. However, unlike capillary devices, for planar microchannel devices, fluids are confined by walls at the upper and lower surfaces of the chip, which normally require special operating conditions such as the surface treatment of the walls.

III. Terrace microfluidic devices

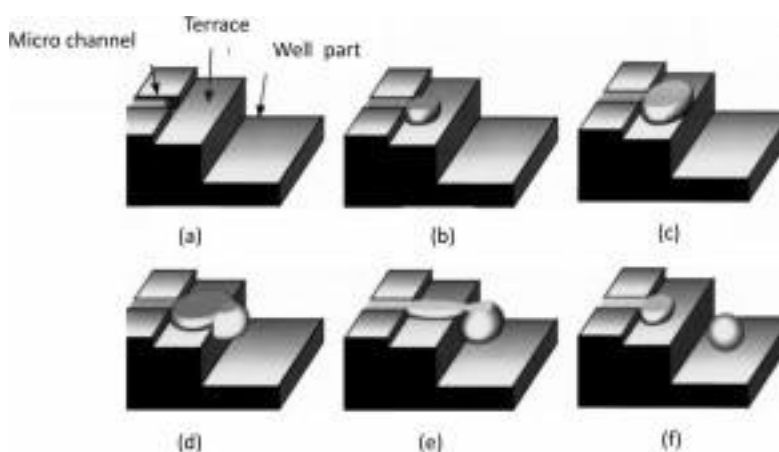


Figure 1.13: Schematic of a terrace geometry microfluidic device. (Images are reprinted from “Spontaneous droplet formation techniques for monodisperse emulsions preparation– Perspectives for food applications”, Abid, et al., *J. Food Eng.*, 2011, 107, 334–346 with permission from ELSEVIER)

For terrace microfluidic devices, droplets are generated as shown in (Fig 1.13). Firstly, the dispersed phase in a microchannel is driven to a terrace area filled with a continuous phase, which can be stagnant. Continuously, a disk-shaped droplet with a high Laplace pressure will be formed because of the shallow depth of the terrace, resulting in thermodynamically instability until the droplet reaches the edge of the terrace. The droplet then moves spontaneously to a deeper region and assumes a thermodynamically more favorable spherical shape. Diverse designs based on terrace micro-channels have been developed for improving and increasing the throughput of the droplets. For example, symmetrical straight-through microchannels⁸² with circular or rectangular cross-sections or symmetrical channels⁷⁹ with circular and rectangular sections upstream and downstream, respectively, have been developed. The terrace structures afford droplets with improved performance, independent of the properties of the phases, but dependent on the step height between phases, which has been described as step emulsification in microfluidic chips. Devices using terrace result in smooth droplet detachment, with an excellent diameter coefficient of variation (<5%), and high throughput and productivity of droplets capabilities (>100 l/h).

This becomes a potentially useful tool for industrial applications ⁸³. However, the cost of fabrication of these devices is higher than that of the fabrication of planar.

There are some recent advancements of microfluidic technology involving innovative designs. The recently developed paper-based microfluidic device can direct flow to different regions of the device through micro-channel networks without the need for external pumps used in traditional microfluidic devices ⁸⁴. With the assistance of advanced computation and sensor technologies, the newly developed digital microfluidic device is able to detect and control the velocity and viscosity of the flow in micro-channels accurately and on-time ⁸⁵. What can be considered as the most recent advancement of microfluidic technology is the 3D printed microfluidic device. 3D printing technology can be used to design and print micro-channels with specific demands ⁸⁶ and microfluidic devices with microneedle architecture in micro-channels for transdermal drug delivery. However, all these advancements are based on conventional micro-channel architecture. While research on the application of such microfluidic devices based on micro-channel architecture at a laboratory scale abound, there is a clear gap in applying and commercializing microfluidic devices, from fundamental research to complex, multi-component products produced on a large scale. A major challenge for the implementation of microfluidic devices in the industry is the need to be able to adjust the processing conditions depending on the properties of the samples. Complex samples have complex rheology that can lead to channel clogging, as well as difficulties in fluid injection and fluid stabilization. Another concern is the cost of using advanced manufacturing techniques to fabricate structures down to sub-micrometer dimensions, which may require cleanroom processing, expensive facilities, high-technology workers, and more.

1.3.3. Applications of microfluidic devices in food processing

There are extensive studies on the applications of microfluidic devices in food processing, which are summarized in the following table.

Table 1.2. Microfluidic devices result in improvements compared to conventional processing methods, especially associated with processing of emulsification and downstream processing of food safety control.

Applications		Outcomes	Ref.
Emulsion	Single emulsion	Increasing the viscosity of the continuous phase in the microfluidic channel increases the average diameter of water-in-oil droplets, but decreases for oil-in-water droplets.	Isao, <i>et al.</i> , 2008
	Double emulsion	Double emulsions of water-in-oil-in-water are prepared using an upstream hydrophobic T-junction enclosed with organic droplets formed at a downstream hydrophilic T-junction.	Takasi, <i>et al.</i> , 2005
		Double emulsions of water-in-oil-in-water and oil-in-water-in-oil emulsions were prepared by reversing the order of the hydrophobic and hydrophilic cross-junction microfluidics.	Garti, <i>et al.</i> , 1999
		Solid-in-oil-in-water pectin microcapsules were prepared using gelatin in the internal water phase and a calcium solution containing Tween 20 in the external water phase.	Goran, <i>et al.</i> , 2005
Food safety control	Micro-organisms	A microfluidic chip integrating glass beads covalently immobilized with anti- <i>E. coli</i> O157:H7 antibody was used to detect <i>E. Coli</i> O157:H7, concentration 3.2×10^1 CFU μl^{-1} to 3.2×10^5 CFU μl^{-1} within 20 min, overcoming the limitations of low surface area for antibody-pathogen binding using conventional methods.	Madhukar, <i>et al.</i> , 2007
	Heavy metals	A low-cost and simple paper-based microfluidic device integrated with fluorescence-labeled single-stranded DNA functionalized with a graphene oxide sensor, for simultaneous detecting Hg^{2+} and Ag^{2+} .	Jeong-Yeol, <i>et al.</i> , 2012
	Biogenic amines	On-chip electro-membrane extraction coupled with high-performance liquid chromatography used to monitor trace levels of biogenic amines, with comparable accuracy to that of conventional methods but requiring fewer samples.	Fereshteh, <i>et al.</i> , 2018
Bioactive compound detection and extraction	Polyphenols	The developed microchip only requires 20 s to determine the polyphenol content in white wines. This microchip is a prototype for the determination of polyphenols in other liquid food samples.	Sandoval-Ventura, <i>et al.</i> , 2017
microporous material production	Microporous calcium alginate gels	Microporous calcium alginate gels are prepared in a T-junction device incorporating monodispersed air bubbles, 177 μm in diameter, increasing the volume to energy content ratio of the product.	Joseph, <i>et al.</i> , 2019

I. Emulsification

Emulsions are dispersions common in many food products. The most simplified structures of emulsion are of two types, namely oil-in-water (e.g., salad dressings and mayonnaise) and water-in-oil (e.g., butter and margarine)⁸⁷. In addition, emulsions can be employed in functional applications, such as in vehicles for stabilizing bioactive compounds⁸⁸. Food emulsions generated using conventional methods involve inducing energy through physical means in mixing equipment, such as a homogenizer and magnetic stirrer, and then into the bulk of a two-phase mixture, leading to shearing strains that disperse one phase into another⁸⁹. However, these methods have limited control of the particle size distribution, resulting in highly poly-dispersed emulsions. Furthermore, there is a limitation in the amount of power per unit volume that can be introduced by such conventional physical means. For example, for the classical processing using a homogenizer, typically only 5% of the supplied energy is used to generate the emulsion, with the rest dissipated as heat⁷⁴. Not only is it energy-inefficient, but it can also cause denaturation of any bioactive compounds in the emulsion. Though several modifications have been made, such as high-pressure homogenization, ultrasonic homogenization and membrane homogenization⁹⁰, the energy-efficiency of homogenization is questionable. In contrast, microfluidic devices can dispense emulsions in a controlled manner, for tailoring the properties of emulsions. They not only have greater control of the size distribution of emulsified particles⁹¹, they can make emulsion processing much more energy efficient⁹². Recent investigations into manipulating emulsions with microfluidic devices have focused on two directions, the size control of emulsified droplets and producing more elaborately structured emulsions.

II. Controlling the particle size of emulsified droplets using microfluidic devices

Microfluidic devices have the potential to disperse emulsion droplets with control over their size, which is difficult to achieve using conventional emulsion processing methods. A T-junction microfluidic device has been used to control the size of emulsion droplets, from 100 to 380 nm, by adjusting the velocity of the continuous phase of two channels⁹³. Microfluidic devices with a Y-junction and cross junction in their planar have also been applied to control the size of the emulsion droplets⁹⁴. However, the flow of the two phases in microfluidic devices with planar must be precisely and equally controlled for all droplet formation units, which is not straightforward, especially for long-term operations⁹⁵. In consequence, microfluidic device based on terrace and capillaries are more commonly used for this purpose. A terrace-based microfluidic device fabricated is effective for generating monodispersed emulsions with droplets as large as 100 μm , using a depth of 16 μm and a terrace length of 240 μm ⁹⁶. The authors also reported that larger emulsion droplets could be fabricated using a larger terrace length. Using alginate to emulsify oil, the droplet size, between 72 and 256 μm , and between 203 μm and 337 μm were able to be controlled by changing the diameters of the inner channel of the capillary microfluidic device⁹⁷. Furthermore, with the assistance of other technology, such as membrane filtration, during microfluidic processing, the emulsified droplet size can not only be accurately controlled, but also reduced from 10 μm to 0.1 μm ⁹⁸. Although the resulting uniform droplets were significantly affected by the design of the microfluidic device, they were also sensitive to other features, such as the flow rate and pressure during the processing⁹⁹.

III. Elaborately structured emulsions

Given the aforementioned control provided by microfluidic devices, more elaborate structures of emulsions, such as a double-emulsion structure and multiple-emulsion structure, can be created. Two types of double emulsions are water-in-oil-in-water (W/O/W) or oil-in-water-in-oil (O/W/O), which offer better functionality for emulsifying hydrophilic and hydrophobic compounds in one emulsion system. Using a microfluidic device with two successive T-junctions (Fig 1.14-1), W/O/W double emulsion with a droplet size of approximately 50 μm can be generated. Aqueous droplets ruptured at the upstream hydrophobic junction are enclosed with organic droplets formed at the downstream hydrophilic junction¹⁰⁰. The capillaries of a circular cross-section were combined (Fig 1.14-2) and produced double emulsion (W/O/W) in a single step¹⁰¹. It is concluded that different emulsion structures can be generated by different microfluidic devices. And this study especially emphasized that the W/O/W droplet radius can be controlled from 60 to 100 μm using a capillary microfluidic device by varying the flow rate¹⁰². W/O/W emulsions were generated with lipid molecules acting as surfactants using a planar microfluidic device. Importantly, the emulsion droplet size can be quantitatively predicted from the flow profiles of the fluids¹⁰³.

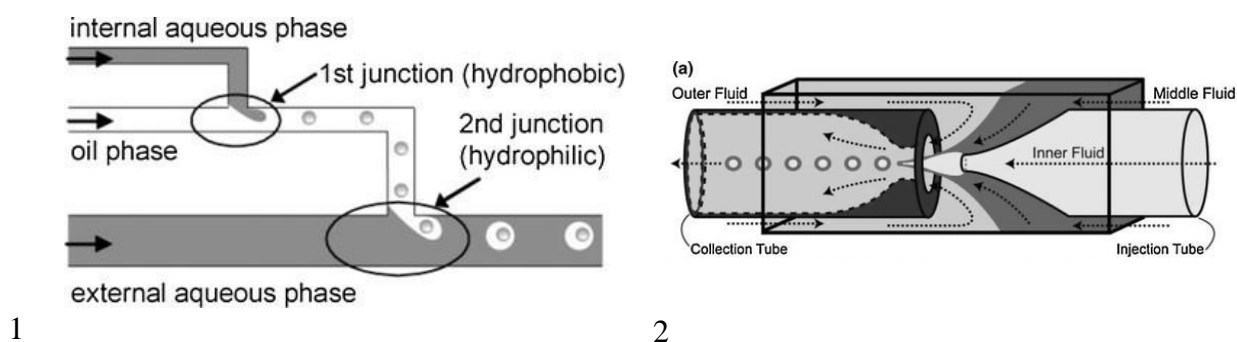


Figure 1.14: Schematic of a microfluidic device with two successive T-junctions. 1) (images are reprinted from “Controlled production of monodisperse double emulsions by two-step droplet breakup in microfluidic devices”, Shingo, et al., *Langmuir*, 2004, 20, 9905–9908 with permission from the American Chemical Society). 2) Schematic of a microfluidic device with the combined capillaries of a circular cross section (images are reprinted from “Controlled production of emulsions and particles by milli- and microfluidic techniques”, Engl, et al., *Curr. Opin. Colloid Interface Sci.*, 2008, 13, 206–216 with permission from ELSEVIER).

Multiple emulsions can also be formed in sequential micro-channels. Double, triple, quadruple, and quintuple emulsions with sizes of approximate 200 μm are formed using linear sequences of multiple cross-junction micro-channels from 2 to 5 (Fig 1.15) ¹⁰⁴.

1.3.4 Microfluidic device for food safety control

The worldwide economic impact of food safety outbreaks is substantial. Pathogens caused over 1.52 million foodborne illnesses and 386 deaths in the United States alone in 2018, with an estimated USD 2.12 billion in associated medical costs, productivity losses, and costs of premature death¹⁰⁵. Traditional methods for the detection of foodborne pathogens rely on culturing the bacteria onto agar plates, which is time-consuming. Traditional methods for the detection of food hazard chemicals also rely on time-consuming processes and expensive equipment. Microfluidic devices allow cheap, efficient, real-time temporal and spatial detection of the presence of residue, trace chemicals, antibiotics, pathogens, and toxins in the food. With the customized design of different microfluidic devices, it is possible to obtain

food safety data within a few minutes. This advantage leads to the possibility of food safety control onsite, from farm to the dinner table.

I. Microfluidic devices for food pathogen detection

The detection and quantification of pathogens in food are achieved by the quantification of pathogen cells or pathogen-related metabolites, such as DNA¹⁰⁶. A microfluidic flow cell with an embedded gold interdigitated array of microelectrodes integrated with magnetic nanoparticle-antibody conjugates has been developed to detect pathogenic bacteria in ground up beef.

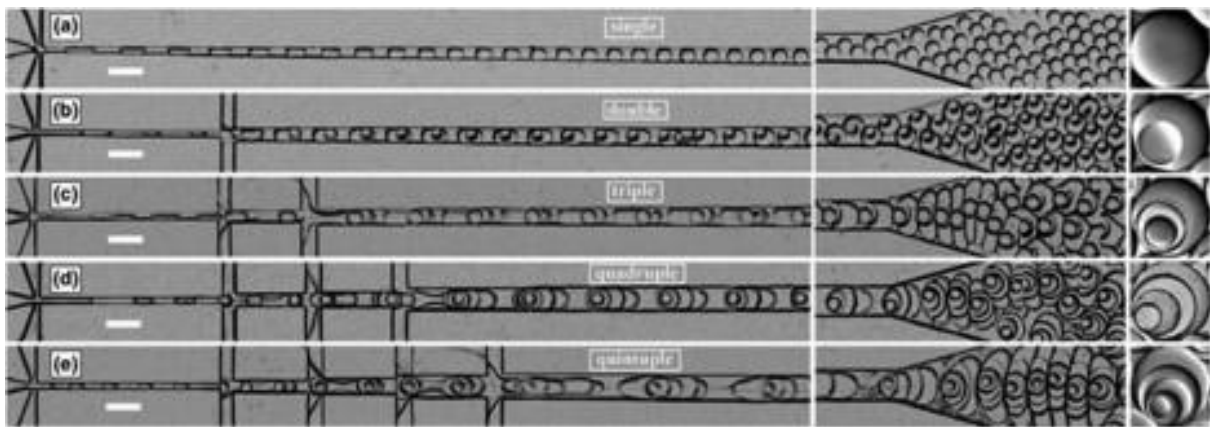


Fig. 1.15 A microfluidic device with linear sequences of multiple cross-junction micro-channels (images are reprinted from “Microfluidic emulsification in food processing”, Abid, et al., *J. Food Eng.*, 2015, 147, 1–7 with permission from ELSEVIER).

This microfluidic biosensor was able to detect as low as 1.2×10^3 cells of Escherichia Coli O157:H7 in beef samples in just 35 min¹⁰⁷. Conversely, the conventional method for E.coli O157:H7 testing from food samples requires over 24 hrs, and this is not including the multiple steps and labor cost required. A centrifugal microfluidic device was developed to integrate the three main steps of Salmonella detection, namely DNA extraction, isothermal recombinase polymerase amplification, and detection, into one step. For example, the entire procedure for milk was complete within 30 min in a fully automated fashion. In

contrast, it takes conventional methods 3–5 days using multiple steps to complete a Salmonella detection test, and this conventional method does not allow instant food safety detection onsite ¹⁰⁸. Microfluidic devices have also been applied in detecting other foodborne pathogens, such as *Listeria monocytogenes* ¹⁰⁹ and Norovirus ⁹³.

II. Microfluidic devices for food-based toxic chemical detection

Similarly, microfluidic devices are used for detecting various toxic chemicals in food, such as biogenic amines, pesticides, and extra food additives. A microfluidic device was developed to incorporate electrochemical enzyme sensor arrays for the detection of biogenic amines, as an indicator of edibility for fishery products ¹¹⁰. The authors found that under optimized conditions, the relative standard deviation narrowed to less than 8.0% and the limit of detection was in the range of 3.0–8.0 $\mu\text{g/L}$. This is more accurate and much less time consuming than the conventional testing method for biogenic amines using HPLC, which requires days to complete, repetitive manual labor operations, multiple steps, and expensive equipment. Given the potential toxicity to humans, the pesticide residue on fruits and vegetables needs to be closely monitored. A simple paper-based luminol- H_2O_2 chemiluminescence (CL) micro-fluidic chip device was developed for the detection of Dichlorvos (2,2-dichlorovinyl dimethyl phosphate) (DDV) (a commonly used pesticide). This chip is able to detect DDV residues in 12 min utilizing 100 μL of the developing reagent. This device was successful for detecting DDV on cucumbers, tomatoes, and cabbages, with a detection time of 12 min and has the potential for daily household testing of fruits and vegetables ⁸⁴. The addition of colorants to food has become a normal practice to enhance or change the color of food to make it more attractive to consumers. However, these colorants can be harmful to human health after excessive consumption. A poly-functionalized paper-based micro-fluidic device was developed for the rapid separation and detection of colorants in drinks made up of complex components, using surface-enhanced Raman spectroscopy. In the trial, sunset yellow and lemon-yellow colorants were detected in grape juice and orange juice, with detection limits as low as 10^{-5} M and 10^{-4} M, respectively ¹¹¹.

1.3.5 Microfluidic devices for other food processing

Microfluidic devices have also been demonstrated as efficient tools in the extraction and detection of bioactive compounds which are used as food supplements, and from plant-based products. As antioxidants, polyphenols are useful for indicating the anti-oxidative activity of wine. However, conventional measurements for determining polyphenol content in wine use HPLC which require large wine samples due to low-level sensitivity of the technique which costs time and labor. To resolve this drawback, a coupled-optical-fiber-poly-dimethyl-siloxane micro-device was developed which increased the levels of sensitivity of detection in quantifying the polyphenol content in wine. The results showed that not only was the required sample volume significantly reduced, but the relative errors were also reduced, by 13% compared to the conventional HPLC flow-injection analysis method⁶⁷. Natural product screening for new bioactive compounds can also benefit from droplet-based microfluidic systems. By coupling HPLC with a droplet generating microfluidic device, the eluted bioactive compounds can be sequentially screened. A Y- junction microfluidic device was developed then successfully identified and screened the inhibitors of Clostridium perfringens neuraminidase present in a root extract of the Pelargonium sidoides plant¹¹². In 'materials science' microfluidic devices have been used for preparing microporous materials as ingredients of functional food. A microfluidic T-junction device was employed in the preparation of microporous calcium alginate gels by incorporating monodisperse air bubbles 177 μm in diameter, which increases the volume to energy content ratio of the product and improves the homogeneity of the samples¹¹³.

In summary, microfluidic devices have been broadly applied in various food processing sectors, for processing applications and food safety control. However, these studies have been limited to laboratory-scale tests. The restrictions for scaling up are mainly due to the following:

- (1) Channel clogging of microfluidic devices, which results from the complexity of microfluidic device systems and causes difficulties in fluid injection and fluid stabilization.
- (2) The high labor cost resulting from intensive manual labor in the fabrication and alignment of microfluidic devices.
- (3) The low production capacity of single microfluidic devices in continuous processing due to volume limitations of the micro-channel, which are dramatically short of the requirements of the food industry.

1.3.6 Future research and development directions

The applications of microfluidic devices in food processing have been comprehensively studied in laboratory settings. Future research should focus on transferring these laboratory achievements into commercial value in the market place, with identified key future research directions discussed below.

I. Development and application of other microfluidic devices

A diversity of microfluidic devices has been developed, as in capillary devices, planar devices, and terrace devices. However, regardless of the design of these devices, the confined micro-fluid is generated by directional pressure, which is an energy penalty, and there are other disadvantages of scaling-up to match the requirements of industry. These include:

- (1) The use of high energy directional pressure results in high production cost of the channel directing device which need to be aligned, and this covers the labor component.
- (2) Clogging of the micro channels in the device.
- (3) Micro-channel-based devices have low production yield, necessitating large parallel arrays of channels.

Technology-wise, these microfluidic devices can limit their scaling-up capacity for industry, and other types of microfluidic process intensification are required. Apart from directional pressure, centrifugal pressure also features in food processing, not only in the laboratory but also as a typical unit of operation in an industrial setting, such as in the purification of bioactive compounds like Fucoïdan from seaweed¹¹⁴ and in the separation of liquid phases with different densities, such as in skim milk production. Thus far, the application of centrifugal pressure in food processing always involves a “top-bottom” model; through centrifugation, the phase with a lower density separates at the top, and the phase with a higher density is separated at the bottom. Centrifugal pressure of this “top-bottom” model has already been implemented for modification of the aforementioned microfluidic devices. A large-volume centrifugal disc-based microfluidic device was developed for blood plasma separation, capable of processing 2 mL of undiluted blood samples¹¹⁵. A sequential operation of multiple microvalves was invented on a centrifugal microfluidic device which was able to disperse 10 nm-sized ferro oxide nanoparticles in paraffin wax¹¹⁶. By enforcing the “top-bottom” centrifugal pressure, the flow rate in micro channels can be drastically increased. However, apart from this “top-bottom” processing, centrifugal pressure can also be generated using an “inside-outside” approach involving the rotation of centrifuge tubes, rather than spinning of the centrifuge tubes or discs associated with the “top-bottom” approach. Centrifugal force in the “inside-outside” approach is a feature of the Vortex Fluidic Device (VFD) (Fig. 1.16), which has been developing since 2012. The rapidly rotating tube in this microfluidic platform generates a thin film on the internal surface of the tube, which is energy efficient in operating at ambient pressure and avoids the use of micro-channels. It harnesses the high shear force produced by rotating centrifugation, intense micro mixing, and high mass transfer, thereby overcoming the limitations of traditional microfluidic devices.

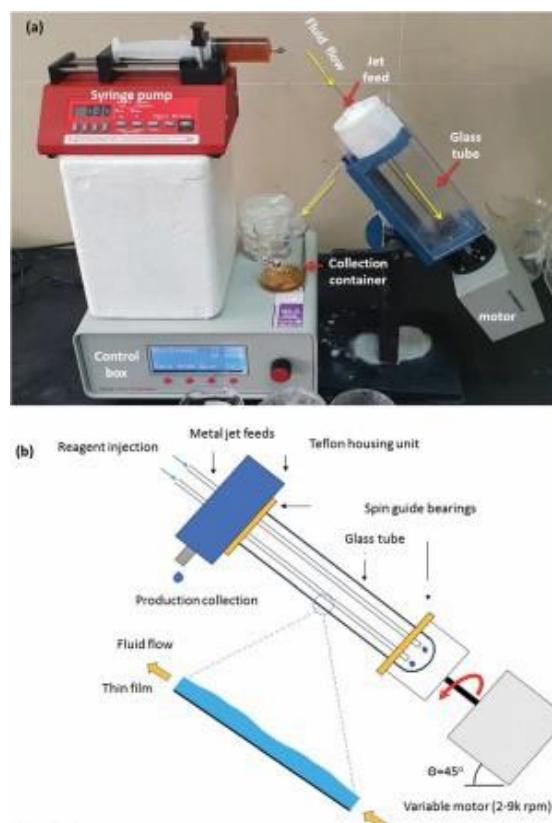


Figure 1.16: Vortex Fluidic Device (VFD). (a). Photograph of the VFD, highlighting its salient features. (b). Schematic of the VFD showing the fluid flow.

The mechanical energy imparted in the liquid in the VFD is effective in mediating a diversity of processes, ranging from small-molecule synthesis involving many steps in a single pass for generating functional materials and manipulating single-celled organisms¹¹⁷. Enzymatic reactions in the VFD typically have a sevenfold enhancement in their rates⁶⁹, depending on the choice of processing parameters of the device, including the rotational speed of the inclined glass tube¹¹⁸. Optimal processing in the VFD is usually at a 45° tilt angle of the tube, as in enhancing enzymatic reactions. Tethering enzymes to the surface of the glass tube has also been achieved for the synthesis of complex molecules in a single pass under continuous flow in the device¹¹⁹. The VFD is also versatile in fabricating nanomaterials under continuous flow, with remarkable findings, for example, in assembling fullerene

C60 molecules into hollow nanotubes 100–400 nm in diameter, in the absence of any surfactants and without the need for further downstream processing ¹²⁰. Other noteworthy applications of the VFD include converting sunflower oil to biodiesel at room temperature with no saponification and avoiding the conventional use of co-solvents or complex catalysts ¹²¹, as well as the direct transesterification of microalgae ¹²¹. While studies on the use of VFD in food processing are limited, given its simple plug-and-play operation and relatively low cost (USD 15K versus USD 150K for high pressure, industrial-scale microfluidic devices), it is likely that the VFD will have a significant impact in the field. This is further highlighted by the inside-out, centrifugal-pressure-driven device not suffering from clogging. In previous studies, we have established that the VFD significantly reduces the processing time of enzymatic hydrolysis of milk protein, from 3 h to 20 mins, and reduces the pasteurization time of raw milk from 30 mins to 10 mins at 60°C ¹²², suggesting that the VFD has potential in other models of food processing.

II. Continuous flow high production microfluidic devices for industrial applications

Presently, a continuous mode of production with high production capacity is a compulsory requirement across food processing and many other processing sectors. However, the micro-scale/micro-channel flow of liquid volume in current channel based microfluidic devices greatly restricts their production capacity and they have a high risk of clogging. Therefore, it is not surprising is that successful scaled-up applications of current microfluidic devices have not yet been reported. Unlike conventional channel based microfluidic devices, the VFD does not use micro-channels to generate the micro-fluid, rather centrifugal force to create a microfluidic film of liquid. Thus, the limitations of conventional microfluidic devices for continuous production do not apply to VFD processing. The production capacity of the conventional 20 mm diameter VFD operating under continuous mode can be set at a milliliter scale, which is much higher than that of conventional microfluidic devices. In our previous study, by applying a single VFD, we successfully passed 100 mL of encapsulated fish oil solution within 18 h, with the solution found to

have the same overall characteristics as a 10 mL scale VFD production¹²³. This success not only demonstrates the high production capacity of VFD processing under continuous flow mode, but also highlights the stability of such processing at a larger scale. Overall, VFD processing has advantages and more potential over conventional microfluidic devices for future food processing applications.

III. Microfluidic mediated protein-polysaccharide mixing

Due to the wide range of applications of polysaccharides and proteins in healthy food, protein-polysaccharide interactions and the formation of composites thereof have been widely studied. The exploitation of protein-polysaccharide interactions offers opportunities for the design of new ingredients and interfacial structures of food products. After isolation from a food matrix, nutraceuticals, including antioxidants (tocopherols, flavonoids, and phenolic compounds), and carotenoids (*b*-carotene, lycopene, lutein, and zeaxanthin), have been the focus of research¹²⁴. Most of these nutraceuticals are unstable to chemical or physical degradation. This can be addressed by encapsulation or entrapment, thereby providing a delivery vehicle for uptake in the human body. Protein-polysaccharides are emerging ingredients and have been applied for such encapsulation purposes. This involves a variety of proteins, such as milk and soy proteins, and polysaccharides, such as alginate from seaweed and fungal polysaccharides, for fabricating a structured encapsulation delivery system. Microfluidic devices provide an opportunity to manipulate protein-polysaccharide interactions at the micro-level dimensionality regime. However, this is limited by the viscous nature of many protein and polysaccharide solutions with the likelihood of micro-channels of conventional microfluidic devices becoming clogged. In contrast, as previously mentioned, thin-film microfluidics in the VFD microfluidic platform, with high shear and intense micromixing, can overcome these limitations, and this augurs well for microfluidic processing involving protein-polysaccharide, in optimizing their interplay, even at the submicron dimensions.

IV. Microfluidic derived ingredients for nutritional enhancement of food

The trend of global desire for food is drastically changing from sufficiency to healthy. However, it's rare to find reports that show contributions of conventional microfluidic devices on technologies regarding nutritional enhancement for food, such as encapsulation and entrapment. This unfortunate reality is most likely caused by the frequently encountered clogging of micro-channels, especially when processing multiple ingredients, and the low output efficacy. Rapid high through-put microfluidics devices, such as the VFD, which doesn't suffer from clogging, provide an opportunity for solving these problems. In this context, we have successfully contributed the further development of encapsulation and entrapment through VFD processing. Regarding encapsulation, the use of such processing was successful in encapsulating fish oil in nano size particles without clogging of the VFD. Omega-3 fatty acid content, as a valuable nutritional ingredient, was significantly increased from approximately 30% in raw and un-encapsulated fish oil to approximate 60% in encapsulated fish oil after 14 days post-VFD processing ¹²⁵. Regarding entrapment of viscous solutions of many proteins and polysaccharides where clogging of micro-channels in conventional microfluidic devices is likely, the VFD has potential to produce regular micro network structures based on interacting gelatin (protein) and alginate (polysaccharide). Furthermore, we have established that this sole protein-polysaccharide composite material was effective in entrapping multiple nutrients of amino acids, vitamin and trace nutritional elements ¹²⁶. These promising preliminary studies suggest that general nutritional enhancement is possible using VFD processing.

V. Microfluidic derived ingredients in food formulation

Product development and sensory study involving ingredients produced by microfluidic devices in food formulation would be the "last punch" before the uptake of this technology in commercial food processing. The lack of such reports possibly relates to the low output efficacy of conventional channel-based microfluidic devices, even when massively parallelized. Any comprehensive product development

and sensory study requires large volumes of ingredients and final food products, which appear to be beyond the capability of such devices. Rapid high through-put microfluidics devices that do not suffer from clogging, for example in the VFD, provide an opportunity for solving these problems. In this context, we have produced sufficiently encapsulated fish oil powder using VFD processing for product development and a sensory study (40 participants) ¹²⁷. This highly improved production capacity establishes the feasibility of VFD processing for “last punch” application studies on ingredients produced by microfluidic devices.

1.3.7 Conclusions

With the rapid growth of the global population, there is an increasing demand for advanced technologies in food processing, to design safer and more functional food. This review critically analyzed the current state-of-the-art designs for microfluidic devices, their applications in food processing, and identified future research directions of microfluidic technology in such processing. Currently, three droplet degeneration systems (capillary, planar, and terrace) are used in the design of microfluidic devices, being based on channels. The applications of these devices in food processing, such as emulsification, food safety measurement, and bioactive compound extraction, have been broadly studied. However, the design of these devices as such greatly restricts their utility in scaling-up processes for the food industry, notably where there is potential for channel clogging, high labor costs, low productivity, and associated high energy penalty “directional pressure” processing. This review highlights the utility of the paradigm- shift thin-film vortex fluidic device (VFD) involving “inside-out centrifugal force”, for application in food processing. This continuous flow microfluidic platform has the potential for fast-tracking commercialization of food processing with scalability incorporated at the inception of the research. The high shear stress and intense micro-mixing in the VFD are effective in controlling the interplay between protein and polysaccharide, despite the high viscosity of their solutions. We foreshadow that this breakthrough sets the scene for a diversity of commercially viable food processing, especially where there are limitations associated with processing viscous liquids.

Cite this: *Food Funct.* 2020, **11**, 5726

Application of microfluidic technology in food processing

Shan He,^{a,†} Nikita Joseph,^{†,b} Shilun Feng,^{b,†,c} Matt Jellicoe^b and Colin L. Raston^{b,*}

Microfluidic technology is interdisciplinary with a diversity of applications including in food processing. The rapidly growing global population demands more advanced technologies in food processing to produce more functional, and safer food, and for such processing microfluidic devices are a popular choice. This review critically critiques the state-of-the-art designs of microfluidic devices and their applications in food processing, and identifies the key research trends and future research directions for maximizing the value of microfluidic technology. Capillary, planar, and terrace droplet generation systems are currently used in the design of microfluidic devices, each with their strengths and weaknesses as applied in food processing, for emulsification, food safety measurements, and bioactive compound extraction. Conventional channel-based microfluidic devices are prone to clogging, and have high labor costs and low productivity, and their "directional pressure" restricts scaling-up capabilities. These disadvantages can be overcome by using "inside-out centrifugal force" and the new generation continuous flow thin-film microfluidic Vortex Fluidic Device (VFD) which facilitates translating laboratory processing into commercial products. Also highlighted is controlling protein–polysaccharide interactions and the applications of the produced ingredients in food formulations as targets for future development in the field.

Received 16th May 2020,
Accepted 31st May 2020
DOI: 10.1039/d0fo01278e
rsc.li/food-function

1. Introduction

Microfluidics is defined as a system that processes and manipulates small amounts of fluid, up to 10^{-6} to 10^{-9} L (Fig. 1).¹ Microfluidic technology is interdisciplinary covering physics, chemistry, engineering, biotechnology, and other fields. The dimensions of the devices ranges from micrometers to a few millimeters.² The strengths of microfluidic devices come from two of their properties, namely the reduced particle size generated and the laminar flow characteristics of fluids. These devices offer several advantages, including low fabrication costs, rapid processing, and the reuse of molds.³ As such they help to ameliorate important scientific problems that are difficult to resolve by applying conventional technologies. Moreover, compared with conventional fluidic systems, microfluidic devices are cheap to fabricate, using less chemical

reagent as well as offering improved analytical performance, chemical reactivity, and biocompatibility. These advantages greatly contribute to the development of sustainable technologies with reduced financial burden.⁴ Applications of microfluidic devices emerged at the beginning of the 1990s, and encompass blood rheology⁵ and chemical analyses.⁶ Subsequently, applications have expanded into capillary electrophoresis,⁷ flow cytometry,⁸ multiple component reactions,⁹ bio-sensors,¹⁰ genetic analyses,¹¹ and drug screening.¹² The

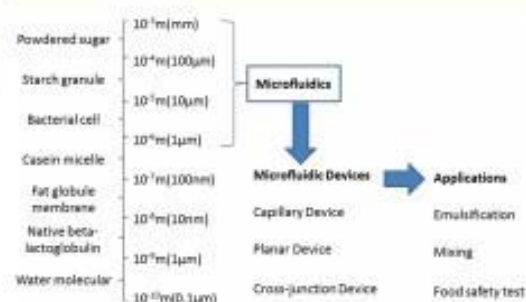


Fig. 1 Range of the length scale of material involved in microfluidics, microfluidic devices, and microfluidic applications (images are reprinted from "Applications of Microfluidic devices in food engineering", Skurtyus, et al., *Food Biophys.*, 2008, **3**, 1–15 with permission from Springer).

^aDepartment of Food Science, School of Chemistry and Chemical Engineering, Guangzhou University, Guangzhou, Guangdong, 510005, China. E-mail: he0091@gmail.com; Tel: +86 20 39386230

^bFlinders Institute for Nanoscale Science and Technology, College of Science and Engineering, Flinders University, Bedford Park, South Australia, 5042, Australia. E-mail: colin.raston@flinders.edu.au; Tel: +61 8 82017958

^cSchool of Electrical and Electronic Engineering, Nanyang Technological University, 639798, Singapore

†These authors contributed equally to this work.

1.4 The Vortex Fluidic Device (VFD)

The Vortex Fluidic Device (VFD) is an emerging thin film flow microfluidic platform which involves a rapidly rotating glass tube, with two different diameters of 10mm – 20 mm, this can be open at one end ('continuous mode') or closed at both end ('confined mode'). Under rapid rotation, the sub-millimeter volumes of liquid are forced into a dynamic thin film (Fig 1.17). VFD generates thin films typically below 500 nm. Under continuous mode in the VFD one or more than one jet-feeds can deliver reagents to the hemispherical base of the rapidly rotating sample tube leading to intense shearing and micro mixing within the dynamic thin film. The properties of the VFD thin film is governed by a number of parameters that include the tilt angle of the rotating tube, θ , the rotational speed, fluid viscosity and density, flow rates, hydrophilic/ hydrophobic inner surface of the tube and the length and diameter of the tube¹²⁸. The VFD can also operate under a confined mode where a finite volume of liquid is rapidly rotated.

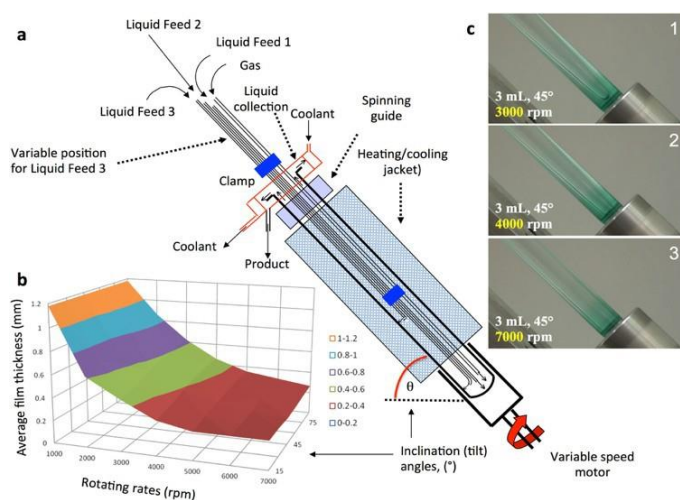


Figure 1.17: Schematic representation of the VFD (a). b, average film thickness vs rotating speed. c, behavior of thin film at different rotational speeds¹²⁸.

This mode of operation is effective in shearing where small quantities of material is required, as a proven approach for translating to continuous flow processing¹²⁹. Also, a change in surface tension of the thin film can result from the intense shear, which can enable high mass transfer of gases into and out of the

liquid typically at higher rotational speeds ¹³⁰. Additional advantages of the VFD as compared to conventional channel-based systems are, that it does not suffer from clogging unlike conventional microfluidics. The VFD, however, is inexpensive to construct, is simple to operate and be set up within minutes (plug and play), allowing scaling-up through parallel processing. In addition, VFD is emerging platform, for real time monitoring during *in situ* reaction optimization. Recent applications of the VFD include a three-minute synthesis, in a single VFD unit, of a lidocaine, a drug which requires a number of steps for preparation ¹³¹. Similarly, the assembly line synthesis of α -amino-phosphonates has been developed in the VFD ¹³², other applications such as refolding of proteins¹³³, lateral slicing of carbon nanotubes using laser irradiation ¹³⁴, and accelerating enzymatic catalysis ¹³⁵. Such applications are discussed in detail in coming sections.

1.4.1 Applications of Vortex Fluidics in Materials Transformations

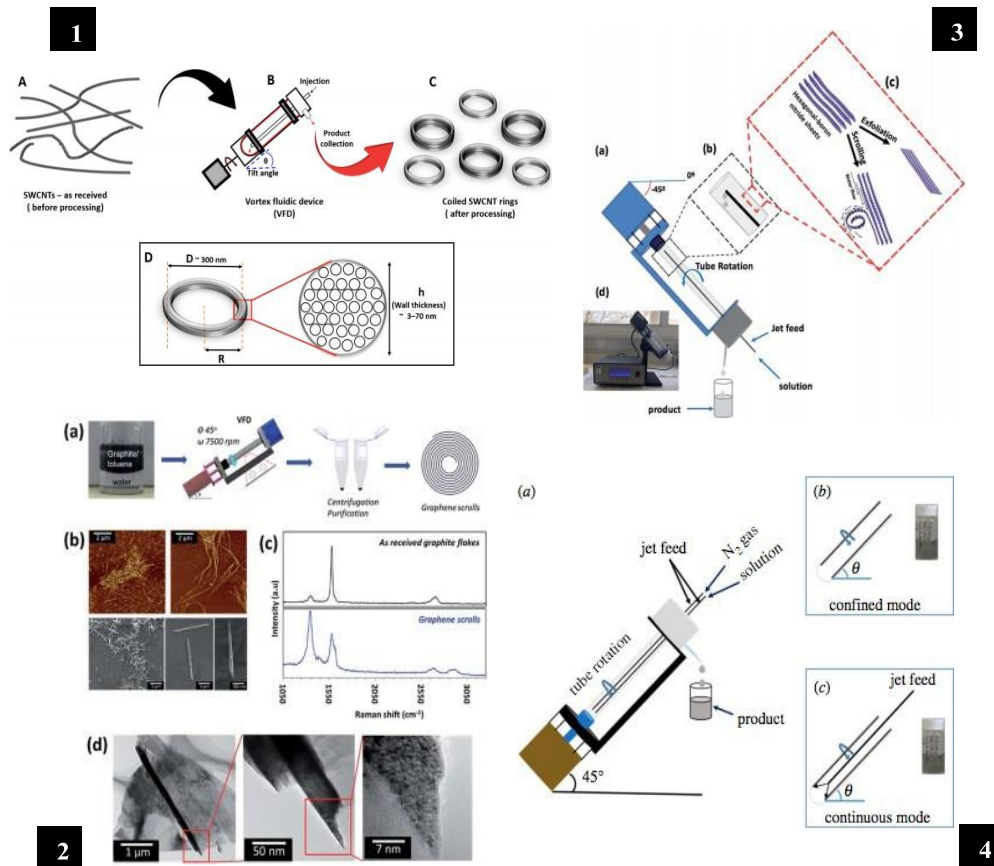


Figure 1.18: Applications of vortex fluidics in materials transformation. (1) Schematic representation for VFD mediated SWCNT coiled rings (a) SWCNTs entangled pre-processing VFD, (b) Schematic of the VFD setup, (c) post processing coiled SWCNTs and (d) defining parameters for the coiled rings.¹³⁶ (2) VFD manipulated graphite into highly conducting scrolls, (a) Schematic representation of the VFD processing from graphite flakes into graphene scrolls (b) AFM phase images and SEM images for the graphene scrolls (c) Raman spectra of the graphene and as receive graphite flakes (d) TEM and HRTEM characterization for the graphene scrolls¹³⁷. (3) An inverted VFD for fabricating exfoliating and scrolling Hexagonal Boron Nitride (h-BN). (a) schematic representation of the VFD (b) A zoomed in illustration for the delivery of liquid inside the VFD tube. (c) schematics for exfoliation of h-BN and scrolling of h-BN. (d) photograph of the VFD in inverted position -45° relative to the horizontal position¹³⁸. (4) VFD mediated exfoliation and fragmentation of two dimensional Mxene (Ti_2CT_x)¹³⁹. (a) schematic representation of the VFD (b) & (c) indicates two different setups of VFD in continuous and confined mode with an images of the post VFD product in IPA and water.

The vortex fluidics dynamic thin film platform has shown plethora of application in field of nano-materials fabrication and manipulation. Alharbi et.al.¹³⁶ reported fabrication of SWCNTs coiled rings in a continuous flow method with a maximum of 80% yield without utilizing any toxic chemicals or surfactants. The group also reported the magnetic interaction of these coiled rings which was strongly dependent on the thickness of the rings (Fig 1.18-1)¹³⁶. Another work from Vimalanathan et.al.¹³⁷ reported on fabricating graphene scrolls from graphite flakes. These two-dimensional materials possess remarkable properties for many applications. The work also reported that these graphene scrolls open up into buckled graphene sheets when heated at a temperature or above 450 °C and at high yield with continuous recycling through-out the microfluidic platform (Fig 1.18 – 2). Another unique class of two-dimensional 2D materials are Hexagonal Boron Nitride (h-BN) and Mxene (Ti_2CT_x), Alnataki et.al reported fabrication and manipulation of these materials utilizing VFD. Mxene was exfoliated down to ca 3nm multi-layered sheet via VFD processing. An inert atmosphere was created to avoid the oxidation of the material while processing in the rapidly rotating VFD tube. Also, no toxic chemicals and surfactants were utilized and a benign reaction processing was carried out (Fig. 1.18- 4)¹³⁹. Similarly, another two-dimensional material exfoliation and scrolling was reported by utilizing VFD. Hexagonal Boron Nitride (h-BN) was manipulated using VFD operating under continuous flow system with a tilt angle of - 45° relative to the horizontal position (Fig 1.18– 3). This setup was carried out to avoid the aggregation and build-up of material which occurs due to high centrifugal force during processing¹³⁸.

A single pass reaction was achieved with a yield of ca 22% using only water as a solvent. This defines the green chemistry metrics of the processing. Thus, VFD reports research unequivocally in field of materials transformations as an emerging microfluidic platform. The shear stress generated and dynamic thin films formed can manipulate and alter different types of nanomaterials. From different allotropes of carbon to unique 2D materials VFD is explored as a benign processing microfluidic platform.

1.4.2 Applications of Vortex Fluidics in Chemical Transformations

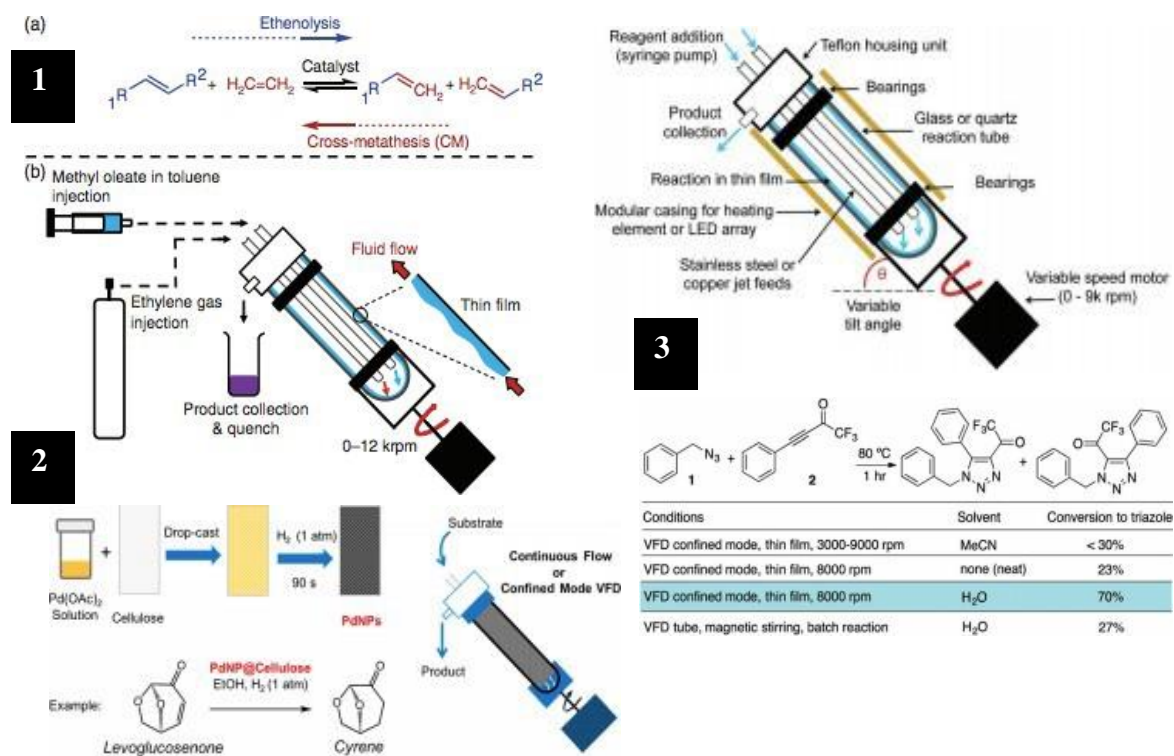


Figure 1.19: Application of vortex fluidics in chemical transformations. 1- a) Schematic mechanism for ethenolysis type – Olefin Metathesis (OM) reaction. 1-b) Schematic illustration for VFD mediated processing of methyl oleate (MO)¹⁴⁰. 2) Schematic illustration for processing chemo selectivity of bio-based molecule Cyrene via utilizing cellulose immobilized palladium nanoparticles onto the VFD tube for a continuous scalable process¹⁴¹. 3 – top) schematic illustration for utilizing VFD for Azide-Alkyne cycloaddition reactions, 3-bottom) optimized conditions and total conversion for the VFD processed cycloaddition product with water as a suitable solvent for the reaction¹⁴².

The Vortex Fluidic Device possesses a rapidly rotating tube which can be operated in either confined or continuous flow setup where a finite volume of liquid can be delivered to the bottom of the tube via a jet feed or a confined amount of liquid can be processed. These abilities have demonstrated for delivering various gaseous agents safely for aerobic oxidation and processing of plant and microbial oils^{143, 122}. Various other microfluidic platforms have also been an area of interest for process intensification and developing greener and benign reaction platform¹⁴⁴. In such growing and developing pharmaceutical industry vortex fluidics have opened a new paradigm with showing progress for sustainable environment.

Pye et.al.¹⁴⁰ reported vortex fluidic device for ruthenium catalyzed ethenolysis under continuous flow within the VFD. His work utilizes the rapid mass transfer as an advantage for gaseous agent such as oxygen under continuous flow for quenching of these ruthenium-based olefin metathesis catalyst. This quenching opens up a new side for the previously based toxic quenching agents such as isocyanides which are widely reported with a non-toxic and inexpensive N-acetyl L-cysteine (AcCysOH) quencher. This work has opened up a new direction in solving difficulties with gas/liquid reactions and quenching and separation of catalysts¹⁴⁰. Philips et.al.¹⁴¹ also reported a chemical transformation utilizing the VFD. the work reported an inexpensive robust technology for continuous flow hydrogenation reactions with the help of paper-based palladium catalyst. Palladium nanoparticles were fabricated and immobilized on a cellulose paper, this cellulose paper was mounted inside the VFD glass tube. This catalyst system can be prepared in minutes and reused through-out the processing. Excellent chemo-selectivity and catalytic activity for reduction reactions is observed with very low generation of wastage and energy. Moreover, another typical reaction in organic synthesis such as Azide-Alkyne cycloaddition is also explored with the VFD. Oksdath-Mansilla et.al.¹⁴² reported a novel approach for metal-free Azide-Alkyne cycloaddition reaction via keeping water as a suitable solvent while copper and stainless-steel jet-feed was utilized for the copper based azide-alkyne cycloaddition reaction. In VFD confined mode the azide-alkyne cycloaddition was achieved with a conversion of 70% which was compared to batch processing via a magnetic stirrer and only 27% of the conversion was achieved. While in a copper based cycloaddition reaction, a copper or stainless steel jet feed was utilized and to maintain the copper catalyst, ascorbic acid was used as a reducing agent. Few other alterations were also maintained by using eosin Y and green LED lights which improved the overall conditions and almost conversion for cycloadditions products was reported to be higher than 75%. Such transformations have shown immense progress in the field of pharmaceutical and chemical industry. Various other chemical transformations have also been reported such as rapid mass transfer, accelerating enzymatic reaction, and also accelerated multiphase

reactions ^{135, 143}. VFD has also opened progress in the field of polymers and biomaterials technology which is discussed in detail in the next section.

1.4.3 Applications of Vortex Fluidics in Biomaterials Processing.

Different materials are processed these days which can mimic the function of natural organ, tissue or function at cellular level when a patient suffers with an ailment or losses the vital organs or functions during an accident. Such materials are often termed as “biomaterials” and are becoming a cornerstone in the field of biomedical and technology. From hydrogels to enzyme-based biosensors, new research is explored for the improvement in human life. Due to a vast potential applications of the Vortex Fluidic Device (VFD) another leading area is explored and research has shown outstanding applications in the area of biomaterials.

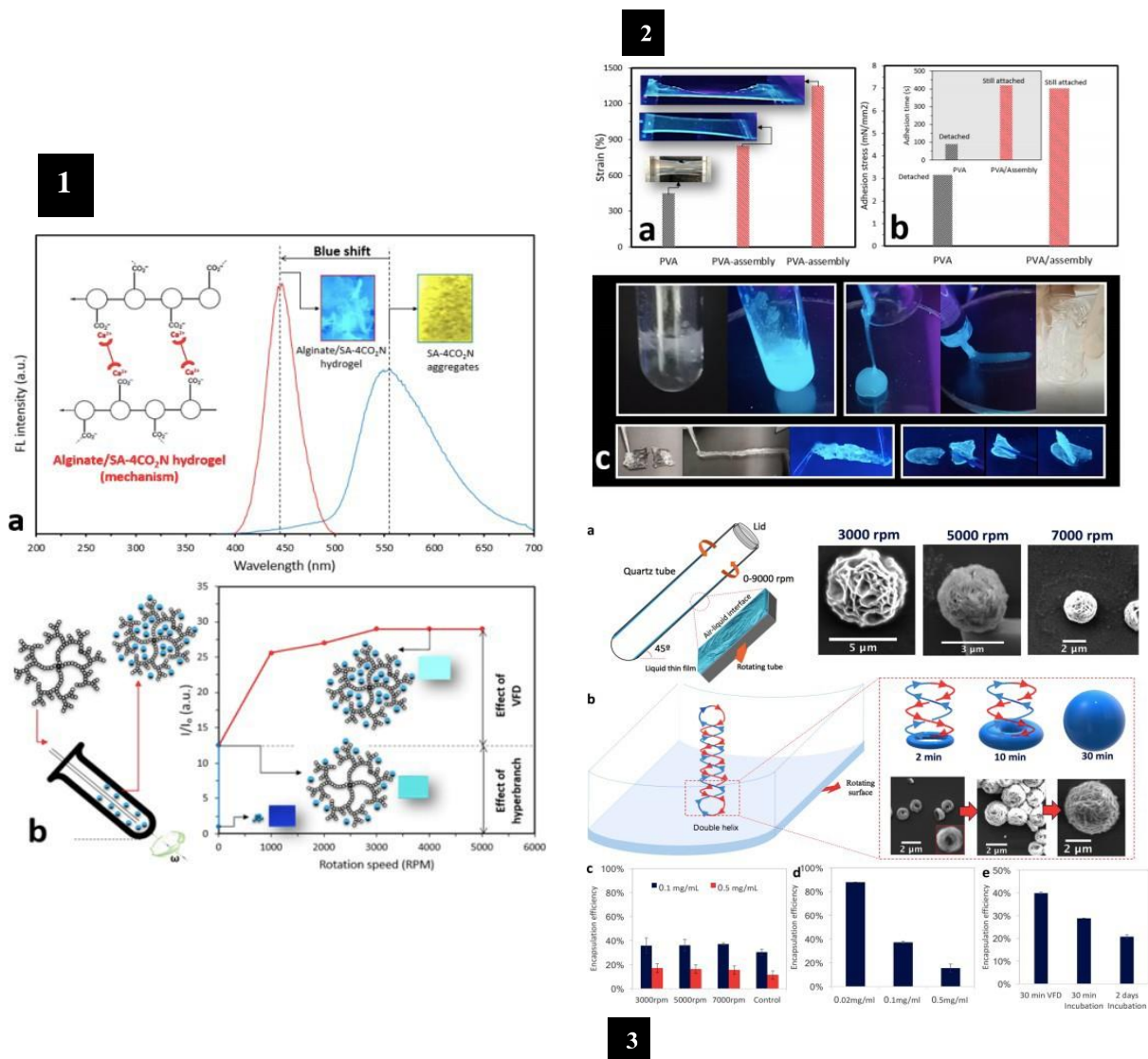


Figure 1.20: Applications of vortex fluidics in biomaterials processing. 1-a) Schematic representation of aggregation induced emission alginate hydrogel with fluorescence properties excited at 350 nm in presence of UV light. 1-b) schematic representation of AIE hyper-branched self-assembly and change its structure by utilizing VFD¹⁴⁶. 2-a), Data analysis for elongation at the break for PVA alone and PVA with AIE 2-b), crosslinking with borax and self-healing properties for PVA alone and PVA with AIE. 2-c) PVA crosslinked with borax images¹⁴⁶. 3-a) Schematic representation of the VFD and rotational effects on the BSA incorporated Nano-Flowers (BNFs) 3-b) BNFs processing at 2, 10 and 30 min. 3-c) Encapsulation Efficiency of BSA on BNFs at different rotational speed 3-d) Encapsulated Efficiency of BSA at given concentrations 3-e) Encapsulated Efficiency at optimized conditions 5000 rpm for 30min and 2-day incubation¹⁴⁵.

Luo et.al. ¹⁴⁵ reported a novel process in fabricating a hybrid material from copper ions and laccase enzymes termed as $\text{Cu}^3(\text{PO}_4)_2$ nanoflowers (NFs) via utilizing the vortex fluidic device. The further studies also revealed a new laccase Nano Flowers (LNFs) immobilization platform via incorporated silica hydrogel with the LNFs which causes gelation along the glass tube and is very stable and reusable showing excellent catalytic activity up to 16-fold enhancement activity than LNF@silicagel in glass vials. This immobilization of enzymes in gels gives protection to the enzymes during bio-sensing applications. Thus, due to the mechanoenergy provided from the VFD, more stronger interactions are produced between the Bovine Serum Albumin (BSA) protein or the laccase enzyme which forms novel hybrid Nano Flowers as new smart materials for bio-sensing technology. Another research also reported in this area of biomaterials such as Tavakoli et.al. ¹⁴⁶ reported a fresh work on hydrogel via utilizing AggregationInduced Emission (AIE) technique. Tavakoli et.al work showcased AIEgen hyperbranched self-assembly with enhanced fluorescence properties and tunable size with the aid of VFD which helps creating an environment for strong hydrogen bond interactions. These interactions cause the AIEgens confinement into the self-assembly and resists the intramolecular rotation which dynamically increases the photon emission for the self-assembly. They are 30 times highly fluorescent self-assembly is fabricated without losing a negligible decrease in the fluorescence intensity for almost 7 days. Furthermore, his work also demonstrated the crosslinking of the PVA films with 100mM Borax, the self-healing properties were dramatically increased than just the PVA alone, almost 150% higher adhesion stress after 420 s tension testing.

Thus, there is vast applications with the VFD in different areas of science from materials manipulation, chemical transformations to biomaterials processing, VFD has showcased infinite possibilities with a high impact on research and development in all these areas as a benign sustainable thin film microfluidic reactor.

1.5 Research Program

The main concept of the research program in this thesis is to demonstrate the ability of the Vortex Fluidic Device (VFD) to manipulate soft matter materials such as nanoparticles, emulsions, gels and protein based nano-carriers for food processing technology and drug delivery applications. Studies of nanoparticles such as phospholipid based self-assembly including Liposomes, form a significant part of this thesis, from fabricating liposomes to controlling their size and also understanding the mechanism as 100-nm bottom up self-assembly. Emulsions such as W/O fish-oil emulsions and controlling their size and homogeneity with an increased omega-3 content for better nutraceutical value is also investigated. Protein-Polysaccharides gel interactions are investigated in presence of polyphenols. Moreover, protein based nano-carrier such as ferritin is processed with VFD for a better uptake of the anti-cancer drug, the preliminary results are a part of the future work in this thesis. Another integral part of this thesis is developing an *In-situ* Small-Angle Neutron Scattering (SANS) technique for monitoring the self-assembly of liposomes and fish-oil emulsions in real-time affording invaluable insights to their mechanisms. Such advances in the soft matter realms unequivocally provides a toxic chemicals free processing and sustainable and scalable process intensification technique for future research and development.

1.5.1 Aims of the Program

The following are the aims of this thesis:

Aim 1: Vortex fluidic fabrication of liposomes and labelling with different fluorophores

Aim 2: Developing *In-situ* Small-Angle Neutron Scattering (SANS) technique for understanding the self-assembly and dis-assembly of liposomes as a mechanism within the VFD.

Aim 3: Vortex fluidics processing of fish-oil emulsions with a controlled size and homogeneity.

Aim 4: Developing *In-situ* Small-Angle Neutron Scattering (SANS) technique for monitoring the effects of the VFD on the surfactant self-assembly utilized for fish-oil emulsions.

Aim 5: Vortex fluidics fabrication on protein non-covalent crosslinked gels with polyphenols and its application on effectively encapsulating nutrients.

Aim 6: Vortex fluidics assisting anti-cancer drug encapsulation within a protein based nano-carrier.

1.5.2 Thesis Outline

Initially the VFD was explored for the food processing industry in demonstrating suitable nano-carriers and different emulsions for the encapsulation of active ingredients, enzymatic hydrolysis and milk pasteurization processing. All the results are compared with conventional technique homogenization. The rest of the thesis develops into individual projects from liposomes fabrication to studying protein and polysaccharide interactions.

Chapter 2: This chapter is focused on fabricating W/O/W emulsions from fish-oil and phospholipid as an amphiphilic surfactant. The results are compared with a traditional technique homogenization demonstrating that VFD controls the size of particle in nano-dimensions than the homogenization. Different characterization techniques are studied for evaluating the size of the particles.

Chapter 3: This chapter is focused on three different initial results obtained with the VFD when exploring its potential in the food industry. Encapsulation on curcumin was shown in O/W emulsions in presence of a non-ionic surfactant and compared with homogenization. Enzymatic hydrolysis of milk powder reduced of about 2–3 hours to 20 minutes, while the processing time of raw milk pasteurization reduced from 30 to 10 minutes. Different characterizations were studied such as MALDI mass spectroscopy for analyzing the milk hydrolysis data. All the experiments were compared with conventional technique homogenization and sonication.

Chapter 4: This chapter is focused on the Omega-3 Polyunsaturated Fatty Acids (PUFAs) content in the fish-oil emulsions processed with aid of VFD in a continuous flow setup. Bio-active ingredients such as curcumin and quercetin is encapsulated in the formulation for improving the nutritional value. Moreover, an *In-situ* Small-Angle Neutron Scattering (SANS) technique is developed for monitoring the effects of the VFD on the surfactant self-assembly and dis-assembly. The results were compared with conventional homogenization technique.

Chapter 5: This chapter is focused on the protein gelatin and polyphenol tannin for effective non-covalent crosslinked gels. The gels were later utilized for encapsulating different nutrients for a better nutritional value. All the results were compared with conventional homogenization technique.

Chapter 6: This chapter is focused on fabricating liposomes in continuous flow VFD set-up, labelling liposomes with two different fluorophores and monitoring their dis-assembly in the VFD via *In-situ* Small-Angle Neutron Scattering (SANS) technique. The results reveal vital intermediates for bottom-up self-assembly to be 100 nm and also highlights the disassembly process instead of membrane fusion when two different fluorophore liposomes are processed together in a confined mode of VFD.

Chapter 7: This is the final chapter of the thesis which is focused on the conclusion and future work, herein for future work a protein based nano-carrier such as ferritin is explored for loading anti-cancer drug doxorubicin. This, results are compared with conventional technique utilized such as water bath and heating it up to 40 °C for optimum drug loading. A heating jacket is utilized for the VFD processing to ensure heating up to 40 °C is provided.

References

1. Hirst, L. S. (2020). *Fundamentals of Soft Matter Science* (2nd ed.). Milton: CRC Press.
2. Vilanova N., Voets I.K. (2016) Introduction to Soft Matter. In: Lang P., Liu Y. (eds) *Soft Matter at Aqueous Interfaces*. Lecture Notes in Physics, vol 917.
3. G. Gompper, J.K.G. Dhont, D. Richter, A unified view of soft matter systems? *Eur. Phys. J. E* 26(1–2), 1–2 (2008).
4. Loescher, Sebastian, Groer, Saskia, & Walther, Andreas. (2018). 3D DNA Origami Nanoparticles: From Basic Design Principles to Emerging Applications in Soft Matter and (Bio)Nanoscience. *Angewandte Chemie (International Ed.)*, 57(33), 10436-10448.
5. Seeman, N. (1982). Journal of theoretical biology. *Journal of Theoretical Biology.*, 99, 237-247.\
6. P. Izquierdo et al., A study on the influence of emulsion droplet size on the skin penetration of tetracaine. *Skin Pharmacol. Physiol.* **20**(5), 263–270 (2007)
7. Nasser, Behrooz, & Fasciolo, Alessandro. (2005). Exploring soft matter: Liposomal vesicles and their tethers. *Journal of Drug Targeting*, 13(8-9), 471-477.
8. Michel, Raphael, & Gradzielski, Michael. (2012). Experimental Aspects of Colloidal Interactions in Mixed Systems of Liposome and Inorganic Nanoparticle and Their Applications. *International Journal of Molecular Sciences*, 13(9), 11610-11642.
9. Rajesh Krishna, Natashia McIntosh, K. Wayne Riggs, & Lawrence D. Mayer. (1999). Doxorubicin Encapsulated in Sterically Stabilized Liposomes Exhibits Renal and Biliary Clearance Properties That Are Independent of Valspodar (PSC 833) under Conditions That Significantly Inhibit Nonencapsulated Drug Excretion. *Clinical Cancer Research*, 5(10), 2939-2947.
10. Busquets, M. Antonia, Estelrich, Joan, & Sánchez-Martín, María Jesús. (2015). Nanoparticles in magnetic resonance imaging: From simple to dual contrast agents. *International Journal of Nanomedicine*, 10(Default), 1727-1741.
11. Pasut, Gianfranco, Paolino, Donatella, Celia, Christian, Mero, Anna, Joseph, Adrian Steve, Wolfram, Joy, . . . Fresta, Massimo. (2015). Polyethylene glycol (PEG)-dendron phospholipids as innovative constructs for the preparation of super stealth liposomes for anticancer therapy. *Journal of Controlled Release*, 199, 106-113.
12. Van der Geest, Tessa, Laverman, Peter, Metselaar, Josbert M, Storm, Gert, & Boerman, Otto C. (2016). Radionuclide imaging of liposomal drug delivery. *Expert Opinion on Drug Delivery*, 13(9), 1231-1242.

13. Bonacucina, Giulia, Cespi, Marco, Misici-Falzi, Monica, & Palmieri, Giovanni F. (2009). Colloidal soft matter as drug delivery system. *Journal of Pharmaceutical Sciences*, 98(1), 1-42.
14. Dong, Zhao, Xie, Shuyu, Zhu, Luyan, Wang, Yan, Wang, Xiaofang, & Zhou, Wenzhong. (2011). Preparation and in vitro, in vivo evaluations of norfloxacin-loaded solid lipid nanoparticles for oral delivery. *Drug Delivery*, 18(6), 441-450
15. Jao, Dave, Xue, Ye, Medina, Jethro, & Hu, Xiao. (2017). Protein-Based Drug-Delivery Materials. *Materials*, 10(5), 517.
16. Cho, Sun-Hee, Kim, Ahreum, Shin, Woojung, Heo, Min Beom, Noh, Hyun Jong, Hong, Kwan Soo, . . . Lim, Yong Taik. (2017). Photothermal-modulated drug delivery and magnetic relaxation based on collagen/poly(γ -glutamic acid) hydrogel. *International Journal of Nanomedicine*, 12, 2607-2620.
17. Pritchard, Eleanor M, & Kaplan, David L. (2011). Silk fibroin biomaterials for controlled release drug delivery. *Expert Opinion on Drug Delivery*, 8(6), 797-811.
18. Khoshnejad, Makan, Parhiz, Hamideh, Shuvaev, Vladimir V, Dmochowski, Ivan J, & Muzykantov, Vladimir R. (2018). Ferritin-based drug delivery systems: Hybrid nanocarriers for vascular immunotargeting. *Journal of Controlled Release*, 282, 13-24.
19. Zhen, Zipeng, Tang, Wei, Chen, Hongmin, Lin, Xin, Todd, Trever, Wang, Geoffrey, . . . Xie, Jin. (2013). RGD-Modified Apoferritin Nanoparticles for Efficient Drug Delivery to Tumors. *ACS Nano*, 7(6), 4830-4837.
20. Van Der Sman, R. G. (2012). Soft matter approaches to food structuring. *Advances in Colloid and Interface Science*, 176-177, 18-30.
21. Vilgis, T. A. (2015). Gels: Model systems for soft matter food physics. *Current Opinion in Food Science*, 3, 71-84.
22. Van der Sman, R. (2012). Soft matter approaches to food structuring. *Advances in Colloid and Interface Science*, 176-177, 18-30.
23. Zuidam, N., & Nedovic, Viktor. (2010). *Encapsulation Technologies for Active Food Ingredients and Food Processing* (1st ed. 2010. ed.).
24. Turasan, Hazal, Sahin, Serpil, & Sumnu, Gulum. (2015). Encapsulation of rosemary essential oil. *Food Science & Technology*, 64(1), 112-119.
25. Sultana, Khalida, Godward, Georgia, Reynolds, N, Arumugaswamy, R, Peiris, P, & Kailasapathy, Kaila. (2000). Encapsulation of probiotic bacteria with alginate–starch and evaluation of survival in simulated gastrointestinal conditions and in yoghurt. *International Journal of Food Microbiology*, 62(1), 47-55.

26. Syrbe, A, Bauer, W.J, & Klostermeyer, H. (1998). Polymer Science Concepts in Dairy Systems— an Overview of Milk Protein and Food Hydrocolloid Interaction. *International Dairy Journal*, 8(3), 179-193.
27. Gentile, L. (2020). Protein–polysaccharide interactions and aggregates in food formulations. *Current Opinion in Colloid & Interface Science*, 48, 18-27.
28. Baeza, R.I, Carp, D.J, Pérez, O.E, & Pilosof, A.M.R. (2002). κ -Carrageenan—Protein Interactions: Effect of Proteins on Polysaccharide Gelling and Textural Properties. *Food Science & Technology*, 35(8), 741-747.
29. Peanparkdee, Methavee, Iwamoto, Satoshi, Borompichaichartkul, Chaleeda, Duangmal, Kiattisak, & Yamauchi, Ryo. (2016). Microencapsulation of bioactive compounds from mulberry (*Morus alba* L.) leaf extracts by protein–polysaccharide interactions. *International Journal of Food Science & Technology*, 51(3), 649-655
30. Kim, J. (2016). Liposomal drug delivery system. *Journal of Pharmaceutical Investigation*, 46(4), 387-392.
31. Fouladi, F., Steffen, K., & Mallik, S. (2017). Enzyme-Responsive Liposomes for the Delivery of Anticancer Drugs. *Bioconjugate Chemistry*, 28(4), 857-868.
32. Dario Carugo, Elisabetta Bottaro, Joshua Owen, Eleanor Stride, & Claudio Nastruzzi. (2016). Liposome production by microfluidics: Potential and limiting factors. *Scientific Reports*, 6, Scientific Reports, 2016, Vol.6.
33. Immordino, M. L., Dosio, F., & Cattell, L. (2006). Stealth liposomes: review of the basic science, rationale, and clinical applications, existing and potential. *International Journal of Nanomedicine*, 1(3), 297–315.
34. Gibbs, Bernard F., Kermasha, Selim, Alli, Inteaz, & Mulligan, Catherine N. (1999). Encapsulation in the food industry: A review. *International Journal of Food Sciences and Nutrition*, 50(3), 213.
35. Zhang, Yumin, Yang, Cuihong, Wang, Weiwei, Liu, Jinjian, Liu, Qiang, Huang, Fan., Liu, Jianfeng. (2016). Co-delivery of doxorubicin and curcumin by pH-sensitive prodrug nanoparticle for combination therapy of cancer. *Scientific Reports*, 6(1), 21225.
36. Meng, J., Guo, F., Xu, H., Liang, W., Wang, C., & Yang, X. (2016). Combination Therapy using Co-encapsulated Resveratrol and Paclitaxel in Liposomes for Drug Resistance Reversal in Breast Cancer Cells in vivo. *Scientific Reports (Nature Publisher Group)*, 6, 22390.
37. Shah, Rhutesh K, Shum, Ho Cheung, Rowat, Amy C, Lee, Daeyeon, Agresti, Jeremy J, Utada, Andrew S, . . . Weitz, David A. (2008). Designer emulsions using microfluidics. *Materials Today (Kidlington, England)*, 11(4), 18-27.

38. Mazzitelli, Stefania, Capretto, Lorenzo, Quinci, Federico, Piva, Roberta, & Nastruzzi, Claudio. (2013). Preparation of cell-encapsulation devices in confined microenvironment. *Advanced Drug Delivery Reviews*, 65(11-12), 1533-1555.
39. Khoo, Bee Luan, Greci, Gianluca, Jing, Tengyang, Lim, Ying Bena, Lee, Soo Chin, Thiery, Jean Paul, . . . Lim, Chwee Teck. (2016). Liquid biopsy and therapeutic response: Circulating tumor cell cultures for evaluation of anticancer treatment. *Science Advances*, 2(7), E1600274.
40. Liu, Dongfei, Zhang, Hongbo, Fontana, Flavia, Hirvonen, Jouni T, & Santos, Hélder A. (2017). Microfluidic-assisted fabrication of carriers for controlled drug delivery. *Lab on a Chip*, 17(11), 1856-1883.
41. Liu, Dongfei, Zhang, Hongbo, Herranz-Blanco, Bárbara, Mäkilä, Ermei, Lehto, Vesa-Pekka, Salonen, Jarno, . . . Santos, Hélder A. (2014). Microfluidic Assembly of Monodisperse Multistage pH-Responsive Polymer/Porous Silicon Composites for Precisely Controlled Multi-Drug Delivery. *Small (Weinheim an Der Bergstrasse, Germany)*, 10(10), 2029-2038.
42. Shum, Ho Cheung, Lee, Daeyeon, Yoon, Insun, Kodger, Tom, & Weitz, David A. (2008). Double Emulsion Templated Monodisperse Phospholipid Vesicles. *Langmuir*, 24(15), 7651-7653.
43. Xu, Qiaobing, Hashimoto, Michinao, Dang, Tram T, Hoare, Todd, Kohane, Daniel S, Whitesides, George M, . . . Anderson, Daniel G. (2009). Preparation of Monodisperse Biodegradable Polymer Microparticles Using a Microfluidic Flow-Focusing Device for Controlled Drug Delivery. *Small (Weinheim an Der Bergstrasse, Germany)*, 5(13), 1575-1581.
44. Jahn, Andreas, Vreeland, Wyatt N, Gaitan, Michael, & Locascio, Laurie E. (2004). Controlled Vesicle Self-Assembly in Microfluidic Channels with Hydrodynamic Focusing. *Journal of the American Chemical Society*, 126(9), 2674-2675.
45. Matosevic, Sandro, & Paegel, Brian M. (2011). Stepwise Synthesis of Giant Unilamellar Vesicles on a Microfluidic Assembly Line. *Journal of the American Chemical Society*, 133(9), 2798-2800.
46. Wang, Rui-Jin, & Li, Zhi-Hua. (2012). Influence on droplet formation in the presence of nanoparticles in a microfluidic T-junction. *Thermal Science*, 16(5), 1429-1432.
47. Baxani, Divesh K, Morgan, Alex J. L, Jamieson, William D, Allender, Christopher J, Barrow, David A, & Castell, Oliver K. (2016). Bilayer Networks within a Hydrogel Shell: A Robust Chassis for Artificial Cells and a Platform for Membrane Studies. *Angewandte Chemie (International Ed.)*, 55(46), 14240-14245.
48. Yeh, Chia-Hsien, Zhao, Qiaole, Lee, Sheng-Ji, & Lin, Yu-Cheng. (2009). Using a T-junction microfluidic chip for monodisperse calcium alginate microparticles and encapsulation of nanoparticles. *Sensors and Actuators. A. Physical.*, 151(2), 231-236.

49. Carugo, Dario, Bottaro, Elisabetta, Owen, Joshua, Stride, Eleanor, & Nastruzzi, Claudio. (2016). Liposome production by microfluidics: Potential and limiting factors. *Scientific Reports*, 6(1), 25876.
50. Zhang, Qiongli, Zhang, Ming, Djeghlaf, Lyas, Bataille, Jeanne, Gamby, Jean, Haghiri-Gosnet, Anne-Marie, & Pallandre, Antoine. (2017). Logic digital fluidic in miniaturized functional devices: Perspective to the next generation of microfluidic lab-on-chips. *Electrophoresis*, 38(7),953-976.
51. Michelon, Mariano, Oliveira, Davi Rocha Bernardes, De Figueiredo Furtado, Guilherme, Gaziola de la Torre, Lucimara, & Cunha, Rosiane Lopes. (2017). High-throughput continuous production of liposomes using hydrodynamic flow-focusing microfluidic devices. *Colloids and Surfaces, B, Biointerfaces*, 156, 349-357.
52. Xu, H., Yu, S.Z., Grissel, T.S., Mario, M.A., Joao,R., Steven, J.J., Paul, S.W., Anne, M.A., Joanna, A. & Ali, K. (2017). Interplay between materials and microfluidics. *Nature reviews materials*, 17016.
53. Chia-Wen, T. (2016). Polymer microfluidics: simple, low-cost fabrication process bridging academic lab research to commercialized production. *Micromachines*, 7(12), 225.
54. Joana, C., Diana, P., Francisco, J.G., Rui, L. & Laura, C. (2016). Particulate blood analogues reproducing the erythrocytes cell-free layer in a microfluidic device containing a hyperbolic contraction. *Micromachines*, 7(1), 4.
55. Adrian, M.N., Adexander, D.B. & Matthew, C.M. (2015). Trends in microfluidic system for in situ chemical analysis of natural waters. *Sensors and Actuators B: Chemical*, 221(31), 1398-1405.
56. Erin, A.R., Nicholas, G.B., Scott, M. & Michael, R. (2015). Integrated microfluidic capillary electrophoresis-electrospray ionization devices with online MS detection for the separation and characterization of intact monoclonal antibody variants. *Analytical Chemistry*, 87(4),2264-2272.
57. Jian, C., Chengcheng, X., Yang, Z., Deyong,C., Min-Hsien, W. & Junbo, W. (2015). Microfluidic impedance flow cytometry enabling high-throughput single-cell electrical property characterization. *International Journal of Molecular Sciences*, 16(5), 9804-9830.
58. Kelley L.P., Inge, C., Lindsay, M.K., Kyle, Z., Jucas, B. & Bruce, R.M. (2015). Simultaneous colorimetric detection of improvised explosive compounds using microfluidic paper-based analytical devices. *Analytical Methods*, 7, 63-70.
59. Darius, G.R., Mohtashim, H.S. & Aaron, R.W. (2015). Electrochemistry, biosensors and microfluidics: a convergence of fields. *Chemical Society Reviews*, 44, 5320-5340.
60. Na, W., Zhan, Z., Bei yuan, F., Deyong, C., Dong, M., Junbo, W. & Jian, C. (2016). Development of droplet microfluidics enabling high-throughput single-cell analysis. *Molecules*, 21(7), 881.

61. Samar, D., Uday, B.K., Safa, A.D. & Rimantas, K. (2018). Microfluidic devices for drug delivery systems and drug screening. *Genes*, 9(2), 103.
62. You, Xiangshen, Wang, Bingsheng, Xie, Shuting, Li, Lanhui, Lu, Han, Jin, Mingliang, . . . Shui, Lingling. (2020). Microfluidic-Assisted Fabrication of Monodisperse Core-Shell Microcapsules for Pressure-Sensitive Adhesive with Enhanced Performance. *Nanomaterials (Basel, Switzerland)*, 10(2), 274.
63. Karin, S., Olesya, B., Kelly, M., Sami, S. & Claire, C.B. (2015). Microfluidic emulsification devices: from micrometer insights to large-scale food emulsion production. *Current Opinion in Food Science*, 3, 33-40.
64. Elisabeth, K., Varun, V., Deborah, L. & Yvonne, P. (2015). Microfluidic-controlled manufacture of liposomes for the solubilisation of a poorly water soluble drug. *International Journal of Pharmaceutics*, 485 (1), 122-130.
65. Xingjun, Y., Yan, Z., Lingyun, D., Junhai, L. & Jianfeng, Y. (2015). Review of the applications of microreactors. *Renewable and Sustainable Energy Reviews*, 47, 519-539.
66. Boce, Z., Yaguang, L., Bin,Z., Qin, W. & Patricia, D.M. (2015). A novel microfluidic mixer-based approach for determining inactivation kinetics of *Escherichia coli* O157:H7 in chlorine solutions. *Food Microbiology*, 49, 152-160.
67. Sandoval-Ventura, O., Olguin-Contreras, L.F. & Canizares-Macias, P. (2017). Total polyphenols content in white wines on a microfluidic flow injection analyzer with embedded optical fibers. *Food Chemistry*, 221(15), 1062-1068.
68. Fereshteh, Z., Yadollah, Y., Mahroo, B. & Mohammad, F. (2018). Electromembrane extraction of biogenic amines in food samples by a microfluidic-chip system followed by dabsyl derivatization prior to high performance liquid chromatography analysis. *Journal of Chromatography*, 1556, 21-28.
69. Merve, G., Xinyue, J., Cem, B., Kezban, U. & Mohan, E. (2018). Honeycomb-like PLGA-b-PEG structure creation with T-junction microdroplets. *Langmuir*, 34(27), 7989-7997.
70. Xuan, W. & Suresh, N. (2017). Ensuring food safety: quality monitoring using microfluidics. *Trends in Food Science & Technology*, 65, 10-22.
71. Suresh, N., Isao, K., Mitsutoshi, N, Dan, W., Saravanan, N. & Francis, L. (2011). Microfluidics for food, agriculture and Biosystems industries. *Lab on a Chip*, 11, 1574-1586.
72. Ana, L.R.C., Andresa, G. & Rosiane, L.C. (2017). Studies of droplets formation regime and actual flow rate of liquid-liquid flows in flow-focusing microfluidic devices. *Experimental Thermal and Fluid Science*, 85, 167-175.

73. Xiaoming, C., Tomaz, G., Naiwen, C. & Carolyn, L.R. (2015). Model of droplet generation in flow focusing generators operating in the squeezing regime. *Microfluidics and Nanofluidics*, 18, 1341-1353.
74. Tengyang, J., Ramesh R., Majid, E.W., Jongyoon, H., Chwee, T.L. & Chia-Hung, C. (2015). Jetting microfluidics with size-sorting capability for single-cell protease detection. *Biosensors and Bioelectronics*, 66(15), 19-23.
75. Yunru, Y., Fanfan, F., Luoran, S., Yao, C., Zhongze, G. & Yuanjin, Z. (2017). Bioinspired helical microfibers from microfluidics. *Advanced Materials*, 29(18), 1605765.
76. Kunqiang, J., Annie, X.L., Panagiotis, D., Don, L.D. % Srinivasa, R.R. (2015). Microfluidic generation of uniform water droplets using gas as the continuous phase. *Journal of Colloid and Interface Science*, 448(15), 275-279.
77. Ankur, S.C. & Shahriar, S. (2015). Millimetric core-shell drops via buoyancy assisted non-confined microfluidics. *Chemical Engineering Science*, 129(16), 260-270.
78. Ushikudo, F.Y., Birribilli, F.S., Oliveira, D.R.B. & Cunha, R.L. (2014). Y- and T-junction microfluidic devices: effect of fluids and interface properties and operating conditions. *Microfluidics and Nanofluidics*, 17, 711-720.
79. Piotr, G., Michael, J.F., Howard, A.S. & George, M.W. (2006). Formation of droplets and bubbles in a microfluidic T-junction-scaling and mechanism of break-up. *Lab on a Chip*, 6, 437-446.
80. Ushikubo, F.Y., Oliveira, D.R.B., Michelin, M. & Cunha, R.L. (2015). Designing food structure using microfluidics. *Food Engineering Reviews*, 7, 393-416.
81. Laurent, S., Martin, M., Imre, B., Olivier, S. & Martin, E.L. (2017). Self-assembly in food-a concept for structure formation inspired by nature. *Current Opinion in Colloid & Interface Science*, 28, 87-95.
82. Goran, T.V., Ekanem, E.E., Zilin, Z., Nauman, K., Isao, K. & Mitsutoshi, N. (2018). Long-term stability of droplet production by microchannel (step) emulsification in microfluidic silicon chips with large number of terraced microchannels. *Chemical Engineering Journal*, 333(1), 380-391.
83. Michael, H., Jean-Baptiste, F. & Ralf, S. (2015). Coexistence of different droplet generating instability: new breakup regimes of a liquid filament. *Soft Matter*, 11, 5246-5252.
84. 35. C. Carrell, A. Kava, M. Nguyen, R. Menger, Z. Munshi, Z. Call, M. Nussbaum and C. Henry, *Microelectron. Eng.*, 2019, 206, 45-54.
85. I. Swyer, R. Fobel and A. R. Wheeler, *Langmuir*, 2019, 35, 5342-5352.
86. C. Yeung, S. Chen, B. King, H. Lin, K. King, F. Akhtar, G. Diaz, B. Wang, J. Zhu, W. Sun, A. Khademhosseini and S. Emaminejad, *Biomicrofluidics*, 2019, 13. 064125.

87. Sabina, G. & Justyna, K. (2015). Food applications of emulsion-based edible films and coatings. *Trends in Food Science & Technology*, 45(2), 273-283
88. Verica, D., Bojina, B., Ana, B., Steva, L., Kata, T., Ana, K., Ivana, K., Drazenka, K., Brako, B. & Viktor, N. (2014). Trends in encapsulation technologies for delivery of food bioactive compounds. *Food Engineering Reviews*, 7, 452-490.
89. Skurtys, O. & Aguilera, J.M. (2008). Applications of Microfluidic devices in food engineering. *Food Biophysics*, 3, 1-15.
90. J. Kenar, International News on Fats Oils, 2005.
91. Paul, S.C., Joe, W.T. & Pete, J.W. (2016). One-step production of multiple emulsion: microfluidic, polymer-stabilized and particle-stabilized approaches. *Soft Matter*, 12, 998-1008.
92. Xuan, W. & Suresh, N. (2017). Aptamer-based fluorometric determination of norovirus using a paper-based microfluidic device. *Microchimica Acta*, 184, 4545-4552.
93. Takasi, N., Toru, T. & Toshiro, H. (2002). Droplet formation in a microchannel network. *Lab on a Chip*, 2, 24-26.
94. Jean-Christophe, B., Felix, K., Abdeslam, E.H. & Andrew, D. G. (2009). Kinetic aspects of emulsion stabilization by surfactants: a microfluidic analysis. *Langmuir*, 2009, 6088-6093.
95. Maartje, L.J.S., Karin, G.P.H.S. & Remko, M.B. (2009). Characterization of emulsification at flat microchannel Y-junctions. *Langmuir*, 25(6), 3396-3401.
96. Shinji, S., Mitsutoshi, N., Satoshi, I. & Minoru, S. (2001). Interfacial tension driven monodispersed droplet formation from microfabricated channel array. *Langmuir*, 17(18), 5562-5566.
97. Ping-wei, R., Xiao-jie, J., Rui, X. & Liang-yin, C. (2010). Monodisperse alginate microcapsules with oil core generated from microfluidic device. *Journal of Colloid and Interface Science*, 343 (1), 392-395.
98. G. T. Vladislavjevic, I. Kobayashi and M. Nakajima, *Microfluid. Nanofluid.*, 2012, 13, 151-178.
99. Seyed, A.N., Sai, G., Goran, T.V. & Ekanem, E.E. (2015). Dynamics of double emulsion break-up in three phase glass capillary microfluidic. *Journal of Colloid and Interface Science*, 450(15), 279-287.
100. Shingo, O., Takasi, N., Toru, T. & Toshiro, H. (2004). Controlled production of monodisperse double emulsions by two-step droplet breakup in microfluidic devices. *Langmuir*, 20(23), 9905-9908.
101. Utada, A.S., Lorenceau, E., Link, D.R., Kaplan, P.D., Stone, H.A. & Weitz, D.A. (2005). Monodisperse double emulsion generated from a microcapillary device. *Science*, 308 (5721), 537-541
102. G. Muschiolik and E. Dickinson, *Compr. Rev. Food. Sci. Food Saf.*, 2017, 16, 532-555.

103. L. Kong, A. Levin, Z. Toprakcioglu, Y. Xu, H. Gang, R. Ye, B.-Z. Mu and T. P. J. Knowles, *Langmuir*, 2020, 36, 2349-2356.
104. Abate, A.R., Lee, D., Do, T., Holtze, C. & Weitz, D.A. (2009). High-order multiple emulsions formed in poly microfluidics. *Nano Micro Small*, 5, 2030-2032.
105. United States Department of Agriculture, Cost estimates of foodborne illnesses, 2020.
106. Jeong-Yeol, Y. & Bumsang, K. (2012). Lab-on-a-chip pathogen sensors for food safety. *Sensors*, 12(8), 10713-10741
107. Madhukar, V., Yanbin, L., Balaji, S. & Steve, T. (2007). A label-free, microfluidics and interdigitated array microelectrode-based impedance biosensor in combination with nanoparticles immunoseparation for detection of Escherichia coli O157:H7 in food samples. *Sensors and Actuators B: Chemical*, 128(1), 99-107.
108. Tae-Hyeong, K., Juhee, P., Chi-Ju, K. & Yoon-Kyoung. (2014). Fully integrated lab-on-a-disc for nucleic acid analysis of food borne pathogens. *Analytical Chemistry*, 86(6), 3841-3848.
109. A. A. Sayad, F. Ibrahim, S. M. Uddin, K. X. Pei, M. S. Mohktar, M. Madou and K. L. Thong, *Sens. Actuator B-Chem.*, 2016, b227, 600-609.
110. Fereshteh, Z., Yadollah, Y., Mahroo, B. & Mohammad, F. (2018). Electromembrane extraction of biogenic amines in food samples by a microfluidic-chip system followed by dabsyl derivatization prior to high performance liquid chromatography analysis. *Journal of Chromatography*, 1556, 21-28.
111. L. Kong, R. Chen, X. Wang, C.-X. Zhao, Q. Chen, M. Hai, D. Chen, Z. Yang and D. A. Weitz, *Lab Chip*, 2019, 19, 2089-2095.
112. Abraham, O., Enrique, A., Eduardo, C. & Luis F. O. (2017). Detection of enzyme inhibitors in crude natural extracts using droplet-based microfluidics coupled to HPLC. *Analytical Chemistry*, 89(9), 4889-4896.
113. Joseph, M.R., Jaekung, K. & Dino, D.C. (2019). Scalable high-throughput production of modular microgels for in situ assembly of microporous tissue scaffolds. *Advanced Functional Materials*, 29(25), 1900071
114. Thanh, T.T.T., Bui, M.L., Tran, T.T.T., Ngo, V.Q., Ho, C.T. & Usov, A. (2015). Anti-HIV activity of focoidans from three brown seaweed species. *Carbohydrate Polymers*, 115, 122-128.
115. Seguin-Devaux, B. Mi and U. Ai, *Carbohydr. Polym.*, 2015, 115, 122-128.
116. M. Amasia and M. Madou, *Bioanalysis.*, 2010, 2, 1701-1710.
117. J.-M. Park, Y.-K. Cho, B.-S. Lee, J.-G. Lee and C. Ko, *Lab Chip*, 2007, 7, 557-564.
118. Britton, J. , & Raston, C. L. (2017). Multi-step continuous-flow synthesis. *Chemical Society Reviews*, 46(5), 1250.

119. Britton J , Meneghini L , Raston C , et al.(2016). Accelerating Enzymatic Catalysis Using Vortex Fluidics. *Angewandte Chemie*, 128(38),11559-11563.
120. Britton, J. , Stubbs, K. A. , Weiss, G. A. , & Raston, C. L. (2017). Vortex fluidic chemical transformations. *Chemistry - A European Journal*. 2017, 23, 13270.
121. Vimalanathan, K., Shrestha, R.G., Zhang, Z., Zou, J., Nakayama, T. & Rastion, C.L. (2017). Surfactant-free fabrication of fullerene C 60 nanotubules under shear. *Angewandte Chemie*,129, 9518-8521.
122. Sitepu, E. K. , Kendall, C. , Xuan, L. , Pye, S. J. , Youhong, T. , & Leterme, S. C. , et al. (2018). Vortex fluidic mediated direct transesterification of wet microalgae biomass to biodiesel. *Bioresource Technology*, 266, 488-497.
123. He, S., Nikita, J., Xuan, L., & Colin R. (2019). Vortex fluidic mediated food processing. *PLOS-ONE*, 14(5), e0216816.
124. He, S., Nikita, J., Xuan, L., & Colin R. (2019). Continuous flow thin film microfluidic mediated nano-encapsulation of fish oil. *LWT-Food Science and Technology* (103), 88-93
125. Xuan, T.L., Laurie, R. & Sylvie, L.R. (2017). Formation and functional properties of protein-polysaccharide electrostatic hydrogels in comparison to protein or polysaccharide hydrogels. *Advances in Colloid and Interface Science*, 239, 127-135.
126. He, Shan, Joseph, Nikita, Mirzamani, Marzieh, Pye, Scott J, Al-anataki, Ahmed Hussein Mohammed, Whitten, Andrew E, . . . Raston, Colin L. (2020). Vortex fluidic mediated encapsulation of functional fish oil featuring in situ probed small angle neutron scattering. *NPJ Science of Food*, 4(1), 12.
127. Cao, X., Joseph, N., Jellicoe, M., Alantak, A., Luo, X., & Su, D. et al. (2020). Vortex fluidics mediated non-covalent crosslinking of tannic acid and gelatin for entrapment of nutrients. *Food & Function*. doi: 10.1039/d0fo02230f.
128. Yasmin, L.C., X.; Stubbs, K. A.; Raston, C. L.(2013). *Optimising a vortex fluidic device for controlling chemical reactivity and selectivity*. *Scientific Reports*, 3 (2282).
129. Britton, J.C., J. M.; Raston, C. L.(2015) *Rapid Vortex Fluidics: Continuous Flow Synthesis of Amides and Local Anesthetic Lidocaine*. *Chemistry - A European Journal*, 21(30),10660-10665.
130. Britton, J., S.B. Dalziel, and C.L. Raston (2016). *The synthesis of di-carboxylate esters using continuous flow vortex fluidics*. *Green Chemistry*, 18(7): p. 2193-2200.
131. Britton, J., S.B. Dalziel, and C.L. Raston, (2015) *Continuous flow Fischer esterifications harnessing vibrational-coupled thin film fluidics*. *RSC Advances*, 2015. 5(3), 1655-1660
132. Britton, J., et al., *Harnessing Thin-Film Continuous-Flow Assembly Lines*. *Chemistry - A European Journal*, 2016.

133. Yuan, T.Z.O., C. F. G.; Kudlacek, S. T.; Kunche, S.; Smith, J. N.; Brown, W. A.; Pugliese, K. M.; Olsen, T. J.; Iftikhar, M.; Raston, C. L.; Weiss, G. A.(2015) *Shear-Stress-Mediated Refolding of Proteins from Aggregates and Inclusion Bodies*. *ChemBioChem*,16, p. 393-396.
134. Vimalanathan, K.G., J. R.; Suarez-Martinez, I.; Marks, N. A.; Kumari H.; Garvey, C. J.; Atwood, J. L.; Lawrence, W. D.; Raston, C. L., (2016) *Fluid dynamic lateral slicing of high tensile strength carbon nanotubes*. *Scientific Reports*, 6(22865).
135. Britton, J., et al., (2016) *Accelerating Enzymatic Catalysis Using Vortex Fluidics*. *Angewandte Chemie*.
136. Alharbi, Thaar M. D, Shingaya, Yoshitaka, Vimalanathan, Kasturi, Nakayama, Tomonobu, & Raston, Colin L. (2019). High Yielding Fabrication of Magnetically Responsive Coiled Single-Walled Carbon Nanotube under Flow. *ACS Applied Nano Materials*, 2(8), 5282-5289.
137. Vimalanathan, Kasturi, Suarez-Martinez, Irene, Peiris, M. Chandramalika R, Antonio, Joshua, De Tomas, Carla, Zou, Yichao, . . . Raston, Colin L. (2019). Vortex fluidic mediated transformation of graphite into highly conducting graphene scrolls. *Nanoscale Advances*, 1(7), 2495-2501.
138. Al-Antaki, Ahmed Hussein Mohammed, Luo, Xuan, Alharbi, Thaar M. D, Harvey, David P, Pye, Scott, Zou, Jin, . . . Raston, Colin L. (2019). Inverted vortex fluidic exfoliation and scrolling of hexagonal-boron nitride. *RSC Advances*, 9(38), 22074-22079.
139. Mohammed Al-antaki, Ahmed Hussein, Kellici, Suela, Power, Nicholas P, Lawrence, Warren D, & Raston, Colin L. (2020). Continuous flow vortex fluidic-mediated exfoliation and fragmentation of two-dimensional MXene. *Royal Society Open Science*, 7(5), 192255.
140. Pye, Scott J, Chalker, Justin M, & Raston, Colin L. (2020). Vortex Fluidic Ethenolysis, Integrating a Rapid Quench of Ruthenium Olefin Metathesis Catalysts. *Australian Journal of Chemistry*, Australian journal of chemistry, 2020.
141. Phillips, Jessica M, Ahamed, Muneer, Duan, XiaoFei, Lamb, Robert N, Qu, Xianlin, Zheng, Kun, . . . Raston, Colin L. (2019). Chemoselective and Continuous Flow Hydrogenations in Thin Films Using a Palladium Nanoparticle Catalyst Embedded in Cellulose Paper. *ACS Applied Bio Materials*, 2(1), 488-494.
142. Oksdath-Mansilla, Gabriela, Kucera, Renata L, Chalker, Justin M, & Raston, Colin L. (2020). Azide-alkyne cycloadditions in a vortex fluidic device: Enhanced "on water" effects and catalysis in flow. *Chemical Communications (Cambridge, England)*, Chemical communications (Cambridge, England), 2020-12-21.
143. Pye, Scott J, Dalgarno, Scott J, Chalker, Justin M, & Raston, Colin L. (2018). Organic oxidations promoted in vortex driven thin films under continuous flow Electronic supplementary information (ESI) available: Full experimental details and analytical characterisation. CCDC 1552986 and

1552987. For ESI and crystallographic data in CIF or other electronic format see DOI:
10.1039/c7gc03352d. 2(1), 118-124.

144. Busacca, Carl A, Fandrick, Daniel R, Song, Jinhua J, & Senanayake, Chris H. (2011). The Growing Impact of Catalysis in the Pharmaceutical Industry. *Advanced Synthesis & Catalysis*, 353(11-12), 1825-1864.
145. Luo, Xuan, Mohammed Al-Antaki, Ahmed Hussein, Igder, Aghil, Stubbs, Keith A, Su, Peng, Zhang, Wei, . . . Raston, Colin L. (2020). Vortex Fluidic-Mediated Fabrication of Fast Gelated Silica Hydrogels with Embedded Laccase Nanoflowers for Real-Time Biosensing under Flow. *ACS Applied Materials & Interfaces*, 12(46), 51999-52007.
146. Tavakoli, Javad, Raston, Colin L, & Tang, Youhong. (2020). Tuning Surface Morphology of Fluorescent Hydrogels Using a Vortex Fluidic Device. *Molecules (Basel, Switzerland)*, 25(15), 3445.

Chapter 2: Continuous Flow Thin Film Microfluidic Mediated Nano

Encapsulation of Fish-Oil

Shan He ^{A, B, *,1}, Nikita Joseph ^{B,1}, Xuan Luo ^B, Colin Raston ^{B, *}

A Department of Food Science and Engineering, School of Chemistry Chemical Engineering,
Guangzhou University, 510006, China

B Institute for Nanoscale Science and Technology, College of Science and Engineering, Flinders
University, Bedford Park, Sa, 5042, Australia.

¹ These Authors Contributed Equally to This Work.

Author Contributions

The publication was published in journal LWT – Food Science and Technology 2019. The author contributions are as follows, NJ wrote the original manuscript, concept and design of the experiments, NJ characterized the formulations, carried out the experiments such as particle size, SEM, TEM, AFM and encapsulation studies and conducted the data analysis. SH helped in encapsulation studies, reviewed the original manuscript and finalizing the final manuscript from submission, XL helped in the setup of initial experiment. C.L.R supervised the project.

Abstract

A facile process has been developed for the encapsulation of fish oil using a thin film vortex fluidic device (VFD) operating under continuous flow, allowing control over the size of the encapsulated particles which are spheroidal in shape with diameters ranging from 50 to 250 nm. This microfluidic platform simplifies the processing procedure of water-in-oil-in-water (W/O/W) encapsulation, as now a time and cost saving one-step process devoid of any organic solvents, in contrast to the conventional homogenization process which is inherently complex, involving multiple-steps and the use of organic solvents. Moreover, use of homogenization (as a benchmark to encapsulate fish oil) afforded much larger macro-particles, ranging in size from 2 to 4 μm . Smaller encapsulated particles fabricated using VFD processing could lead to improved absorption from fish oil. Overall, VFD processing provides a new alternative bottom-up approach to easy, scalable processing, without the need for organic solvents which are counterproductive in the food industry.

2.1 Introduction

Long chain omega-3 polyunsaturated fatty acids (PUFAs) are the major component in fish oil, and they are beneficial for human health, improving the fluidity and function of components of cell membranes, and thus enhancing cell metabolism ^{1,2}. PUFAs are however prone to oxidation, resulting in poor bioavailability to the body ^{1,2}. This is compounded by their lipophilic property imparting poor water solubility, and this can be counterproductive for commercial applications of PUFAs. Encapsulation technologies and various colloidal delivery carriers can be used to overcome the bioavailability of omega-3 in our diet, while also allowing its improved controlled release. The conventional method for oil encapsulation involves the use of a surfactant which forms a layer in stabilizing the oil-water interface. These encapsulated particles are conventionally processed through high-energy methods, such as homogenization. The purpose of this is to break the bigger particles into smaller particles through mechanical shear force. Homogenized whey protein isolates and beeswax forms beeswax encapsulation particles ranging in size from 0.5 to 2.0 μm ³. Another group used monodispersed latex to stabilize a water and oil encapsulation system ⁴, with the average diameter of the encapsulated particle ranging from 35 to 75 μm . Compared with “ μm encapsulation”, “nano-encapsulation” provides better characteristics for commercial use in foods, in providing higher absorption in the body and instantaneous release of flavor, and for use in injection medication ^{1,2}. However, it is difficult for conventional homogenization to generate particle-sizes at the nanometer dimensions, unless operating the processing at high pressures, some studies produced nano-crystalline suspensions under such conditions, approximately 200 nm in

diameter ⁵. Moreover, the high cost of a high-pressure homogenizer (approximately USD 150k) limits its application mainly to laboratory operations, rather than extending them into industry.

The vortex fluidic device (VFD), (Fig 2.1), represents a relatively new thin film microfluidic processing platform that has a plethora of diverse research and industrial applications ⁶. VFD processing technology emerged from research efforts focused on the application of thin film microfluidics and thin film flow chemistry ^{7,8,9}. It harnesses high shear forces, intense micro mixing, and high heat and mass transfer, overcoming mixing and heat transfer limitations of traditional batch processing ⁹.

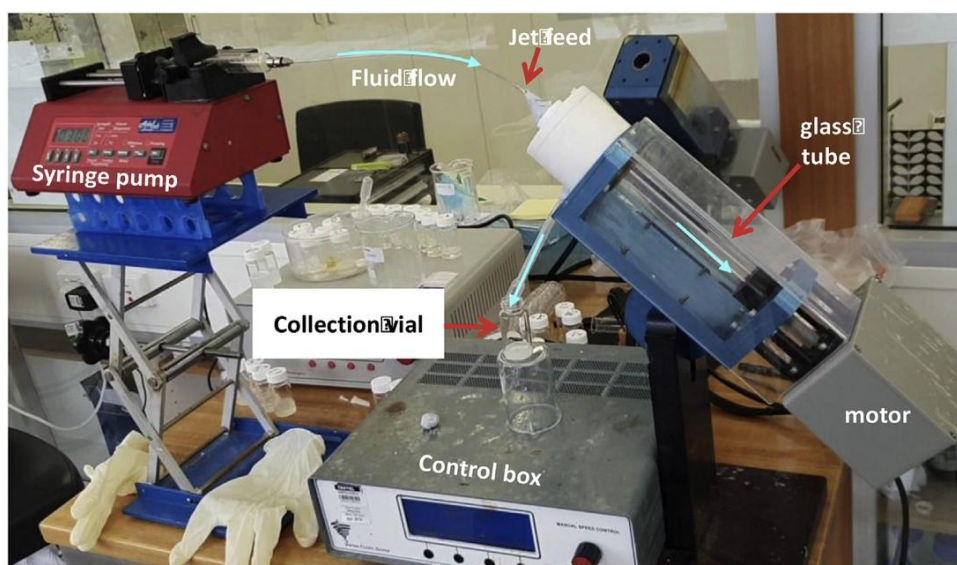


Figure 2.1: Photograph of the vortex fluidic device (VFD) highlighting its salient features. The reagents are delivered via syringe pump into the bottom of the glass tube, gets processed at optimized conditions and collected in the vial.

Processing capabilities of the VFD are rapidly growing, from small molecule synthesis through to processing functional materials for drug delivery, and manipulating single cell organisms ^{8,9,10}. The VFD can be operated under a confined mode where a tube containing a finite volume of liquid is spun at high speed, or operated under continuous flow whereby jet feeds deliver liquid to the bottom of the tube or at positions along the tube, with the device operating otherwise under the same conditions. At high rotational speeds, the liquid in the tube forms a dynamic thin film with the thickness of the film controlled

by varying the rotational speed, tilt angle of rotation, and the volume of liquid in the tube ^{9,10}. The utility of the VFD has been established for a number of chemical transformations, with control over reactivity and selectivity, and the ability to prepare complex molecules in a single pass. Dramatic enhancement of enzymatic reactions has been established, with an average seven-fold acceleration in their catalytic reactions, which arises from Faraday pressure waves within the thin film ¹⁰. Tethering enzymes to the surface of the tube has also been achieved, for the synthesis of complex molecules in a single pass ¹⁰. Then, there are the remarkable results for materials processing under continuous flow, for example, in assembling fullerene C60 molecules into nanotubes ¹². The micron length nanotubes, with hollow diameters of 100–400 nm, are formed in the absence of surfactant, and without the need for further downstream processing ¹². The 3 major VFD operating parameters are rotational speed, flow rate and tilt angle, and these determine the outcome of the high throughput processing. Therefore, the optimization of these 3 parameters is essential for VFD processing and changing them may significantly affect the processing outcome. For example, VFD processing is effective in converting sunflower oil to biodiesel at room temperature, with no saponification, and avoiding the conventional use of co-solvent or complex catalysts. When the flow rate increased from 1 mL/min to 5 mL/min, the percentage of conversion to biodiesel dropped from 100% to 80% ¹¹. VFD processing is also effective in direct transesterification to produce biodiesel from wet microalgae biomass at room temperature. When the rotational speed is increased from 4000 rpm to 8000 rpm, the conversion efficiency of fatty acid methyl ester increased from 30% to 90% ¹³. We were motivated to explore the aforementioned high shear forces and intense micro mixing in the VFD for encapsulation purposes. While the VFD has not been previously used for this purpose, it has been used for uptake of anti-cancer drugs in preformed vesicles of phospholipid mimics ¹⁴. The purpose of the present study is to investigate nano-encapsulation of fish oil, which is rich in poly unsaturated fatty acids, under shear stress in the dynamic thin film in the VFD, in the presence of phospholipids, which act as stabilizers between the aqueous and non-aqueous phases. This VFD-mediated process was compared with the conventional homogenization process, and their encapsulation

efficiencies calculated. This has led to establishing a one-step, time-saving process for the formation of nano-encapsulated particles, which is without precedent.

2.2 Materials

Fish-oil enriched with omega-3 fatty acids was provided by Chemist Warehouse (Australia), and the non-ionic surfactant 1-palmitoyl-2-oleoyl phosphatidylcholine (POPC) was obtained from Sapphire Bioscience (NSW, Australia). Milli-Q water was used throughout the preparations of encapsulated fish oil.

2.3 Methods

2.3.1 Preparation of nano-encapsulations.

Nano-encapsulations were formulated using fish-oil, as a bioactive ingredient, and a mixture of liposome as surfactant, and water. Oil in water nano-encapsulations had a liposome to oil ratio of 1:1 (w:w) with a concentration of the content of liposome and oil to total volume of the suspension in 2 mg/mL. Briefly, 10 mL lipid, oil and water suspension were prepared which contained 20 mg of fish oil, 20 mg of lipid, and 10 mL of water, affording both concentration of lipid and oil at 2 mg/mL with the ratio of lipid to oil at 1:1 (w/w). This suspension was premixed, and then introduced into the borosilicate glass tube (20 mm OD, 17 mm ID) in the VFD through jet-feeds. The VFD operational parameters were: rotational speed of 8000 rpm, flow-rate 0.1 mL/min, tilt angle of 45°. These conditions were applied as the optimal conditions after optimization of speed (4000 rpm to 8000 rpm, Fig S1; Fig S4), flowrate (0.3 mL/min to 0.5 mL/min, Fig S2; Fig S4), and tilt angle (30° to 60°, Fig S3; Fig S4). The device was operated at room temperature and the product processed in the tube was collected and sonicated for 20 min. The traditional homogenization method was also applied for comparison with the VFD processing. Here the same

volume, concentrations and ratio (10 mL lipid, oil and water suspension) was prepared which contained 20 mg of fish oil, 20 mg of lipid, and 10 mL of water, with the concentration of both lipid and oil at 2 mg/mL and the ratio of lipid to oil at 1:1 (w/w) (as used in the VFD). This was then homogenized (homogenizer T25 digital ULTRA-TURRAX) at 13,500 rpm for 10 min at 25 °C. Products processed by homogenization were also collected and sonicated for 20 min.

2.3.2 Particle Size Distribution

The nano-encapsulation particle size distribution and polydispersity index were determined at 25 °C using dynamic light scattering (DLS) (Nano ZS90, Malvern instruments, Worcester, UK) operating with a HeNe 633 nm wavelength laser and a detector angle of 173°. Three independent measurements were performed for each sample. The Malvern zeta sizer instrument measured the time dependent fluctuations of light scattered based on the particle sizes. Samples were too viscous to be analyzed immediately using DLS, but this dropped with time, with the data recorded 20 min after VFD processing. Also, noteworthy is that there was two phase-separation of sample using homogenization processing over 24 h. In contrast, two-phase-separation was not observed from samples generated using VFD processing.

2.3.3 Scanning Electron Microscopy (SEM)

Samples with nano-encapsulated particles were analysed using an Inspect FEI F50 SEM (PS216) instrument. The spot size was 2.0, voltage was 5.0 kV and magnification were 50,000. Sample preparation for SEM was as follows: 20 µL of as-prepared sample was drop cast on a silicon wafer and air dried overnight, followed by platinum sputter coating of a 2 nm thick layer, for SEM imaging.

2.3.4 Transmission Electron Microscopy (TEM)

The nano-encapsulated particles were analyzed using transmission electron microscopy (TEM) (FEI Titan Themis 80-200). The sample preparation was as follows: 20 µL of sample was fixed on the carbon

grids and left to air dry for 1 h, with the excess sample removed using blotting paper, followed by staining using 2 g/100 mL uranyl acetate solution. TEM images were then taken at 250 Å magnification under voltage of 300 keV.

2.3.5 Atomic Force Microscopy (AFM)

Samples with nano-encapsulated particles were analysed using atomic force microscope (AFM) (Nanoscope V, Multimode 2 SPM). Images were acquired using silicon probes in tapping mode in air with Scanner “E” from 500 nm-µm scan sizes. The sample preparation for AFM was as follows: 20 µL of 1: 100 diluted sample was drop casted onto silicon wafer and air dried overnight whereupon the samples were washed 3 times with Milli-Q water prior to recording the AFM images.

2.4 Results and Discussions

2.4.1 Formation of fish-oil in water encapsulations

Processing carried out in the VFD with the tube rotating at 8000 rpm, using a flow rate of 0.1 mL/min, tilt angle 45 °C, and a temperature of 25 °C, afforded a solution that was distinctly different in appearance relative to encapsulation using conventional homogenization. The fish oil solution produced using VFD processing was clear (Fig 2.2c), whereas the solution produced using conventional homogenization was milky (Fig 2.2b). After processing using both techniques, samples were sonicated for 20 min, prior to characterization. Sonication alone (no VFD) effects the physical appearance of the different samples if it was applied for a long period of time.

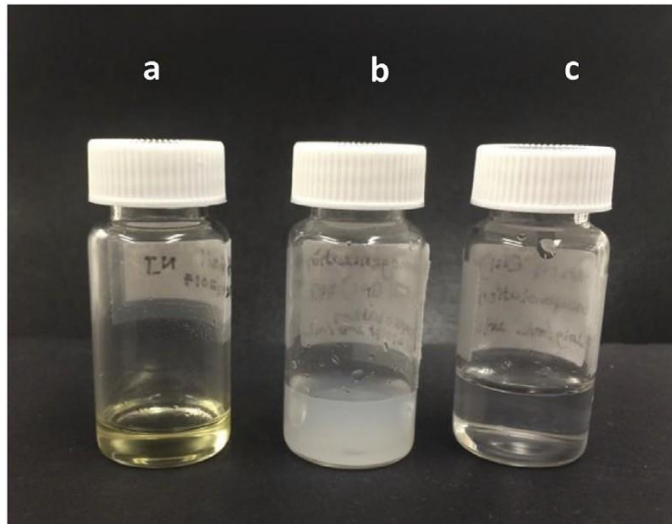


Figure 2.2: Photographs of different samples of fish oil: (a) As received fish oil. (b) Fish oil formulation processed using the homogenization method (speed: 13,500 rpm; time: 10 min; temperature: 25 °C; sonication: 20 min; homogenizer: T25 digital ULTRA-TURRAX). (c) Fish oil formulation processed using a vortex fluidic device (VFD) (dispersed phase: 2 g/100 mL, lipid/oil: 1/1 (w/w), speed: 8000 rpm, flow-rate: 0.1 mL/min, tilt angle: 45°, temperature: 25 °C; sonication post VFD processing for 20 min).

A research report advised that bath sonication has to be applied for a minimum of 30 min to have an impact on physical appearance of nanoparticle suspension¹⁸ the shorter sonication time used in the present study, 20 min, was applied to avoid aggregation of particles, and thus the results from VFD processing and conventional homogenization can be directly compared. The particle size in solution is one of the decisive factors for determining if the solution is transparent or otherwise. Another research reported that solutions change from milky to clear when the particle size is reduced from micrometers in dimensions to about 200–300 nm^{15,16}. A similar particle size encapsulation has also been reported¹⁷. Thus, previous studies are consistent with the different physical appearance between the encapsulation solutions in (Fig 2.2 b and c). To further understand the origin of the difference, a number of imaging characterization techniques were used.

2.4.2 Scanning electron microscopy (SEM)

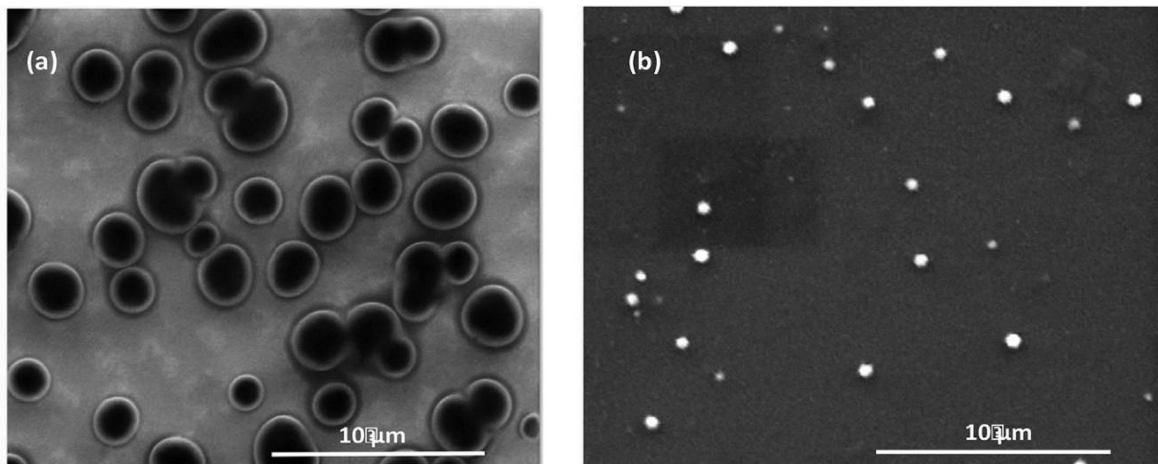


Figure 2.3: SEM images of fish oil encapsulation in phospholipids: (a) Generated using the homogenization method (speed: 13,500 rpm; time: 10 min; temperature: 25 °C, sonication: 20 min). (b) Generated using VFD processing. Samples in (a) and (b) were coated with 2 nm Pt; dispersed phase: 2 g/100 mL, lipid/oil: 1/1 (w/w), speed: 8000 rpm, flowrate: 0.1 mL/min, tilt angle: 45°, temperature: 25 °C; sonication: 20 min.

SEM images of the particle are consistent with the results shown in (Fig 2.2) The conventional homogenization method produced particles approximately 3–4 μm in diameters (Fig 2.3a). In contrast, the particles generated using VFD processing, (Fig 2.3 b), are much smaller, in the nanometer-dimensions, <300 nm in diameter. We note that while this is similar to those generated using an expensive high-pressure homogenization system, the VFD is relatively inexpensive processing technology. Thus, VFD processing potentially represents a significant cost saving approach for encapsulation at the nanometer-dimensions, noting that the VFD is a relatively inexpensive device.

2.4.3 Dynamic light scattering (DLS)

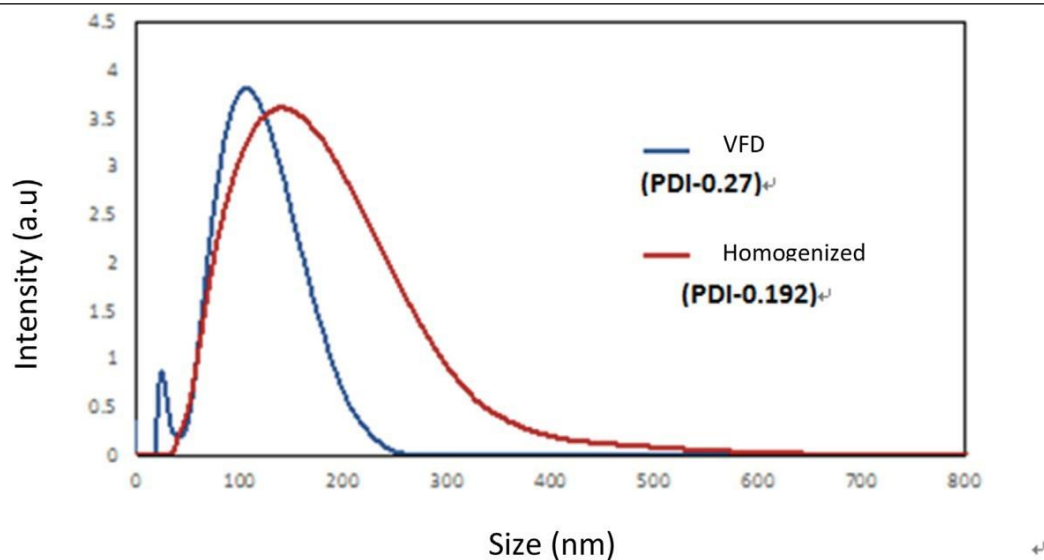


Figure 2.4: Dynamic light scattering (DLS) data (temperature 25 °C; HeNe laser: 633 nm; detector angle: 173°) for encapsulated particles produced using VFD processing, for the optimized processing parameters in (Fig 2.3 caption).

The polydispersity, and the hydrodynamic diameter of the particles generated using VFD processing and homogenization processing were determined using DLS analysis (Fig. 2.4), revealing similar polydispersity (0.27 for VFD process, 0.192 for homogenization process), and 20–250 nm particles with the majority of them distributed between 50 nm and 250 nm in diameter. DLS showed a similarity in diameters of the particles (approximate 50–250 nm, Fig. 2.4) relative to diameters from SEM data (approximate 100–200 nm, Fig. 2.3), for particles generated using VFD processing (hundreds of nm regime). The DLS measurement of particles generated using homogenization processing is different to that determined using SEM (Fig. 2.3a) which were between 2 μm and 4 μm . This is not surprising given that homogenization samples were turbid, unstable, and not transparent, and for such samples DLS is expected to be problematic. The characteristics of the homogenization sample also explain its aforementioned two phase-separation over 24 h.

2.4.4 Transmission Electron Microscopy (TEM)

The internal structure of the fish oil particles encapsulated using a VFD was studied using TEM. For the image in (Fig 2.4), the sample was stained with a 2 g/mL solution of uranyl acetate. The oil phase, which has PUFAs with carbon backbones, takes up more of the uranyl acetate than the aqueous phase, and thus appears darker. The Image shows multiple w/o/w encapsulations in which water particles are trapped in the oil-phase. W/O/W encapsulations are formed when an oil phase, in the presence of surfactant, is rapidly stirred or homogenized at high speed in an aqueous medium. Previous studies also report the formation of the W/O/W encapsulation system. Bodmeier et.al.¹⁵ used ethyl acetate as the organic solvent to form the W/O/W double encapsulation, formed the multiphase of W/O/W microspheres by applying a multiple encapsulation solvent evaporation technique.

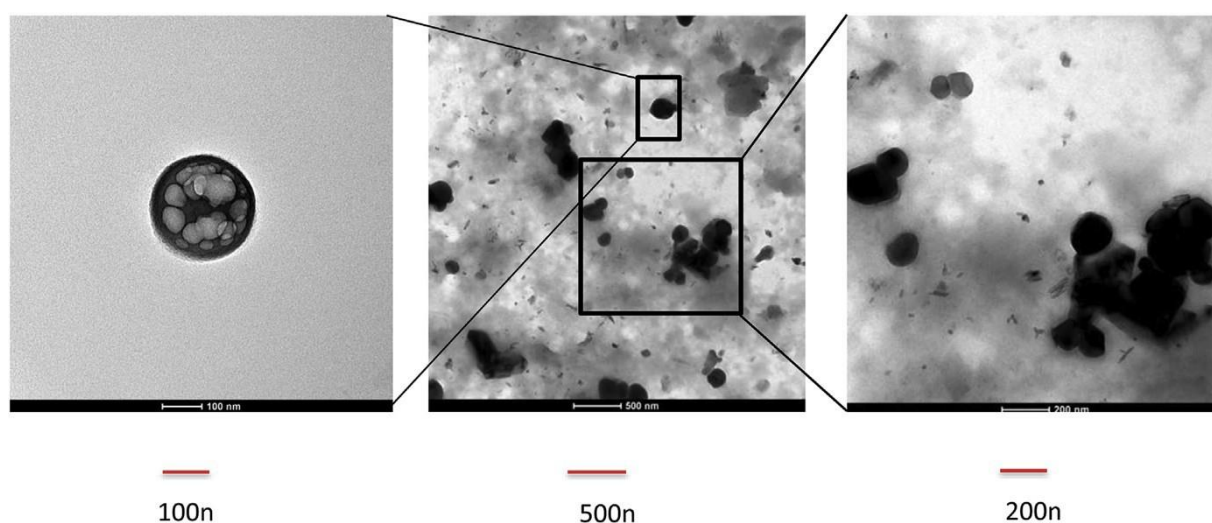


Figure 2.4: *Transmission electron microscopy images of encapsulated particles produced using VFD processing under different magnification, for the optimized processing parameters in (Fig 2). (Sample volume: 20 μ L; staining: 2 g/100 mL uranyl acetate solution).*

However, these earlier processes are complicated, Herrmann et al.¹⁵ taking 3 steps to form the W/O/W encapsulation system, both using organic chemicals. In contrast, the VFD method is a one-step process, which is time-saving, and its use circumvents the need

for using any organic solvents, and thus the overall process is more environmentally friendly. Importantly, processing in the VFD simplifies the processing relative to previous methods for W/O/W encapsulation.

2.4.5 Atomic Force Microscopy (AFM)

The particles generated in the VFD were further studied using AFM, as shown in (Fig 2.5) (Bruker's AutoMET software analysis) with the height of the encapsulated particles estimated to range from 10 to 20 nm (Fig 2.5), interestingly with a 10 nm height approximating to the dimension of two bi-layers of the self-assembled phospholipid, without any content inside the particles.

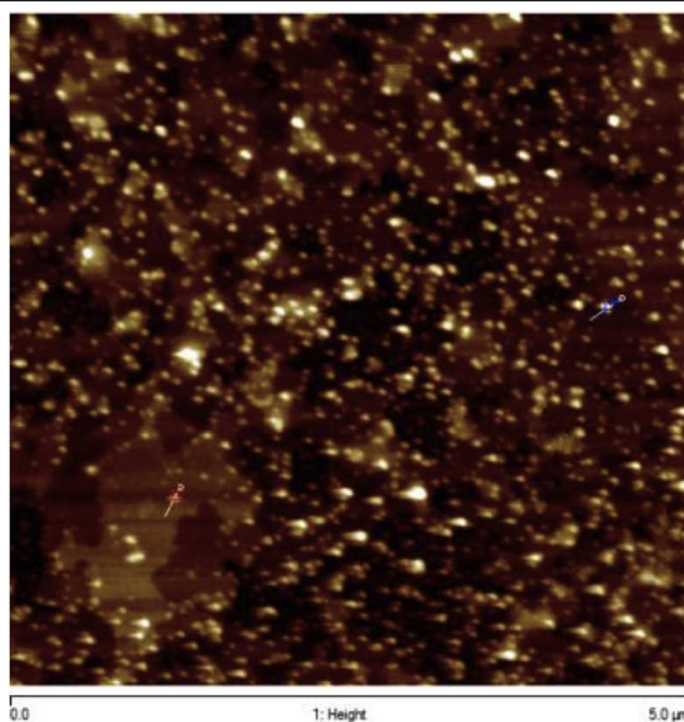


Figure 2.5: Atomic Force Microscopy image (sample volume: 20 μL , dispersed phase: 2 g/100 mL, lipid/oil: 1/1 (w/w), speed: 8000 rpm, flow-rate: 0.1 mL/min, tilt angle: 45°, temperature: 25 °C; sonication post VFD processing for 20 min).

2.4.6. Volume of particles

DLS provides information on the hydrodynamic diameter of the particles, treating them as spherical particles, whereas any anisotropy in shape can come from imaging techniques. The 50–250 nm diameter of particles from DLS corresponds to volumes of the particles 65,500 nm³ to 8,177,000 nm³. TEM measurement established that a typical diameter of a particle is approximate 200 nm. AFM measurement showed that the height of the particles as 10 nm and 20 nm, which corresponds to volumes between 314,000 nm³ and 628,000 nm³, and are within the volumes of particles established using DLS.

2.4.7. Scale-up VFD processing to produce encapsulated fish oil solution

The VFD is designed with the ability to operate under continuous flow for on-demand processing of large volumes of liquid. To establish this herein, we readily translated the processing of a 10 mL solution, as used for all of the above studies, to passing 100 mL of solution within 18 h through the device, with the solution found to have the same overall characteristics, including colloidal stability. The success of this trial demonstrated the stability of VFD process, and the consistency of the quality in the final products, for translating into a larger scale.

2.5 Conclusion

The use of VFD processing of fish oil for its encapsulation was compared with use of conventional homogenization. The diameter of encapsulated particles generated using homogenization ranged from 2 to 4 μm in diameter, whereas much smaller encapsulated particles were generated in the VFD, w/o/w spheroidal particles 50–250 nm in diameter, which potentially are more beneficial towards absorption of the fish oil. The VFD simplifies the procedure for water-in-oil-in-water (w/o/w) encapsulation, avoiding complicated and expensive processing, the use of organic solvents, and dramatically reduces the number of processing steps. Overall, the VFD provides a new direction for bottom– up facial and scalable processing with potential for food processing. Further studies on the use of the VFD in forming nano-

meter dimension particles will focus on further systematically varying the different operating parameters of the VFD (rotational speed, tilt angle, concentrations and ratio of components, temperature, and flow rates), the choice of phospholipid and combinations thereof, and the nature of the fish oil.

Acknowledgements

The authors acknowledge support of this work by the Australian Research Council and the Australian Microscopy and Microanalysis Research Facility (AMMRF) and Australian National Fabrication Facility for SEM, dual target sputter coater and AFM imaging. Authors also acknowledge Adelaide Microscopy at The University of Adelaide, South Australia for TEM imaging, and funding support from "Hundreds of Talents Program ", Guangzhou University, China (funding code:28099201-302).

References

1. Li, J., Shen, Z., Ma, X., Ren, W., Xiang, L., Gong, A., et al. (2015). Neuropeptide YY1 receptors mediate targeted delivery of anticancer drug with encapsulated nanoparticles to breast cancer cells with high selectivity and its potential for breast cancer therapy. *ACS Applied Materials and Interfaces*, 7, 5574–5582.
2. Li, S., Tan, H., Wang, N., Zhang, Z., Lao, L., Wong, C., et al. (2015). The role of oxidative stress and antioxidants in liver disease. *International Journal of Molecular Sciences*, 16, 26087–26124.
3. Nazar, M. R., Hafeezullah, K., & Shahzad, N. (2010). Encapsulation and characterization of controlled release flurbiprofen loaded microspheres using beeswax as an encapsulating agent. *Journal of Materials Science: Materials in Medicine*, 21, 1621–1630.
4. Sacanna, S., & Philipase, A. P. (2006). Preparation and properties of monodisperse latex spheres with controlled magnetic moment for field-induced colloidal crystallization and chain formation. *Langmuir*, 22, 10209–10216.
5. Mostafa, N., Jean-Rene, A., Marc-Antoine, P., & Harivardhan, R. L. (2018). Comparison of high pressure homogenization and stirred bead milling for the production of nanocrystalline suspensions. *International Journal of Pharmaceutics*, 547, 61–71.
6. Britton, J., & Raston, L. C. (2017). Multi-step continuous-flow synthesis. *Chemical Society Reviews*, 46, 1250–1271.

7. Britton, J., Dyer, R. P., Majumdar, S., Raston, C. L., & Weiss, G. A. (2017). Ten-minute protein purification and surface tethering for continuous-flow biocatalysis. *Angewandte Chemie*, 129, 2336–2341.
8. Chen, X., Smith, N. M., Iyer, K. S., & Raston, C. L. (2014). Controlling nanomaterial synthesis, chemical reactions and self-assembly in dynamic thin films. *Chemical Society Reviews*, 5, 1387–1399
9. Britton, J., Chalker, M. J., & Raston, L. C. (2015). Rapid vortex fluidics: Continuous flow synthesis of amides and local anesthetic lidocaine. *Chemistry-A European Journal*, 21, 10660–10665.
10. Britton, J., Meneghini, L. M., Raston, C. L., & Weiss, G. A. (2016). Accelerating enzymatic catalysis using vortex fluidics. *Angewandte Chemie*, 55, 11387–11391.
11. Britton, J., & Raston, L. C. (2014). Continuous flow vortex fluidic production of biodiesel. *RSC Advances*, 4, 49850–49854.
12. Vimalanathan, K., Shrestha, R. G., Zhang, Z., Zou, J., Nakayama, T., & Rastion, C. L. (2017). Surfactant-free fabrication of fullerene C60 nanotubes under shear. *Angewandte Chemie*, 129, 9518-8521.
13. Sitepu, E. K., Corbin, K., Luo, X., Pye, S. J., Tang, Y., Leterme, S. C., et al. (2018). Vortex fluidic mediated direct transesterification of wet microalgae biomass to biodiesel. *Bioresource Technology*, 266, 488–497.
14. Mo, J., Eggers, P. K., Chen, X., Ahamed, M. R. H., Becher, T., Lim, L. Y., et al. (2015). Shear induced carboplatin binding within the cavity of phospholipid minic for increased anticancer efficacy. *Scientific Reports*, 5, 10414.
15. Herrmann, J., & Bodmeier, R. (1995). Somatostatin containing biodegradable microspheres prepared by a modified solvent evaporation method based on W/O/W-multiple emulsions. *International Journal of Pharmaceutics*, 126, 129–138.
16. Honary, S., Ebrahimi, P., & Hadianamrei (2014). Optimization of particle size and encapsulation efficiency of vancomycin nanoparticles by response surface methodology. *Pharmaceutical Development and Technology*, 19, 987–988.
17. Betoret, E., Betoret, N., Rocculi, P., & Rosa, M. (2015). Strategies to improve food functionality: Sstructure-property relationships on high pressures homogenization, vacuum impregnation and drying technologies. *Trends in Food Science & Technology*, 46, 1–12.
18. Adeyemi, S. A., Jon, R. C., Thomas, P., Paige, R., & Arturo, A. K. (2014). Influence of extracellular polymeric substances on the long-term fate, dissolution, and speciation of copper-based nanoparticles. *Environmental Science and Technology*, 48, 12561–12568.



Contents lists available at ScienceDirect

LWT - Food Science and Technology

journal homepage: www.elsevier.com/locate/lwt

Short communication

Continuous flow thin film microfluidic mediated nano-encapsulation of fish oil

Shan He^{a,b,*}, Nikita Joseph^{b,1}, Xuan Luo^b, Colin Raston^{b,*}^a Department of Food Science and Engineering, School of Chemistry Chemical Engineering, Guangzhou University, 510006, China^b Institute for Nanoscale Science and Technology, College of Science and Engineering, Flinders University, Bedford Park, SA, 5042, Australia

ARTICLE INFO

Keywords:

Vortex fluidic device

Encapsulation

Nano-particles

Continuous flow

ABSTRACT

A facile process has been developed for the encapsulation of fish oil using a thin film vortex fluidic device (VFD) operating under continuous flow, allowing control over the size of the encapsulated particles which are spheroidal in shape with diameters ranging from 50 to 250 nm. This microfluidic platform simplifies the processing procedure of water-in-oil-in-water (w/o/w) encapsulation, as now a time and cost saving one-step process devoid of any organic solvents, in contrast to the conventional homogenization process which is inherently complex, involving multiple-steps and the use of organic solvents. Moreover, use of homogenization (as a benchmark to encapsulate fish oil) afforded much larger macro-particles, ranging in size from 2 to 4 μm. Smaller encapsulated particles fabricated using VFD processing could lead to improved absorption from fish oil. Overall, VFD processing provides a new alternative bottom-up approach to easy, scalable processing, without the need for organic solvents which are counterproductive in the food industry.

1. Introduction

Long chain omega-3 polyunsaturated fatty acids (PUFAs) are the major component in fish oil, and they are beneficial for human health, improving the fluidity and function of components of cell membranes, and thus enhancing cell metabolism (Li, Shen et al., 2015; Li, Tan et al., 2015). PUFAs are however prone to oxidation, resulting in poor bio-availability to the body (Li, Shen et al., 2015; Li, Tan et al., 2015). This is compounded by their lipophilic property imparting poor water solubility, and this can be counterproductive for commercial applications of PUFAs. Encapsulation technologies and various colloidal delivery carriers can be used to overcome the bioavailability of omega-3 in our diet, while also allowing its improved controlled release.

The conventional method for oil encapsulation involves the use of a surfactant which forms a layer in stabilising the oil-water interface. These encapsulated particles are conventionally processed through high energy methods, such as homogenization. The purpose of this is to break the bigger particles into smaller particles through mechanical shear force. Nazar, Hafeezullah, and Shahzad (2010) homogenized whey protein isolate and beeswax, forming beeswax encapsulation particle ranging in size from 0.5 to 2.0 μm. Sacanna and Philipase (2006) used monodispersed latex to stabilize a water and oil

encapsulation system, with the average diameter of the encapsulated particle ranging from 35 to 75 μm. Compared with “μm encapsulation”, “nano-encapsulation” provides better characteristics for commercial use in foods, in providing higher absorption in the body and instantaneous release of flavour, and for use in injection medication (Li, Shen et al., 2015; Li, Tan et al., 2015). However, it is difficult for conventional homogenization to generate particle-sizes at the nano-meter dimensions, unless operating the processing at high pressures, as reported by Mostafá, Jean-Rene, Marc-Antoine, and Harivardhan (2018) who produced nano-crystalline suspensions under such conditions, approximately 200 nm in diameter. Moreover, the high cost of a high pressure homogenizer (approximately USD 150k) limits its application mainly to laboratory operations, rather than extending them into industry.

The vortex fluidic device (VFD), Fig. 1, represents a relatively new thin film microfluidic processing platform that has a plethora of diverse research and industrial applications (Britton & Raston, 2017). VFD processing technology emerged from research efforts focused on the application of thin film microfluidics and thin film flow chemistry (Britton & Raston, 2017; Chen, Smith, Iyer, & Raston, 2014). It harnesses high shear forces, intense micro mixing, and high heat and mass transfer, overcoming mixing and heat transfer limitations of traditional

* Corresponding author.

** Corresponding author. Department of Food Science and Engineering, School of Chemistry Chemical Engineering, Guangzhou University, 510006, China.

E-mail addresses: he0091@gmail.com (S. He), colin.raston@flinders.edu.au (C. Raston).

¹ These two authors contributed equally to this work.<https://doi.org/10.1016/j.lwt.2018.12.066>

Received 13 August 2018; Received in revised form 15 November 2018; Accepted 24 December 2018

Available online 26 December 2018

0023-6438/ © 2018 Published by Elsevier Ltd.

Chapter 3: Vortex Fluidic Mediated Food Processing

Shan He ^{1, A, ^*}, Nikita Joseph ^{A, ^}, Xuan Luo ^A, Colin L. Raston ^{A,*}

¹ Department of Food Science, School of Chemistry and Chemical Engineering, Guangzhou University, Guangzhou, Guangdong, 510006, China.

^A Flinders Institute for Nanoscale Science and Technology, College of Science and Engineering, Flinders University, Bedford Park, South Australia, 5042, Australia

[^] As the First Author(S), These Two Major Authors Contributed Equally to This Work.

Author Contributions

The publication was published in journal Plos One 2019. The author contributions are as follows, NJ wrote the original manuscript, concept and design of the experiments, NJ characterized the formulations and carried out the experiments such as curcumin encapsulation, particle size, UV-spectroscopy and fluorescence measurements. SH reviewed the original manuscript and finalized for the submission. SH carried out raw milk pasteurization and enzymatic hydrolysis experiments. XL helped in the setup of initial experiment. C.L.R supervised the project

Abstract

The high heat and mass transfer, and controlled mechanoenergy, in angled vortex fluidics has been applied in chemical and material sciences and allied fields, but its utility in food processing remains largely unexplored. Herein we report three models of food processing incorporating such vortex fluidics, including enzymatic hydrolysis, raw milk pasteurization and encapsulation. The processing times of enzymatic hydrolysis was reduced from about 2–3 hours to 20 minutes, with the processing time of raw milk pasteurization reduced from 30 to 10 minutes, and an encapsulated particle size reduced approximately 10-fold, from micro meters to hundreds of nanometers. These findings highlight exciting possibilities, in exploiting the value of vortex fluidic mediated processing in the food industry.

3.1 Introduction

The advance of modern technologies has significantly improved the traditional methods of food processing. This has resulted in shorter processing times as well as the development of “new food” with better nutritional or functional values than traditional food products. For example, protein hydrolysates with smaller molecular weights from fish or milk ^{1,2} enhance its absorbance in the body, therefore increasing its nutritional values ¹ and yoghurt, cheese or other traditional food with encapsulated fish oil or other nutritional substances is possible without destabilizing the food system. In comparison with the traditional pasteurization method, the application of advanced Ultra Heat Temperature (UHT) pasteurization has significantly increased the shelf life of milk without reducing its nutritional value ³. Nevertheless, there are a number of challenges in the current food processing industries. Most of these relate to the balance between the quality of the final products and the cost of production. While protein hydrolysis from fish, milk and other protein sources provided the protein-based food with higher nutritional value, the processing time required to hydrolyze food protein into small peptides is about 2–3 hours ⁴. This is at odds with food industry practice and cost considerations, requiring an acceptable processing time within 0.5 hours ⁵. Regarding encapsulation of small particles, this results in instantaneous release of flavor and functioning of the confined substances. Currently it is difficult for conventional homogenization to generate particle-sizes at the nano-meter dimensions, unless operating the processing at high pressures, as reported by ⁶ for generating nano-crystalline suspensions under such conditions, with the particles approximately 200 nm in diameter. However, the high cost of a high-pressure homogenizer (approximately USD 150k) limits its application mainly to laboratory operations, rather than extending them into industry. Indeed, in comparison with the traditional pasteurization method, the application of advanced Ultra High Temperature (UHT) pasteurization has significantly increased the shelf life of milk without reducing its nutritional value. Nonetheless, an UHT system costs over USD 1 million and is therefore difficult for small farms and small businesses to implement, in comparison with the cost of only USD 15,000 for establishing a traditional pasteurization system ².

Therefore, an innovative low-cost system with dramatically improved heat transfer and/or high shear has the potential to revolutionize the food processing industry⁷. Vortex fluidics represents a new processing capability that enables new tools and synthetic strategies with a diversity of research and industrial applications. Core processing technology has emerged from research efforts focused on the application of thin film microfluidics and thin film flow chemistry. This has resulted in the ability to harness high shear forces, intense micro mixing, and high heat transfer to enhance and explore reactivity relative to traditional batch processing⁸. This led to the development of the Vortex Fluidic Device (VFD) (Fig 3.1) which has a rapidly growing number of processing capabilities, from small molecule synthesis to processing advanced materials, for various applications such as in drug delivery, and manipulating



Figure 3.1: Photograph of the vortex fluidic device (VFD) highlighting its salient features. The reagents are delivered via syringe pump into the bottom of the glass tube, gets processed at optimized conditions and collected in the vial.

single cell organisms⁹. The VFD can operate under the confined mode of operation where a tube containing a finite volume of liquid is spun at high speed, or operate under continuous flow where jet feeds deliver liquid to the base of the tube or at positions along the tube under the same conditions. A dynamic thin film is formed at high rotational speeds with the thickness of the thin film controlled by

varying the rotational speed and tilt angle of the tube or the volume of liquid in the VFD tube, which under continuous flow, depends on the flow rate ⁸. The utility of the VFD has been established for a number of chemical transformations, with control over reactivity and selectivity, and the ability to prepare complex molecules in a single pass in the thin film microfluidic platform. Dramatically enhancing enzymatic reactions has been established, with an average seven-fold acceleration for a diversity of enzymes ¹⁰. This arises from the Faraday pressure waves contained within the thin film. Tethering enzymes to the surface of the tube has also been established, for the synthesis of small molecules in a single pass ⁹. The VFD has also been applied in materials processing under continuous flow, such as in assembling fullerene C60 molecules into nanotubes ¹¹. The micron length nanotubes, with hollow diameters 100 to 400 nm, are formed in the absence of surfactant, and without the need for further downstream processing. The operating parameters of VFD can be systematically explored, as high throughput processing, in optimizing any process, as in effectively converting sunflower oil to biodiesel at room temperature, with no saponification and avoiding the conventional use of co-solvent or complex catalysts ¹². The thin film generated by the VFD significantly increases heat transfer and shear forces, which are two critical conditions/requirements in food processing, as discussed above. Thus far, the VFD as the showcase tool for vortex fluidics, has not been applied in food processing, other than preliminary findings on the encapsulation of fish oil ¹³. This involved operating the VFD under continuous flow for controlling the size of spheroidal encapsulated fish oil particles, from 50 to 250 nm. Moreover, use of homogenization (as a benchmark to encapsulate fish oil) afforded much larger macro-particles, ranging in size from 2 to 4 μ m. Smaller encapsulated particles fabricated using VFD processing could lead to improved absorption from fish oil.

Herein we explore the utility of the VFD thin film microfluidic platform in food processing, targeting three models of food processing, namely enzymatic hydrolysis, pasteurization and encapsulation. The effects of VFD processing are compared with the traditional processing technology. Overall, the data in

this communication letter establishes a conceptual basis with respect to the application of the VFD in food processing

3.2 Materials

Both milk powder (Coles, Australia) and fish oil (Swiss, Australia) were food grade and purchased from local markets. Neutrase was purchase from Novozyme Australia (U3/22 Loyalty Road, North Rocks, NSW, 2151). Raw milk (unpasteurised) was provided by Bd farm Paris Creek PTY LTD (9/7 Paris Creek Rd, Paris Creek SA 5201) 24 hours before the commencement of the trial processing. Sucrose monolaurate and curcumin were purchased from Sigma- Aldrich, Australia (12 Anella Avenue, Castle Hill, NSW, 2154).

3.3 Methods

3.3.1 Enzymatic hydrolysis of protein in milk powder.

Ten grams of milk powder was fully dissolved in 50 mL of water. One percent Neutrase (w/w, enzyme to milk powder, 0.1 g) was added in the milk powder solution. For the conventional enzymatic hydrolysis method, 1 mL of the dissolved milk powder along with the enzyme was transferred into a 5mL container and heated at 55°C for 2 hours using a water bath, followed by heating at 95°C for 15 minutes to deactivate the enzyme. For VFD enzymatic hydrolysis method, 1 mL of the dissolved milk with enzyme was transferred into the VFD tube (20 mm O.D. and 17.5 mm I.D., 18.5 cm in length). The confined mode of operation of the VFD was used, with the tube spun at 8000 rpm for 20 minutes, at a tilt angle of 45 degrees. The processing conditions of 8000 rpm rotation speed and tilt angle of 45 degrees were recognized as the optimal processing conditions for a number of previous VFD studies ^{14,9}. The temperature of the VFD tube was maintained at 55°C using a heating jacket. After that, the temperature

of the VFD tube was elevated to 95°C and maintained at this temperature for 15 minutes in the VFD to deactivate the enzymes. Matrix-assisted laser desorption/ionization (MALDI) mass spectrometry was conducted for both the liquid samples after hydrolysis of the dissolved raw milk powder, for determining the molecular weights, which were used as the indicator of hydrolysis efficiency.

3.3.2 Curcumin encapsulation with fish oil and sucrose mono-laurate as an emulsifier.

Nano-encapsulations were formulated using curcumin, as a bioactive ingredient, and a mixture of non-ionic surfactant and water. Briefly, 10 mg of curcumin was mixed and dissolved in 60 mg of fish oil. Then the curcumin-fish oil mixture was premixed with 10 mg of sucrose mono-laurate and 10 mL of water using a benchtop vortex mixer, which was required because of the viscous nature of fish-oil, with the uniform suspension then introduced into the borosilicate glass tube (20 mm OD) in the VFD through jet-feeds, with the tube rotating at 8000 rpm, at a flow-rate of 0.1 mL/min, with the tilt angle of the tube at 45° and the device operating at room temperature. The solution was collected and sonicated for 20 minutes. The traditional homogenization method was also applied for comparison with the VFD processing. Here the same concentrations as used above in the VFD were homogenized (homogenizer T25 digital ULTRA-TURRAX) at 13,500 rpm for 10 minutes at 25°C and similarly the homogenized solution was sonicated for 20 minutes.

3.3.3 Particle size measurements.

Oil in water (O/W) emulsions particle size distribution and polydispersity index were determined at 25°C using dynamic light scattering (DLS) (Nano ZS90, Malvern instruments, Worcester, UK) operating with a He-Ne 633 nm wavelength laser and a detector angle of 173°. Three independent measurements were performed for each sample. The Malvern zeta sizer instrument measured the time dependent fluctuations of light scattered based on the particle sizes. All the o/w emulsions were diluted in 1:10 with Milli Q water for all measurements.

3.3.4 UV-visible absorption spectroscopy measurements.

The absorption spectra for all the samples were measured on Cary 50 Bio UV-visible spectrophotometer at 25°C. The maximum absorption of curcumin was recorded at pH 7 at 25°C using a quartz cuvette of path-length 10 mm.

3.3.5 Fluorescence spectroscopy measurements.

All the fluorescence measurements were carried out with a Cary Eclipse Fluorescent Spectrophotometer, Agilent Technologies, using a quartz cuvette with a path-length 10 mm. Both excitation and emission band slits were fixed at 10 nm and the scan rate was selected at 1800 nm/min. The excitation wavelength was selected at 425 nm while emission spectra were collected in the range of 450 to 600 nm.

3.3.6 Raw milk pasteurization.

For the conventional processing, 1mL of raw milk was sealed in a 5mL container and pasteurized at 60°C for 30 minutes in a water bath. VFD processing used the confined mode with 1mL of raw milk transferred into a VFD tube and spun at 8000 rpm with the tilt angle at 45°. For different trials, the heating temperatures were set at 60°C, 50°C and 40°C, and for each temperature the VFD was operated for 30, 20, 10 and 5 minutes, respectively. Alkaline Phosphatase tests were carried out on all pasteurized samples for determining the efficiency of the pasteurization.

3.3.7 Measurement tests.

MALDI mass spectrometry was used to determine the enzymatic hydrolysis efficiency, and Alkaline Phosphatase tests were used to determine the pasteurization efficiency, carried out according to standard methods.

3.4 Results and Discussions

3.4.1 Enzymatic hydrolysis of protein in milk powder

The appearances of dissolved milk powder, dissolved milk powder after VFD-enzymatic hydrolysis, and dissolved milk powder after conventional enzymatic hydrolysis are shown in (Fig 3.2). The hydrolyzed protein after enzymatic hydrolysis is a protein that has been partially broken down, and therefore possesses lower molecular weight in comparison with intact protein. The cloudiness of the liquid in (Fig 3.2-c) might indicate poor efficiency of hydrolysis, as reported by ¹⁵. In comparison, the clear solution of (Fig 3.2-b) is consistent with improved efficiency of hydrolysis, even though the processing was much shorter (20 minutes compared with 2 hours for conventional processing). This observation was confirmed using MALDI mass spectrometry analysis. The peaks on the left and right side in (Fig 3.2) indicate protein with the lowest and highest MW, respectively. Milk protein is composed of a mixture of proteins with various sizes with wide m/z values from 0 to 25000 (Fig 3-A). Prior to processing, there were several peaks from 12500 to 25000 m/z for the non-processed dissolved milk powder (Fig 3.2-A). However, these peaks were not observed after hydrolysis using either the VFD or conventional processing (Fig 3.2-B and 3.2-C). Comparing the two processing techniques, it can be seen that the peaks in (Fig 3-B) were more concentrated on the left than those in (Fig 3.2-C). This indicates that the MW of the dissolved milk powder after VFD-enzymatic hydrolysis is smaller than the dissolved milk after conventional enzymatic hydrolysis, thereby demonstrating greater efficiency of hydrolysis assisted by VFD processing. Enzymatic hydrolysis has been carried out in an industrial scale, although there are some concerns, including the cost of enzymes as reported by ⁵, and processing time. The current enzyme cost for the cellulose to ethanol process is approximately USD 5 per gallon ethanol. However, the market-acceptable price is USD 1.07 per gallon, which requires a 10-fold reduction in the cost of the enzyme ¹⁶. As to processing time, this can be up to 3 hours with the food industry preferring enzymatic hydrolysis

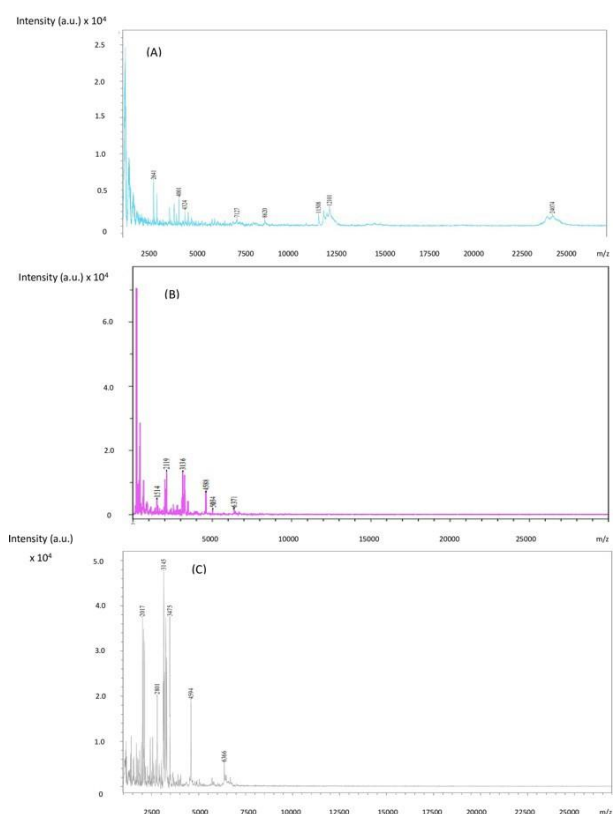
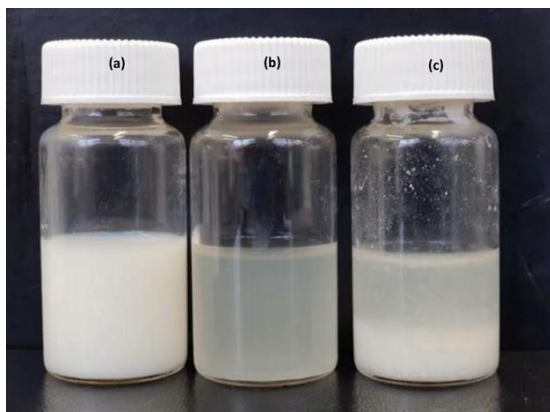


Figure 3.2: Enzymatic hydrolysis of protein. (Left) Appearance of dissolved milk powder with (a) no treatment; milk powder: water = 1:5 (w/v). (b) VFD-enzymatic hydrolyzation; milk powder: water = 1:5 (w/v); temperature at 55 °C; processing time of 20 mins; VFD speed at 8000 rpm; VFD tilt angle of 45°. (c) Conventional enzymatic hydrolyzation; milk powder: water = 1:5 (w/v); temperature at 55 °C; processing time of 20 min. (Right) MALDI mass spectra analysis of dissolved milk powder before and after different treatments (a) No treatment; milk powder: water = 1:5 (w/v). (b) VFD-enzymatic hydrolyzation; milk powder: water = 1:5 (w/v); temperature at 55 °C; processing time of 20 mins; VFD speed at 8000 rpm; VFD tilt angle at 45°. (c) Conventional enzymatic hydrolyzation; milk powder: water = 1:5 (w/v); temperature at 55 °C; processing time of 20 min.

processing time down to 20 min⁵. The current trend is to develop new technologies to increase the efficiency of enzymes, to reduce the amount of enzyme required and/or the time of 20 mins; processing time.¹⁷ immobilized glucose oxidase on TiO₂ /Polyurethane for removal of a dye, with the resulting decolorization efficiency increased from approximate 60% for no immobilization to almost 100%.⁵

developed a microwave-assisted enzymatic process which increased the production yield from 42% to 62.5%, and shortened the processing time from 2hrs to 20 min. The development of VFD technologies in this study presented another technology with the potential to enrich this trend.

3.4.2 Curcumin encapsulation in O/W emulsions.

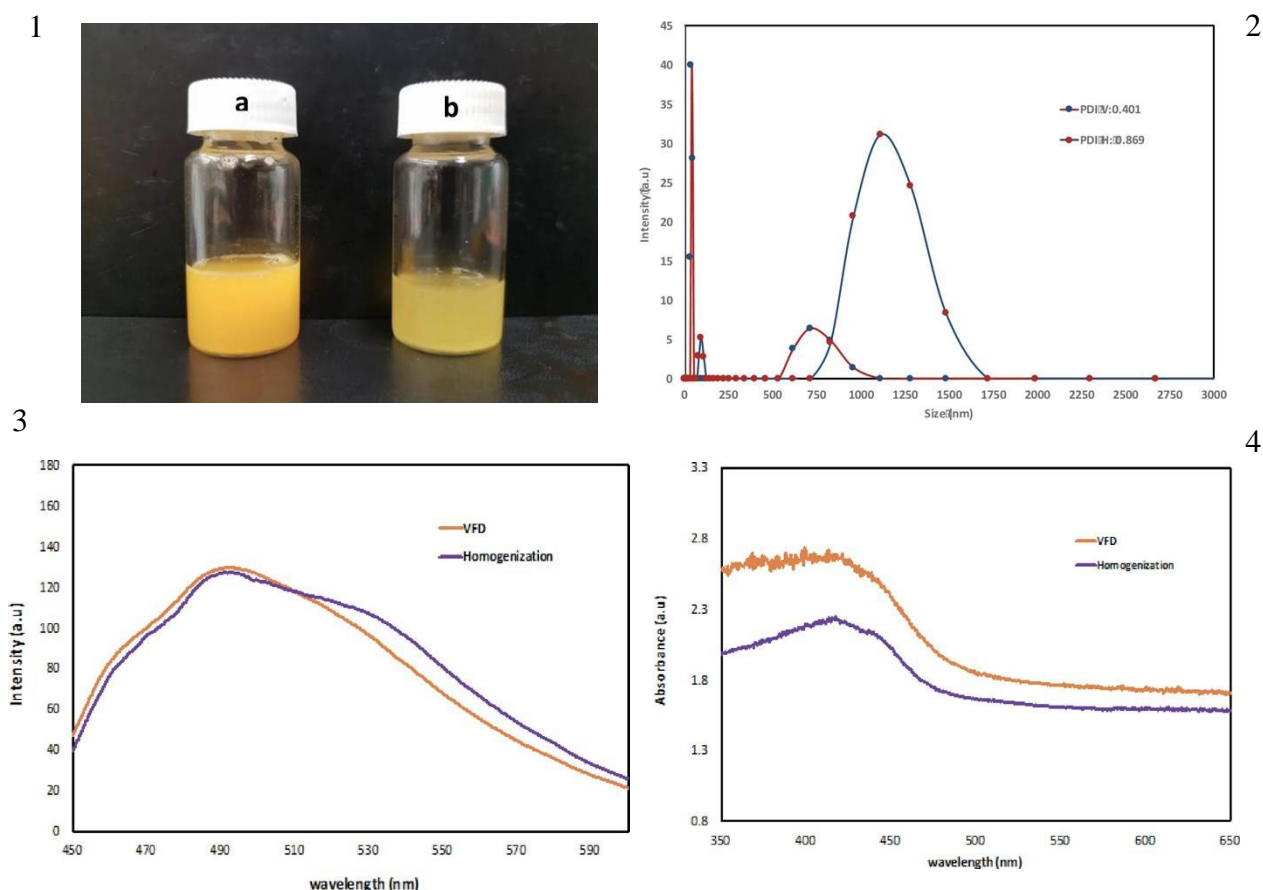


Figure 3.3: Curcumin encapsulation of O/W emulsions. 1-a) O/W emulsion homogenized 1-b) O/W emulsion of VFD. 2) Particle size data for homogenized and VFD samples. 3) Fluorescence spectrum of homogenized and VFD samples. 4) UV-spectrum of homogenized and VFD samples.

(Fig 3.3) demonstrates that there are significant differences of particle size between the curcumin encapsulated by conventional homogenization method and VFD processing. Though there are 2 peaks shown for the diagrams of both conventional homogenization method and VFD processing, the conventional homogenization method produced capsules with the major size distribution above 1000 nm.

In contrast, VFD processing significantly reduced the majority of the particles to the size of less than 1000 nm. This finding is supported by the different appearance of curcumin encapsulated from different treatments. The solution of encapsulated curcumin processed using VFD processing was clearer (Fig 3.3-a), whereas the solution of encapsulated curcumin processed by homogenization method was less transparent (Fig 3.3-b). In this context, the particle size in solution is one of the decisive factors for transparency of solution or otherwise. Another group reported that the cloudiness of solution is drastically reduced once the particle size is less than 200 nm¹⁸. A similar particle size of encapsulated curcumin has been previously reported¹⁹. However, to achieve this, high-pressure homogenization using a system costing about USD 150,000 was required. In contrast, the current cost of approximate USD 20,000 for VFD makes it a dramatically less expensive technology, and thus VFD processing represents a significant cost saving processing, in achieving quality encapsulation. Scaling up of the VFD processing will be a focus of future studies, with the aim of improving the current industrial production of homogenization at large scale. The effectiveness of encapsulation was further measured using fluorescent spectroscopy (Fig 3.3-3). Curcumin has intrinsic fluorescence with a wide intensity band between 540–550 nm in aqueous medium²⁰. A shift is observed at 500 nm for both VFD and homogenization samples. This shift is indicative of interactions between sucrose mono-laurate and curcumin micelles. However, comparing with the VFD generated sample, the homogenization sample has a broader fluorescent spectrum curve at 530 to 540 nm. This is likely to be due to the presence of curcumin not encapsulated during the homogenization processing. UV-visible spectroscopy was also used to characterize the samples (Fig 3.3-4). Curcumin has a strong absorbance band at 425 nm associated with $\pi - \pi$ excitation of the di-ketone rings²¹. A 5nm blue shift is observed at 420 nm, highlighting a change in the molecular environment of the curcumin, noting curcumin in a more hydrophobic environment typically has such a blue-shift⁶.

3.4.3 Pasteurization of raw milk






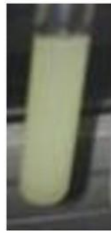






time \ temperature	30 min	20 min	10 min	5 min
60°C				
50°C				
40°C				

Figure 3.4: Pasteurization of raw milk. The effect of VFD-pasteurization with different processing times (5–30 min) and temperatures (40–60°C) on raw milk (VFD Mode: confined mode; VFD rotation speed: 9000 rpm; VFD tilt angle: 45°).

The effect of VFD-pasteurization with different processing times and temperatures on raw milk is shown in (Fig 3.4). The white color in (Fig 3.4) shows that there is no color change during the test, which would arise from complete deactivation of Alkaline Phosphatase. The lack of color change confirmed the complete pasteurization. In contrast, the yellow color in (Fig 3.4) is indicative of incomplete pasteurization. The standard conventional pasteurization method requires the raw milk to be processed at 60°C for 30 minutes. As seen from (Fig 3.4), the VFD-pasteurization is unable to reduce the pasteurization temperature, but it was effective in reducing the processing time from 30 minutes to 10 minutes. While this is still longer than the standard processing time for UHT, which is 1–2 seconds at

135°C, the shorter processing time in the VFD preserves the nutritional value. This aside, the UHT equipment costs approximately USD 1–2 million, considerable more than the cost of a VFD, as discussed above. Overall, VFD-pasteurization provides the balance between cost and nutritional value for milk pasteurization, but this will require addressing scaling up for the processing using, for example in using a larger diameter tube in the VFD.

3.5 Conclusion

We have established the utility of the VFD in food processing, for three different food models. The high heat transfer and shear stress (mechanoenergy) in the VFD is effective in shortening the processing time of enzymatic hydrolysis from about 2–3 hours to 20 minutes. In the same vein, the VFD was effective in reducing the processing time of standard pasteurization from 30 minutes to 10 minutes, and in reducing the size of encapsulated curcumin particles, from approximate 1000 nm to less than 100 nm, without requiring expensive processing homogenization equipment. This initial data and analysis demonstrates a potential of VFD processing in the food industry, noting that the device itself is relatively inexpensive.

Acknowledgements

The authors acknowledge support from the Australian Research Council (ARC Discovery Grant DP170100453) and Flinders Analytical Facility for MALDI measurements, and acknowledge the provision of in kind by Bd farm Paris Creek PTY LTD (9/7 Paris Creek Rd, Paris Creek SA 5201).

References

1. Valle B.C.S., Dantas E.M., Silva J.F.X., Bezerra R.S., Correia E.S., Peixoto S.R.M., et.al. (2015). Replacement of fishmeal by fish protein hydrolysates and biofloc in the diets of *Litopenaeus vannamei* postlarvae. *Aquaculture Nutrition*, 21 (1), 105–112.

2. Awad S., El-Sayed M.I., Wahba A., Attar A., Yousef M.I., & Zedan M. (2016). Antioxidant activity of milk protein hydrolysate in alloxan-induced diabetic rats. *Journal of Dairy Science*, 99 (11), 8499–8510. <https://doi.org/10.3168/jds.2015-10626> PMID: 27592424
3. Zhang Y.D., Zheng N., Han R.W., Zheng B.Q., Yu Z.N., Li S.L., et.al. (2014). Occurrence of tetracyclines, sulfonamides, sulfamethazine and quinolones in pasteurized milk and UHT milk in China's market. *Food Control*, 36 (1), 238–242.
4. He S., Franco C. & Zhang W. (2012). Process optimization and physicochemical characterization of enzymatic hydrolysates of protein from co-products of Atlantic Salmon and Yellowtail Kingfish. *International of Journal of Food Science and Technology*, 47(11), 2397–2404.
5. He S., Franco C. & Zhang W. (2015). Fish Protein Hydrolysates: Application in Deep-fried Food and Food Safety Analysis. *Journal of Food Science*, 80 (1), E108–E115. <https://doi.org/10.1111/1750-3841.12684> PMID: 25559171
6. Ming Y., Fengwen H., Haidong Y., Hong X., Liangliang S., Tianwen H., et.al. (2015). Study on interaction between curcumin and pepsin by spectyoscopic and docking methods. *International Journal of Biological Macromolecules*, 79, 201–208. <https://doi.org/10.1016/j.ijbiomac.2015.04.057> PMID: 25940524
7. Chemat F., Rombaut N., Meullemiestre A., Turk M., Perino S., Fabiano-Tixier A. et.al. (2017). Review of green food processing techniques. Preservation, transformation, and extraction. *Innovative Food Science & Emerging Technologies*, 41, 357–377.
8. Britton J., Chalker M.J., & Raston C.L. (2015). Rapid vortex fluidics: continuous flow synthesis of amides and local anesthetic lidocaine. *Chemistry-A European Journal*, 21(30), 10660–10665.
9. Britton J., Dyer R.P., Majumdar S., Raston C.L. & Weiss G.A. (2017). Ten-minute protein purification and surface tethering for continuous-flow biocatalysis. *Angewandte Chemie*, 129 (9), 2336–2341.
10. Britton J., Meneghini L.M., Raston C.L. & Weiss G.A. (2016). Accelerating enzymatic catalysis using vortex fluidics. *Angewandte Chemie*, 55 (38), 11387–11391. <https://doi.org/10.1002/anie.201604014> PMID: 27493015
11. Vimalanathan K., Shrestha R.G., Zhang Z., Zou J., Nakayama T. & Rastion C.L. (2017). Surfactant-free fabrication of fullerene C60 nanotubules under shear. *Angewandte Chemie*, 129 (29), 9518–8521.
12. Britton J., & Raston C.L. (2014). Continuous flow vortex fluidic production of biodiesel. *RSC Advances*, 4, 49850–49854.
13. He S., Joseph N., Luo X., & Raston C. (2019). Continuous flow thin film microfluidic mediated nanoencapsulation of fish oil. *LWT-Food Science and Technology*, 103, 88–93.

14. Luo X., Smith P., Raston C.L. & Zhang W. (2016). Vortex fluidic device-intensified aqueous two phase extraction of C-phycoerythrin from *Spirulina maxima*. *ACS Sustainable Chemistry & Engineering*, 4 (7), 3905–3911.
15. Al-Shamsi A., Mudgil P., Mohamed H. & Maqsood H. (2018). Camel milk protein hydrolysates with improved technofunctional properties and enhanced antioxidant potential in in vitro and in food model systems. *Journal of Dairy Science*, 10(1), 47–60.
16. Liu G., Zhang J., & Bao J. (2015). Cost evaluation of cellulose enzyme for industrial-scale cellulosic ethanol production based on rigorous Aspen Plus modelling. *Bioprocess and Biosystems Engineering*, 39 (1), 133–140. <https://doi.org/10.1007/s00449-015-1497-1> PMID: 26541585
17. Shoabargh S., Karimi A., Dehghan G., & Khataee A. (2014). A hybrid photocatalytic and enzymatic process using glucose oxidase immobilized on TiO₂ /polyurethane for removal of a dye. *Journal of Industrial and Engineering Chemistry*, 20 (5), 3150–3156.
18. Honary S., Ebrahimi P., & Hadianamrei K (2014). Optimization of particle size and encapsulation efficiency of vancomycin nanoparticles by response surface methodology. *Pharmaceutical Development and Technology*, 19 (8), 987–988. <https://doi.org/10.3109/10837450.2013.846375> PMID: 24147898
19. Betoret E., Betoret N., Rocculi P., & Rosa M. (2015). Strategies to improve food functionality: structure- property relationships on high pressures homogenization, vacuum impregnation and drying technologies. *Trends in Food Science & Technology*, 46 (1), 1–12.
20. Wu Y., & Wang X. (2017). Binding, stability, and antioxidant activity of curcumin with self-assembled casein–dextran conjugate micelles. *International Journal of Food Properties*, 20(12), 3295–3307.
21. Kaur, Kumar, & Mehta. (2015). Nanoemulsion: A new medium to study the interactions and stability of curcumin with bovine serum albumin. *Journal of Molecular Liquids*, 209, 62–70.

RESEARCH ARTICLE

Vortex fluidic mediated food processing

Shan He^{1,2,4*}, Nikita Joseph^{2,4‡}, Xuan Luo², Colin L. Raston^{2*}

1 Department of Food Science, School of Chemistry and Chemical Engineering, Guangzhou University, Guangzhou, Guangdong, China, **2** Flinders Institute for NanoScale Science and Technology, College of Science and Engineering, Flinders University, Bedford Park, South Australia, Australia

* These authors contributed equally to this work

‡ These authors are co-first authors on this work

* colin.raston@flinders.edu.au (CLR); he0001@gmail.com (SH)

Abstract

The high heat and mass transfer, and controlled mechanoenergy, in angled vortex fluidics has been applied in chemical and material sciences and allied fields, but its utility in food processing remains largely unexplored. Herein we report three models of food processing incorporating such vortex fluidics, including enzymatic hydrolysis, raw milk pasteurization and encapsulation. The processing times of enzymatic hydrolysis was reduced from about 2–3 hours to 20 minutes, with the processing time of raw milk pasteurization reduced from 30 to 10 minutes, and an encapsulated particle size reduced approximately 10-fold, from micrometers to hundreds of nanometers. These findings highlight exciting possibilities, in exploiting the value of vortex fluidic mediated processing in the food industry.

OPEN ACCESS

Citation: He S, Joseph N, Luo X, Raston CL (2019) Vortex fluidic mediated food processing. PLoS ONE 14(5): e0216816. <https://doi.org/10.1371/journal.pone.0216816>

Editor: Stuart Prescott, University of New South Wales, AUSTRALIA

Received: December 3, 2018

Accepted: April 29, 2019

Published: May 30, 2019

Copyright: © 2019 He et al. This is an open access article distributed under the terms of the [Creative Commons Attribution License](https://creativecommons.org/licenses/by/4.0/), which permits unrestricted use, distribution, and reproduction in any medium, provided the original author and source are credited.

Data Availability Statement: All relevant data are within the manuscript and its Supporting Information files.

Funding: The authors acknowledge support from the Australian Research Council (ARC Discovery Grant DP170100453) and Flinders Analytical Facility for MALDI measurements, and acknowledge the provision of in kind by B&I farm Paris Creek PTY LTD (977 Paris Creek Rd, Paris Creek SA 5201). The funders had no role in study design, data collection and analysis, decision to publish, or preparation of the manuscript.

2. Introduction

The advance of modern technologies has significantly improved the traditional methods of food processing. This has resulted in shorter processing times as well as the development of “new food” with better nutritional or functional values than traditional food products. For example, protein hydrolysates with smaller molecular weights from fish or milk [1,2] enhance its absorbance in the body, therefore increasing its nutritional values [1] and yoghurt, cheese or other traditional food with encapsulated fish oil or other nutritional substances is possible without destabilizing the food system. In comparison with the traditional pasteurization method, the application of advanced Ultra Heat Temperature (UHT) pasteurization has significantly increased the shelf life of milk without reducing its nutritional value [3].

Nevertheless, there are a number of challenges in the current food processing industries. Most of these relate to the balance between the quality of the final products and the cost of production. While protein hydrolysis from fish, milk and other protein sources provided the protein-based food with higher nutritional value, the processing time required to hydrolyze food protein into small peptides is about 2–3 hours [4]. This is at odds with food industry practice and cost considerations, requiring an acceptable processing time within 0.5 hours [5]. Regarding encapsulation of small particles, this results in instantaneous release of flavor and functioning of the confined substances. Currently it is difficult for conventional homogenization to generate particle-sizes at the nano-meter dimensions, unless operating the processing at high

Chapter 4: Vortex Fluidic Mediated Encapsulation of Functional Fish Oil

Featuring *in Situ* Probed Small Angle Neutron Scattering

Shan He ^{1,5}, Nikita Joseph ^{2,5}, Marzieh Mirzamani ^{3,5}, Scott J. Pye ², Ahmed Hussein Mohammed Alanataki ², Andrew Whitten ⁴, Yaonan Chen ¹, Harshita Kumari ^{3*}, Colin L. Raston ^{2*}

¹ Department of Food Science and Engineering, School of Chemistry Chemical Engineering, Guangzhou University, 510006, China

² Flinders Institute for Nanoscale Science and Technology, College of Science and Engineering, Flinders University, Bedford Park, SA 5042, Australia

³ Division of Pharmaceutical Sciences, James L. Winkle College of Pharmacy, University of Cincinnati, Cincinnati, OH 45267-0004, USA

⁴ Australian Nuclear Science and Technology Organization (ANSTO), New Illawarra Road, Lucas Heights, NSW 2234

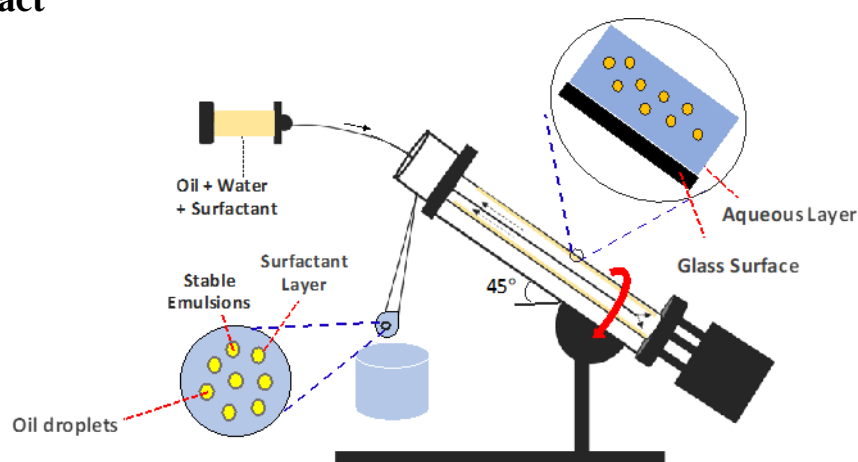
⁵ Authors contributed equally to this work

Author Contributions

The publication was published in Nature Publishing Journal – Science of food 2020. The author contributions are as follows, S.H.: formed the general frame of the idea for this project, wrote the main manuscript text, revised/reviewed manuscript for final version approval, and prepared figures, concept, design, and literature review for the research. N.J.: wrote the main manuscript text, revised/reviewed manuscript for final version approval, prepared figures, concept, design, and literature review for the research, and carried out experimental studies at Australian Nuclear Science and Technology Organization (ANSTO). NJ carried out the encapsulation studies, the neutron scattering experiments at ANSTO, particle size, TEM, UV-spectroscopy measurements for all the encapsulation studies. M.M.

carried out data analysis/interpretation and writing for the Small Angle Neutron Scattering (SANS) section. S.J.P. and A.H.M.A.: assisted the SANS experiments at ANSTO. A.W. assisted the setup of experiments at ANSTO. Y.C.: carried out the sensory evaluation and confocal microscopy in china for this research. H.K.: supervised and carried out data analysis/ interpretation and writing for the SANS section. C.L.R.: supervised the whole project and guided for all the experiments.

Graphical Abstract



Abstract

Major challenges for optimizing the benefits of fish oil on human health are improved bioavailability while overcoming the strong odor and avoiding significant oxidation of the omega-3 polyunsaturated fatty acids (PUFAS). The scalable continuous flow thin film vortex fluidic device (VFD) improves the tween 20 encapsulation of fish oil relative to conventional homogenization processing, with the fish oil particles significantly smaller and the content of the valuable omega-3 fatty acids higher. In addition, after 14 days storage the remaining omega-3 fatty acids content was higher, from ca 31.0% for raw fish oil to ca 62.0% of freeze-dried encapsulated fish oil. The VFD mediated encapsulated fish oil was used to enrich the omega-3 fatty acid content of apple juice, as a model water-based food product, without changing its sensory values. the versatility of the VFD was further demonstrated in forming homogenous suspensions of fish oil containing water-insoluble bioactive molecules, curcumin and quercetin. We also

captured, for the first time, real-time structural changes in nano-encapsulation by installing a VFD with *in situ* small angle neutron scattering. Real-time measurements as such afford valuable insight into the self- assembly occurring in solution.

4.1 Introduction

Fish oil is an excellent dietary source of omega-3 polyunsaturated fatty acids (PUFAS) having positive effects on human health. However, it has a strong odor and is easily oxidized at ambient conditions¹ and omega-3 PUFAS cannot be synthesized in the human body, and thus it needs to be sourced from food². Capsules of fish oil protect omega-3 PUFAS from oxidation, but their large size limits their utility as nutritional supplements. Encapsulating fish oil in nanoparticles also protects omega-3 PUFAS from oxidation, and has exciting possibilities in food processing. Although such confinement of one substance (active agent) within another (wall material)³ has been broadly studied for fish oil^{4,5}, the methods used either require multiple steps or expensive processing equipment. The vortex fluidic device (VFD) (Fig 1) is a continuous flow thin film microfluidic platform with diverse applications⁶. It harnesses high shear forces, intense micro mixing, and high mass transfer to overcome the mixing and heat transfer limitations akin to traditional batch processing⁷. Processing capabilities of the VFD are rapidly growing across various fields, ranging from small molecule synthesis involving a number of steps being accomplished in a single pass to processing functional materials for drug delivery and manipulating single-cell organisms⁸. Enzymatic reactions in the VFD have on average a sevenfold acceleration in their catalytic reactions⁹, depending on the choice of processing parameters of the device, including rotation speed of the inclined glass tube⁹. Tethering enzymes to the surface of the glass tube has also been achieved for the synthesis of complex molecules in a single pass under continuous flow conditions¹⁰. Fabricating nanomaterials in the VFD has yielded unexpected results, also under continuous flow, for example, in assembling fullerene C₆₀ molecules into nano-tubules with hollow diameters of 100–400 nm, in the absence of a surfactant and without the need for further downstream processing¹¹. Other noteworthy applications of the VFD are converting sunflower oil to biodiesel at room temperature with no

saponification and avoiding the conventional use of co-solvents or complex catalysts¹², and the direct transesterification of micro-algal¹³. As a preliminary trial, our previous study¹⁴ established that for low concentrations of the fish oil (fish oil: surfactant = 1:1 (w/w), fish oil + surfactant: water = 2 mg/ml), the VFD is effective in encapsulating fish oil particles below 300 nm, whereas those produced by homogenization are 3–4 μm in diameter. Though the low concentration in this study was not industry-applicable because of the high cost of concentrating and drying the material, this proof-of-concept achievement encouraged us to follow up with a high concentration study, to drastically reduce the cost of the overall processing. In the present study, we report a simple low-cost, single pass VFD process for encapsulating fish oil using high concentration feedstocks (fish oil: surfactant = 1:1(w/w), fish oil + surfactant: water = 0.2 g/ml), as well as the ability to simultaneously encapsulate sparingly water-soluble bioactive polyphenols. The encapsulated omega-3 fatty acids become protected from oxidation, and the encapsulation is effective in enriching the omega-3 fatty acid content in liquid food. Also reported is a small angle neutron scattering (SANS) method for studying the shear stress-induced encapsulation process under real time conditions in the VFD. Notably post-VFD SANS studies have been reported¹⁷, however, real-time measurement of self-assembly in solution is being reported here for the first time.

4.2 Materials

Fish oil enriched with omega-3 fatty acids was provided by Chemist Warehouse (Australia). Tween 20 was purchased from Sigma-Aldrich (NSW). Milli-Q water was used throughout the preparations of the encapsulated fish oil.

4.3 Methods

4.3.1 Fish oil encapsulated with Tween 20

The encapsulation process using VFD were operated according to He et al.³⁰ with modifications.

Encapsulation of fish oil, the bioactive ingredient, used a mixture of Tween 20, as a surfactant, and water.

Oil in- water encapsulations had a surfactant-to-oil ratio of 1:1 (w: w) with a total concentration of 0.2 g/mL. Briefly, 10 mL of the Tween 20 oil suspension in water was premixed as an emulsion (1 g of oil, 1 g of Tween 20, and 8mL of water) and then added to a borosilicate glass tube (20mm OD, 17mm ID) in the VFD through jet feeds with the tube rotating at 9000 rpm, at a flow rate of 0.3 mL/min, with the tilt angle of the tube at 45°, and the device operating at room temperature. This condition was deemed as the optimal condition for encapsulation of fish oil after systematically varying the rotational speed (4000–9000 rpm), flow rate (0.3–0.5 mL/min), and tilt angle (30°–60°). The traditional homogenization method was also applied for comparison with VFD processing. Indeed, the oil to surfactant ratio of 1:2 has a slightly better effect, but the implication of this ratio would cause more surfactant to be used in production. This would increase the production cost. Therefore, the conditional optimization was chosen to be 1:1. Homogenization, the conventional method for encapsulation, served as a control for the present study, using the same concentrations that were used for VFD processing with the homogenizer (T25 digital ULTRA-TURRAX) operating at 13,500 rpm for 10 min, at 25 °C. The VFD-mediated encapsulated fish oil solution was freeze-dried for further use.

4.3.2 DLS technique

The particle-size distribution of VFD-encapsulated fish oil and the polydispersity index were determined at 25 °C using DLS (Nano ZS90, Malvern instruments, Worcester, UK) operating with a He–Ne 633 nm wavelength laser and a detector angle of 173°. The Malvern zeta sizer instrument measured the time-dependent fluctuations of light scattered based on the particle sizes.

4.3.3 Epi-fluorescence microscopy

Images of encapsulated particles were recorded using an epi-fluorescent microscope with a monochrome camera (NIKON DS-Qi1Mc), a Cool LED pE300, and appropriate filter cubes. A 20 Å~ long-working-distance (20Å~amplification) objective with an exposure time of 100 ms and a frame rate of

approximately 10 fps was applied. Images taken by the microscope were analyzed using the program ImageJ.

4.3.4 Fatty acid profile of fresh fish oil and VFD-encapsulated fish oil before and after 14 days

Fresh fish oil and freeze-fried VFD-encapsulated fish oil before and after 14 days of storage were subjected to fatty acid profile measurements following the method described by He et al.³¹, with slight modification. Extracted fats were converted to fatty acid methyl esters (FAME), separated, and then measured on a Hewlett-Packard 6890 gas chromatograph equipped with a 50-cm capillary column (0.32 mm internal diameter SGE; Victoria, Australia) coated with 70% cyanopropyl polysilphenylenesiloxane (BPX-70; 0.25- μ m film thickness), which was fitted with a flame ionization detector. Helium was the carrier gas (flow rate 60 mL min⁻¹), and the split ratio was 20:1. The injector temperature was set at 250 °C and the detector temperature at 300 °C. The initial oven temperature was 140 °C and was programmed to rise to 220 °C for 5 min and held for up to 3 min. FAMEs were identified based on the retention time of standards obtained from Nucheck Prep Inc. (Elysian, MN, USA) using the Chemstation software. An external standard was analyzed and used for calibration.

4.3.5 Encapsulation efficiency

The VFD-mediated encapsulated fish oil was freeze-dried, and the oil content of the fish oil particles before and after 14 days of storage was measured according to He et al.³¹. Encapsulation efficiency was calculated as the percentage of the oil content of the freeze-dried VFD-mediated encapsulated fish oil in the fish oil starting material (1 g).

4.3.6 Enrichment of apple juice with nano-encapsulated fish oil

An intake of approximately 0.2 g of omega-3 fatty acids per day is recommended²². Based on this information, 250 mL of commercial apple juice was enriched with 0.2 g of fish oil and 0.4 g of freeze-

dried encapsulated fish oil which contained 0.2 g of fish oil, respectively. This preparation made the concentration of fish oil in enriched apple juice 0.8% (w/v), regardless of VFD-encapsulated fish oil or original fish oil. Samples were stirred with a magnetic stirrer for 1 h.

4.3.7 Sensory tests

Sensory tests were conducted according to Zeng et al.³² with slight modifications. Forty volunteers were recruited according to standard procedures. The sensory evaluation was performed in private booths equipped with Sensory Management System hardware (2006) and computerized sensory software (Sensory Integrated Management System, Morristown, NJ, USA). The volunteers received 1 h of training in discrimination testing, followed by five rounds of practice triangle testing. Volunteers who scored poorly more than twice during these five rounds of practice tests were eliminated from the panelist pool. The number of panelists who passed the practice triangle test was 20. Sensory evaluation consisting of color, taste, aroma, and overall acceptance were based on hedonic scales (1: dislike extremely; 5: like extremely). Each sample was scored individually, and the samples were presented to the panelists in individual plastic containers. The samples were coded and randomly presented to the panel group at each session. Water was presented to rinse their palate between samples³³.

4.3.8 Encapsulation capacity for curcumin and quercetin

Encapsulations were formulated using 30 mg of starting raw material (curcumin or quercetin), 1 g of fish oil, and 1 g of Tween 20. Briefly, 10 mL of a 30mg starting raw material, 1 g of fish oil, and 1 g of Tween 20 suspension in water was premixed as an emulsion, then introduced into a borosilicate glass tube (20mm OD, 17mm ID) in the VFD through jet feeds with the tube rotating at 9000 rpm, at a flow rate of 0.3 mL/min, with the tilt angle of the tube at 45°, and the device operating at room temperature. The product was collected, then centrifuged at 3000 rpm for 20 min. The precipitate after centrifugation, which was non-encapsulated starting raw material, was collected and dissolved in 200 mL of 80% (v/v)

ethanol for the measurement of absorbance at a wavelength of 420 nm. The standard curve with the x-axis of the weight of dissolved starting raw material in 200 mL of 80% (v/v) ethanol and y-axis of absorbance was generated. The weight of precipitated starting raw material was determined according to this standard curve. The encapsulation efficiency of curcumin and quercetin was calculated according to the following

equation:

Encapsulation Efficiency (%).

$$= \frac{30 \text{ mg of original material} - \text{the weight of the precipitated material}}{30 \text{ mg of original material}} \times 100$$

4.3.9 Confocal Microscopy technique

Encapsulations were formulated using 30 mg of curcumin or quercetin, 1 g of fish oil, and 1 g Tween 20. Briefly, 10 mL of 30 mg curcumin or quercetin, 1 g of fish oil, and 1 g of Tween 20 suspension in water was premixed as an emulsion, then introduced into a borosilicate glass tube (20 mm OD, 17 mm ID) in the VFD through jet feeds with the tube rotating at 9000 rpm, at a flow rate of 0.3 mL/min, with the tilt angle of the tube at 45°, and the device operating at room temperature. The product was collected, then centrifuged at 3000 rpm for 20 min. The supernatant was collected for confocal microscopy according to the method described by Coklin et al.³⁴ with slight modifications. Briefly, 25 µL of the supernatant was dripped onto the slide and covered with a glass slide, then dried overnight. Nail varnish was applied to seal the ends of the glass slide after drying overnight. A confocal laser scanning microscope was then applied to observe the microstructure of the encapsulated particles, with the wavelength at 420 nm for curcumin and 370 nm for quercetin, which are the excitation wavelengths of curcumin and quercetin, respectively.

4.3.10 Fluorescence Spectroscopy measurements

All the fluorescence measurements were carried out with Cary Eclipse Fluorescent Spectrophotometer, Agilent technologies using quartz cells of path-length 10 mm. Both excitation and emission band slits were fixed at 10 nm and the scan rate was selected at 1800 nm/min. The excitation wavelength was selected at 425 nm, while emission spectra were collected in the range of 450–600 nm for curcumin and the excitation wavelength for quercetin was 440 nm while the emission was collected in the range 500–600 nm.

4.3.11 Statistical analysis.

The measurements of emulsifying stability and encapsulation capacity for curcumin and quercetin were carried out in triplicate. The measurements of sensory tests were carried out for 20 replicates (20 qualified panelists). Data were presented as the mean with standard deviation. One-way analysis of variance (ANOVA) and least significant difference (LSD) using MINITAB Statistical Software v15 were applied in the statistical analysis. The significance was judged statistically by the F value at a probability (p) below 0.05.

4.3.12 Small-Angle Neutron Scattering (SANS).

Solutions of 10 wt% Tween 20 were prepared in D₂O at room temperature and allowed to equilibrate for 24 h, while 10 wt% Tween 20 with 10 wt% fish-oil were mixed together in D₂O using a magnetic stirrer. D₂O was used as the solvent to improve the contrast between the continuous and dispersed phases. SANS scans were taken at 0 rpm (static) to serve as a baseline of comparison for the higher speeds. Depending on the VFD speed, different volumes of sample were added to a quartz VFD tube to ensure that the thin film would not go too high up the side of the tube. For the real-time 4000 rpm scans, 2mL of sample was added to the sample tube, while 1mL was used for the 7000 and 9000 rpm runs. SANS experiments were carried out at Bilby (small-angle neutron scattering time of flight) (ANSTO) and

Quokka (small-angle neutron scattering) (ANSTO) with neutron wavelength $\lambda=5 \text{ \AA}$. The VFD microfluidic device was mounted on an xyz θ goniometer stage. The stage was adjusted with respect to the neutron beam such that the beam-center was placed 3 cm from above the base of the tube, schematically shown in Fig. 3. For all experiments, a quartz tube is used instead of normal borosilicate glass tube to reduce background for SANS. All the quartz tubes possess 20 mm OD. An aluminum shield was put on the VFD to protect the tube from any outside impacts. Slits were cut from the sides of the shield and covered with aluminum foil in order to reduce the loss of beam intensity due to scattering off of or absorption into the aluminum. Sample detector distances of 1.3, 12.0, and 20.0m were used to achieve a q-range of $0.00216 < q < 0.38125 \text{ \AA}^{-1}$, where $q=(4\pi/\lambda) \sin\theta$, 2θ is the scattering angle, and λ is the wavelength. The acquisition times for all experiments were 60min. each. Mantid software was employed for all data reduction. The 2D data were corrected for background scattering, empty tube scattering, solvent scattering using D2O blanks processed at each VFD speed (0, 4000, 7000, and 9000 rpm), and detector sensitivity, and then set to absolute scale based on the beam transmission. The reduced 2D data were then radially averaged to obtain the 1D data. The 1D data was analyzed in Igor Pro (WaveMetrics, Portland, OR, USA) using the analysis macros developed at NIST19. The general equation describing the scattering for particulate systems is $I(q) = \frac{N}{V} (\rho_1 - \rho_2)^2 P(q) S(q)$ where N is the number of scatterers, V is the total sample volume, ρ_n is the scattering length density (SLD) for the solvent phase or particle phase and $(\rho_1 - \rho_2)^2$ is the contrast factor, P(q) is the form factor that describes the particle geometry, and S(q) is the structure factor describing the inter-particle interactions. Here, the form factor used was spheres with a Gaussian polydispersity term for the radius. This form factor is well-known and can be found in the SANS Toolbox 35 for example, which also provides a great deal of information on the SANS technique and other models in general. The presence of correlation peaks in the scattering data indicated that there were interparticle interactions, necessitating the use of a structure factor. The strong correlation peak could not be modeled well by a hard-sphere interaction, but the screened Coulomb interaction was able to model the peak suggesting that the scattering particles were

charged and repelling each other electrostatically. The repulsive potential, $U(r)$, for the screened

$$\text{Coulomb interaction is } U(r) = \begin{cases} \infty, & r \leq \sigma \\ \left(\frac{z_1 z_2 e^2}{4 \pi \epsilon_0 \epsilon_r} \right) \frac{e^{-\kappa r}}{r}, & r > \sigma \end{cases} \quad \text{where } r \text{ is the center-to-center}$$

distance between the ionic particles, σ is the diameter of the particle, z is the charge of the particle, ϵ is the dielectric constant of the solvent, ϵ_0 is the permittivity of free space, and κ is the Debye–Hückel inverse screening length. By using the mean spherical approximation to solve the Ornstein–Zernike equation for particulate systems, the direct correlation function $c(r)$ becomes $c(r) = -\beta U(r)$, where $\beta = 1/(kBT)$ is the inverse temperature in energy units. This analytical solution was developed by Hayter and Penfold³⁶ and further expanded by Hansen and Hayter³⁷ for instances where $S(q)$ is needed to analyze experimental data. Further discussion of this structure factor can be found in those references.

4.4 Results and Discussion

The oil-in-water encapsulations had a surfactant-to-oil ratio of 1:1 (w: w), and a total concentration of 0.2 g/mL (10 mL of the Tween 20 oil suspension in water was premixed as pretreatment for both VFD processing and the control of homogenization processing, which was composed of 1 g of oil, 1 g of Tween 20, and 8mL of water. The VFD was operated at optimized conditions, where the rotation speed was 9000 rpm, flow rate 0.3 mL/min, tilt angle 45°, and 25 °C. The tilt angle of 45° has been reported as the optimal angle in many previous studies regarding VFD operation^{9,10,14–16}. Our previous study¹⁴ regarding fish oil encapsulation at low concentration also reported that the particle size of encapsulated fish oil was the smallest when the tilt angle was set at 45° while operating the VFD, as measured by dynamic light scattering (DLS). Tween 20 was selected as the surfactant due to its food grade category and long-chain character, which are two fundamental requirements for fish oil encapsulation in high concentration for food application. (Fig 4.1a, b) shows the appearance of the fish oil encapsulation solution immediately after processing and 24 h later, respectively. While both samples were

homogeneous immediately after processing, the sample prepared using homogenization phase separated after 24 h, whereas that prepared using VFD processing was stable over the same period. The encapsulation stability of the immediately prepared mixture (Fig 2e) processed using the VFD (96%) was significantly higher than that processed using homogenization (72%). These results were in accordance with the images shown in (Fig 4.1a, b) and reflect the appearance of white oily foam on top of encapsulation liquid. The combination of these results demonstrated that in comparison with conventional method of homogenization, the VFD method is more efficient to form stable emulsions. Epi-fluorescent microscopy, (Fig 4.1c, d) clearly establishes that the particle sizes of the encapsulation sample processed by homogenization were much larger than those of the sample processed by VFD, and this comparison was further complimented by DLS data (Fig 4.1f).

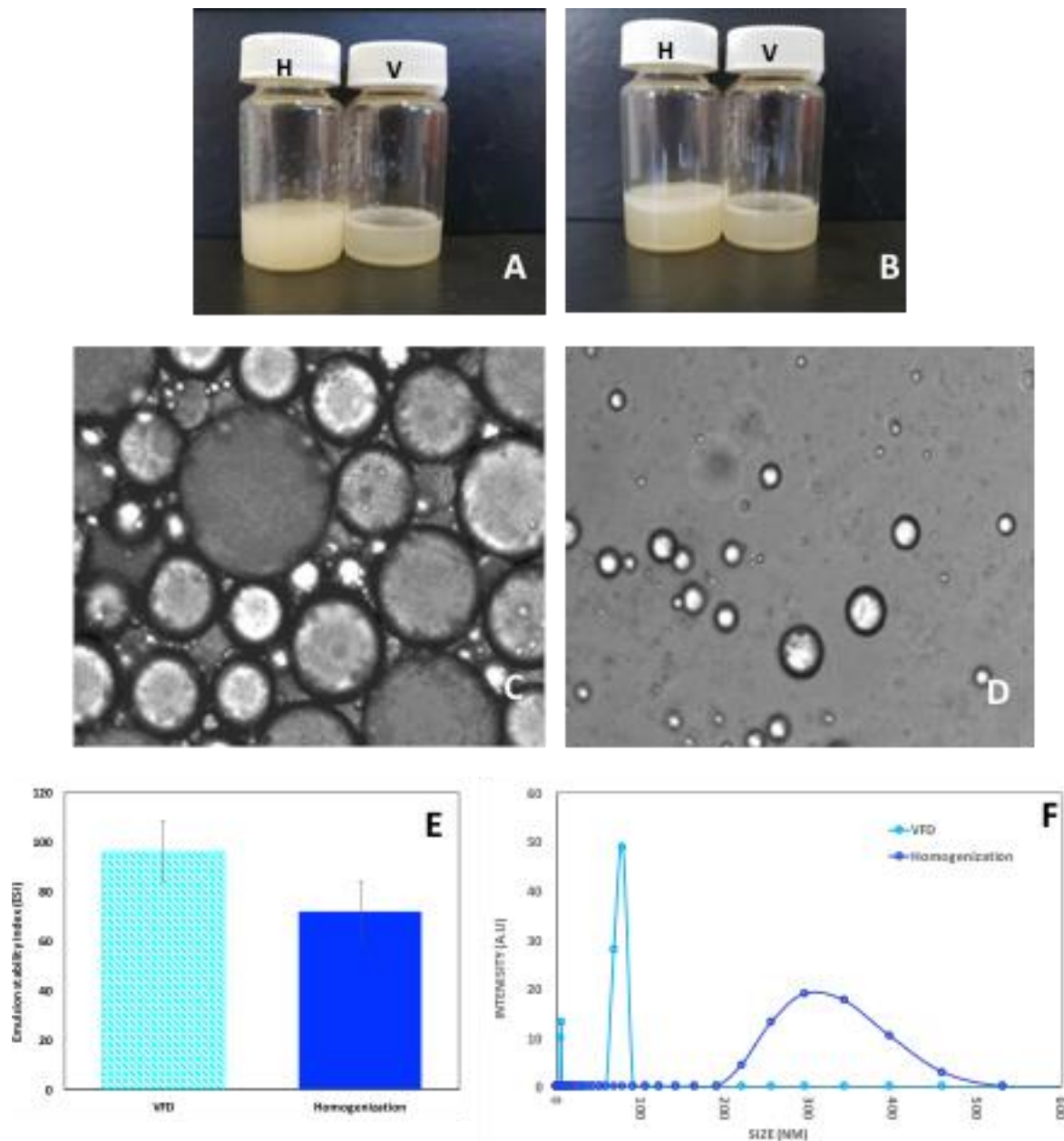


Figure 4.1: Fish oil encapsulation with tween 20 (A) Homogenization processed mixture (speed: 13,500 rpm; time: 10 min; temperature: 25°C) immediately after processing (H) and VFD processed mixture (rotational speed: 9000 rpm; flow rate: 0.3 mL/min; tilt angle: 45°; temperature: 25°C) immediately after processing (V). (B) The mixtures in (A) after 24 hours. (C) and (D) Epi-fluorescence microscopic images (20 X long-working-distance; exposure time 100 ms; frame rate 10 fps) for the homogenization and VFD processed mixtures in (A) respectively. (E) Emulsion stability of homogenization and VFD processed mixtures in (A). (F) Dynamic light scattering (temperature: 25°C; He-Ne wavelength: 633 nm detector angle: 173°C) results of homogenization and VFD mixtures prepared in (A).

Particles of VFD encapsulated fish oil were much smaller than that of homogenization-encapsulated fish oil (Fig 4.1f). Indeed, due to the accuracy of current DLS technique, DLS results were better considered as guidance, but both DLS results and Epi-fluorescent microscopic results demonstrated the dramatic size difference between the samples produced by homogenization and VFD. In comparison with particle sizes of samples produced by homogenization, the particle sizes of samples produced by VFD are drastically reduced. The difference between encapsulated particle size using VFD and homogenization processing for different lipid surfactants was similar to that for low concentrations of lipid ¹⁴. Furthermore, VFD processing is able to provide continuous processing, whereas homogenization is only able to provide batch processing. Considering the industrial production regarding cost of operation, labor, etc., using continuous process is more favorable for industry. To establish this herein, we translated the processing of a 10mL solution, as used for all of the above studies, to passing 100 mL of solution within 18 h through one device. The resulting solution had the same overall characteristics, including colloidal stability. The success of this trial demonstrates the stability of VFD processed material, and the consistency of the quality in the final products, for translating into even larger scale processing involving a number of devices operating simultaneously. It is also noteworthy that a high-pressure homogenization system with micro jet feed might also be able to generate similar results to that of the VFD. However, the high cost of this system (approximately USD 150 k) limits its application mainly to laboratory processing. In contrast, a VFD system is relatively inexpensive and is applicable for both laboratory and industry applications, with the cost of one VFD device USD 15 K. Thus, for the cost of purchasing one high-pressure homogenization system, 10 VFD can be purchased with much larger production capacity when operating under continuous flow in parallel. The energy consumptions of the VFD and homogenizer have also been considered. For the VFD operating at 9000 rpm (optimal rotational speed), the energy input is 232 w and given that it takes 7 min for the first drop of liquid to be collected, for then 35 min of processing to pass 10 mL of solution through the device at of 0.3 mL/min (optimal flow rate), the total energy consumption is 162.4 wh. The energy input of the homogenizer (T25 digital ULTRA-

TURRAX) is 800 w and for 10 min processing of 10 mL of solution (optimal processing parameters), the energy consumption is 136 wh. Clearly the energy consumption for 10 mL of liquid is less in the homogenizer, but under continuous flow processing in the VFD, the energy consumption for this device becomes competitive; passing 420 mL of liquid through the VFD consumes 232 w \times [(7 min + (35 min \times 42))/60] h = 5711 wh, whereas for batch processing in the homogenizer for the same volume of liquid, the energy consumption is 136 wh \times 42 = 5712 wh. Thus, in terms of energy consumption, passing even larger volumes through the VFD will make it an attractive processing platform over the homogenizer. This coupled with other attributes of continuous flow processing in the VFD makes it attractive for industrial processing relative to homogenization. For a better understanding at the nano-dimensions, a new small-angle neutron scattering (SANS) setup and study is carried out in-presence of the VFD. SANS is a powerful technique capable of elucidating the size and geometry of objects on the mesoscopic scale (1–100 nm), making it well-suited to studying soft matter systems such as micelles. The large size of the SANS instrument's sample staging area also allows the sample setup to be changed in order to study the effects of a stimulus on the system size and geometry in real-time. One example of this versatility is rheo-SANS¹⁸, where a rheometer is placed in the sample area and a sample is sheared during the SANS experiment to study how the system responds to shear. Other setups, such as high-pressure and dielectric spectroscopy, have also been used in combination with SANS. Because of this versatility, SANS was chosen to study the real-time effects of the VFD on the size and geometry of this system. Although VFD-treated gels have been studied on SANS¹⁷, this is the first report on real-time SANS measurements. A representation on the setup of the microfluidic platform for the SANS analysis is shown in (Fig 4.2e, f). (Fig 4.2a–d) shows SANS overlays for the real-time VFD data and the post-VFD data of Tween 20 by itself and Tween 20 with fish oil.

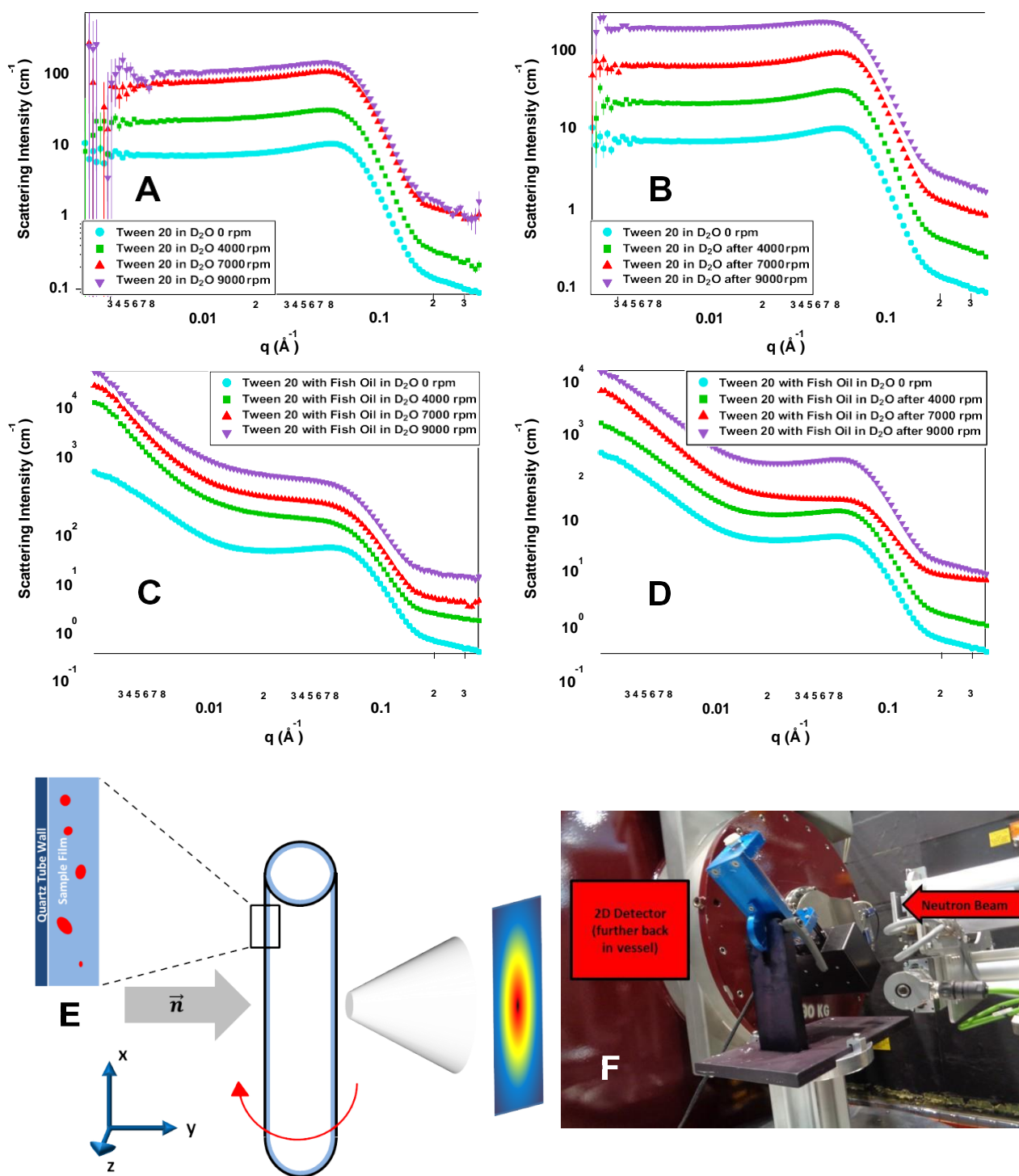


Figure 4.2: Small-angle neutron scattering. (A) SANS data overlay of real-time VFD data of 10wt% Tween 20 alone, (B) SANS data overlay of post-VFD data of 10wt% Tween 20 alone, (C) SANS data overlay of real-time VFD data of 10wt% Tween 20 with 10wt% of fish oil, (D) SANS data overlay of post-VFD data of 10wt% Tween 20 with 10wt% of fish oil, (E) top-down view schematic representation for in situ VFD SANS where the neutron beam is normal to the x - z plane of the VFD tube and the tube is

tilted 45° from vertical, (F) picture of the VFD installed on the sample staging area of the Bilby beam line while out of the path of the neutron beam. The curves shown in the data overlays in (A)-(D) were offset by powers of 3 to improve clarity.

The differences in the overall scattering intensity for a particular SANS overlay are due to the solvent scattering subtraction step, which is complicated by the experiment setup. Some trends can be observed from the overlays. The Tween 20-only samples all had a weak correlation peak during and after the VFD treatment, with the only noticeable change being after the sample was processed in the VFD at 9000 rpm. The Tween 20 with fish oil samples did not have this correlation peak during the VFD treatment, but after treatment the peak returned; additionally, all fish oil samples exhibited strong low- q scattering regardless of the VFD, and the post-7000 rpm sample showed lasting effects. To gain a better understanding of how the size and geometry of the particles changed during and after VFD processing, various models were fitted to the data using non-linear least squares via the NIST macros for Igor Pro (Wave metrics, Portland, OR, USA)¹⁹. Different resolution-smearred models were tested on each data set to determine the most appropriate model. Ultimately, a Gauss Sphere with Screened Coulomb interaction model was used for the Tween 20 only samples during and after VFD processing, a summed Power Law + Gauss Sphere with Screened Coulomb interaction model was used for the fish oil samples after VFD, and a summed Power Law + Gauss Sphere model was used for the fish oil samples during VFD treatment. Gauss Sphere reflects the spherical shape and the size distribution of the micelles that can be observed from the epi-fluorescence microscopic image in (Fig 4.1d). Given that Tween 20 is a non-ionic surfactant, attempts were made to use the hard sphere structure factor with various form factors, such as spheres, oblate and prolate ellipsoids, and core-shell spheres, to model the data, however, none of those were able to fit the correlation peak well. This necessitated the use of the screened Coulomb structure factor, which did fit the correlation peak, thus indicating that the peak was caused by electrostatic repulsions between the micelles. The electrostatic repulsions stem from partial charges on the ether oxygen groups on the ethoxylated polysorbate Tween molecule.

Although these partial charges are usually not enough to cause electrostatic interactions, there can be significant electrostatic repulsions if the surfactant concentration and/or the degree of ethoxylation becomes high enough (>20mM and >20 units, respectively) ²⁰. In the present systems, the Tween 20 concentration is about 200 mM, making this well above the cutoff for electrostatic interactions to become observable. Example fits to the data can be seen in (Fig. 4.3a, b). The fits to the remaining data sets can be found in the SI. Table 4.1 shows the radius and radial polydispersity for the two systems during and after processing at each rotational speed in the VFD. The Tween 20-only samples were not substantially affected by increasing shear in terms of either micelle radius or radial polydispersity, with the micelle radius remaining close to 2.59 nm ²¹.

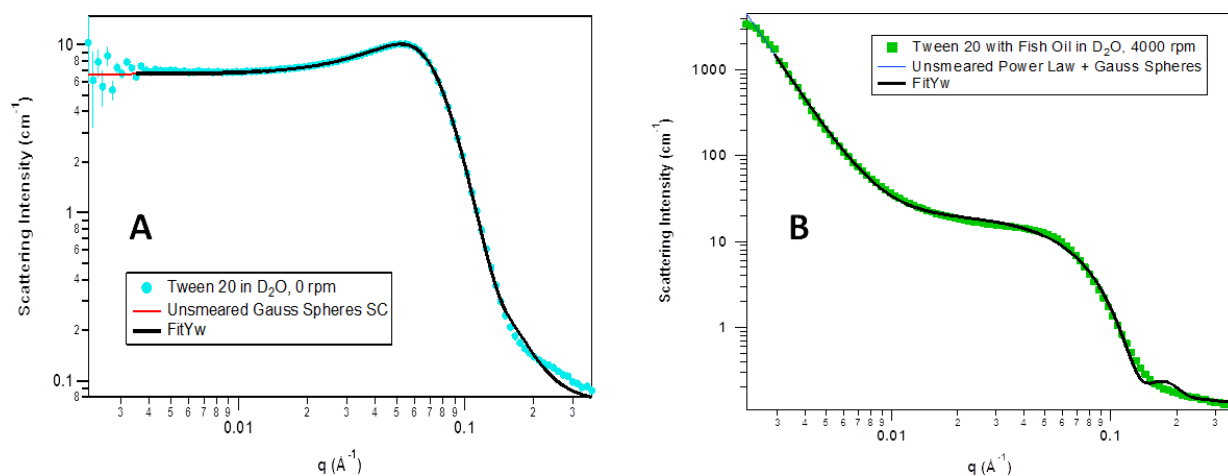


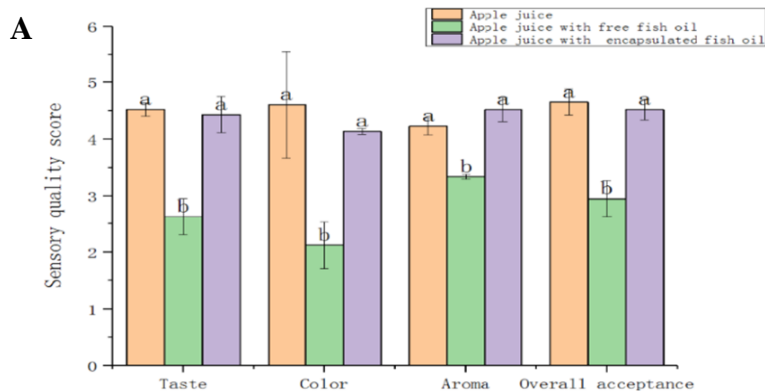
Figure 4.3: Representative fits to the data from the models described above. *a* Gauss Sphere with screened Coulomb interaction model fitted to the 10 wt% of Tween 20-alone sample at 0 rpm (static), *b* summed Power Law + Gauss Sphere model fitted to the 10 wt% of Tween 20 with 10 wt% of fish oil sample while being sheared at 4000 rpm. The fits to the other data sets shown in the SI are similar in fit quality.

Table 4.1. Sphere radius and polydispersity during and after VFD treatment at each speed for 10 wt% of Tween 20 by itself and 10 wt% of Tween 20 with 10 wt% of fish-oil at ratio 1:1.

		Tween 20 alone		Tween 20 with Fish Oil	
	RPM	radius (+/- .03 Å)	radial polydispersity (+/- 0.002)	radius (+/- 0.3 Å)	radial polydispersity (+/- 0.015)
Real-time VFD	0	25.92	0.27	26.55	0.28
	4000	26.04	0.27	30.31	0.13
	7000	25.93	0.29	30.82	0.12
	9000	25.75	0.22	30.94	0.12
After VFD	0	25.92	0.27	26.55	.028
	4000	25.86	0.27	26.52	0.27
	7000	25.87	0.26	22.88	0.31
	9000	25.61	0.28	26.60	0.27

Only during the 9000rpm treatment was there a slight effect on the Tween 20 system, where the micelle radius dropped to 2.57 nm while the micelles became somewhat less poly-dispersed. Once the shear was removed the micelle sizes remained stable, except the micelles that were sheared at 9000 rpm became slightly smaller and more poly-disperse than they were while being sheared. This possibly arises from loss of solvation shell of the micelle under high shear. As the rotational speed increases, the thin film thickness inside the VFD decreases, causing more of the Tween 20 hydrophobic regions to orient toward the oil phase of the emulsions. When fish oil was added, the baseline micelle size at 0 rpm was larger than it was when no fish oil was present, as a result of fish oil being taken up within the micelles. As the systems were sheared at increasing speeds, the micelle sizes grew while the polydispersity dropped, indicating that the system became increasingly homogenized. After they were sheared, the micelle sizes returned to baseline and became similar in polydispersity; however, the system that had been sheared at 7000 rpm ended up having noticeably smaller micelles than baseline (2.29 instead of 2.65 nm) and were more poly-disperse, suggesting that the micelles had been pulled apart and then reformed into smaller micelles on average with a greater range in size. This could have caused by strong eddy currents

associated with Faraday waves that occur at ca 7000 rpm ⁹.



B

Fatty acids	Fatty acids composition			
	Fish oil (fresh)	Fish oil (after 14 days)	Freeze-dried encapsulated fish oil (fresh)	Freeze-dried encapsulated fish oil (after 14 days)
C8:0	0.00%	0.00%	0.00%	0.00%
C10:0	0.00%	0.02	0.00%	0.00%
C12:0	0.00	0.26	4.78%	5.26%
C14:0	1.13	11.44	2.63%	2.90%
C15:0	0.01	1.17	0.00%	0.01%
C16:0	0.19	13.59	2.02%	2.30%
C16:1 N-7	1.06	12.44	0.25%	0.33%
C17:0	0.00%	0.26	0.00%	0.00%
C18:0	4.05	2.84	5.07%	4.93%
C18:1 N-9	14.02	11.03	7.30%	7.22%
C18:1 N-7	4.09	2.43	1.54%	1.47%
C18:2 N-6	2.39	1.91	0.50%	0.49%
C18:3 N-3	1.88	1.23	0.00%	0.00%
C18:4 N-3	4.27	3.09	0.95%	0.95%
C20:0	0.00	0.31	0.00%	0.00%
C20:1 N-9	0.01	3.41	5.33%	5.08%
C20:2 N-6	0.02	0.20	0.38%	0.35%
C20:3 N-6	0.05	0.13	0.29%	0.28%
C20:4 N-6	3.60	1.19	2.74%	2.65%
C20:5 N-3	25.98	14.42	36.39%	35.55%
C22:0	0	0	0.88%	0.94%
C22:1 N-11	0	3.25	0.02%	0.02%
C22:1 N-9	0	3.09	3.59%	3.78%
C22:4 N-6	0	0.08	0.08%	0.08%
C22:5 N-3	0	2.85	3.78%	3.76%
C24:0	0.08	0.00%	0.00%	0.00%
C22:6 N-3	37.17	9.36	21.49%	21.65%
Total FAME	100.00	100.00	100.00	100.00
Omega-3	69.28	30.95	62.61	61.91
Oil content	100%	100%	49.53%	44.46%
Encapsulation efficiency	---	---	99.06%	88.92%

Figure 4.4: Application of encapsulated fish oil using vortex fluidic device. a Sensory evaluation of apple juices with and without fish oil and encapsulated fish oil. **b** Fatty acid profile of fresh fish oil and encapsulated fish oil by VFD processing (speed: 9000 rpm; flow rate: 0.3 mL/min; tilt angle: 45°; temperature: 25 °C) before and after 14 days storage.

(Fig 4.4b) shows that the content of omega-3 fatty acids in fresh fish oil purchased from the market is 69.3%. However, after 14 days of storage in an ambient environment, the content of omega-3 fatty acids are reduced to 31.0%, which approximates to a 38% reduction. The results in Fig. 5b show that freeze-

dried VFD encapsulated fish oil has little change in the omega-3 fatty acid content after 14 days of storage at ambient conditions, 62.6–61.9%. Relative to as-received fish oil there is only an approximate 7% reduction in omega-3 fatty acid content after VFD processing, with oxidation possibly occurring during the VFD processing associated with the high uptake of gases (oxygen) into the dynamic thin film in the device ⁸. Stability of the processed liquid is a prerequisite for the production of encapsulated fish oil powder. (Fig 4.1 a, b, e) shows the instability of the liquid after homogenization, and therefore, only freeze-dry the liquid after homogenization to form a powder is required. The encapsulation efficiency of the fish oil was also established at 99.1% immediately after VFD processing, and there was only about a 10% drop to 88.9% after 14 days of storage. However, while the encapsulation efficiency dropped approximately 10% after 14 days, the omega-3 fatty acids contents were essentially unchanged (from 62.6 to 61.9%). An intake of approximately 0.2 g of omega-3 fatty acids per day is recommended ²². Based on this information, 250 mL of commercial apple juice was enriched with 0.2 g of fish oil and 0.4 g of freeze-dried encapsulated fish oil which contained 0.2 g of fish oil, respectively. This preparation made the concentration of fish oil in enriched apple juice 0.8%(w/v), regardless of VFD-encapsulated fish oil or original fish oil. The quality of the apple juice with different formulations of apple juice with fish oil was evaluated by sensory tests. The average scores with error bars that represent the standard deviation of the sensory evaluations are given in (Fig 4.4a). There was no significant quality difference between apple juice and apple juice with encapsulated fish oil processed by VFD in terms of taste, color, aroma, and overall acceptance. However, panelists showed a preference for these two samples over the apple juice with free fish oil in every category (Fig 4.4a).

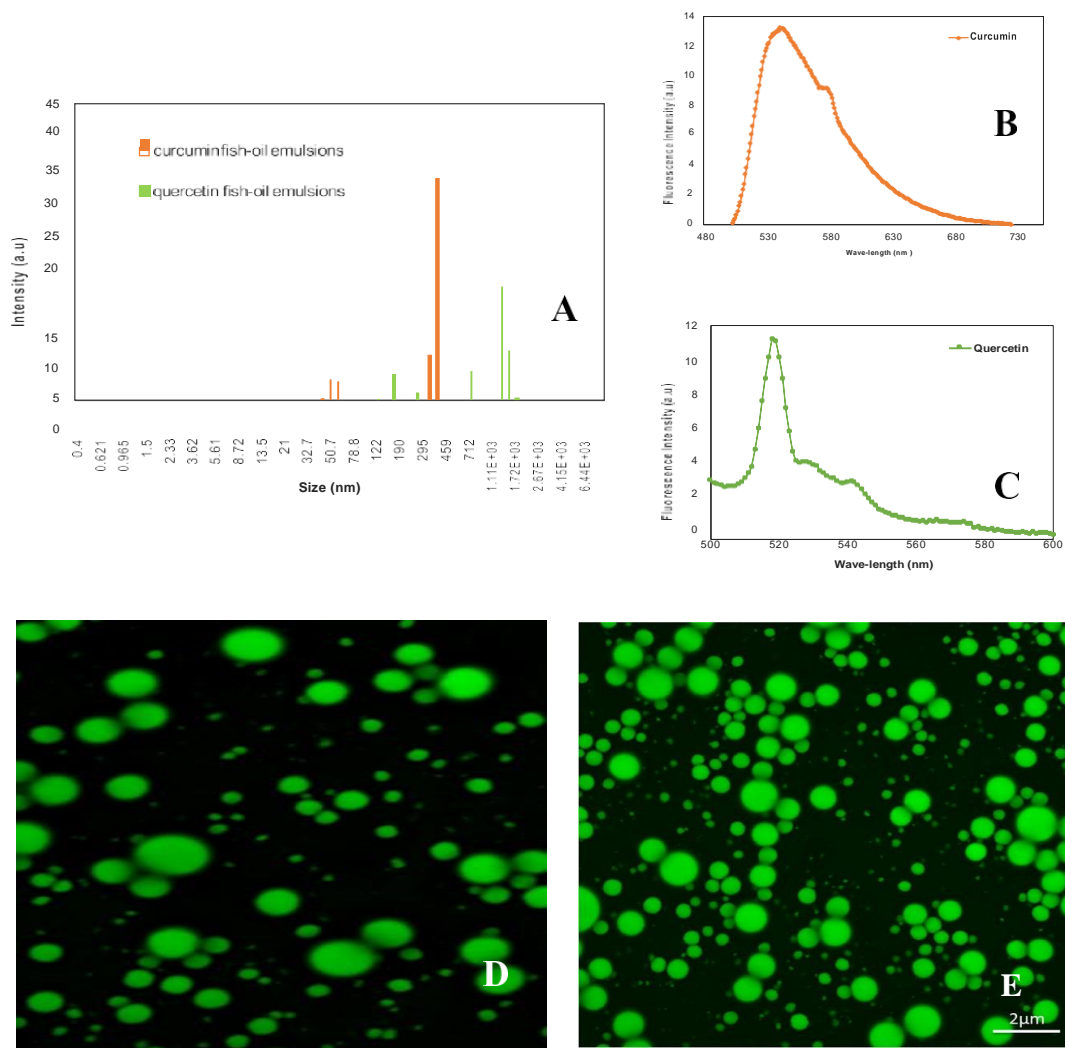


Figure 4.5: Encapsulation capacity for curcumin and quercetin. *a* Dynamic light scattering (DLS) measurements for encapsulated emulsions. *b*, *c* Fluorescence spectra for curcumin and quercetin encapsulated emulsions, respectively. *d*, *e* Confocal micrographic images (wavelength: 420 and 370 nm) of encapsulated fish oil containing curcumin and quercetin, respectively, homogeneously suspended in water.

Encapsulations of curcumin and quercetin, as two typical sparingly water and oil-soluble polyphenolic compounds, were formulated using 30 mg of starting raw material, 1 g of fish oil, and 1 g of Tween 20. The conditions of entire encapsulation processing, including VFD operation, were reported in the section

of Encapsulation capacity for curcumin and quercetin 'Materials and methods'. The outcome was investigated. The particle size distribution was characterized using DLS. Curcumin-encapsulated emulsions are in a distribution range of 200–500 nm, while the quercetin is indicated at higher distribution range of 700 nm–2 μ m (Fig 4.5a). Both curcumin and quercetin have characteristic fluorescence signals, (Fig 6b, c) respectively, with fluorescent micrographs observed by confocal microscopy, as shown in (Fig 6d, e) operating at 420 nm for curcumin and 370 for quercetin. Curcumin and quercetin dissolved in the encapsulated fish oil droplets produced green and light orange round droplets homogenously distributed in the water-based system, respectively, with encapsulation capacities as approximately 67.9% and 51.2%, respectively. The instability of the encapsulated fish oil arises from coagulation of the encapsulated particles ²³. The larger the encapsulated particles, the more they tend to coagulate, and the more unstable they become ²³. Klaypradit and Huang ²⁴ tested the encapsulation of tuna oil using Tween 80 surfactant and found that, in line with the particle sizes changing from 1.56 to 11.89 μ m, the encapsulation stability decreased from 80 to 60%. Previous studies have also reported stable encapsulated fish oil produced by homogenization. However, they either required a multiple-step process, or a high ratio of surfactant to fish oil. Klaypradit and Huang ²⁴ produced stable emulsions using up to 10:1 of surfactant to fish oil, with the maximum concentration of fish oil at 50 mg/mL. Carla et al. ²⁵ produced a stable fish oil encapsulation solution with a higher concentration of fish oil at 500 mg/mL, with a lower ratio of surfactant to oil of 2:1. In addition, the process here involved multiple steps, including micelle and buffer preparations prior to encapsulation. Each of these requirements has limitations for industrial applications of encapsulated fish oil, which can be overcome using the VFD. Our initial study ¹⁴ demonstrated that under low concentration in fish oil, VFD processing was able to overcome these two limitations, producing stable encapsulated fish oil in one step, for 20 mg fish oil, 20 mg lipid as surfactant in 10 mL water.

The present study further demonstrates the utility of the VFD processing in overcoming the same limitations for producing stable solutions of encapsulated fish oil at much higher concentration (1 g fish oil, 1 g Tween 20 as surfactant in 8mL water), depending on the choice of surfactant. SANS measurements of Tween 20 alone and Tween 20 with fish oil were recorded on the Bilby instrument at ANSTO (Lucas Heights, Australia) for increasing speeds (0, 4000, 7000, and 9000 rpm), and measurements were taken again after each speed. The correlation peak indicates the presence of interparticle interactions, which would require a structure factor to be used in the modeling step. The disappearance of the correlation peak in the fish oil samples during VFD treatment is likely to be due to the unincorporated oil interfering with the stabilizing interparticle interactions, which are then able to reform after VFD processing (no shear). The strong low- q scattering in the fish oil samples can be attributed to the globules that are large enough to cause cloudiness on the macroscopic scale, which correspond to the approximately 75 nm particles identified using DLS. At higher rotational speeds more shear stress (mechano-energy) is applied on the surfactants, lowering the interfacial tension between the oil and water phase, associated with Faraday wave eddies driving interplay of the liquids. (This accounts for enhanced separation of proteins in specific immiscible liquids ¹⁶. As a result, more surfactants adsorb strongly, increasing their emulsifying properties and forming stronger and more compact membranes while under shear. The change in the post-VFD processing at 9000 rpm data curve seen in (Fig 4.3b) likely reflects a slight change in the interparticle interaction. When fish oil is added to the Tween 20 system, the micelle radius increased slightly to 2.65 nm as a result of the fish oil being incorporated into the micelles. While being sheared, the micelles gradually became larger while the radial polydispersity became smaller as the VFD rotational speed is increased, indicating that the VFD homogenized the sample even further and resulted in particles more uniform in size. This effect was, however, not permanent, as seen by the micelle radius and polydispersity returning to baseline in the post-VFD results. After the VFD 7000 rpm treatment, however, the micelle radius dropped to 2.29 nm and the polydispersity increased to 0.31, indicating that the VFD appears to tear the micelles apart to form smaller

micelles over a greater size range ²⁶. This is likely caused by eddy currents that strongly form from Faraday waves at 7000 rpm. It should be noted that the micelle sizes reported by SANS are likely related to the 7–8 nm particles seen by DLS in (Fig 4.1f,) as DLS reports the radius of hydration, which is somewhat larger than the sizes determined by SANS. As the SANS data are on absolute scale, the volume fractions determined by SANS (see SI) also indicate that most of the material in these systems is incorporated in the larger particles identified using DLS, while the small amount of remaining material makes up the smaller micelles identified using SANS. Overall, these results demonstrate that although VFD processing does not generally cause lasting changes to the fully equilibrated system, certain speeds may be effective in causing permanent changes depending on the composition of the system. The mechanoenergy in the VFD is effective in driving systems into non-equilibrium states, as shown in the present system where the nanoparticle-sized fish oil particles are generated as such, and then stabilized by the surfactant. The oxidation of fish oil was prevented by encapsulation using VFD processing (Fig 4.4b). Given the ability to minimize oxidation of the fish oil using VFD processing, there is scope to use the freeze-dried encapsulated fish oil as an ingredient to enrich the content of omega-3 fatty acids in food formulations. In order to demonstrate this, apple juice, a commonly consumed food product, was selected as an example for formulation upgrade by adding it to freeze-dried encapsulated fish oil processed by VFD. The results clearly indicated equal preference of the original apple juice and apple juice with encapsulated fish oil processed by the VFD, over the apple juice with free fish oil. Indeed, a similar study has been reported previously. Tahere et. al. ²⁷ applied encapsulated fish-oil into yogurt for the fortification of the omega-3 fatty acids content in yogurt. However, multiple steps were used to form stable fish oil encapsulation, which included preheating, stirring, homogenization, sonication, and storage under nitrogen. In comparison, VFD processing is one step and the thin film microfluidic platform is easy to operate, thereby establishing potential for the fish oil encapsulation in other applications. Several bioactive compounds are not water-soluble, which restricts their application because they cannot form a homogeneous solution for many water-based food formulations. For example, the antioxidative activities

of polyphenolic compounds have been broadly reported. However, many polyphenolic compounds are water-insoluble, although most of the water in soluble polyphenolic compounds are oil-soluble. Therefore, it was interesting to see if these bioactive compounds could be taken up in fish oil, and encapsulated using a homogeneous single step water-based VFD process. The green (Fig 4.5d) and (Fig 4.5e) round droplets indicated that the encapsulated fish oil, which included dissolved curcumin (Fig 4.5d) and quercetin (Fig 4.5e), respectively, were homogeneously distributed in the water-based systems. The fluorescent micrographs for curcumin and quercetin were taken at each polyphenol's respective excitation value of 420 and 370 nm. Fluorescence spectrums indicate emission signals for curcumin and quercetin at 540 and 520 nm when excited at their respective excitation values. Emission peaks at 540 and 520 nm for curcumin and quercetin represents lipophilic environments as encapsulated particles in the fish oil emulsions. The particle size for curcumin and quercetin are in the range 200–500 nm and 700 to 2 μm which is evident from confocal micrographs; the smaller particles at 50 and 100 nm presumably aggregated curcumin and quercetin particles not encapsulated in the emulsions. The encapsulation of water-insoluble polyphenols has previously been reported, but it either required multiple wall materials (surfactants), such as chitosan and tri polyphosphates, for encapsulation involving multiple step processing ²⁸ or the use of expensive equipment, such as an electro-hydrodynamic atomizer ²⁹. VFD processing is effective and the device is relatively inexpensive.

4.4 Conclusion

In summary, a facile process, operating under continuous flow has been developed using a VFD, for encapsulated particles, 100–200 nm in diameter. This VFD simplifies the processing procedure of encapsulation into a time- and cost-saving one-step process devoid of any organic solvents, which is in contrast to the conventional homogenization process, which is inherently complex and involves multiple steps and the use of organic solvents. VFD encapsulation minimized the oxidation of the encapsulated fish oil, from 38.3 % (approximate 69.3–31.0 %) to 7.3% (approximate 69.3–62.0 %). The encapsulated

particles are a storage compartment for omega-3 fatty acid in water-based food products, demonstrated for apple juice, without changing their sensory values. The encapsulation capacity of curcumin and quercetin was 67.9 % and 51.2 %, respectively, and the findings provide a model for producing homogenous suspensions of water-insoluble bioactive compounds in general. Both VFD processes of encapsulated fish oil and simultaneously encapsulating water-insoluble bioactive polyphenols was scaled-up from 10 to 200 mL, with the solutions found to have the same overall characteristics. This study not only presents a new alternative approach as an affordable one process but also for directly scaling up any fish oil process, for a variety of applications in food processing.

Acknowledgements

The authors acknowledge support of this work by the Australian Research Council for funding support, ANSTO, the South Australia Research and Development Institute (SARDI) for the measurement of fatty acid profiles, and microscopy facility of Macquarie University, Sydney, Australia for the microscopy images.

References

1. Shoup, V. A. & Touster, O. Purification and characterization of the alpha-D-mannosidase of rat liver cytosol. *J. Biol. Chem.* 251, 3845–3852 (1976).
2. Lee, S., Gura, K. M. & Puder, M. Omega-3 fatty acids and liver disease. *Hepatology* 45, 841–845 (2010).
3. Rozas, R., Lümmer, N. & Kraska, T. Structure formation of metallic nano-particles in the vapour phase and in disperse materials. *Eur. Phys. J.* 149, 57–70 (2007).
4. Ghorbanzade, T., Jafari, S. M., Akhavan, S. & Hadavi, R. Nano-encapsulation of fish oil in nano-liposomes and its application in fortification of yogurt. *Food Chem.* 216, 146–152 (2017).
5. Moomand, K. & Lim, L. T. Oxidative stability of encapsulated fish oil in electrospun zein fibres. *Food Res. Int.* 62, 523–532 (2014).

6. Britton, J. & Raston, C. L. Multi-step continuous-flow synthesis. *Chem. Soc. Rev.* 46, 1250 (2017).
7. Britton, J., Chalker, M. J. & Raston, L. C. Rapid vortex fluidics: continuous flow synthesis of amides and local anesthetic lidocaine. *Chemistry* 21, 10660–10665 (2015).
8. Britton, J., Stubbs, K. A., Weiss, G. A. & Raston, C. L. Vortex fluidic chemical transformations. *Chemistry* 23, 13270 (2017).
9. Britton, J., Meneghini, L. & Raston, C. Accelerating enzymatic catalysis using vortex fluidics. *Angew. Chem.* 128, 11559–11563 (2016).
10. Britton, J., Dyer, R. P., Majumdar, S., Raston, C. L. & Weiss, G. A. Ten-minute protein purification and surface tethering for continuous-flow biocatalysis. *Angew. Chem.* 56, 2296–2301 (2017).
11. Vimalanathan, K. et al. Surfactant-free fabrication of fullerene C 60 nanotubules under shear. *Angew. Chem.* 129, 9518–8521 (2017).
12. Britton, J. & Raston, L. C. Continuous flow vortex fluidic production of biodiesel. *RSC Adv.* 4, 49850–49854 (2014).
13. Sitepu, E. K. et al. Vortex fluidic mediated direct transesterification of wet microalgae biomass to biodiesel. *Bioresour. Technol.* 266, 488–497 (2018).
14. He, S., Joseph, N., Luo, X. & Raston, C. Continuous flow thin film microfluidic mediated nano-encapsulation of fish oil. *LWT* 103, 88–93 (2019).
15. Chen, X., Smith, N. M., Iyer, K. S. & Raston, C. L. Controlling nanomaterial synthesis, chemical reactions and self-assembly in dynamic thin films. *Chem. Soc. Rev.* 43, 1387–1399 (2014).
16. Xuan, L., Smith, P., Raston, C. L. & Zhang, W. Vortex fluidic device-intensified aqueous two phase extraction of C-phycoerythrin from spirulina maxima. *ACS Sust. Chem. Eng.* 4, 3905–3911 (2016).
17. Kumari, H. et al. Manipulating three-dimensional gel network entanglement by thin film shearing. *Chem. Commun.* 52, 4513–4516 (2016).
18. Dawn, A. & Kumari, H. Low molecular weight gels under shear: rheology as the tool for elucidating structure–function correlation. *Chemistry* 24, 762–776 (2017).
19. Kline, S. Reduction and analysis of SANS and USANS data using IGOR Pro. *J. Appl. Crystallogr.* 39, 895–900 (2006).
20. Penfold, J. et al. Nature of the intermicellar interactions in ethoxylated polysorbate surfactants with high degrees of ethoxylation. *Langmuir* 32, 1319–1326 (2016).
21. Kumari, H., Kline, S. R. & Atwood, J. L. Aqueous solubilization of hydrophobic supramolecular metal–organic nanocapsules. *Chem. Sci.* 5, 2554–2559 (2014).
22. Dayspring, T. D. Understanding hypertriglyceridemia in women: clinical impact and management with prescription omega-3-acid ethyl esters. *Inte. J. Women’s Health* 3, 87–97 (2011)

23. Takeungwongtrakul, S., Benjakul, S. & H-Kittikun, A. Micro-encapsulation of pacific white shrimp oil as affected by emulsification condition. *Food Sci. Hum. Wellness* 3, 175–182 (2014).
24. Klaypradit, W. & Huang, Y. W. Fish oil encapsulation with chitosan using ultrasonic atomizer. *LWT* 41, 1133–1139 (2008).
25. Carla, D. N., Julian, M. & Eric, A. D. Impact of Tween 20 hydroperoxides and iron on the oxidation of methyl linoleate and salmon oil dispersion. *J. Agric. Food Chem.* 49, 4912–4916 (2001).
26. Solheim, T. E. et al. Neutron imaging and modelling inclined vortex driven thin films. *Sci. Rep.* 9, 2817 (2019).
27. Tahere, G., Seid, M. J., Sahar, A. & Roxana, H. Nano-encapsulation of fish oil in nano-liposomes and its application in fortification of yogurt. *Food Chem.* 216, 146–152 (2017).
28. Bakht, R. S. et al. Preparation and optimization of Pickering emulsion stabilized by chitosan-tripolyphosphate nanoparticles for curcumin encapsulation. *Food Hydrocolloid.* 52, 369–377 (2016).
29. Gomez-Estaca, J., Balaguer, M., Lopez-Carballo, G., Gavara, R. & Hernandez-Munoz, P. Improving antioxidant and antimicrobial properties of curcumin by means of encapsulation in gelatin through electrohydrodynamic atomization. *Food Hydrocolloid.* 70, 313–320 (2017).
30. He, S., Joseph, N., Luo, X. & Raston, C. L. Vortex fluidic mediated food processing. *PLoS ONE* 14(5), e0216816 (2019).
31. He, S., Franco, C. & Zhang, W. Characterisation of processing wastes of Atlantic Q6 Salmon (*Salmo salar*) and Yellowtail Kingfish (*Seriola lalandi*) harvested in Australia. *Int. J. Food. Sci. Technol.* 46, 1898–1904.
32. Zeng, Q. et al. Process optimization and anti-oxidative activity of peanut meal MAillard reaction products. *LWT* 97, 573–580 (2018).
33. Schwambach, S. L. & Peterson, D. G. Reduction of stale flavor development in low-heat skim milk powder via epicatechin addition. *J. Agric. Food Chem.* 54, 502–508 (2006).
34. Coklin, T. et al. Temporal changes in the prevalence and shedding patterns of *Giardia duodenalis* cysts and *Cryptosporidium* spp. oocysts in a herd of dairy calves in Ontario. *Can. J. Vet. Res.* 51, 841–846 (2010).
35. Hammouda, B. Probing Nanoscale Structures: The SANS Toolbox. http://www.ncnr.nist.gov/staff/hammouda/the_SANS_toolbox.pdf (2016).
36. Hayter, J. B. & Penfold, J. An analytic structure factor for macroion solutions. *Mol. Phys.* 42, 109–118 (1981).
37. Hansen, J.-P. & Hayter, J. B. A rescaled MSA structure factor for dilute charged colloidal dispersions. *Mol. Phys.* 46, 651–656 (1982).

ARTICLE OPEN



Vortex fluidic mediated encapsulation of functional fish oil featuring in situ probed small angle neutron scattering

Shan He^{1,5}, Nikita Joseph^{1,5}, Marzieh Mirzamani^{1,5}, Scott J. Pye², Ahmed Hussein Mohammed Al-Hanataki^{1,3}, Andrew E. Whitten^{1,5}, Yaonan Chen¹, Harshita Kumari^{1,5} and Colin L. Raston^{1,5}

Major challenges for optimizing the benefits of fish oil on human health are improved bioavailability while overcoming the strong odor and avoiding significant oxidation of the omega-3 polyunsaturated fatty acids (PUFAs). The scalable continuous flow thin film vortex fluidic device (VFD) improves the Tween 20 encapsulation of fish oil relative to conventional homogenization processing, with the fish oil particles significantly smaller and the content of the valuable omega-3 fatty acids higher. In addition, after 14 days storage the remaining omega-3 fatty acids content was higher, from ca 31.0% for raw fish oil to ca 62.0% of freeze-dried encapsulated fish oil. The VFD mediated encapsulated fish oil was used to enrich the omega-3 fatty acid content of apple juice, as a model water-based food product, without changing its sensory values. The versatility of the VFD was further demonstrated in forming homogenous suspensions of fish oil containing water-insoluble bioactive molecules, curcumin and quercetin. We have also captured, for the first time, real-time structural changes in nanoencapsulation by installing a VFD with in situ small angle neutron scattering. Real-time measurements afford valuable insights about self-assembly in solution.

npj Science of Food (2020)4:12; <https://doi.org/10.1038/s41538-020-00072-1>

INTRODUCTION

Fish oil is an excellent dietary source of omega-3 polyunsaturated fatty acids (PUFAs) having positive effects on human health. However, it has a strong odor and is easily oxidized at ambient conditions¹ and omega-3 PUFAs cannot be synthesized in the human body, and thus it needs to be sourced from food². Capsules of fish oil protect omega-3 PUFAs from oxidation, but their large size limits their utility as nutritional supplements. Encapsulating fish oil in nanoparticles also protects omega-3 PUFAs from oxidation, and has exciting possibilities in food processing. Although such confinement of one substance (active agent) within another (wall material)³ has been broadly studied for fish oil^{4,5}, the methods used either require multiple steps or expensive processing equipment.

The vortex fluidic device (VFD) (Fig. 1) is a continuous flow thin film microfluidic platform with diverse applications⁶. It harnesses high shear forces, intense micro mixing, and high mass transfer to overcome the mixing and heat transfer limitations akin to traditional batch processing⁷. Processing capabilities of the VFD are rapidly growing across various fields, ranging from small-molecule synthesis involving a number of steps being accomplished in a single pass to processing functional materials for drug delivery and manipulating single-cell organisms⁸. Enzymatic reactions in the VFD have on average a sevenfold acceleration in their catalytic reactions⁹, depending on the choice of processing parameters of the device, including rotation speed of the inclined glass tube⁹. Tethering enzymes to the surface of the glass tube has also been achieved for the synthesis of complex molecules in a single pass under continuous flow conditions¹⁰. Fabricating nanomaterials in the VFD has yielded unexpected results, also under continuous flow, for example, in assembling fullerene C₆₀ molecules into nano-tubules with hollow diameters

of 100–400 nm, in the absence of a surfactant and without the need for further downstream processing¹¹. Other noteworthy applications of the VFD are converting sunflower oil to biodiesel at room temperature with no saponification and avoiding the conventional use of co-solvents or complex catalysts¹², and the direct transesterification of microalgae¹³.

As a preliminary trial, our previous study¹⁴ established that for low concentrations of the fish oil (fish oil:surfactant = 1:1 (w/w), fish oil + surfactant:water = 2 mg/ml), the VFD is effective in encapsulating fish oil particles below 300 nm, whereas those produced by homogenization are 3–4 μm in diameter. Though the low concentration in this study was not industry-applicable because of the high cost of concentrating and drying the material, this proof-of-concept achievement encouraged us to follow up with a high concentration study, to drastically reduce the cost of the overall processing. In the present study, we report a simple low-cost, single pass VFD process for encapsulating fish oil using high concentration feedstocks (fish oil:surfactant = 1:1 (w/w), fish oil + surfactant:water = 0.2 g/ml), as well as the ability to simultaneously encapsulate sparingly water-soluble bioactive polyphenols. The encapsulated omega-3 fatty acids become protected from oxidation, and the encapsulation is effective in enriching the omega-3 fatty acid content in liquid food. Also reported is a small-angle neutron scattering (SANS) method for studying the shear stress-induced encapsulation process under real time conditions in the VFD. Notably post-VFD SANS studies have been reported¹⁵, however, real-time measurement of self-assembly in solution is being reported here for the first time.

RESULTS

The oil-in-water encapsulations had a surfactant-to-oil ratio of 1:1 (w/w), and a total concentration of 0.2 g/mL (10 mL of the Tween

¹Department of Food Science and Engineering, School of Chemistry Chemical Engineering, Guangzhou University, Guangzhou 510006, China. ²Flinders Institute for Nanoscale Science and Technology, College of Science and Engineering, Flinders University, Bedford Park, SA 5042, Australia. ³Division of Pharmaceutical Sciences, James L. White College of Pharmacy, University of Cincinnati, Cincinnati, OH 45267-0004, USA. ⁴Australian Nuclear Science and Technology Organisation (ANSTO), New Illawarra Road, Lucas Heights, NSW 2234, Australia. ⁵These authors contributed equally: Shan He, Nikita Joseph, Marzieh Mirzamani. [✉]email: kumarhag@gmail.com; colin.raston@flinders.edu.au

Chapter 5: Vortex Fluidics Mediated Non-Covalent Physical

Entanglement of Tannic Acid and Gelatin for Entrapment of Nutrients

Xuejiao Cao^{1 ^}, Nikita Joseph^{2^}, Matt Jellicoe², Ahmed Hussein Mohammed Al-Antaki², Xuan Luo², Dongxiao Su^{1*}, Shan He^{1,2*}, Colin Raston^{2*}

¹ Department of Food Science, School of Chemistry and Chemical Engineering, Guangzhou University, Guangzhou, Guangdong, 510006, China.

² Flinders Institute for Nanoscale Science and Technology, College of Science and Engineering, Flinders University, Bedford Park, South Australia, 5042, Australia

[^] As the First Author(S), These Two Major Authors Contributed Equally to This Work.

Author Contributions

The publication was published in journal Food and Function 2020. The author contributions are as follows, N.J. wrote the main manuscript text, revised/reviewed manuscript for final version approval. N.J. designed the experiments and helped in the data analysis of the particle size and viscosity. N.J. carried out the nutrient entrapped experiments. X.C. prepared figures, concept, design, and literature review for the research and conducted experiments such as preparation of gels, particle size, SEM, viscosity and BET. A.A guided in during the experimental procedure of SEM-EDAX. M.J prepared the figure of VFD. X.L helped in the writing of BET characterization, S.H, D.S revised/reviewed manuscript for final version approval and C.L.R.: supervised the whole project and guided for all the experiments.

Abstract

We have developed a simple process for the entrapment of nutrients in shear stress induced non-covalent physically entangled tannic acid-gelatin gel in a thin film vortex fluidic device (VFD) operating under continuous flow. This allows control of the porosity and surface area of the pores in order to improve the nutrient entrapment capacity. The VFD microfluidic platform simplifies the processing procedure of physically entangled biopolymers, as a time and cost saving one-step process devoid of any organic solvents, in contrast to the conventional homogenization process, which is also inherently complex, involving multiple-step processing. Moreover, the use of homogenization (as a benchmark to entrap nutrients) afforded much larger porosity and surface area of pores, with lower entrapment capacity of nutrients. Overall, the VFD processing provides a new alternative, bottom-up approach for easy, scalable processing for materials with a high nutrient entrapment capacity.

5.1 Introduction

The vortex fluidic device (VFD), (Fig 5.1), is a relatively new thin film microfluidic processing platform with remarkably diverse research and industrial applications¹. VFD processing technology emerged from research efforts focused on the application of thin film microfluidics and thin film flow chemistry^{1,2}. This processing harnesses high shear forces, intense micro mixing, and high heat and mass transfer, overcoming the mixing and heat transfer limitations of traditional batch processing¹. The processing capabilities of the VFD are rapidly growing, from small molecule synthesis through to processing functional materials for drug delivery, and the manipulation of single cell organisms¹.

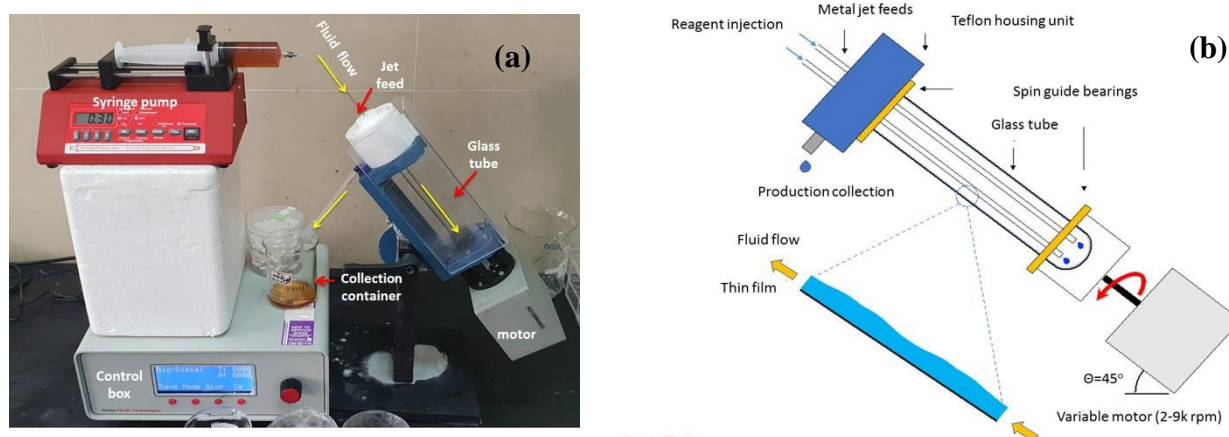


Figure 5.1: Vortex Fluidic Device (VFD). (a). Photograph of the VFD, highlighting its salient features. (b). Schematic of the VFD showing the fluid flow (images are reprinted from our previous publication “Application of microfluidic technology in food processing”, He, et al., *Food and Function*, 2020, advance article, with permission from the Royal Society of Chemistry).

A VFD can be operated under a confined mode, where a tube containing a finite volume of liquid is spun at high speed, or continuous flow, where jet feeds deliver liquid to the bottom of the tube or at positions along the tube, with the device otherwise operating under the same conditions as the confined mode. At high rotational speeds, the liquid in the tube forms a dynamic thin film with the thickness of the film controlled by varying the rotational speed, the tilt angle of rotation, and the volume of liquid in the tube³. The utility of the VFD has been established for a number of chemical transformations, with control over chemical reactivity and selectivity, and the ability to prepare complex molecules in a single pass. Dramatic enhancement of enzymatic reactions has also been established, averaging seven-fold acceleration for a variety of enzymes⁴, and this is understood mechanistically from the effect of Faraday pressure waves contained within the thin film. Related to this is the tethering of enzymes to the surface of the tube, for the synthesis of small molecules in a single pass⁵. VFD processing has also been applied to materials synthesis under continuous flow, for example in assembling fullerene C₆₀ molecules into nano-tubules⁶. Of particular note is that the micron length nano-tubules, with hollow diameters of 100 to 400 nm, are formed in the absence of surfactant, and without the need for further downstream processing. Indeed, this is a common hallmark of use of the VFD where the operating parameters can be systematically explored as high throughput processing in optimizing any process. This is typified, for example, in effectively converting sunflower oil to biodiesel at room temperature of 25°C, with no saponification and avoiding the conventional use of co-solvent or complex catalysts⁷. Mechano-energy delivered in the thin film is optimal for the rapidly rotating tube tilted at 45° where there is increased heat and mass transfer associated with the shear forces. In addition to chemical transformations, the utility of the VFD in food processing has been explored. He, et al.⁸ operated a VFD under continuous flow for controlling the size of spheroidal encapsulated fish oil particles, from 50 to 250 nm. In contrast, conventional homogenization afforded much larger macro-particles, ranging from 2 to 4 μm. Beneficial use of the VFD for food processing has also been established for reducing the processing time of raw

milk pasteurization, from 30 to 10 minutes at 60°C with other beneficial impacts of VFD food processing awaiting^{9,10}.

Gelatin is commonly used to entrap nutrients with the product a form of functional food. Seyed et al¹¹ used fish gelatin to entrap bioactive peptides and tested the load and releasing capacity. Annan et al¹² entrapped probiotic *Bifidobacterium adolescentis* 15703T in alginate-coated gelatin, which protects the probiotic during exposure to adverse environmental conditions. The nutrient entrapment capacity of gelatin is critical for developing functional food which can be improved using physical entanglement agents. Bertrand et al¹³ improved the nutrient entrapment capacity and stability of peppermint oil in gelatin-based high methyl pectin coacervate physically entangled with tannic acid, which is commonly used as a physical entanglement agent in the food industry. It is effective in forming self-assembled colloidal complexes of polyphenol-gelatin which are able to entrap more soybean oil with higher lipid stability¹⁴. The shear stress in the VFD is effective in controlling self-assembly processes and we hypothesized that it has potential for enhancing the nutrient entrapment capacity of gelatin-based materials incorporating physical entanglement agent, and this is the focus of the present studies as applied to food processing. The physical entanglement agent of choice with gelatin was tannic acid which is based on its effectiveness in previous physical entanglement studies. The resulting VFD-mediated process incorporating high shear stress and intense micro-mixing was compared with the conventional homogenization process and this has led to establishing a one-step, time-saving process for the production of material with improved nutrient entrapment capacity.

5.2 Materials

Nutrient supplements of Berocca (vitamins composition of one tablet: 15mg Vitamin B1, 15mg Vitamin B2, 25g Nicotinamide, 10µg Vitamin B6, 400µg Folic Acid, 10mg Vitamin B13, 150µg Biotin, 23mg Pantothenic Acid, 300mg Vitamin C), enriched with vitamins, and Kid's multi-minerals, enriched with

minerals (mineral composition of one tablet: 8mg Iron, 15mg Zinc, 0.4mg Copper, 70µg Iodine, 1mg Manganese, 20µg Chromium, 25µg Selenium, 50µg Molybdenum, 100mg Calcium, 21.5mg Magnesium), were provided by Chemist Warehouse (Australia). Gelatin (food grade) was purchased from Woolworth supermarket (Australia). Tannic acid was obtained from Sapphire Bioscience (NSW, Australia). Milli-Q water was used throughout the preparation of the protein–polysaccharide interactions.

5.3 Methods

5.3.1 The Preparation of physically entangled tannic acid-gelatin materials

Gelatin and tannic acid were mixed with water. The gelatin to tannic acid ratio was 2: 0.375 (w/w) with a total concentration of 0.18 g/mL. Briefly, 10 mL of 2% (w/v) gelatin solution and 3 mL of 0.125% (w/v) tannic acid solution were premixed, and then the solution was added to a VFD borosilicate glass tube (20 mm OD, 17 mm ID) through jet feeds while the tube was rotating at 7000 rpm, at a flow rate of 0.3 mL/min, with the tilt angle of the tube at 45°, and operating at room temperature of 25°C. These conditions were deemed as the optimal conditions for the encapsulation of fish oil after systematically varying the rotational speeds available (4000 to 9000 rpm), flow rate (0.3 to 0.5 mL/min), and tilt angle (30° to 60°). Indeed, these are the typical focused optimizing processing parameters for a VFD with a 20 mm OD tube. The traditional homogenization method was also applied for comparison with VFD processing. Here, the same concentration as used above for VFD processing was homogenized (homogenizer T25 digital ULTRA-TURRAX) at 13,500 rpm for 10 min at 25 °C. The processed liquid samples from the VFD and homogenization were collected, and then freeze-dried until further use.

5.3.2 Dynamic light scattering (DLS)

The size distribution of particles in the aforementioned liquid samples from VFD and homogenization were determined at 25 °C using DLS (Nano ZS90, Malvern instruments, Worcester, UK) operating with

a He-Ne 633 nm wavelength laser and a detector angle of 173°. The Malvern zeta sizer instrument measures the time-dependent fluctuations of light scattered based on the particle sizes.

5.3.3 Scanning Electron Microscopy (SEM)

SEM of samples for material derived from both liquid and freeze-dried forms used an Inspect FEI F50 SEM (PS216) instrument, under different magnifications. The spot size was 2.0 and the voltage was 5.0 Kv. The method of sample preparation for SEM was as follows: For liquid samples, 20 μ L of the prepared sample, immediately after processing, was drop casted on a silicon wafer and air dried overnight, followed by platinum sputter coating a ca 2 nm thick layer; for the freeze-dried material, the sample were submerged into liquid nitrogen for 2 min after being freeze-dried, then cut into slices with dimensions of 5 mm x 5 mm x 2 mm (length x width x thickness) using a surgical knife, followed by platinum sputter coating the sample with a ca 2 nm thick layer prior to characterization.

5.3.4 Fourier Transform Infrared Spectroscopy (FTIR)

FTIR spectra of freeze-dried materials were obtained using a spectrometer equipped with an attenuated total reflection accessory with a diamond crystal, at room temperature of 25°C. The spectral range was 400-4000 cm^{-1} with 40 scans and a resolution of 4 cm^{-1} . Around 10 mg of each freeze-dried sample was deposited on the diamond crystal prior to measurement. Background and sample spectra were also acquired at 4 cm^{-1} resolution with 40 scans from 400 to 4000 cm^{-1} .

5.3.5 Brunauer, Emmett, and Teller (BET) Analysis

Surface area and porosity of the freeze-dried samples were determined by BET analytical method (TriStar II, Micrometric Ltd, Lincoln LN6 3RX, United Kingdom). The freeze-dried samples were crushed to powder in liquid nitrogen; 40 mg of each powdered sample was then placed at the bottom of a BET tube, followed by 12 h of evacuating the BET tube. Thereafter the tube was inserted into the BET

analyzer with the conditions set as: Adsorptive gas, N₂; bath temperature, 77 K; and equilibration intervals, 20 s.

5.3.6 Viscosity measurement

The viscosities of the physically entangled tannic acid-gelatin materials were determined using a Brookfield viscometer equipped with a thermo-container and programmable temperature controller (LV-DVIII, HT-60, HT-110FR, respectively; Brookfield Engineering Laboratories, Inc.; Middleboro, MA, U.S.A). The thermo-container was equipped with a sample chamber and a spindle (HT-2 and SC4-18 respectively; Brookfield Engineering Laboratories, Inc.; Middleboro, MA, U.S.A). The system was cooled using a cooling plug assembly (HT-26Y, Brookfield Engineering Laboratories, Inc.; Middleboro, MA, U.S.A) attached to a pressurized air nozzle. The heating profile for the temperature controller was set as: Heat between 20 °C and 40 °C in increments of 2 °C/min; and the sample weight at 2 g. The spindle was set with a shear rate of 20.00 rad/s and a gap of 4 mm.

5.3.7 Nutrients entrapment by physically entangled tannic acid-gelatin materials

The mineral based nutrient supplement of Kid's multi-mineral and vitamin based nutrient supplement of Berocca were ground into powder prior to entrapment studies. The gelatin, tannic acid, and ground nutrient supplement were mixed with water. The gelatin to tannic acid to each nutrient supplement had a ratio of 2:0.375:1.25 (w/w/w). Briefly, 10 mL of 2% (w/v) gelatin solution and 3 mL of 0.125% (w/v) tannic acid solution were premixed and then mixed with 1.25 g of powdered nutrient supplement. The mixture of gelatin, tannic acid, nutrient supplement, and water was then added to a borosilicate glass tube (20 mm OD, 17 mm ID) in the VFD through jet feeds while the tube was rotating at 7000 rpm, at a flow rate of 0.3 mL/min, with the tilt angle of the tube at 45° and the device operating at room temperature of 25°C. These conditions were the optimum processing conditions for the preparation of VFD-produced non-covalent physically entangled tannic acid-gelatin material. The same concentrations as used above

for VFD processing were homogenized (homogenizer T25 digital ULTRA-TURRAX) at the same conditions as the aforementioned homogenization-produced physically entangled tannic acid-gelatin material (13,500 rpm for 10 min at 25 °C). The processed liquid samples from VFD and homogenization were collected and then freeze-dried.

5.3.8 Quantification of entrapped nutrients in physically entangled tannic acid-gelatin materials

Quantification of entrapped nutrients in physically entangled tannic acid-gelatin materials were characterized using SEM equipped with energy-dispersive X-ray spectroscopy (Inspect FEI F50, Bruker Cooperation, Billerica, Mass, United States). Results were presented as percentage of weight of each entrapped nutrient in comparison with the starting material.

5.4 Results and Discussion

5.4.1 Synthesis and physical characteristics of physically entangled tannic acid-gelatin

The use of physically entangled material for improved function has been applied in various products, such as physically entangled soy protein as material for biodegradable films for food package ¹⁵ and titanium physically entangled chitosan composite for efficient adsorption and detoxification of hexavalent chromium from polluted water ¹⁶. As a typical combination of material and physical entanglement agent, studies on physical entanglement between gelatin and tannic acid have been reported ^{17, 18}. Improved methods regarding the synthesis of physically entangled material are warranted, and processing in the VFD herein afforded a solution that was distinctly stickier in appearance relative to physically entangled tannic acid-gelatin material prepared using conventional methods of homogenization. VFD-mediated physical entanglement between gelatin and tannic acid was optimized with respect to rotational speed (4000- to 9000 rpm, with 7000 rpm deemed as optimized rotational speed), flow rate (0.3 to 0.5 mL/min, with 0.3 mL/min deemed as optimized flow rate), and title angle

(30° to 60°, with 45° deemed as optimized tilt angle). Containers with two different physically entangled tannic-acid-gelatin materials were inverted, showing that the material produced using VFD processing was in gel form and stuck to the bottom of container, whereas the material produced using homogenization was viscous, unable to stick to the tube, and dripped down (Fig 5.2a). Both of the images were for solutions of physically entangled material after 12 h at room temperature of 25°C post fabrication.

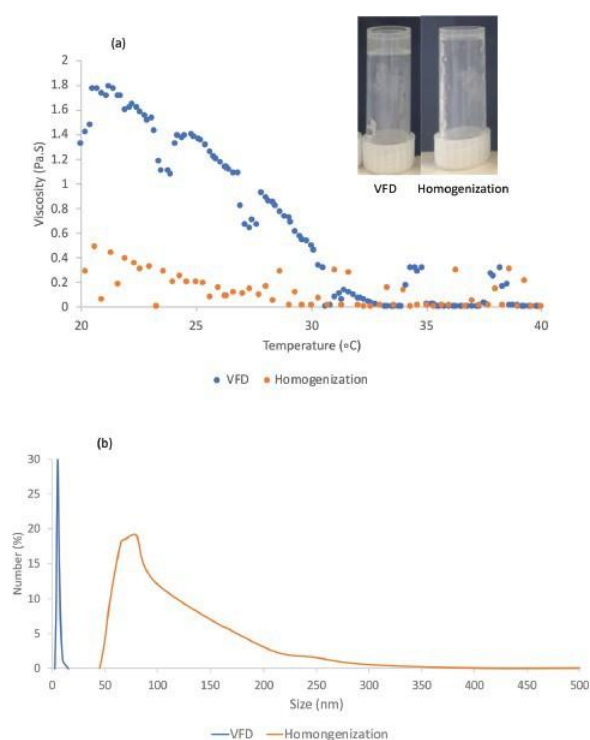


Figure 5.2: Physical characteristics of cross-linked tannic acid-gelatin materials produced using the vortex fluidic device (VFD). (total concentration: 0.18 g mL⁻¹, gelatin/tannic acid: 2: 0.375(w/w); speed: 7000 rpm; flow rate: 0.3 mL min⁻¹; tilt angle: 45 °C; temperature: 25° C) and homogenization (speed: 13 500 rpm; time: 10 min; temperature: 25 °C; homogenizer: T25 digital ULTRA-TURRAX). (a) Viscosity data: measured immediately after processing. Images in (a): taken 12 h after the material was prepared. (b) Dynamic light scattering (DLS) data.

The state of these two samples was unchanged after 5 days at room temperature of 25°C. The above differences in viscosity of physically entangled tannic acid-gelatin materials, between using VFD and homogenization processing, were maintained after 12 h storage at 25°C. Nevertheless, freshly prepared

solutions had substantial differences in viscosity (Fig 5.2a). For the temperature range between 20°C and 30°C, the viscosity of physically entangled tannic acid-gelatin material produced using VFD processing was significantly higher than that produced using homogenization. For example, at a temperature of 25°C, the viscosity of the former was 1.4 Pa.S, with the viscosity of the later much lower at 0.2 Pa.S. The viscosities of physically entangled tannic acid-gelatin materials show no apparent difference for temperature between 30°C and 40°C. The impact of increasing the temperature on a liquid or gel is to reduce the cohesive forces while simultaneously increasing the rate of molecular interchange, thereby substantially reducing the viscosity and the difference in viscosity between materials with different compositions, or the same compositions with different processing ¹⁹. Zhenbin, et.al ²⁰ noted that for temperatures > 35°C, viscosity difference of carrageenan-xanthan-starch gels with different compositions reduce from 2 Pa.S to no apparent difference, all tracking towards 0 Pa.S. There are reports of higher physical entanglement leading to higher viscosity and stickiness of the biopolymers ²¹. Greater amount of physical entanglement arising from using higher concentrations of tannic acid in the high internal phase emulsion based on modified starch, results in the viscosity and shear modulus increasing for increasing concentration of tannic acid, from 0% to 2% (w/w) ²². The increased concentration of tannic acid also results in the appearance of high internal phase emulsion after the process, changing from dripping-down liquid to the solid gel sticking at the bottom of the container, in accordance with the present study (Fig 5.2a). Similar results have been reported using tannic acid for generating hybrid supramolecular nanofibers²³. Overall, the results in (Fig 5.2a) indicate a stronger physical entanglement capacity of tannic acid imposed on gelatin when they were processed in a VFD, in comparison with in a homogenizer. The particle size of physically entangled tannic acid-gelatin generated using VFD and homogenization were determined using DLS analysis (Fig 5.2b), being remarkably different at ~10 nm and ~100 nm respectively. This highlights an advantage of the VFD in accessing smaller particles, with another being that the processing is under continuous flow, such that it is scalable, unlike the limiting batch homogenization processing. Based on the cost of operation, labor, etc., continuous flow VFD

processing process is more favorable for industry. The pH of starting material and processed material after both homogenization and VFD processing are 6.0 which is without change. The zeta potential values of these three materials are between -4.5 mV and -5 mV, and thus without significant difference. This shows that the reported DLS data was reliable, without being affected by differences of pH and zeta potential values of the material.

5.4.2. Scanning Electron Microscopy (SEM)

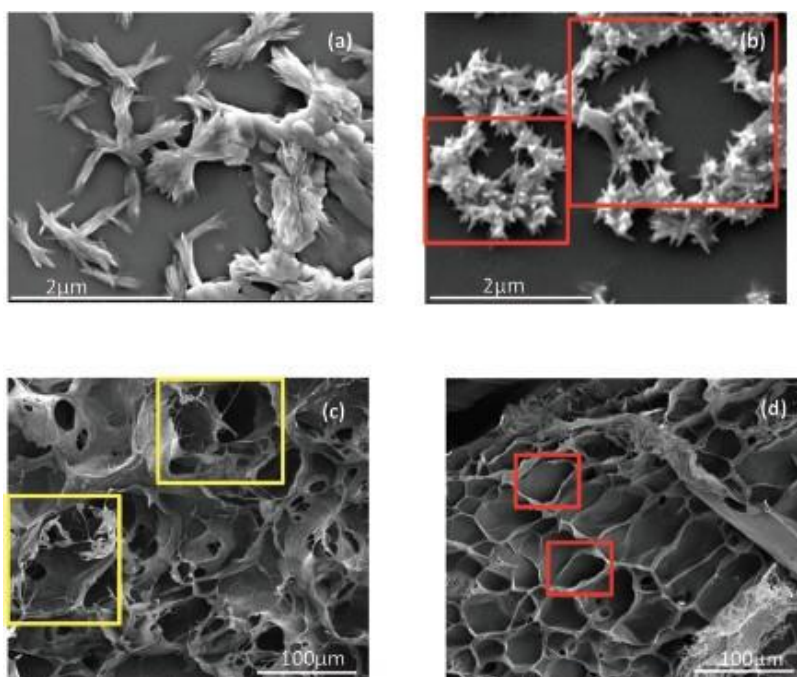


Figure 5.3: Scanning electron microscopy (SEM) images of cross-linked tannic acid-gelatin materials. (a) Material produced using homogenization processing (speed: 13 500 rpm; time: 10 min; temperature: 25 °C; homogenizer: T25 digital ULTRA-TURRAX) immediately drop casted onto a silicon wafer and air dried overnight, followed by platinum sputter coating. (b) Material produced using VFD processing (total concentration: 0.18 g mL⁻¹, gelatin/tannic acid: 2 : 0.375 (w/w); speed: 7000 rpm; flow rate: 0.3 mL min⁻¹; tilt angle: 45 °C; temperature: 25 °C) immediately drop casted onto a silicon wafer and air dried overnight, followed by platinum sputter coating. (c) Material produced using homogenization processing (speed: 13 500 rpm; time: 10 min; temperature: 25 °C; homogenizer: T25 digital ULTRA-TURRAX) after freeze-drying and platinum sputter coating. (d) Material produced using VFD processing (total concentration: 0.18 g mL⁻¹, gelatin/tannic acid: 2 : 0.375 (w/w); speed: 7000 rpm; flow rate: 0.3 mL min⁻¹; tilt angle: 45 °C; temperature: 25 °C) after freeze-drying and platinum sputter coating.

The morphology of physically entangled tannic acid-gelatin was determined using SEM, (Fig 5.3, Fig 5.3a and Fig 5.3b) are SEM images of samples immediately after being produced in the different processing platforms. Homogenization processing afforded rods matted together (Fig 5.3a) whereas the VFD gave enclosed spicular like structures (Fig 5.3b). The difference in structure presumably arises from different topologies of their fluid flow and dimensionalities thereof, as well as different induced shear stress and associated heat generation and rate of heat dissipation. In this context, during homogenization processing, only 5% of the supplied energy is used in processing, with the rest dissipated as heat²⁴. This resulted in apparent incomplete physical entanglement with rods being formed (Fig 5.3a). The VFD is more energy efficient having intense micro-mixing which facilitates physical entanglement of the gelatin and tannic acid, as indicated by closed circle in (Fig 5.3b). We note that the high shear stress in the VFD affords encapsulated fish oil particles 200 nm in diameter, compared with much larger particles of 3 μm using homogenization processing⁸. In addition, the VFD efficiently mixes Neutrase with milk protein, forcing them to be in close contact during the processing under high mass transfer conditions, with the enzymatic hydrolyzation time of milk protein reduced from 2 h in conventional water-bath processing to 20 min for VFD processing⁹. The aforementioned DLS technique is commonly recognized to provide guidance for the particle size in the tested liquid. Given that spicular nature of the particles generated using VFD processing, the DLS results are understood as a guide for the diameters of the physically entangled and enclosed particles, revealed in SEM images, highlighted in the red squares in (Fig 5.3b). The spicular particles are of similar size and their interlocking associated with self-assembly is potentially adding to the formation of a stable gel. This is reminiscent to interlocking of tetraphenylphosphonium cations at the molecular level²⁵.

The morphologies of the material from two freeze-dried samples were also explored using SEM. The surface of the freeze-dried sample prepared using homogenization processing was irregular with larger porosity/surface area ca 22,500 μm^2 (Fig 5.3c), typical pores shown in yellow squares). In comparison,

the surface of the freeze-dried samples prepared using VFD were more regular with smaller porosity/surface area ca $2500 \text{ } \mu\text{m}^2$ (Fig 5.3d, typical pores shown in red squares). Samples show clear morphological difference before (Fig 5.3a, Fig 5.3b) and after freeze-drying (Fig 5.3c, Fig 5.3d). Mechanical forces shred physically entangled materials during the processing of homogenization and VFD. Stronger mechanical force impacted on material during VFD processing will lead to more thorough, complete and homogenous shredding. This was demonstrated by regular, specular and circular structure in (Fig 5.3b), in comparison with rods with different sizes and open structure produced using homogenization, (Fig 5.3a). Reassembling of shred physically entangled materials occurred after processing. The morphologies of physically entangled samples after processing are shown in (Fig 5.3c) and (Fig 5.3d), being reassembled from the samples in (Fig 5.3a) and (Fig 5.3c), respectively. The difference between (Fig 5.3c) and (Fig 5.3d) reflects the different impact of energy input from homogenization relative to VFD processing. Samples with homogenous, specular structure after VFD processing (Fig 5.3b) led to the reassembled regular structure with small porosities. The width of thin, clear and even boundaries in (Fig 5.3d) is in accordance with the diameters of physically entangled and enclosed particles in (Fig 5.3b). However, samples with irregular shapes of rods and open structure after homogenization processing (Fig 5.3a) have large pores, without clear and even boundaries between them (Fig 5.3c). While the high shear mechanical force impacting on the material during VFD processing led to different physical properties, with thorough, complete and homogenous shredding, there was no chemical interaction (bond formation) between the components, as for using homogenization. This was established using FTIR of the physically entangled tannic acid-gelatin materials produced using VFD and homogenization (Fig 5.4), with both having the same spectra.

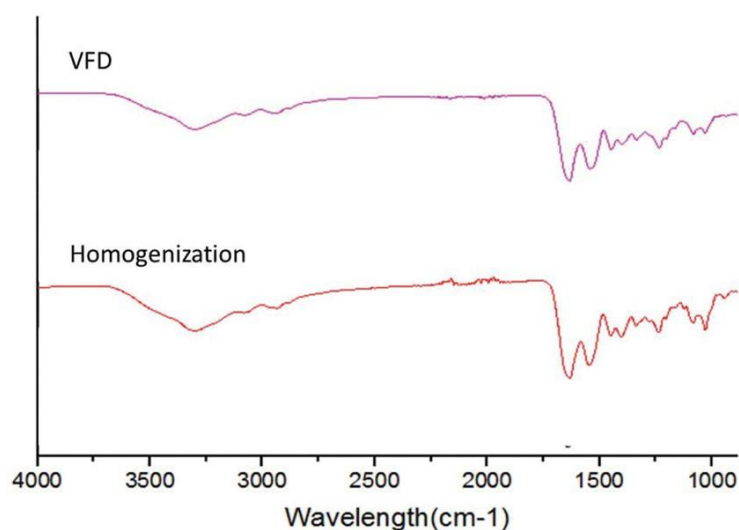


Figure 5.4: Fourier transform infrared (FTIR) spectra of physically entangled tannic acid-gelatin materials produced using the vortex fluidic device (VFD). (total concentration: 0.18 g mL^{-1} , gelatin/tannic acid: 2: 0.375 (w/w); speed: 7000 rpm; flow rate: 0.3 mL min^{-1} ; tilt angle: 45° ; temperature: 25° C) and homogenization (speed: 13 500 rpm; time: 10 min; temperature: 25° C ; homogenizer: T25 digital ULTRA-TURRAX).

The surface areas and porosity of these two materials were quantified by BET analysis. The surface area of the sample processed by homogenization ($7164.7 \text{ m}^2/\text{g}$) was almost double that of the sample processed by VFD ($3776.5 \text{ m}^2/\text{g}$). The same trend was also demonstrated in the porosity, with that of the sample prepared using homogenization processing at $0.1359 \text{ cm}^3/\text{g}$, higher than that prepared using VFD processing, $0.09458 \text{ cm}^3/\text{g}$.

5.4.3 Nutrients entrapment capacity of physically entangled tannic acid-gelatin

The appearances of different physically entangled tannic acid-gelatin materials with the entrapment of minerals and vitamins after freeze-drying are shown in (Fig 5.5). Darker colors represent more entrapped nutrients. The ground nutrient supplements of both minerals and vitamins processed by VFD were darker than those prepared using homogenization processing. This indicates enhanced nutrient entrapment

capacity of the physically entangled tannic acid-gelatin material when processed using a VFD relative to when processed using a homogenizer.

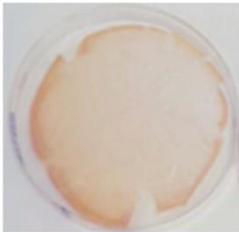
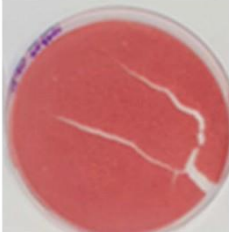
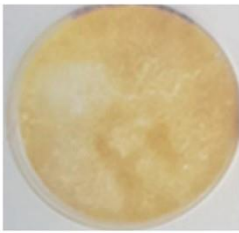

	Cross-linked tannic acid-gelatin	
	Homogenization processing	VFD processing
In the presence of minerals		
In the presence of vitamins		

Figure 5.5: Nutrients Entrapment capacity. Appearances of ground nutrient supplements of minerals and vitamins entrapped by different cross-linked tannic acid-gelatin materials after freeze-drying the sample prepared using VFD processing (gelatin/tannic acid/ground nutrient supplement: 2 : 0.375 : 1.25 (w/w/w); speed: 7000 rpm; flow rate: 0.3 mL min⁻¹; tilt angle: 45 °C; temperature: 25° C) and using a homogenizer (gelatin/tannic acid/ground nutrient supplement: 2 : 0.375 : 1.25 (w/w/w); speed: 13 500 rpm; time: 10 min; temperature: 25 °C; homogenizer: T25 digital ULTRA-TURRAX).

The nutrient entrapment was quantified using SEM equipped with energy-dispersive X-ray spectroscopy. The quantification results (Fig 5.6, Fig 5.7) match the sample appearances in (Fig 5.5) The substantial color changes of mineral entrapment samples between those prepared using a VFD and those prepared using homogenization processing (Fig 5.5) are reflected by substantial differences in weight percentage in (Fig 5.6) (20% in comparison with starting material for the homogenization sample, 30% in comparison with starting material for the VFD sample), with 1%, 2%, 3%, and 4% increase of Mg (4% to 5%), Zn (3% to 5%), Si (5% to 8%), and P (8% to 12%), respectively. Several techniques have been reported to improve entrapment capability of minerals in gel systems, including supercritical impregnation ²⁶.

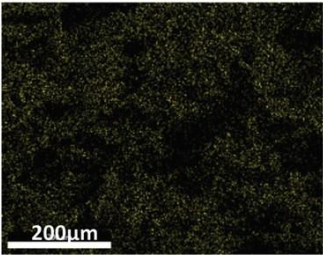
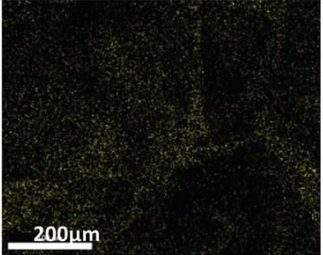
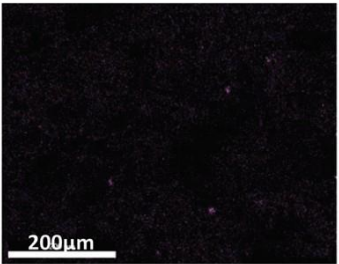
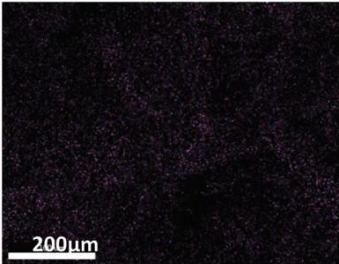
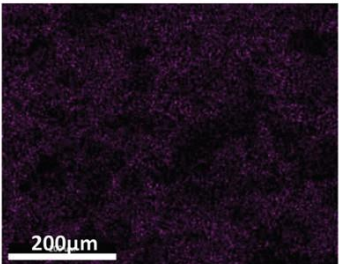
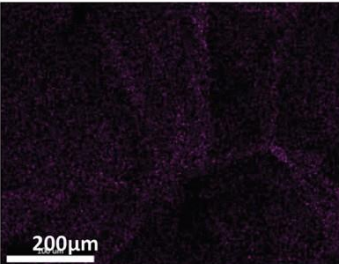
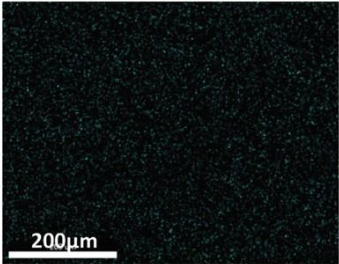
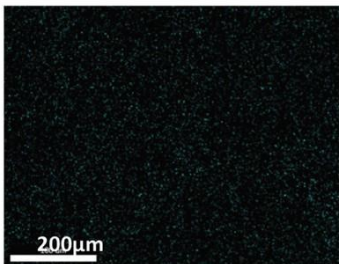
	Homogenization processing	VFD processing
Mg: Magnesium (percentage of testing material)	 (4%)	 (5%)
Si: Silicon (percentage of testing material)	 (5%)	 (8%)
P: Phosphorous (percentage of testing material)	 (8%)	 (12%)
Zn: Zinc (percentage of testing material)	 (3%)	 (5%)
Sum percentage	20%	30%

Figure 5.6: Percentage of entrapped mineral in cross-linked tannic acid-gelatin prepared using homogenization processing (speed: 13 500 rpm; time: 10 min; temperature: 25 °C; homogenizer: T25 digital ULTRA-TURRAX) and a VFD (total concentration: 0.18 g mL⁻¹, gelatin/tannic acid: 2: 0.375. (w/w); speed: 7000 rpm; flow rate: 0.3 mL min⁻¹; tilt angle: 45°; temperature: 25 °C).

The VFD technique presented in (Fig 5.6) and (Fig 5.7) establishes another technique for improved entrapment capability of minerals in comparison with minerals, the color changes of the vitamin

entrapped samples between those prepared using a VFD and those prepared using homogenization processing were minor.

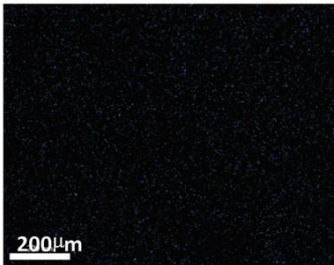
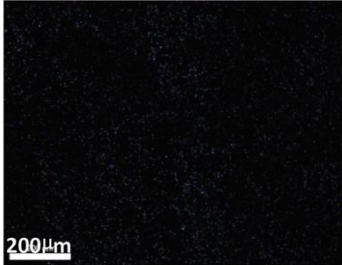
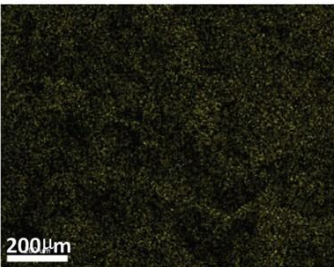
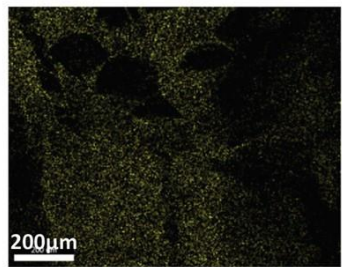
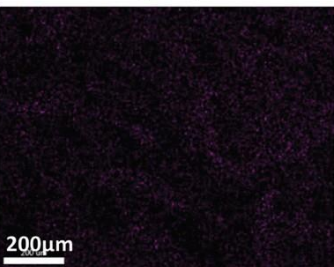
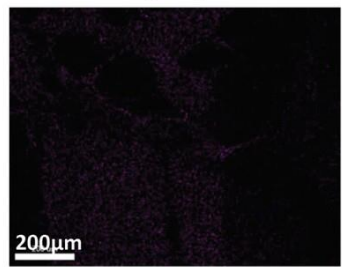
	Homogenization processing	VFD processing
Vitamin B13, represented by Co: Cobalt (percentage of testing material)	 (2%)	 (4%)
Vitamin H and B1, represented by S:Sulfur (percentage of testing material)	 (11%)	 (11%)
Vitamin B6, represented by P:Phosphorous (percentage of testing material)	 (4%)	 (5%)
Sum percentage	17%	20%

Figure 5.7 Percentage of each entrapped vitamin in cross-linked tannic acid-gelatin prepared using homogenization processing (speed: 13 500 rpm; time: 10 min; temperature: 25 °C; homogenizer: T25 digital ULTRA-TURRAX) and a VFD (total concentration: 0.18 g mL⁻¹, gelatin/tannic acid: 2: 0.375(w/w); speed: 7000 rpm; flow rate: 0.3 mL min⁻¹; tilt angle: 45°; temperature: 25 °C).

This is reflected in (Fig 5.7) (17% in comparison with starting material for the homogenization sample, 20% in comparison with starting material for the VFD sample) where the change of weight percentage in comparison with starting material are small at 3%, with 1% and 2% increase of Vitamin B6 (4% to 5%) and Vitamin B13 (2% to 4%), respectively. Given the structure of Vitamin B6 (with P) and Vitamin B12 (with Co).it is common to use the percentages of cobalt (Co), sulfur (S) and phosphorus (P) to

represent the percentages of Vitamin B13, Vitamin H and B1, Vitamin B6, respectively; the analysis uses energy-dispersive X-ray spectroscopy^{17, 27}. As detailed in the ‘Materials and Methods’ section, 10 mL of 2% (w/v) gelatin solution and 3 mL of 0.125% (w/v) tannic acid solution were premixed and then mixed with 1.25 g of powdered nutrient supplement. According to this, the weight of starting material is $10 \times 2\% + 3 \times 0.125\% \times 384 = 0.2375$ g. The entrapped mineral after VFD processing and homogenization is 0.0713 g ($0.2375 \text{ g} \times 30\%$) and 0.0475 g ($0.2375 \times 20\%$), respectively, and the entrapped vitamin after VFD processing and homogenization is 0.0475 g ($0.2375 \times 20\%$) and 0.0333g ($0.2375 \times 17\%$), respectively. The entrapped weight of nutrients is for providing sufficient daily intake of various minerals and vitamins as recommended by World Health Organization (WHO), especially after VFD processing. The entrapped Zn and Mg after VFD processing were both $0.2375 \times 5\% = 0.0119 \text{ g} = 11.9 \text{ mg}$ with the daily intake of Zn and Mg recommended by WHO at 15 mg and 350 mg²⁸, respectively. Accordingly, the daily consumption of starting material only needs to be 0.3 g for Zn and 7 g for Mg in nutritional supplement after VFD processing. The same encouraging outcome was also found for vitamin B6, with $0.2375 \times 5\% = 0.0119 \text{ g} = 11.9 \text{ mg}$ entrapment after VFD processing. The daily intake of B6 recommended by WHO is 6 mg²⁸ and thus the daily consumption of the material after VFD processing for the nutritional supplement is 0.12 g.

5.4.4 Scale-up VFD processing to produce non-covalent physical entanglement of tannic acid and gelatin

The VFD is designed with the ability to operate under continuous flow for on-demand processing of large volumes of liquid. To establish this herein, we readily translated the processing of a 10mL solution, as used for all of the above studies, to passing 100 mL of solution within 18 h through the device, with the solution found to have the same overall characteristics. The success of this trial demonstrates both the stability and scalability of VFD processing, and the consistency of the quality of the final products, for translating into industrial scale demands.

5.5 Conclusion

The use of VFD processing of physically entangled tannic acid-gelatin has been established, for nutrient entrapment which was compared with material and entrapment using conventional homogenization processing. As observed using SEM for the liquid samples, greater non-covalent physical entanglement prevails in samples produced using VFD processing relative to those produced using homogenization. SEM established that for freeze-dried samples, the surface area of the pores and porosity of the samples produced using VFD processing were both substantially reduced compared with samples prepared using homogenization processing. The nutrient entrapment capacity for minerals and vitamins for physically entangled tannic acid-gelatin material produced using VFD was significantly higher than for the material produced using homogenization. The overall these findings establish that VFD processing provides a new direction for bottom-up, scalable processing for non-covalent physical entanglement of biopolymers with potential for food processing.

Acknowledgements

The authors acknowledge support of this work by the Australian Research Council, and the Australian Microscopy and Microanalysis Research Facility (AMMRF), and the Australian National Fabrication Facility for SEM, along with funding from "Hundreds of Talents Program ", Guangzhou University, China (funding code:28099201-302).

References

1. J. Britton and C. L. Raston, *Chem. Soc. Rev.*, 2017, 46, 1250-1271.
2. X. Chen, N. M. Smith, K. S. Iyer and C. L. Raston, *Chem. Soc. Rev.*, 2014, 43, 1387-1399.
3. J. Britton, J. M. Chalker and C. L. Raston, *Chem.-Eur. J.*, 2015, 21, 10660-10665.
4. J. Britton, L. M. Meneghini, C. L. Raston and G. A. Weiss, *Angew. Chem.-Int. Edit.*, 2016, 55, 11387-11391.

5. J. Britton, R. P. Dyer, S. Majumdar, C. L. Raston and G. A. Weiss, *Chem.-Int. Edit.*, 2017, 56, 2296-2301.
6. K. Vimalanathan, R. G. Shrestha, Z. Zhang, J. Zou, T. Nakayama and C. L. Raston, *Chem.-Int. Edit.*, 2017, 56, 8398-8401.
7. J. Britton and C. L. Raston, *RSC Adv.*, 2014, 4, 49850-49854.
8. S. He, N. Joseph, X. Luo and C. Raston, *LWT-Food Sci. Technol.*, 2019, 103, 88-93.
9. S. He, N. Joseph, X. Luo and C. L. Raston, *PLoS One*, 2019, 14, e0216816.
10. S. He, N. Joseph, S. L. Feng, M. Jellicoe and C. L. Raston, *Food Funct.*, 2020, 11, 5726-5737.
11. S. F. Hosseini, L. Ramezanzade and M. Nikkhah, *Int. J. Biol. Macromol.*, 2017, 105, 1455-1463.
12. N. T. Annan, A. D. Borza and L. T. Hansen, *Food Res. Int.*, 2008, 41, 184-193.
13. B. Muhoza, S. Xia and X. Zhang, *Food Hydrocolloids*, 2019, 97, 105174.
14. Y. Huang, A. Li, C. Qiu, Y. Teng and Y. Wang, *Food Funct.*, 2017, 8, 3145-3154.
15. A. Gonzalez, M. Cristina Strumia and C. I. Alvarez Igarzabal, *J. Food Eng.*, 2011, 106, 331-338.
16. L. Zhang, W. Xia, X. Liu and W. Zhang, *J. Mater. Chem. A*, 2015, 3, 331-340.
17. C. Bertoni-Freddari, C. Giuli, G. Lustyik and I. Nagy, *Mech. Ageing Dev.*, 1981, 16, 169-180.
18. M. d. L. Linhares Rodrigues Menezes, N. d. R. Pires, P. L. Rodrigues da Cunha, M. d. F. Rosa, B. W. Silva de Souza, J. P. de Andrade Feitosa and M. d. S. Moreira de Souza Filho, *FOOD PACKAGING SHELF*, 2019, 19, 7-15.
19. N. E. Noren, M. G. Scanlon and S. D. Arntfield, *Trends Food Sci. Technol.*, 2019, 88, 290-301.
20. Z. Liu, B. Bhandari, S. Prakash, S. Mantihal and M. Zhang, *Food Hydrocolloids*, 2019, 87, 413-424.
21. M.-F. Li, Z.-Y. He, G.-Y. Li, Q.-Z. Zeng, D.-X. Su, J.-L. Zhang, Q. Wang, Y. Yuan and S. He, *Food Hydrocolloids*, 2019, 90, 482-489.
22. Y. Liu, C. Yan, J. Chen, Y. Wang, R. Liang, L. Zou, D. J. McClements and W. Liu, *Food Hydrocolloids*, 2020, 109, 10683.
23. M. Allais, D. Mailley, P. Hebraud, D. Ihiwakrim, V. Ball, F. Meyer, A. Hebraud and G. Schlatter, *Nanoscale*, 2018, 10, 9164-9173.
24. K. Schroen, O. Bliznyuk, K. Muijlwijk, S. Sahin and C. C. Berton-Carabin, *CURR OPIN FOOD SCI*, 2015, 3, 33-40.
25. I. Dance and M. Scudder, *Chem.-Eur. J.*, 2010, 2, 481-486.
26. A. Abu-Fayyad and S. Nazzal, *Int. J. Pharm.*, 2017, 528, 463-470.
27. R. Ranguin, M. C. Ncibi, T. Cesaire, S. Lavoie, C. Jean-Marius, H. Grutzmacher and S. Gaspard, *Environ. Sci. Pollut. Res.*, 2020, 27, 41122-41131.
28. M. Kim, Y. Lee and K. Park, *Nutrients*, 2018, 10, 50



Cite this: DOI: 10.1039/d0fo02230f

Vortex fluidics mediated non-covalent physical entanglement of tannic acid and gelatin for entrapment of nutrients†

Xuejiao Cao,^{†‡} Nikita Joseph,^{†‡} Matt Jellicoe,[‡]
Ahmed Hussein Mohammed Al-Antaki,[‡] Xuan Luo,[‡] Dongxiao Su,[‡]
Shan He[‡] and Colin Raston[‡]

We have developed a simple process for the entrapment of nutrients in shear stress induced non-covalent physically entangled tannic acid-gelatin gel in a thin film vortex fluidic device (VFD) operating under continuous flow. This allows control of the porosity and surface area of the pores in order to improve the nutrient entrapment capacity. The VFD microfluidic platform simplifies the processing procedure of physically entangled biopolymers, as a time and cost saving one-step process devoid of any organic solvents, in contrast to the conventional homogenization process, which is also inherently complex, involving multiple-step processing. Moreover, the use of homogenization (as a benchmark to entrap nutrients) afforded much larger porosity and surface area of pores, with lower entrapment capacity of nutrients. Overall, the VFD processing provides a new alternative, bottom-up approach for easy, scalable processing for materials with a high nutrient entrapment capacity.

Received 24th August 2020,
Accepted 22nd November 2020
DOI: 10.1039/d0fo02230f
rsc.li/food-function

1. Introduction

The vortex fluidic device (VFD), Fig. 1, is a relatively new thin film microfluidic processing platform with remarkably diverse research and industrial applications.¹ VFD processing technology emerged from research efforts focused on the application of thin film microfluidics and thin film flow chemistry.^{1,2} This processing harnesses high shear forces, intense micro mixing, and high heat and mass transfer, overcoming the mixing and heat transfer limitations of traditional batch processing (Britton *et al.*, 2015).³ The processing capabilities of the VFD are rapidly growing, from small molecule synthesis through to processing functional materials for drug delivery, and the manipulation of single cell organisms.¹

A VFD can be operated under a confined mode, where a tube containing a finite volume of liquid is spun at high speed, or continuous flow, where jet feeds deliver liquid to the

bottom of the tube or at positions along the tube, with the device otherwise operating under the same conditions as the confined mode. At high rotational speeds, the liquid in the tube forms a dynamic thin film with the thickness of the film controlled by varying the rotational speed, the tilt angle of rotation, and the volume of liquid in the tube.³

The utility of the VFD has been established for a number of chemical transformations, with control over chemical reactivity and selectivity, and the ability to prepare complex molecules in a single pass. Dramatic enhancement of enzymatic reactions has also established, averaging seven-fold acceleration for a variety of enzymes,⁴ and this is understood mechanistically from the effect of Faraday pressure waves contained within the thin film. Related to this is the tethering of enzymes to the surface of the tube, for the synthesis of small molecules in a single pass.⁵

VFD processing has also been applied to materials synthesis under continuous flow, for example in assembling fullerenes C₆₀ molecules into nanotubes.⁶ Of particular note is that the micron length nanotubes, with hollow diameters of 100 to 400 nm, are formed in the absence of surfactant, and without the need for further downstream processing. Indeed, this is a common hallmark of use of the VFD where the operating parameters can be systematically explored as high throughput processing in optimizing any process. This is typified, for example, in effectively converting sunflower oil to biodiesel at room temperature of 25 °C, with no saponification and avoid-

[†]Department of Food Science, School of Chemistry and Chemical Engineering, Guangzhou University, Guangzhou, Guangdong, 510006, China.
E-mail: he0091@gmail.com, dongxiao@126.com

[‡]Flinders Institute for Nanoscale Science and Technology, College of Science and Engineering, Flinders University, Bedford Park, South Australia, 5042, Australia.
E-mail: colin.raston@flinders.edu.au; Tel: +61 8 82017958

† Electronic supplementary information (ESI) available. See DOI: 10.1039/d0fo02230f

‡ As the first author(s), these two major authors contributed equally to this work.

Chapter 6: Vortex Fluidic Regulated Equilibria Involving Liposomes

Down to Solvated Phospholipids

(This manuscript is close to submission)

Nikita Joseph^{1,5}, Marzieh Mirzamani^{2,5}, Tarfah Abudiyah¹, Ahmed Alanataki¹, Matt Jellicoe¹, David P Harvey¹, Emily Crawley¹, Andrew Whitten⁴, Elliot Gilbert⁴, Michael Michael³, Harshita Kumari^{2*},
Colin L Raston^{1*}

¹ Flinders Institute for Nanoscale Science and Technology (INST), College of Science and Technology,
Flinders University, Bedford park, SA 5042 Australia

² James L. Winkle College of Pharmacy, University of Cincinnati, Cincinnati, OH 45267-0004, USA

³ Flinders Centre for Innovation in Cancer (FCIC), Flinders Medical Centre (FMC), Bedford Park, SA
5042 Australia

⁴ Australian Nuclear Science and Technology Organization (ANSTO), Lucas heights, NSW 2234
Australia.

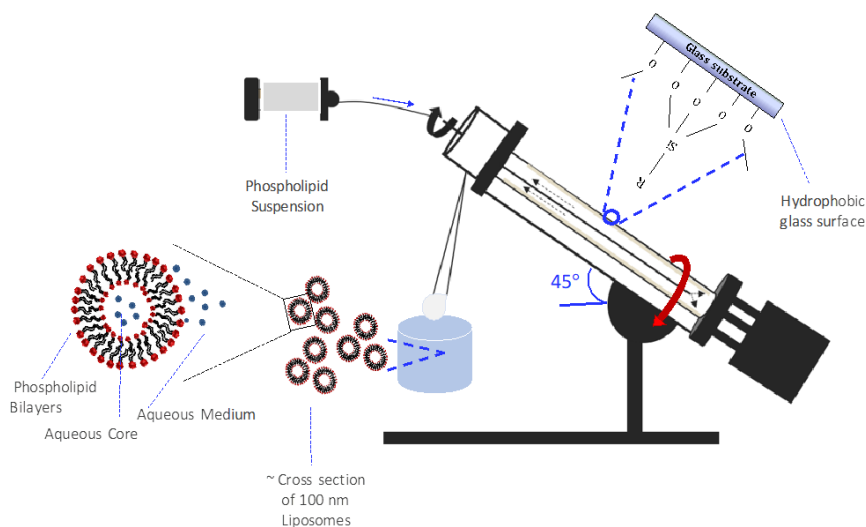
⁵ Co-first Authors.

Author Contributions

N.J.: wrote the main manuscript text, revised/reviewed manuscript for final version approval, prepared figures, concept, design, and literature review for the research, and carried out experimental studies at Australian Nuclear Science and Technology Organization (ANSTO). M.M.: carried out data analysis/interpretation and writing for the Small Angle Neutron Scattering (SANS) section. T.A and M.J helped in experimental section. D.H. and E.C: assisted the SANS experiments at ANSTO. A.W and E.G: assisted the setup of experiments at ANSTO. H.K.: supervised and carried out data analysis/

interpretation and writing for the SANS section. C.L.R.: supervised the whole project and guided for all the experiments.

Graphical Abstract



Abstract

Conventional channel based microfluidic platforms have gained prominence in controlling the bottom-up formation of phospholipid-based nanostructures including liposomes. However, there are challenges in gaining access to liposomes from rapid scalable processes and from high concentrations of phospholipids. These have been overcome using a vortex fluidic device (VFD), as a thin film microfluidic platform rather than channel based, affording ca 100 nm diameter liposomes. The high yielding and high throughput continuous flow process has a rapidly rotating glass tube with an inner hydrophobic surface, tilted at 45°. Processing is also possible in the confined mode of operation of the VFD which is effective for labelling pre-VFD prepared liposomes with fluorophore tags for then

mechanistic studies on the fate of liposomes under shear stress in the VFD. *In-situ* small-angle neutron scattering established the co-existence of liposomes ca 100 nm in diameter and small rafts, micelles, distorted micelles, or solvated phospholipid, for increasing rotation speeds. The equilibria between one of these small entities and ca 100 nm liposomes for a specific rotational speed of the tube is consistent with the spatial arrangement and dimensionality of topological fluid flow regimes in the VFD. The commonality of ca 100 nm diameter liposomes establishes that this is the most stable structure from the bottom up self-assembly of the phospholipid, and this is in accord with the typical dimension of both exosomes and endosomes.

6.1 Introduction

Liposomes are composed of self-assembled bilayers of phospholipid which confine space, segregating the inner compartments from aqueous surrounding environment. They have emerged as vehicles for drug and gene delivery applications, which relates to the liposomes mimicking cells behaviour and protecting themselves from the immune responses of the body ^{1, 2}. They are of interest in mimicking the size and function of exosomes ^{3, 4}, and they are also used as bio-analytical tools, as in immunoassays, biosensors and liposome-nanotube networks ^{1, 2}. These lipid assemblies can be altered and manipulated in specific carrier systems for developing novel approaches towards clinical and analytical applications. Fabricating liposomes using conventional methods involves a number of critical steps including dissolving lipid molecules in a suitable solvent, solvent evaporation for producing a thin film and extracting liposomes by hydrating the thin film on the addition of different solvents ⁵. This complex processing was given a new direction using channel based microfluidic platforms. Such microfluidic systems can result in high response to controlling the properties of the liposomes in terms of size, distribution, lamellarity and polydispersity⁵⁻⁹. Transforming this technology to clinical scale processing raises a number of challenges in addressing the viability of generating liposomes at macro-scale where the processing is diffusion controlled under laminar flow, with low Reynolds numbers typically >200. These challenges arise

With restrictions associated with the focus of the microfluidic hydrodynamic approach (MHF), as a lab-on-a-chip device⁵. They can be addressed using the more recently developed thin film microfluidic platforms, as in the vortex fluidic device (VFD), (graphical abstract), where the thickness of the film is typically less than 500 nm, which is in the realms of microfluidics. The VFD has a rapidly rotating tube open at one end, and at high rotational speed shear stress is generated, producing thin films of different thickness, depending on the orientation and rotational speed of the tube. The associated dynamic thin films are pivotal for applications of the device in chemical and materials transformations¹⁰⁻¹³.

The VFD is operated in the confined mode, where a finite amount of liquid is allowed to under-go processing for a specific time, and continuous flow mode for scaling up the process⁸. For the latter, the liquid is continuously delivered into the rapidly rotating tube via syringe pumps or the like at different flow rates and different rotational speeds, and the product is collected at the other end. In addition, sequential processing can be done by connecting the out flow of one VFD to another VFD⁸. We report herein the processing of liposomes at a macro-scale with the formation of approximately 100 nm liposomes in water across the rotation landscape when the tube is tilted at 45°. Moreover, we establish the ability to prepare fluorophore labelled liposomes based on the same phospholipids in the VFD, depending on its operating parameters, in particular at lower rotational speeds. The VFD has a diverse range of applications including protein folding¹⁴, accelerating enzymatic reactions¹², controlling chemical selectivity and reactivity¹⁵⁻¹⁶, tuning hydrogel properties¹⁷, manipulating the surfactant and interface for functional food structure and encapsulation¹⁸⁻²⁰, fabricating porous spheres of cross linked BSA protein with glutaraldehyde and²¹ and also monitoring real-time bio-sensing application²². The optimal operating parameters for any application depend on the rotational speed of the hemispherical based tube, with the tilt angle usually at 45°, and the signature of the liquid²¹. The latter is defined as the impact of rotational speed on mixing times for a drop of liquid to mix halfway up the tube, change in temperature monitored midway along the tube, and the average film thickness²¹. The thin film has high

Reynold's numbers with different high shear stress topological fluid flows down to sub-micron dimensions²³. We hypothesized that these fluid flows would be effective in reorganizing phospholipids into different structures through shear stress disassembly, with then reassembly away for the topological fluid flows, to the thermodynamically favored structure. Formation of the liposomes occurs at lower phospholipid concentrations relative to that used in the conventional batch processes⁵ as the critical micelle concentration is reached much faster in the VFD due to high mass transfer under controlled topological shear stress²³. This bottom-up control of self-assembly in forming liposomes is a paradigm shift for rapid, high throughput and scalable processing for generating liposomes. Its simplicity is in contrast to the otherwise requirements of membrane extrusion to prepare liposomes. The mechanism of VFD mediated formation of liposomes has been studied using *in situ* Small-Angle Neutron Scattering (SANS)²⁴ establishing the formation of small assembled arrays of phospholipid down the micelles and solvated phospholipids which are in equilibria with ca 100 nm liposomes. This is the thermodynamically favored bottom up assembly of phospholipid molecules not experiencing shear stress topological fluid flows within the thin film of liquid in the VFD, (Fig 6.2) Interestingly, the formation of ca 100 nm liposomes matches the approximate size of endosomes and exosomes^{3,4}.

6.2 Materials

1-Palmitoyl-2-Oleoyl-sn-Glycerol-3-Phosphocholine (POPC) was purchased from sapphire biosciences NSW, Fluorophore lipids are selected such as, Rh-PE 1,2-Dipalmitoyl-sn-Glycero-3-Phosphoethanolamine-N-(Lissamine Rhodamine B Sulfonyl) (Ammonium Salt), and NBD-PE (1-Oleoyl-2-Hydroxy-sn-Glycero-3-Phosphoethanolamine-N-[Tetra (Ethylene Glycol)]-N'-(7-Nitro-2-1,3-Benzoxadiazol-4-yl) (Ammonium Salt). Milli Q water was utilised for all the experiments.

6.3 Methods

6.3.1 Fabrication of Liposomes

A phospholipid suspension of 50 µg/mL in Milli q water was processed through VFD at an optimized speed of 9000 rpm, 0.1 mL/min flow-rate, 45° tilt angle in continuous flow in a hydrophobic tube.

6.3.2 Labelling liposomes with fluorophore lipids.

Liposomes fabricated by VFD were isolated through ultracentrifugation at 113,000 g's and redispersed in PBS. 1% of the fluorophore lipid was added to this population and processed through VFD at lower rotational speed of 5000 rpm.

6.3.3 Mixing of Fluorophore labelled liposomes

In this processing, 1 mL of RH-PE labelled liposomes were mixed with 1 mL of NBD-PE labelled liposomes using the confined mode of operation in the VFD, for 15 minutes, with a rotational speed of 5000 rpm, with a tilt angle of 45°, in a hydrophobic tube.

6.3.4 Nanoparticle Tracking Analysis (NTA)

The size distribution of the liposomes was analyzed using a Nano Sight LM10 instrument (Malvern instruments Ltd, Worcestershire, UK) equipped with NTA software version 2.3. The particle suspensions were diluted with PBS to a concentration of 1–8 × 10⁸ particles/mL for analysis. Data were taken in triplicate 60s videos to get a standard error for the data, for nanoparticle tracking analysis.

6.3.5 Scanning Electron Microscopy (SEM)

Samples were analyzed using an Inspect FEI F50 SEM (PS216) instrument. The spot size was 3.0, voltage was 5.0 kV and magnification were 50,000. Sample preparation for SEM was as follows: 20 µL of as-prepared sample was drop casted on a silicon wafer and air dried overnight, followed by platinum sputter coating of a 2 nm thick layer, for SEM imaging.

6.3.6 Atomic Force Microscopy (AFM)

Samples were analyzed with atomic force microscope (AFM) (Nanoscope V, Multimode 2 SPM). Images were acquired using silicon probes in tapping mode in air with Scanner “E” from 500 nm 3 μ m scan sizes. The sample preparation for AFM was as follows: 20 μ L of 1: 100 diluted sample was drop casted onto silicon wafer and air dried overnight whereupon the samples were washed 3 times with Milli-Q water prior to recording the AFM images.

6.3.7 Transmission Electron Microscopy (TEM)

Samples were analysed with transmission electron microscopy (TEM) (FEI Titan Themis 80-200). The sample preparation was as follows: 20 μ L of sample was fixed on the carbon grids and left to air dry for 1 h, with the excess sample removed using blotting paper, followed by staining using 2g/100 mL uranyl acetate solution. TEM images were then taken at 250Å~magnification under the voltage of 100 keV.

6.3.8 Small-Angle Neutron Scattering (SANS) sample preparation

Solutions of 0.1 wt% POPC phospholipid solutions were prepared in D₂O. Then 2 mL of solution was added in a quartz VFD tube OD 20mm with an inner hydrophobic surface in confined mode at lower speed of 3800 rpm, 4000, 4500 rpm and 5000 rpm, while 1 mL of solution was added for higher speeds such as 7000, 8000 and 9000 rpm. All the VFD samples were collected and characterized post-VFD with conventional SANS. As-received sample without any processing was also characterized with SANS.

6.3.9 SANS data acquisition and analysis

All the SANS experiments were carried out on Bilby (ANSTO, Lucas Heights, Australia). The VFD microfluidic device was mounted on the xyz θ goniometer stage. An aluminum shield with a foil slit was covering the VFD tube and the beam was passed through the slit. The stage was adjusted with respect to the neutron beam such that the beam-centre was placed 3 cm from above the base of the tube. The beam

had a neutron wavelength of $\lambda = 5 \text{ \AA}$ and sample-detector distances were set to 1.3m, 12.0m and 20.0m to achieve the full q -range of $0.00216 \text{ \AA}^{-1} < q < 0.36309 \text{ \AA}^{-1}$. The scattering vector $q = (4\pi/\lambda) \sin(\theta/2)$, λ is the neutron wavelength, and θ is the scattering angle. All the datasets were corrected for solvent scattering using D2O blanks measured at each speed, background scattering, empty quartz tube scattering, and detector sensitivity. The data were then set to absolute scale using sample transmission measurements. Finally, the reduced 2D data were radially averaged to yield the 1D scattering curve. Mantid version was employed for all data reduction while the NIST macros for Igor Pro were used for the data fitting. The data sets did not exhibit clear scattering features that supported the use of any particular form factor, with the exception of the 3800 rpm and 4500 rpm in-situ and post-shear data. In order to analyze most of the data, empirical models were fitted to the data using nonlinear-least squares method. The Guinier- Porod model or a summed Guinier-Porod + Gaussian Peak model ^[17] were used to fit the data. A summed Uniform Ellipsoid + Dilute Lamellar model was fitted to the in-situ 3800 and 4500 rpm data and the post-shear 3800 rpm data, while the Dilute Lamellar model was used to model the post-shear 4500 rpm data. The models were not resolution-smeared, because the reduction procedure for the VFD setup caused the q -resolution to be inaccurate.

6.3.10 Fluorescence spectroscopy measurements

All the fluorescence measurements were carried out with Cary Eclipse Fluorescent Spectrophotometer, Agilent technologies using quartz cells of path-length 10 mm. Both excitation and emission band slits were fixed at 10 nm and the scan rate was selected at 1800 nm/min. The excitation wavelength was selected at 460 nm for the NBD-PE fluorophore while emission spectra were collected in the range of 480–600 nm. The excitation wavelength for Rh-PE was selected as 560 nm and emission was collected from 570-650 nm.

6.4 Results and Discussions

The optimal conditions in the VFD under continuous flow, where a flow rate of 0.1 mL/min with the glass tube spun at 9000 rpm at a tilt angle of 45° relative to the horizontal position is required for generating liposomes (graphical abstract). This was established by systematically (See SI section 3,4,5 & 6) exploring the operating parameters of the device, notably rotational speed, tilt angle of the tube and the nature of the inner surface of the tube, and flow rate, along with the concentration of the phospholipid, POPC, in Milli Q water, which was established at 50 g/mL (See SI section 3,4,5 & 6). Initially the confined mode of operation of the VFD was used for process optimization, as a proven strategy for translating processes in general into continuous flow⁸. The tubes were made of borosilicate glass or quartz, 20 mm in diameter tube (ca 17.5 mm internal diameter), 18.5 cm in length with a hemispherical base, which is the most widely used tube. We found that the phospholipid covered the Inner surface of the tube when using the confined mode of operation of the device. This was overcome by rendering the inner surface hydrophobic by coating with Trichloro-DodecylSilane (See SI section 2).

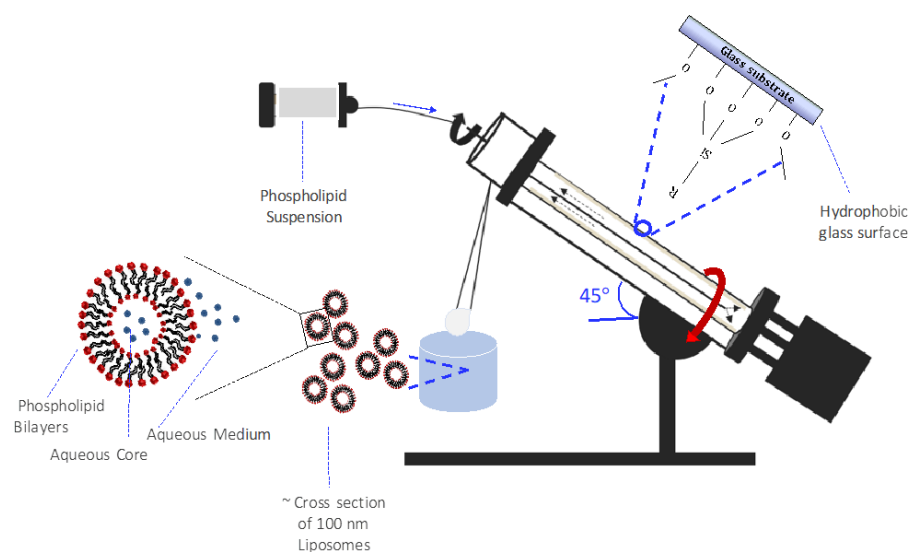


Figure 6.1: Schematic representation of The Vortex Fluidic Device. The phospholipid suspension is passed to the bottom of the tube through one jet feed at a concentration of 1mg/mL, 9000 rpm, 0.1 mL/min, 45° tilt angle in continuous flow in a hydrophobic tube. The collected product yields unilamellar liposomes of ~ 100 nm in size.

Processed solutions (confined mode and continuous flow) were analyzed using Nanoparticle Tracking Analysis (NTA), in providing particle size distributions. The mean diameter of the liposomes at the optimal conditions was 110 nm, (Fig 6.1). The morphology of the spheroidal particles was determined using Scanning Electron Microscopy (SEM), Transmission Electron Microscopy (TEM) and Atomic Force Microscopy (AFM). The diameter size obtained from SEM is within the range of 100 – 200 nm. The diameter size obtained from TEM is at 100 nm. Atomic Force Microscopy (AFM) established the diameter of the particles within the range 80 – 150 nm, as well as the height profile of the liposomes on the silicon substrate ¹⁴. A phospholipid bilayer is 4.5 nm ¹⁴ and a deflated unilamellar liposome has a height thickness of ca 10 – 12 nm. ¹⁴ Given that the particles were sputter coated with 2 nm of platinum, the determined average thickness of 15.9 nm, as determined from counting 100 -200 particles on an AFM

image and an average distribution plot were carried out, in accord with the formation of unilamellar liposomes.

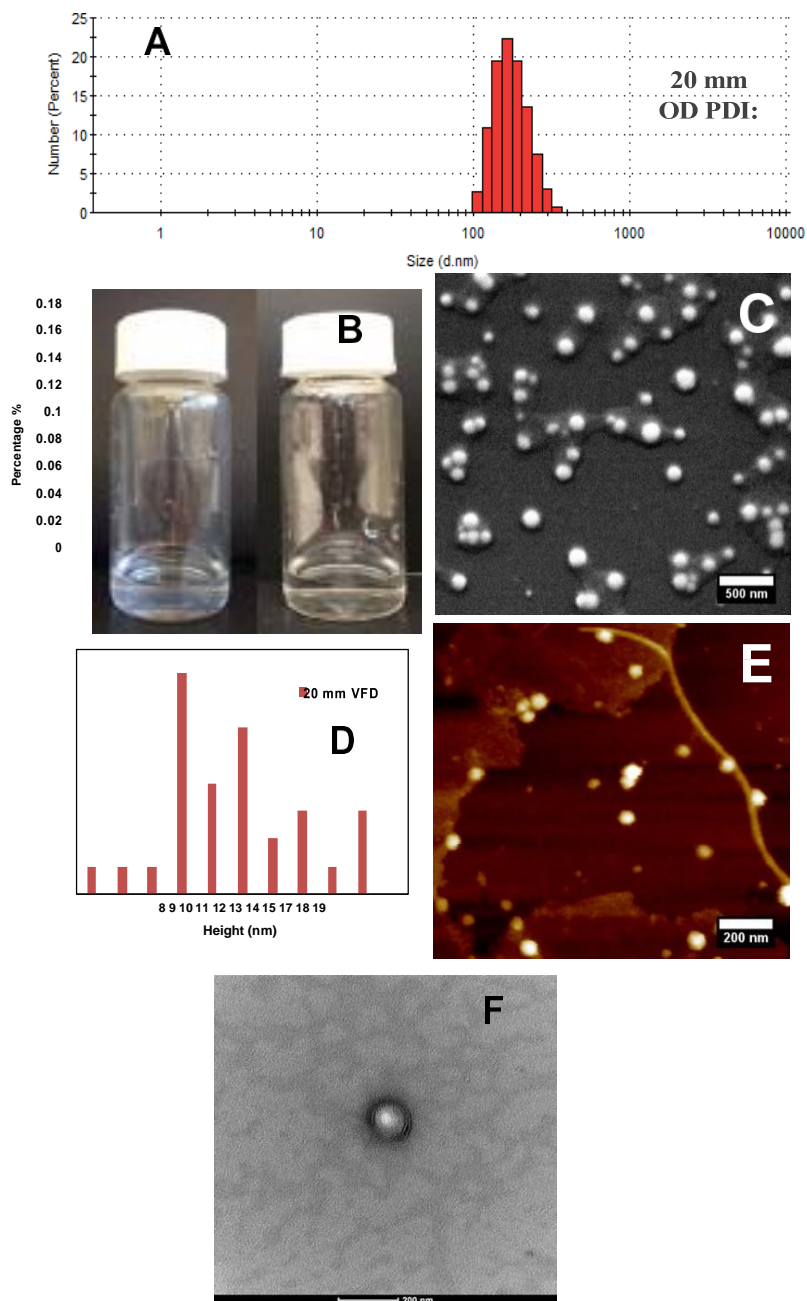


Figure 6.2: VFD processed Liposomes. (A) Dynamic Light Scattering data with the highest number of particles at 200 nm with a polydispersity index (PDI) of 0.3 (B) pre-VFD and post VFD solutions for 1 mg/mL phospholipid (POPC) solution in Milli-Q water processed at 9000 rpm, 0.1 mL/min, 45° tilt angle in continuous flow in a hydrophobic tube. (C) SEM image for VFD processed liposomes at 9000 rpm,

0.1 mL/min, 45° tilt angle in continuous flow in a hydrophobic tube, the sample was sputter coated with 2 nm Pt deposition before imaging. Scale bar is 500 nm. (D) AFM Height Distribution Profile for VFD processed liposomes IN 20 mm OD tube as in (E), the sample being imaged with a fast scan assist peak force microscope in tapping mode on a silicon surface. Scale bar is 200 nm. (F) TEM image for VFD processed liposomes as in (B) with the sample stained with 2% uranyl acetate and air dried on a copper grid before imaging. The voltage applied was 80 – 100 kv. Scale bar is 200 nm

The nature of the inner surface of the tube also affects the processing outcome in forming liposomes, beyond the POPC initially coating the surface of the tube when it is hydrophobic. The hydrophobic tube avoids such coating and improves the PDI for dynamic light scattering determination of the particle sizes generated in a continuous flow setup. The reason for the higher PDI for hydrophilic tubes, where there is less control over the self-assembly processes, is unclear. Nevertheless, it is more energetically favorable for the hydrophobic chain in the phospholipid to associate with other hydrophobic chains in reducing the surface area when dispersed in water, as a free energy driven process with a decrease in entropy. The arrangement of phospholipids with their hydrophilic head group in contact with water lowers the interfacial tension, but in a hydrophilic tube the expected drag of the polar head groups with the hydrophilic glass surface will perturb the fluid dynamics, and presumably this is at the expense of some loss in control of the self-assembly process. It should be noted that the choice of hydrophilic or hydrophobic tube is essentially another operating parameter of the VFD and an understanding on how this impact on chemical reactions, and self-assembly in the present study, is yet to be realized. The above results are for the 20 mm OD diameter VFD tube (17.5 mm internal diameter), and subsequently studied the processing in smaller diameter tubes, 10 mm OD and 15 mm OD glass tubes. This is possible using interchangeable bearing in the standard 20 mm diameter VFD.

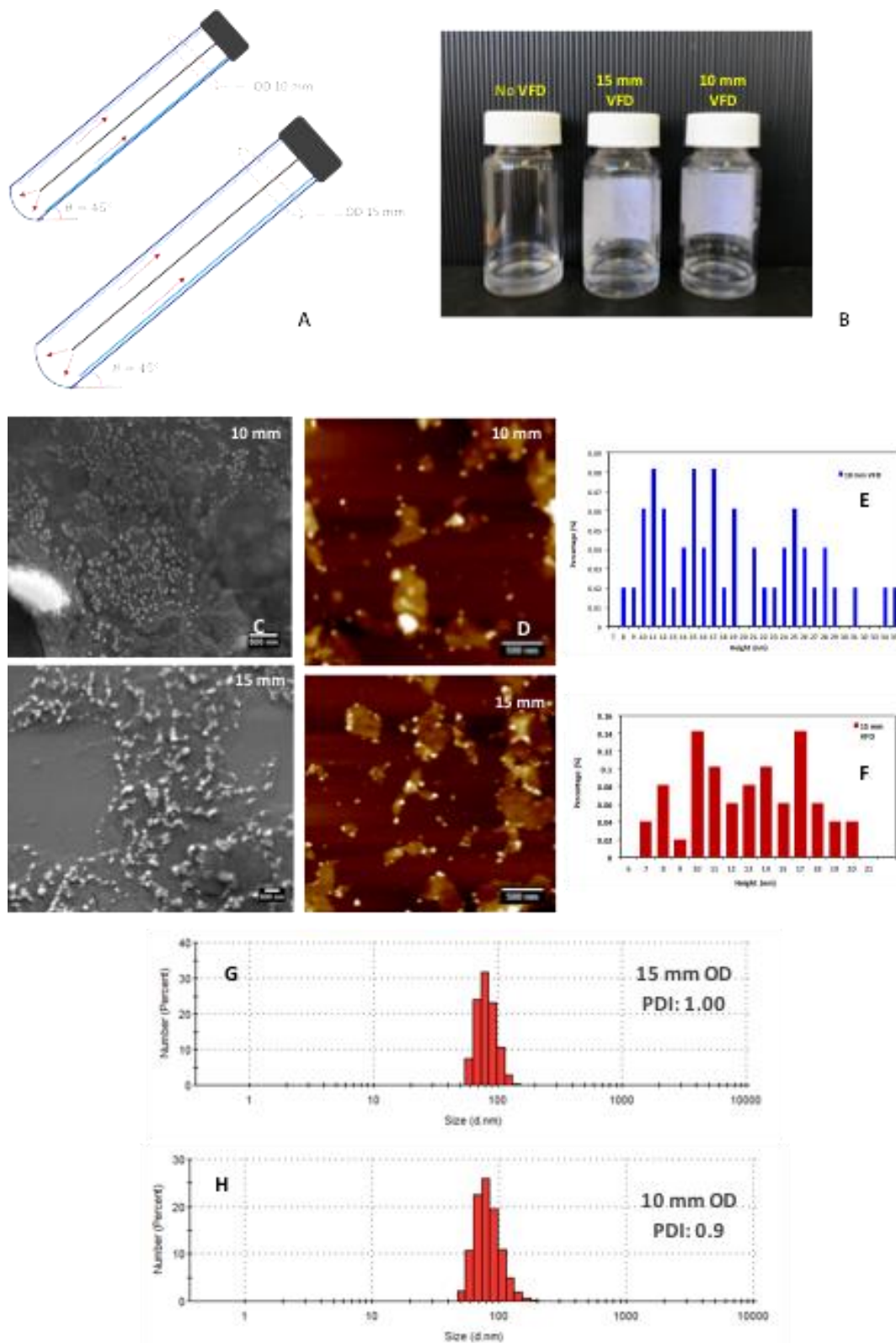


Figure 6.3: Influence of different size VFD tube. (A) Schematic representation for hydrophobic coated VFD tube, 10 mm and 15 mm OD. (B) pre-VFD and post VFD solutions processed at 9000 rpm in confined mode, concentration 1 mg/mL, tilt angle 45° in both tubes. (C) SEM image for VFD processed

liposomes; the sample was sputter coated with 2 nm Pt deposition before imaging. Scale bar 500 nm. (D) AFM images and height distribution profile for VFD processed liposomes in 10 and 15 mm OD tubes; the sample were scanned with SPM multimode 2 in tapping mode on a silicon surface. Scale bars 500 nm. (E) and (F) AFM height thickness of the particles formed in 10 and 15 mm OD tubes respectively. (G) and (H) DLS distribution plots for particles formed in 10 and 15 mm OD tubes respectively.

Due to multiple applications in the VFD microfluidic platform, different materials can be processed in different glass tube with different OD's. Herein, 10 mm and 15mm is applied for the liposome scaling application. Due to smaller OD in 10 mm the liposomes polydispersity is not controlled as less surface area is accessed and a thicker thin film formation, similar observations were found in 15mm OD tube. Thus, due to larger access to surface area and thinner thin film formation at 9000 rpm the best polydispersity and size control is observed using 20mm VFD glass tube in a hydrophobic surface tube. As the self-assembly process is inherently complex, different techniques are widely utilized to understand the self-organization in soft matter. Here, we have developed an in-situ process utilizing Small-Angle Neutron Scattering (SANS). This capability of performing *in-situ* measurements while measuring structures on the nano-meter scale (10-300 nm) makes SANS an excellent technique to use in studying the VFD and its effect on liposomes.

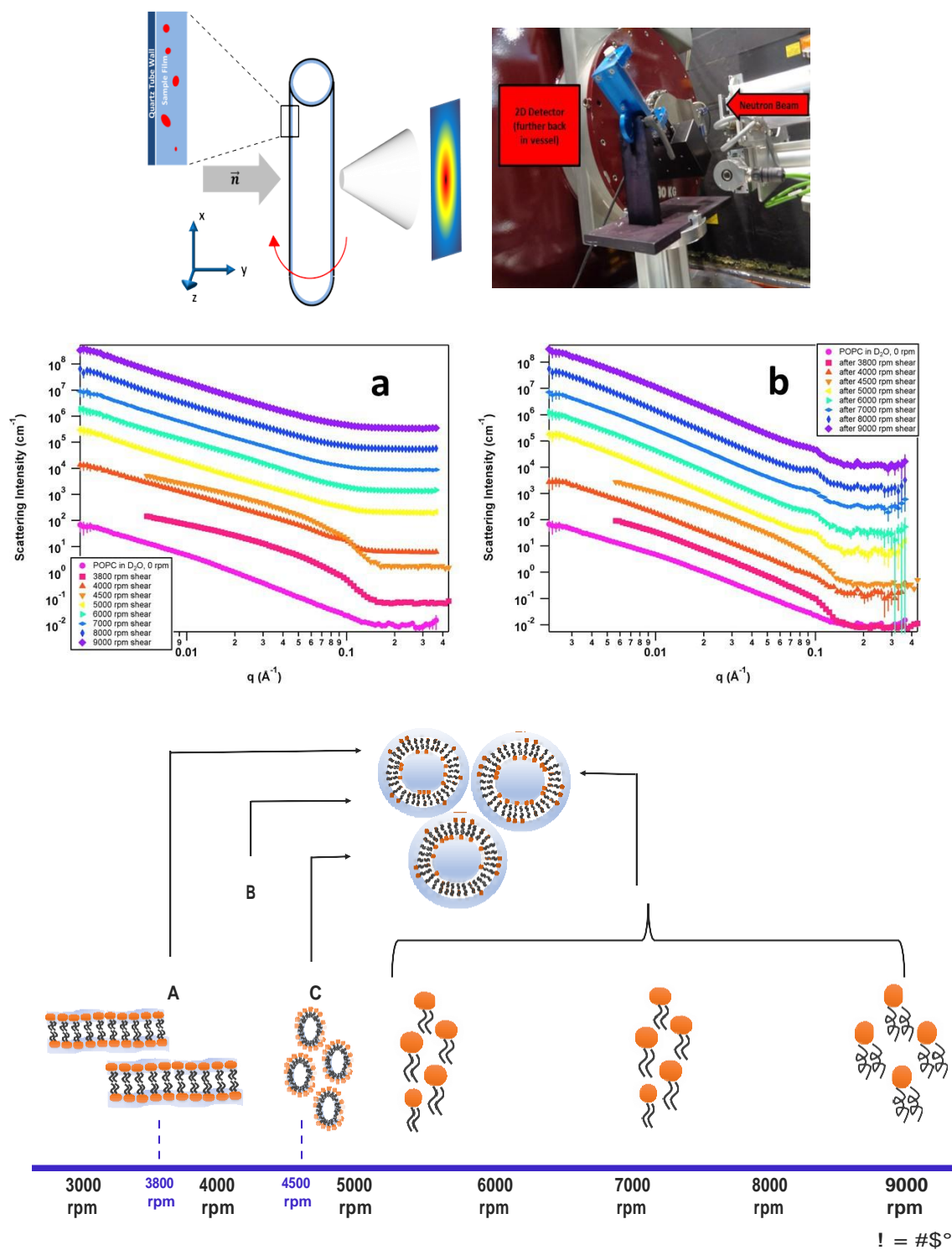


Figure 6.4: SANS data overlays of POPC liposomes in D₂O at each shear level generated at the specified rotational speeds: (a) overhead-view schematic of the VFD tube, the sample film, and the neutron beam passing through and being scattered by the tube and sample film before meeting the 2D-detector; (b) BILBY sample staging area depicting the VFD setup; (c) real-time VFD-SANS data as a

function of increasing rotational speeds (d) static SANS measurements after each real-time VFD study, (e) schematic mechanism on the observed lipid self-assembly at each rotational speed as determined via in-situ SANS and post-shear static SANS. Each data set in (a) and (b) were offset by powers of 6 for improved visibility.

SANS data overlays are shown in (Fig 6.4). During the shearing process (Fig 6.4a), some changes to the results were observed. At 3800 rpm and 4500 rpm, the scattering data appeared similar to each other while being noticeably different from the un-sheared data set and the data from higher shear levels. A weak peak at about 0.1 \AA^{-1} was also seen at both shear levels, suggesting the presence of a structure or building block with a repeating distance. At 5000 rpm and above, the scattering data was featureless and maintained a similar slope, indicating that increasing shear did not affect the general shape of the structure. After shearing (Fig 6.4b), the scattering data at all shear levels except 3800 rpm and 4500 rpm appeared similar to the 0 rpm scattering data, with the addition of a weak scattering peak at 0.1 \AA^{-1} . This suggested that the liposome structure returned to baseline after shearing, although a new structure or building block with a repeating distance was also generated *in-situ* as a transient species. After shearing at 3800 rpm and 4500 rpm, however, the scattering data mostly retained the same appearance that the *in-situ* data had, indicating that the liposome structure underwent lasting changes.

Table 6.2: SANS fitting results for the real-time VFD-SANS data at increasing VFD speeds

The 0 rpm sample did not undergo shear in order to serve as a baseline. The 0 rpm, 5000 rpm, 6000 rpm, 7000 rpm, 8000 rpm, and 9000 rpm samples were fitted with the Guinier-Porod model which is typically used to fit spherical micelles or lamellar micelles. The 3800 rpm, 4000 rpm, and 4500 rpm samples were fitted with a summed Guinier-Porod + Gauss Peak model. The cross-section/thickness values were calculated from the R_g value based on the geometry specified by the dimension variable. The d-spacing value was calculated from the peak position determined by the Gauss Peak model. Errors are $\pm 5\%$.

Parameter	0 rpm	3800 rpm	4000 rpm	4500 rpm	5000 rpm	6000 rpm	7000 rpm	8000 rpm	9000 rpm
Dimension Variable, s	1.83	--	1.55	--	1.81	1.77	1.86	1.85	1.94
R_g (Å)	28.9	--	14.7	--	10.5	13.8	10.8	10.5	8.24
Porod Exponent	2.47	--	4.00	--	4.00	2.91	2.99	2.83	3.60
Cross-section/ Thickness (Å)	100.0	--	51.1	--	36.4	47.7	37.3	36.3	28.5
Peak position (Å ⁻¹)	--	--	0.0940	--	--	--	--	--	--
Std Dev (Å ⁻¹)	--	--	0.0090	--	--	--	--	--	--
d-spacing (Å)	--	--	66.9	--	--	--	--	--	--
Ellipsoid R_a (Å)	--	179.8	--	180.3	--	--	--	--	--
Ellipsoid R_b (Å)	--	35.4	--	33.6	--	--	--	--	--
Lamellar Bilayer Thickness (Å)	--	26.2	--	26.8	--	--	--	--	--

To better identify trends during and after shearing the liposomes, a nonlinear least-squares fitting procedure was used to fit the data with appropriate models. The Guinier-Porod model was used to fit the 0rpm data, 5000-9000 rpm *in-situ* data, and the 4000 rpm post-shear data sets. A Guinier-Porod + Gaussian Peak summed model was used to fit the 4000 rpm *in-situ* data and the 5000-9000 rpm post-shear data sets. A Dilute Lamellar + Uniform Ellipsoid summed model was fitted to the 3800 rpm and 4500 rpm *in-situ* data and the 3800 rpm post-shear data, and finally the Dilute Lamellar model was fitted

to the 4500 rpm post-shear data. Table 1 shows the fitting results to the *in-situ* VFD SANS data, while Table 2 contains the results for the post-shear data modelling. The Guinier-Porod model provided information on the radius of gyration (R_g) of the scattering particle, the general shape(s) of the scattering particle (globular, rod-like, or lamellar/flat), and the Porod exponent. The Gaussian Peak model was included in the model to analyze data sets that showed a peak in the high- q region, and provided information on the position of the peak and how broad it was. The cross-section or thickness of the particle was calculated from the R_g value while the characteristic repeat distance (d-spacing) was calculated from the peak position. Before the samples were sheared, i.e. the milky POPC suspension (0 rpm, Table 1), the particles appeared to be 100 Å thick and mostly flat with a slight rod-like character. Once the sample was sheared at 3800 rpm, two different geometries became apparent: a lamellar structure and an ellipsoidal structure. The ellipsoidal structure was a large prolate ellipsoid ($R_a > R_b$) with an aspect ratio ($R_a: R_b$) of approximately 5.1:1. The lamellar structure was fairly thin in comparison, with the bilayer having a thickness of 26.2 Å. At 4000 rpm, the scattering structure became equally rod-like and lamellar-like. The thickness of the particle went up to 51 Å while the d-spacing of the repeating structure decreased to 67 Å. Increasing the shear to 4500 rpm again resulted in the formation of prolate ellipsoids and lamellar structures; however, the aspect ratio of the ellipsoids increased to approximately 5.4:1 and the bilayers became slightly thicker than they were at 3800 rpm, at 26.8 Å. Once the shear increased to 5000 rpm and higher, the scattering particles became flat, similar to how the structure was before being sheared. The particles were thinner than the pre-sheared particles, however, becoming around 40 Å thick. As the shear increased beyond 5000 rpm, the thickness tended to decrease. This fluid phenomena are due to the Coriolis driven circular flow which is followed by double helical topological fluid flow once the Faraday waves are induced as the mechanical response from the vibrations, this was previously reported

¹⁵ The behavior at 4000 rpm being similar to what happened at 3800 rpm.

Table 6.3: SANS fitting results to the post-shear data sets.

<i>Parameter</i>	0 rpm	3800 rpm	4000 rpm	4500 rpm	5000 rpm	6000 rpm	7000 rpm	8000 rpm	9000 rpm
<i>Dimension Variable, s</i>	1.83	--	1.52	--	1.69	1.69	1.58	1.92	1.64
<i>R_g (Å)</i>	28.9	--	80.6	--	114.7	99.1	117.9	99.3	98.6
<i>Porod Exponent</i>	2.47	--	2.49	--	2.60	2.61	2.60	2.68	2.59
<i>Cross-section/ Thickness (Å)</i>	100.0	--	279.4	--	397.5	343.5	408.5	343.9	341.6
<i>Peak position (Å⁻¹)</i>	--	--	--	--	0.0933	0.0909	0.0881	0.0922	0.0890
<i>Std Dev (Å⁻¹)</i>	--	--	--	--	0.00861	0.0107	0.0136	0.0122	0.0121
<i>d-spacing (Å)</i>	--	--	--	--	67.4	69.1	71.3	68.1	70.6
<i>Ellipsoid R_a (Å)</i>	--	22.3	--	--	--	--	--	--	--
<i>Ellipsoid R_b (Å)</i>	--	37.7	--	--	--	--	--	--	--
<i>Lamellar Bilayer Thickness (Å)</i>	--	73.8	--	34.1	--	--	--	--	--

The 0 rpm sample did not undergo shear in order to serve as a baseline. The 0 rpm and 4000 rpm samples were fitted with the Guinier-Porod model. The 3800 rpm, 4500 rpm, 5000 rpm, 6000 rpm, 7000 rpm, 8000 rpm, and 9000 rpm samples were fitted with a summed Guinier-Porod + Gauss Peak model. The cross-section/thickness values were calculated from the R_g value based on the geometry specified by the dimension variable. The d-spacing value was calculated from the peak position determined by the Gauss Peak model. Errors are $\pm 5\%$.

After the shearing process, a number of lasting changes to the structure of the scattering particles could be noticed (Table 2). After being sheared at 3800 rpm, the ellipsoid and lamellar structures remained. Interestingly, the ellipsoids transitioned to oblate ($R_b > R_a$) and the bilayers thickened by a factor of 2.8 to become 73.8 Å, demonstrating that the high shear had a great effect on the structural dimensions. After the sample was sheared at 4000 rpm, the repeating structure that caused the high-q peak disappeared, the scattering particle became equally rod-like and lamellar-like in structure, and its thickness dramatically increased to 280 Å. It is not clear why the building block or repeating structure disappeared after the shear ended. After shearing at 4500 rpm, the ellipsoidal structures disappeared, leaving only the lamellar

structures. The lamellar bilayers became thicker at 34.1 Å than they were while undergoing shear. After shearing at 5000 rpm and above, the particle structure became similar to how it was after shearing at 4000 rpm, in terms of the rod-like/lamellar-like geometry and how the structure became significantly thicker. However, the repeating structure or building block that caused the high-q peak still remained and maintained a d-spacing of around 67 Å. The differences in the final geometry, structural thickness, and d-spacing as a function of shear may be due to the effects of the Coriolis and Faraday waves that were present while the sample was being sheared. Thus, the in-situ SANS provides understanding on the formation of liposomes through this simple VFD processing technique. The high shear in the VFD produce higher curvature in the liposomes bilayer which distorts into transient ellipsoidal species and down to solvated phospholipids. A fundamental understanding is achieved in the self-assembly and disassembly of liposomes which are fabricated through this high shear microfluidic platform. Furthermore, fluorophore labelling of the liposomes and their exchange was studied through this processing technique. This gives insights on encapsulating different bio-active molecules and on membrane fusion of the liposomes.

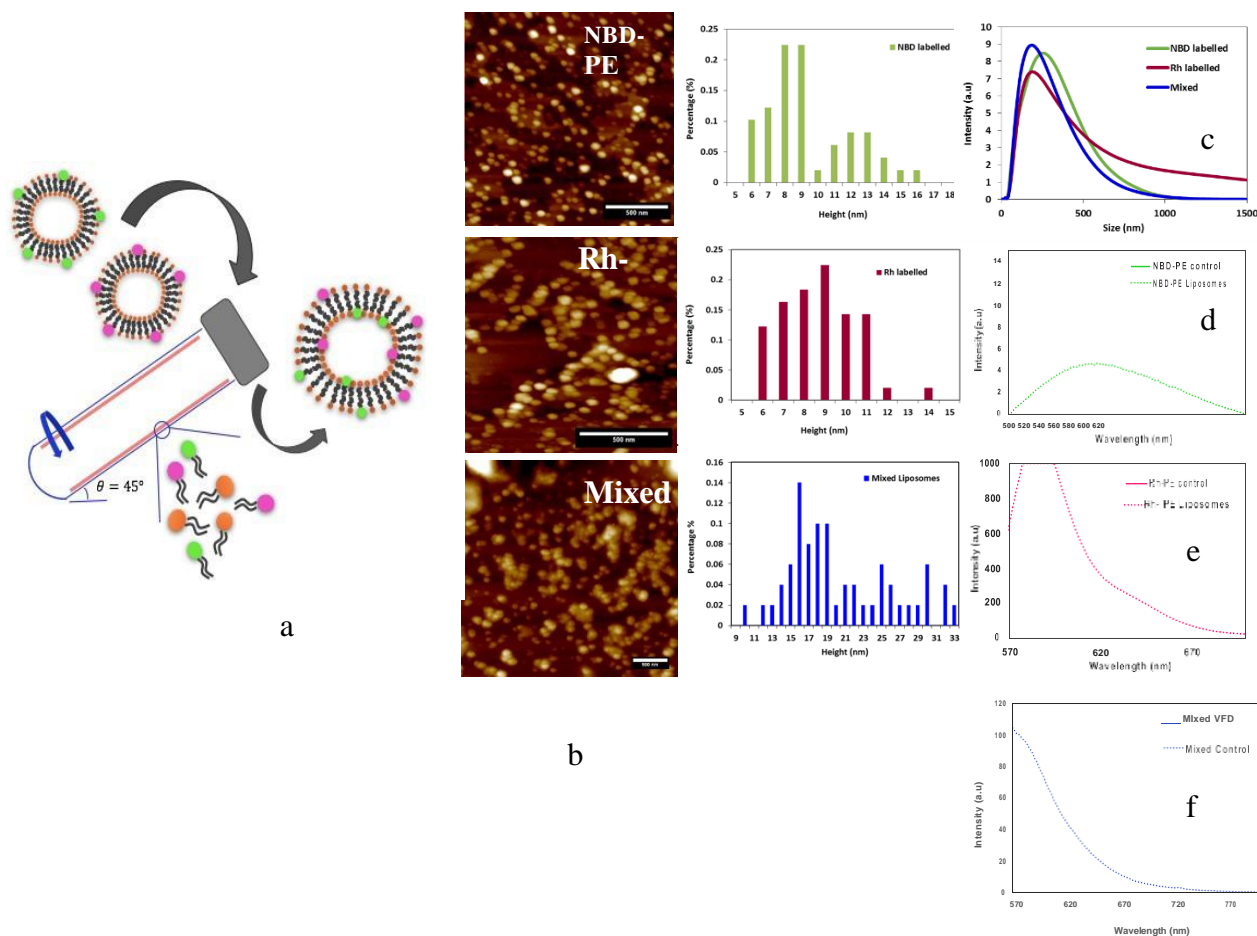


Figure 6.5: Fluorophore labelling and exchange of labelled liposomes. (a) Schematics for VFD NBD-PE liposomes and VFD Rh-PE liposomes and mixed fluorophore labelled liposomes processed through VFD at given conditions of 5000 rpm, 0.1% of fluorophore dye, confined mode, 1 mL of solution at 45° in 20 mm VFD tube. (b) Atomic Force Microscopy (AFM) images and height distribution profile for VFD processed fluorophore labelled liposomes and mixed fluorophore VFD liposomes. (c) DLS size distribution for VFD NBD-PE liposomes and VFD Rh-PE labelled liposomes and mixed fluorophore VFD liposomes. (d) Fluorescence spectrum for the VFD NBD-PE liposomes, (e) VFD Rh-PE fluorophore labelled liposomes and (f) VFD mixed liposomes.

The two-prepared fluorophore labelled liposomes were prepared initially by processing unlabeled liposomes at an optimized condition with phospholipid suspension of 50 µg/mL in Milli Q water was processed through VFD at an optimised speed of 9000 rpm, 0.1 mL/min flow-rate, 45° tilt angle in

continuous flow in a hydrophobic tube, these VFD processed liposomes population were further isolated through ultracentrifugation at 113,000 g's and redispersed in PBS. 1% of the fluorophore lipid was added to this population and processed through VFD at lower rotational speed of 5000 rpm were then characterized using DLS, measuring the size of generated fluorophore liposomes. The size of fluorophore labelled liposomes incorporating NBD-PE dye did not show any significant change relative to the size of the liposomes prepared for just VFD processed POPC (un-labelled liposomes). Similarly, a comparison made between the size of POPC (un-labelled liposomes) and fluorophore labelled liposomes using RH-PE dye did not show any significant change in the size of the liposomes. Mo et al. reported that the lamellarity thickness of a phospholipid bilayer mimic was approximately 5 nm, (Fig 6.5). The results from the AFM height profile, (Figure 3), in the present study indicates that the formed liposomes are unilamellar. In addition, shows that the diameter of the deflated collapsed vesicles is about 15 nm and this is also consistent with vesicles generated using a similar thin film process with a unilamellar or two bilayers before collapsing. The height of NBD-PE formed fluorophore labelled liposomes, and RH-PE fluorophore labelled liposomes are shown in (Fig 6.5). These observations indicate that there is no change in the final geometry of the liposomes even after addition of a foreign entity. Due to the dynamic nature of the phospholipids and the intense shear stress from the VFD the liposomes dis-assemble into solvated phospholipids which was shown through the in-situ VFD SANS, these solvated phospholipids incorporate the fluorophore tags and re-organizes into 100 nm liposomes once the shear stress stops. This reassembly of NBD-PE with POPC liposomes resulting in probe dilution (lipid-dye mixing) and an increased distance between NBD-PE molecules in spreading throughout the POPC liposome, thus resulting in a reduced measurable emission intensity. Conventionally this was only observed through a membrane fusion process, Herein, with the disassembly of liposomes and reassemble of liposomes we encounter a similar reduced emission intensity. While in the presence of another fluorophore which is RH- PE, there is an increase in the emission intensity. Previously it was reported that acceptor molecules such as Rh-PE can easily undergo – conjugations and which results into an increased emission

intensity¹⁶. While when both the labelled fluorophore liposomes were mixed together 1mL solution of each and processed through VFD at speed 5000 rpm and was compared to the control solution with no VFD processing there was a decrease in the emission intensity than the control data. This unequivocally proves the molecular exchange between the two fluorophores while processing in the VFD which causes the quenching of the donor molecule due to the close proximity during shear and thus reduces the overall emission intensity.

6.5 Conclusion

A facile and new process has been developed for fabricating liposomes under continuous flow processing in a high shear vortex fluidic device (VFD), as a scalable process. The optimum processing parameters were determined for the concentration of the phospholipid, the rotational speed of the 45° inclined tube in the thin film microfluidic platform, and flow rate. *In-situ* SANS was used to determine the nature of the species present under shear in the VFD, where liposomes approximately 100 nm in diameter are in equilibria with disassembled species, down to solvated phospholipid, depending on the level of shear stress associated with rotational speed induced topological fluid flow. Fluorophore tags can be introduced into the liposomes without disturbing the final geometry (no-VFD processing) and when two types of liposomes bearing 1% fluorophores are mixed in the VFD the resulting liposomes have equal populations of the two fluorophores, in accordance with the SANS findings. This study is a paradigm shift in fabricating liposomes with the ability to have control over the disassembly and re-organization without the need for downstream processing.

Acknowledgements

The authors acknowledge support of this work by the Australian Research Council for funding support, Australian Nuclear Science & Technology organization ANSTO for the beam-times to carry out the experiments and their guidance and support throughout this project. The authors acknowledge the

Australian Microscopy and Microanalysis Research Facility (AMMRF) and Australian National Fabrication Facility (AMMRF) for SEM, dual target sputter coater and AFM imaging. Authors also acknowledge Adelaide Microscopy at The University of Adelaide (UoA), South Australia for TEM imaging and Flinders Centre for Innovation in Cancer (FCIC), South Australia for the guidance and support throughout this project.

References

1. Allen, T. & Cullis, P. Liposomal drug delivery systems: From concept to clinical applications. *Advanced Drug Delivery Reviews* 65, 36-48 (2013).
2. Salim, M., Minamikawa, H., Sugimura, A. & Hashim, R. Amphiphilic designer nano-carriers for controlled release: from drug delivery to diagnostics. *Med. Chem. Commun.* 5, 1602-1618 (2014).
3. Luan, X. et al. Engineering exosomes as refined biological nanoplateforms for drug delivery. *Acta Pharmacologica Sinica* 38, 754-763 (2017).
4. Sato, Y. et al. Engineering hybrid exosomes by membrane fusion with liposomes. *Scientific Reports* 6, (2016).
5. Carugo, D., Bottaro, E., Owen, J., Stride, E. & Nastruzzi, C. Liposome production by microfluidics: potential and limiting factors. *Scientific Reports* 6, (2016).
6. Shum, H., Lee, D., Yoon, I., Kodger, T. & Weitz, D. Double Emulsion Templated Monodisperse Phospholipid Vesicles. *Langmuir* 24, 7651-7653 (2008).
7. Xu, Q. et al. Preparation of Monodisperse Biodegradable Polymer Microparticles Using a Microfluidic Flow-Focusing Device for Controlled Drug Delivery. *Small* 5, 1575-1581 (2009).
8. Jahn, A., Vreeland, W., Gaitan, M. & Locascio, L. Controlled Vesicle Self-Assembly in Microfluidic Channels with Hydrodynamic Focusing. *Journal of the American Chemical Society* 126, 2674-2675 (2004).
9. Matosevic, S. & Paegel, B. Stepwise Synthesis of Giant Unilamellar Vesicles on a Microfluidic Assembly Line. *Journal of the American Chemical Society* 133, 2798-2800 (2011).
10. Britton, J., Stubbs, K., Weiss, G. & Raston, C. Frontispiece: Vortex Fluidic Chemical Transformations. *Chemistry - A European Journal* 23, (2017).
11. Britton, J., Meneghini, L., Raston, C. & Weiss, G. Accelerating Enzymatic Catalysis Using Vortex Fluidics. *Angewandte Chemie* 128, 11559-11563 (2016).
12. Britton, J. & Raston, C. Multi-step continuous-flow synthesis. *Chemical Society Reviews* 46, 1250-1271 (2017).

13. Vimalanathan, K. et al. Surfactant-free Fabrication of Fullerene C60 Nanotubules Under Shear. *Angewandte Chemie* 129, 8518-8521 (2016).
14. Yuan, T. et al. Shear-Stress-Mediated Refolding of Proteins from Aggregates and Inclusion Bodies. *ChemBioChem* 16, 393-396 (2015).
15. Phillips, J. et al. Chemoselective and Continuous Flow Hydrogenations in Thin Films Using a Palladium Nanoparticle Catalyst Embedded in Cellulose Paper. *ACS Applied Bio Materials* 2, 488-494 (2018).
16. Oksdath-Mansilla, G., Kucera, R., Chalker, J. & Raston, C. Azide–alkyne cycloadditions in a vortex fluidic device: enhanced “on water” effects and catalysis in flow. *Chemical Communications* 57, 659-662 (2021).
17. Tavakoli, J., Raston, C. & Tang, Y. Tuning Surface Morphology of Fluorescent Hydrogels Using a Vortex Fluidic Device. *Molecules* 25, 3445 (2020).
18. He, S., Joseph, N., Luo, X. & Raston, C. Continuous flow thin film microfluidic mediated nano-encapsulation of fish oil. *LWT* 103, 88-93 (2019).
19. He, S. et al. Vortex fluidic mediated encapsulation of functional fish oil featuring in situ probed small angle neutron scattering. *npj Science of Food* 4, (2020).
20. Cao, X. et al. Vortex fluidics mediated non-covalent physical entanglement of tannic acid and gelatin for entrapment of nutrients. *Food & Function* (2021). doi:10.1039/d0fo02230f
21. Luo, X. et al. Vortex Fluidic Mediated Synthesis of Macroporous Bovine Serum Albumin-Based Microspheres. *ACS Applied Materials & Interfaces* 10, 27224-27232 (2018).
22. Luo, X. et al. Vortex Fluidic-Mediated Fabrication of Fast Gelated Silica Hydrogels with Embedded Laccase Nanoflowers for Real-Time Biosensing under Flow. *ACS Applied Materials & Interfaces* 12, 51999-52007 (2020).
23. Alharbi, T. M. D. et al. Sub-Micron Moulding Topological Mass Transport Regimes in Angled Vortex Fluidic Flow. <https://doi.org/10.26434/chemrxiv.13141352.v1> (2020)
24. Hammouda, B. Temperature Effect on the Nanostructure of SDS Micelles in Water. *Journal of Research of the National Institute of Standards and Technology* 118, 151 (2013).
25. Mo, J. et al. Shear induced carboplatin binding within the cavity of a phospholipid mimic for increased anticancer efficacy. *Scientific Reports* 5, (2015).
26. Gao, F. et al. High-efficiency blue thermally activated delayed fluorescence from donor–acceptor–donor systems via the through-space conjugation effect. *Chemical Science* 10, 5556-5567 (2019).

Chapter 7: Conclusions and Future Work

7.1 Conclusions

The vortex fluidic device shown significance outcomes in a number of research areas including in materials processing¹⁻¹⁰, chemical transformations¹¹⁻¹², bio-materials fabrication¹³⁻¹⁵, polymer synthesis¹⁶, folding proteins¹⁷, controlling self-assembly¹⁸⁻²⁰ and biodiesel production²¹⁻²³. The mechanoenergy in the VFD is able to control and manipulate the size, shape and homogeneity of the materials being processed, as well as controlling different reactions to increase the total conversion and rates of conversion when compared with batch processes. Outcomes of processing in the thin film microfluidic platform depend on the nature of liquid including viscosity, rotational speed, tilt angle, and concentration. This holds for either the confined mode of operation of the VFD where a finite amount of liquid is processed or for continuous flow where material is delivered at optimized flow rates using one or more jet feeds. Research undertaken in this thesis significantly advances the applications of the device and provide insight into the nature of the fluid flow. Our work establishes that the dynamic thin film in the VFD and associated mechanoenergy can manipulate “soft materials” and alter their properties according to specific applications.

A continuous flow process for fabricating W/O/W emulsions comprised of 50 to 250 nm diameter particles has been established with the results published in journal LWT- Food Science and Technology. The VFD induced mechanoenergy affords much smaller particles relative to conventional batch homogenization where the particle range in size from 2 to 5 mm. Optimization of the process followed a systemic approach in varying different processing parameters of the VFD, and are as follows: Dispersed phase 2 g/100 mL, lipid/oil: 1/1 (w/w), rotational speed 8000 rpm, flow-rate 0.1 mL/min, tilt angle 45°, temperature 25 °C followed by sonication post VFD processing for 20 min. The findings confirm the potential of vortex fluidic processing in the food industry, especially given the green chemistry metrics of the technology which avoids the use of toxic chemicals or the need for other

additives.

Different food models further highlight the potential of the VFD in food technology, with the results published in journal *Plos one*. Raw milk pasteurization was compared with the homogenization technique with the VFD reducing the pasteurization time from 30 to 10 minutes and the enzymatic hydrolysis for the milk powder from 2–3 hours to 20 minutes, along with the encapsulated particle size being reduced approximately 10-fold, from micro meters to hundreds of nanometers. This again opens up potential in food industry as a time-saving and cost-effective technology, as well as having a small capital outlay for the VFD technology relative to homogenization technology for comparable volume processing. Similarly, the fabrication of fish-oil emulsions in the VFD was established with better nutritional value of the product with the results published in the prestigious journal *npg Science of Food*. This is a paradigm shift in the area of food science, and the findings are destined to create the next generation of products with better nutritional value for the body, again in cost-effective and time-saving set-up. This work also developed a new technique for real time study of assembly-disassembly processing in the VFD using *in-situ* SANS, which provided valuable insight into the processing, as well as setting a new benchmark for studying liquids under shear stress. The findings show that the VFD can manipulate materials at nano- dimensions with potential for aiding the development of new products in the marketplace.

Different proteins are crosslinked with polyphenols or polysaccharides for fabricating gels or gel-based nanoparticles. Research undertaken herein uses the VFD to fabricate stronger gels with gelatin and non-covalently crosslinking with polyphenol tannin, with the results published in *Food and Function*. They show that nutrients can be encapsulated and utilized for products with better nutritional value.

Liposomes which are widely used in pharmaceutical and health industry for a number of applications can be fabricated using VFD technology as a rapid and facile process. This also involved extensive studies on real time small angle neutron scattering which established that the mechanical energy in the liquid in

the VFD can disassemble liposomes in a controlled way down to micelles and even solvated phospholipid, and the results are without precedent. These are in equilibrium with liposomes in the VFD and this establishes that the most stable structure for the bottom up self-assembly of lipids is about 100 nm, and interestingly this dimensionality occurs at the cellular level for producing exosomes and endosomes which are liposomes with membrane protein.

The findings established that the VFD has potential in manipulated soft matter relevant to food processing in general, and also liposomes at the cross roads with other fields including medicine and cosmetics.

7.2 Future Work

The outcomes of each project undertaken in this thesis are reported as separate chapters, collectively providing a platform for applications of the corresponding materials and processes reported. In addition, the findings provide insight for further applications of the VFD. The VFD is a relatively new microfluidic platform, with few research groups around the world having access to such technology. The findings in this thesis feature in five publications and one manuscript on manipulating soft matter is to be submitted. Collectively they further highlight the remarkable utility of the VFD in being applicable for processing of soft materials in a controlled way. It is the unique fluid flow in the VFD that sets the device aside as a paradigm shift in microfluidics devices and in materials synthesis in general. Inroads into understanding the topological fluid flow in the VFD have been made, involving a major international research effort.²⁴ The dimensionality of the topological fluid flow in the 20mm diameter tube in the VFD is submicron, depending on the rotational speed for the tube set at 45° tilt angle, which is the optimized angle for all processing thus far in the device. This has provided a level of predictability of the outcomes of processing in the device, and this opens up other possibilities in using the VFD to further manipulate and transform materials in wide range of disciplines, including soft matter. Indeed, the findings in this thesis contribute to an understanding of the fluid flow, and for soft materials the scene is set for a myriad of application, especially in the food,

drug delivery and cosmetic arenas. Larger VFD tubes can be predictably used for soft matter processing, and future work in this regard is the use of the recently commissioned 50 mm diameter VFD in the Raston research laboratory.

7.2.1 Vortex Fluidics Mediated Enhanced Drug Loading in Ferritin Nano-Carriers

Ferritin has a unique 24 subunit structure with an outer diameter of 12 nm. It possesses a hollow cavity of 8 nm, which can be used to encapsulate drugs and modified chemically to be utilized as nano-carriers. Due to its unique architecture, self-assembly and withstand to temperature and pH these are widely studied as novel protein-based drug carriers²⁵. As the natural ferritin structure has two types of protein units known as H-ferritin (Hfn) and L-ferritin (Lfn) and have an iron core obtained through the biomineralization of the excess iron in the body. The ferritin drug carriers (FDC's) are engineered ferritin obtained by expression and purification and is mainly dominated by Hfn and an empty core. The major advantage of utilizing FDC's as nano-carrier due to its simple structure and no extra modification is required for the stability or to be target specific as the protein has an innate affinity towards Tfr1 receptors²⁵. VFD has shown significant results in improving the drug-efficacy of carboplatin into p-calixarenes based phospholipid mimics²⁶. Due to the previous significant results, we aimed to utilize ferritin with improve drug loading by applying mechanoenergy in the VFD. Due to robust nature of the structure of ferritin, in conventional processing the protein is mixed with the drug and the mixture heated at 60 degrees with stirring for 4 hours. Through this process the loading is very low. Thus, we also aimed to apply the mechanoenergy and shear stress from the VFD to improve the drug loading content and also reduce the processing time below 4 hours. This will also enable us to understand protein self-assembly and folding under shear stress and how this can be used to design systems for improved drug efficacy. Moreover, this will also test some of the fundamental understanding of the fluid dynamics in the VFD, which is now understood as Faraday waves primarily driving the process along the rotational landscape, with a defined physical dynamic equilibrium state, depending on the viscosity and density of the liquid.

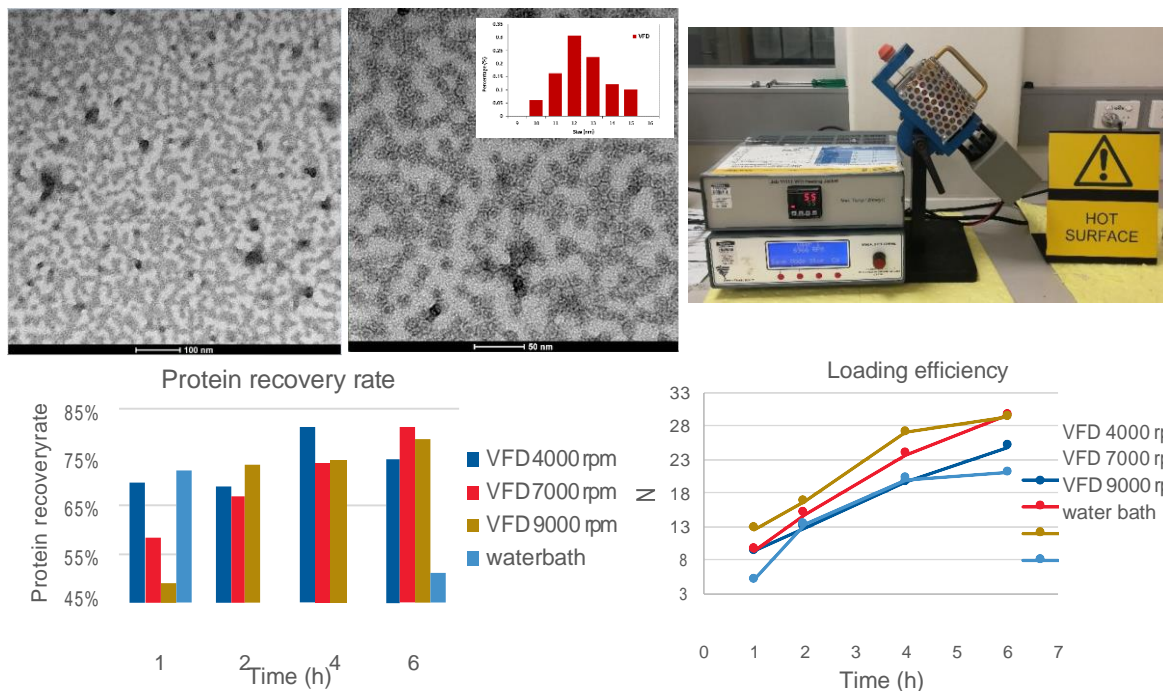


Figure 7.1: Application of VFD in drug delivery technology. 1) TEM images of the protein carrier ferritin. 2) photograph of the VFD with the heating unit assembled. 3) protein recovery rate for the VFD at different speeds and water bath system. Loading efficiency of the drug in the protein at different speeds and the water bath system.

The results from the drug loading experiments indicated that there is an increase in the protein recovery rate with the help of VFD. The mechanoenergy of the VFD aids to reduce the aggregation of the protein clusters enhance the recovery rate after the drug loading when compared with the conventional water bath system. But it is also observed that at the same time there is no significance increase in the drug loading efficiency N when processed for 1, 2, 4 and 6 hours at 4000 rpm, 7000 rpm and 9000 rpm when compared with water bath system for the same amount of time. This result shows the robustness of the protein and the interaction with the model drug. But this also shows the potential of VFD in future drug delivery application for enhancing drug loading in different carriers. The progress VFD has is just “the tip of the iceberg” there is still plenty of avenues to be achieved.

Acknowledgements

The author acknowledges University of Adelaide School of Chemical Engineering for their help in the drug loading experiments and TEM facility for their assistance with the TEM images.

References

1. Chen, X.; Dobson, J. F.; Raston, C. L., Vortex fluidic exfoliation of graphite and boron nitride. *Chemical Communications* 2012, 48 (31), 3703-3705.
2. Wahid, M. H.; Eroglu, E.; Chen, X.; Smith, S. M.; Raston, C. L., Functional multi-layer graphene–algae hybrid material formed using vortex fluidics. *Green Chemistry* 2013, 15 (3), 650-655.
3. Wahid, M. H.; Eroglu, E.; Chen, X.; Smith, S. M.; Raston, C. L., Entrapment of *Chlorella vulgaris* cells within graphene oxide layers. *RSC Advances* 2013, 3 (22), 8180-8183.
4. Wahid, M. H.; Eroglu, E.; LaVars, S. M.; Newton, K.; Gibson, C. T.; Stroehrer, U. H.; Chen, X.; Boulos, R. A.; Raston, C. L.; Harmer, S.-L., Microencapsulation of bacterial strains in graphene oxide nano-sheets using vortex fluidics. *RSC Advances* 2015, 5 (47), 37424-37430.
5. Alharbi, T. M. D.; Harvey, D.; Alsulami, I. K.; Dehbari, N.; Duan, X.; Lamb, R. N.; Lawrance, W. D.; Raston, C. L., Shear stress mediated scrolling of graphene oxide. *Carbon* 2018, 137, 419-424.
6. Vimalanathan, K.; Suarez-Martinez, I.; Peiris, M. C. R.; Antonio, J.; de Tomas, C.; Zou, Y.; Zou, J.; Duan, X.; Lamb, R. N.; Harvey, D. P.; Alharbi, T. M. D.; Gibson, C. T.; Marks, N. A.; Darwish, N.; Raston, C. L., Vortex fluidic mediated transformation of graphite into highly conducting graphene scrolls. *Nanoscale Advances* 2019, 1 (7), 2495-2501.
7. Vimalanathan, K.; Gascooke, J. R.; Suarez-Martinez, I.; Marks, N. A.; Kumari, H.; Garvey, C. J.; Atwood, J. L.; Lawrance, W. D.; Raston, C. L., Fluid dynamic lateral slicing of high tensile strength carbon nanotubes. *Scientific reports* 2016, 6, 22865.
8. Vimalanathan, K.; Raston, C. L., Dynamic Thin Films in Controlling the Fabrication of Nanocarbon and Its Composites. *Advanced Materials Technologies* 2017, 2 (6), 1600298.

9. Alharbi, T. M. D.; Vimalanathan, K.; Lawrance, W. D.; Raston, C. L., Controlled slicing of single walled carbon nanotubes under continuous flow. *Carbon* 2018, 140, 428-432.
10. Luo, X.; Al-Antaki, A. H. M.; Vimalanathan, K.; Moffatt, J.; Zheng, K.; Zou, Y.; Zou, J.; Duan, X.; Lamb, R. N.; Wang, S.; Li, Q.; Zhang, W.; Raston, C. L., Laser irradiated vortex fluidic mediated synthesis of luminescent carbon nanodots under continuous flow. *Reaction Chemistry & Engineering* 2018, 3 (2), 164-170.
11. Britton, J.; Raston, C. L.; Weiss, G. A., Rapid protein immobilization for thin film continuous flow biocatalysis. *Chemical Communications* 2016, 52 (66), 10159-10162.
12. Britton, J.; Meneghini, L. M.; Raston, C. L.; Weiss, G. A., Accelerating Enzymatic Catalysis Using Vortex Fluidics. *Angewandte Chemie International Edition* 2016, 55 (38), 11387-11391.
13. Luo, X.; Al-Antaki, A. H. M.; Pye, S.; Meech, R.; Zhang, W.; Raston, C. L., High- Shear- Imparted Tunable Fluorescence in Polyethylenimines. *ChemPhotoChem* 2018, 2 (4), 343-348.
14. Luo, Xuan, Mohammed Al-Antaki, Ahmed Hussein, Igder, Aghil, Stubbs, Keith A, Su, Peng, Zhang, Wei, . . . Raston, Colin L. (2020). Vortex Fluidic-Mediated Fabrication of Fast Gelated Silica Hydrogels with Embedded Laccase Nanoflowers for Real-Time Biosensing under flow. *ACS Applied Materials & Interfaces*, 12(46), 51999-52007.
15. Tavakoli, Javad, Raston, Colin L, & Tang, Youhong. (2020). Tuning Surface Morphology of Fluorescent Hydrogels Using a Vortex Fluidic Device. *Molecules (Basel, Switzerland)*, 25(15), 3445.
16. Igder, Aghil, Pye, Scott, Mohammed Al-Antaki, Ahmed Hussein, Keshavarz, Alireza, Raston, Colin L, & Nosrati, Ata. (2020). Vortex fluidic mediated synthesis of polysulfone. *RSC Advances*, 10(25), 14761-14767.
17. Yuan, T. Z.; Ormonde, C. F.; Kudlacek, S. T.; Kunche, S.; Smith, J. N.; Brown, W. A.; Pugliese, K. M.; Olsen, T. J.; Iftikhar, M.; Raston, C. L., Shear-Stress-Mediated Refolding of Proteins from Aggregates and Inclusion Bodies. *ChemBioChem* 2015, 16 (3), 393-396.
18. Vimalanathan, K.; Shrestha, R. G.; Zhang, Z.; Zou, J.; Nakayama, T.; Raston, C. L., Surfactant-free Fabrication of Fullerene C60 Nanotubules Under Shear. *Angewandte Chemie* 2017, 129 (29), 8518-8521.

19. Boulos, R. A.; Zhang, F.; Tjandra, E. S.; Martin, A. D.; Spagnoli, D.; Raston, C. L., Spinning up the polymorphs of calcium carbonate. *Scientific Reports* 2014, 4, 3616.
20. 19. Alsulami, I. K.; Alharbi, T. M.; Harvey, D. P.; Gibson, C. T.; Raston, C. L., Controlling the growth of fullerene C60 cones under continuous flow. *Chemical Communications* 2018, 54 (57), 7896-7899
21. Britton, J.; Raston, C. L., Continuous flow vortex fluidic production of biodiesel. *RSC Advances* 2014, 4 (91), 49850-49854.
22. Britton, J.; Raston, C. L., Rapid high conversion of high free fatty acid feedstock into biodiesel using continuous flow vortex fluidics. *RSC Advances* 2015, 5 (3), 2276-2280.
23. Sitepu, E. K.; Corbin, K.; Luo, X.; Pye, S. J.; Tang, Y.; Leterme, S. C.; Heimann, K.; Raston, C. L.; Zhang, W., Vortex fluidic mediated direct transesterification of wet microalgae biomass to biodiesel. *Bioresource Technology* 2018, 266, 488-497
24. Alharbi, Thaar M. D.; Jellicoe, Matt; Luo, Xuan; Vimalanathan, Kasturi; Alsulami, Ibrahim K; Harbi, Bedia S Al; et al. (2020): Sub-Micron Moulding Topological Mass Transport Regimes in Angled Vortex Fluidic Flow. *ChemRxiv*. Preprint. <https://doi.org/10.26434/chemrxiv.13141352.v1>
25. He, Jiuyang, Fan, Kelong, & Yan, Xiyun. (2019). Ferritin drug carrier (FDC) for tumor targeting therapy. *Journal of Controlled Release*, 311-312, 288-300.
26. Mo, Jingxin, Eggers, Paul K, Chen, Xianjue, Ahamed, Muhammad Rizwan Hussain, Becker, Thomas, Yong Lim, Lee, & Raston, Colin L. (2015). Shear induced carboplatin binding within the cavity of a phospholipid mimic for increased anticancer efficacy. *Scientific Reports*, 5(1), 10414.